NOAA

Professional Paper 7

Three-Dimensional Triangulation With Satellites

HELLMUT H. SCHMID
National Ocean Survey, Geodesy Division

U.S. DEPARTMENT OF COMMERCE, Frederick B. Dent, *Secretary*
NATIONAL OCEANIC AND ATMOSPHERIC ADMINISTRATION, Robert M. White, *Administrator*

Rockville, Md., October 1974

For sale by the Superintendent of Documents, U.S. Government Printing Office
Washington, D.C. 20402 - Price $1.65 (paper cover)
Stock Number 0321-00011

Contents

551-596

FIGURES

TABLES

Three-Dimensional Triangulation with Satellites

Hellmut H. Schmid

ABSTRACT.—Geometric satellite triangulation is an application of analytical photogrammetry. In the World Net Project, recently completed, passive satellites were photographed against the star background from 45 globally distributed stations and the resulting directions were combined to determine three-dimensional Cartesian coordinates for each. This volume presents, in detail, the rationale of this method together with a description of the equipment and, in part 2, the mathematical background of the computation programs used in the adjustment of the observed data. Part 3 gives results of the triangulation project and an evaluation of these results from the standpoint of error theory.

1. FOUNDATIONS OF SATELLITE GEODESY AND THE CREATION OF WORLDWIDE GEODETIC REFERENCE SYSTEMS

1.1 Geometric and Geophysical Aspects of Satellite Geodesy

Artificial satellites in near-Earth orbits have contributed to the field of geodesy a new technique which, theoretically speaking, is capable of completely reorienting the methods and procedures of the geodetic discipline. Application of newly developed methods of precision measurements in satellite triangulation constitute, in a practical sense, a reformation in the domain of classical geodetic field operations [1].

Without entering here into questions concerning the dividing line between geodesy and geophysics, it can be stated that the fundamental problem of geodesy is the mathematical description of the Earth's gravity field together with the determination of the geometry of the physical surface of the Earth, with unambiguous correspondence between the Earth-fixed coordinate systems or datums and the spherical coordinate system for a given epoch that serves as a frame of reference for metric astronomy. With satellite geodesy it is possible to find a synoptic solution to the fundamental problem, i.e., with reference to the whole Earth. Furthermore, triangulation with satellites in conjunction with position and time determinations of satellite orbits, eventually provides the necessary link between the geometric and geophysical measuring concepts of geodesy.

Thus, with the aid of satellite geodesy it becomes possible to undertake the geometric description of the surface and the analytical description of the gravity field of the Earth by means of worldwide measuring systems, and to derive results in the form of three-dimensional models based on a minimum of a priori hypotheses.

These mathematical models then represent the frame of reference into which one can fit existing geodetic results from the various local datums, as well as all future geodetic measurements. The relevant adjustment should not confine itself to the limited (in practice) classical concept of the treatment of accidental errors. With the aid of a generalization of the Gaussian algorithm it must take advantage of the increasing knowledge derived from interdisciplinary research concerning the various geophysical parameters involved. It must also include the corresponding variance-covariance matrices.

From a formalistic mathematical point of view, the significance of artificial satellites for geodesy consists in the ability to express the time-position curve of the orbit of a close-to-Earth satellite in

terms of functions of certain parameters which, in turn, give information with respect to geometric and geophysical properties of the Earth and its surrounding space. In this development the quantities describing the gravitational field are of prime importance to gravimetry; the remainder of the geophysical forces affecting the orbit or arising from the satellite itself are treated as perturbation sources.

The parameters appearing in the mathematical simulation of the satellite orbits are determined quantitatively by setting up observation equations that functionally relate the measurements made for the orbit determination with the parameters describing the orbit. It is then apparent that, in addition to these orbital parameters, these equations will involve the position coordinates of the Earth-fixed observation stations which, in the geophysical content of the problem, represent the position of these stations relative to the Earth's center of mass. Assuming a sufficiently large number of optimally distributed observations, it is possible to determine from the corresponding adjustment not only the geophysical parameters affecting the orbit but also the geocentric parameters of the observing stations. This presents the opportunity of a simultaneous solution of the geometric and gravimetric problems of geodesy in a worldwide frame.

From a purely theoretical standpoint, this attractive train of thought has found great appeal among astronomers and geophysicists in particular and has already led to impressive results and new insight [2]. Being more intimately connected with triangulation measurements proper, however, the measurement engineer and, in particular, the practicing geodesist will have certain reservations, because the relatively large number of parameters appearing in the complex system of equations of such an adjustment are all more or less strongly correlated. In direct consequence of the simultaneous solution there exists, first of all, correlation among the various parameters of the same type, e.g., the coefficients of the harmonic functions describing the gravity field. In addition, there is statistical dependence between the gravimetric quantities and the geophysical parameters introduced to describe certain orbital perturbations. Also, the coordinates of the observing stations introduced into the solution and adjusted together with the other parameters are not only correlated among themselves but also with these nongeometric quantities. In practice, the number of observations as well as their distribution in time and space leaves much to be desired, which serves only to amplify these correlations.

Even when, by using a large-capacity electronic computer, it is possible to unite a very large number of observations in a single solution, it is important not to overlook the fact that the geometry of the observing stations obtained from such a solution does not necessarily represent actual spatial relations. While the computed parameters in their entirety are well suited to describe the geometry of the satellite orbits, within the limits of accuracy of the original observations, the possibility nevertheless exists that an isolated group of parameters such as the station coordinates may have only limited accuracy. Their significance must be judged in the light of the underlying geophysical and astronomical hypotheses. In short, the geometry of the observation stations is prejudiced by the specific properties of the mathematical model chosen to simulate the geophysical-dynamic nature of the satellite orbit.

This state of affairs also explains why, despite the initial lack of interest in a purely geometric solution in satellite geodesy, a worldwide three-dimensional satellite triangulation is now in progress.

This in no way lessens the significance of the geophysical solution. On the contrary, dynamic satellite geodesy gains thereby. Once the three-dimensional geometry of a sufficiently large number of points on the Earth's surface has been established with a purely geometric solution, based only on Euclidean (flat space) geometry and the Right Ascension-Declination System of metric astronomy, orbital observations from these stations can be used for the exclusive purpose of determining geophysical parameters. Such a system will not require the computation of station coordinates in the adjustment.

Thus the number of unknowns to be determined from a given, available set of observations is reduced. This in itself is a desirable objective but, in addition, correlation is eliminated between the geometry and the geophysics, at least with respect to the station coordinates and the orbital elements.

Given the results of the geometric solution, the opportunity is presented, by way of a purely geometric satellite orbit determination, to ascertain the geometrical shape of the surface of the oceans by using laser and radar techniques to measure the distances between the satellite and the ocean surface. The influence of weather and tides on the measured profiles can be eliminated with measurements over a sufficiently long period of time. This would not only help to complete the presentation of the geometry of the physical surface of the Earth, but would also give a purely geometric (hence unconstrained by hypothesis) representation

of a large portion of a surface that would be a very good but not rigorous approximation to the geoid. The objection that, considering the preceding comments on a purely geometric solution, the information content of the dynamic solution is not completely exhausted can be countered by seeing the eventual solution of the problem of satellite geodesy as a combination of the separate, individual geometric and dynamic solutions. In such a solution, the station coordinates will no longer be treated as free variables for the dynamic solution but will be introduced with their associated covariances from the geometric adjustment.

This will be the real contribution of satellite geodesy to the principal geodetic mission. The problems of describing the Earth's gravity field and determining the geometry of the physical surface are solved in a consistent formulation, yielding optimal results from a geophysical-hypothetical as well as from a metrological standpoint, with the geometric and geophysical concepts mutually supporting each other. The amalgamation of the outputs of geometric and dynamic satellite geodesy must in the end be consummated, from the theoretical as well as practical standpoint, by the inclusion of geodetic data measured on the surface of the Earth. This requirement seems necessary because, although satellite geodesy's significant contribution to physical geodesy has been to open up the third dimension in the investigation of the Earth's gravity field, the fact still remains that the essential tasks of geodesy are the determination of the geometry of the physical surface of the Earth and the representation of the gravity field in detail close to the crust [3].

1.2 Development and Organization of a Geodetic Satellite Program for the Creation of a Worldwide Geodetic Reference System

The history of satellite geodesy and its theoretical development began with the implementation of an idea that had been, for decades, an intermediary goal for scientists concerned with rocket development. This goal was to increase the velocity of the rocket to the point where it would balance the component due to gravity, and go into orbit around the Earth. This is shown schematically for a circular orbit in figure 1.

The realization of this technical goal with the launch of the first Russian artificial satellite and, shortly thereafter, of the first American satellite, created renewed interest among experts in the fields of astronomy and aeronomy in the theoretical problems concerned with the description of the track of a body of negligible weight orbiting around

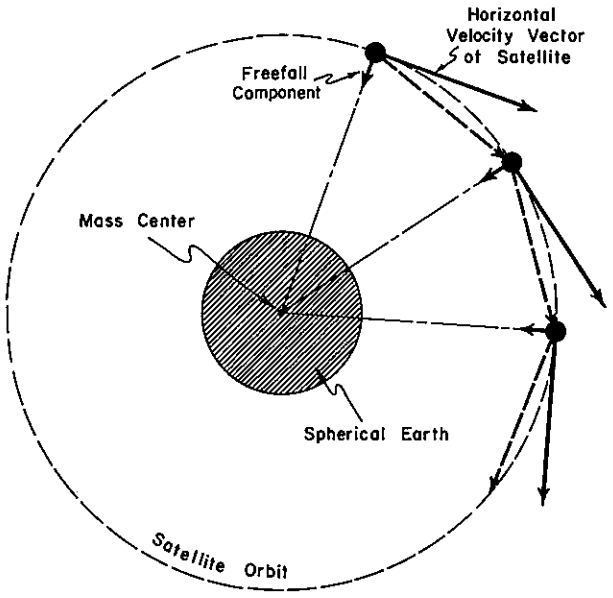

Figure 1.—Basic forces producing the satellite orbit.

an oblate mass, specifically around the Earth. Because the classical theories and procedures of physical geodesy are inadequate to the solution of all these problems, it has become the practice to apply, almost exclusively, the classical principles of celestial mechanics together with theories and results from the fields of aeronomy and related geosciences. These, with the aid of rocket experiments, had already made considerable advances in the subject.

This development explains the dominating influence of dynamic satellite geodesy to this day; this factor also was reflected in the planning and execution of the first American geodetic satellite program. The basic requirement for the launch of the satellite for the first American geodetic experiment, known as ANNA, and for the subsequent GEOS satellite program was compact construction and rotation-symmetric form to the highest possible degree. The resulting mass-to-cross-section ratio is designed to minimize the perturbing influence of the atmosphere and other geophysical forces such as solar radiation pressure, in order not to complicate unnecessarily the adjustment of the orbit relative to the gravitational field.

In order to be able to sense the essential components of the Earth's gravitational field while keeping perturbing influences within bounds, a problem intimately connected with that of assuring the satellite a sufficiently long lifetime, the necessary experiments are executed at heights of 1,000 to 1,600 km above the Earth and the nearly circular orbits are distributed over as wide a band of

inclination as possible. The equipment for this type of satellite is typical for its purpose. Determination of the orbit is accomplished with satellite-borne instrumentation enabling the measurement of direct distances, distance differences, and directions. All these observations are related to absolute time measurements.

At the present time the distance measurements are based on the measurement of time lag of individual pulses or of the phase differences of continuously emitted frequencies, while distance difference observations are based on the use of the Doppler effect. A distance measuring method promising increased absolute accuracy is being developed with laser techniques. To measure directions, flashes of short duration—on the order of 1/1000 s—are emitted in groups of 5 to 7 at intervals of a few seconds and repeated a number of times in the course of a single orbit. Repetition depends on the power source available, but, on the whole, this method yields only few observations.

While the observation of such flashes has some application in geometric satellite triangulation, the basic use is for the calibration of electronic measurement systems.

Viewed in the light of the present state of development it is apparent that, in general, the program of dynamic satellite geodesy faces two complexes of questions requiring further study in planning for future geodetic satellite projects. From the theoretical side, for one, the question arises as to what extent the concepts derived from classical celestial mechanics and applicable to spherical fields are valid in the immediate vicinity of an oblate spheroidal mass. Of perhaps even greater significance are the questions regarding the validity of our concepts with respect to the various geophysical forces other than gravity that influence the orbit of an Earth satellite. So far as practical measuring techniques are concerned, assuming proper professional use of the equipment, there is little left to be desired with respect to data density and interior accuracy of the electronic data. However, even when exercising care in the necessary time and spatial distribution of the measurements, there remains sufficient reason to suspect that even today occasional systematic errors creep in, not so much because of the lack of reliability in the electronic components as because of uncertainties in the corrections necessary to transform the velocity of light in vacuo into the wave propagation velocity existing at the time of observation. The frequencies currently in use are particularly affected by periodic changes in the ionosphere. The possibility, mentioned above, of calibrating with light flashes by way of position and time determination offers little hope in a long term program if only for sighting reasons. Particularly ineffective in this connection have been the unsuccessful attempts to initiate an efficient and sufficiently extensive calibration program in which all the measuring methods to be used are examined systematically under typical observation conditions by simultaneous orbit observations from previously and precisely surveyed observation sites. The current method of judging the metric accuracy of the various procedures from the internal accuracy of, at times, very arbitrarily selected series of observations, or to derive absolute accuracy from the differences between end results of measuring systems employing quite different techniques in measuring and adjusting, is generally unsatisfactory for the metrological engineer and even more so for the geodesist.

In addition to GEOS satellites, used primarily for dynamic satellite geodesy, a balloon type satellite (PAGEOS) is used exclusively for geometric satellite triangulation within the framework of the present American geodetic satellite program. The PAGEOS balloon is similar in material and construction to the balloon satellite ECHO I; it is 30 m in diameter, its casing is 0.013 mm thick, and it reflects sunlight specularly, unlike the ECHO II satellite whose somewhat thicker casing reflected more diffusely. PAGEOS (passive geodetic satellite) was launched June 23, 1966, into a nearly circular, nearly polar orbit, with an average altitude of 4,200 km. Its launch established a suitable elevated target for worldwide satellite triangulation. The order of the stations in the worldwide triangulation network is listed in table 1 (cf. also figs. 44 to 49 and sec. 3.3). Part of the world net is shown in figure 2.

The compromise in the distribution of the stations necessitated by logistic and political considerations represents a good approximation to an optimal solution. The open mesh in the South Pacific Ocean is due to the lack of any kind of island, while the open space over Central Asia is political in nature. The optimal execution of worldwide geophysical experiments depends ultimately on whether the political world will come to the recognition that worldwide cooperation is required to enrich our geophysical and geodetic knowledge. In this sense, it is gratifying to see that the first worldwide geometric satellite triangulation under the technical supervision of the U.S. Coast and Geodetic Survey[1] is a program free of any kind of security restriction, whose results will be accessible to everyone.

[1] Now National Ocean Survey.

TABLE 1.—*World net stations*

Station No.	Station name	Latitude ϕ°	Longitude λ°
001	Thule, Greenland, Denmark	76.5 N	68.5 W
002	Beltsville, Maryland, USA	39.0 N	76.8 W
003	Moses Lake, Washington, USA	47.2 N	119.3 W
004	Shemya, Alaska, USA	52.7 N	174.1 E
006	Tromsø, Norway	69.7 N	18.9 E
007	Lajes AFB, Terceira, Azores	38.8 N	27.1 W
008	Paramaribo, Surinam	5.5 N	55.2 W
009	Quito, Ecuador	0.1 S	78.4 W
011	Maui, Hawaii, USA	20.7 N	156.3 W
012	Wake Island, USA	19.3 N	166.6 E
013	Kanoya, Kyushu, Japan	31.4 N	130.9 E
015	Mashad, Iran	36.2 N	59.4 E
016	Catania, Sicily, Italy	37.4 N	15.0 E
019	Villa Dolores, Argentina	31.9 S	65.1 W
020	Easter Island, Chile	27.2 S	109.4 W
022	Pago Pago, Samoa, USA	14.3 S	170.7 W
023	Thursday Island, Australia	10.6 S	142.2 E
031	Invercargill, New Zealand	46.4 S	168.3 E
032	Perth, Australia	31.9 S	116.0 E
038	Revilla Gigedo Isl., Mexico	18.7 N	111.1 W
039	Pitcairn Island, UK	25.1 S	130.1 W
040	Cocos Island, Australia	12.2 S	96.8 E
042	Addis Ababa, Ethiopia	9.0 N	38.7 E
043	Cerro Sombrero, Chile	52.8 S	69.2 W
044	Heard Island, Australia	53.1 S	73.7 E
045	Mauritius, Mascarene	20.4 S	57.7 E
047	Zamboanga, Philippines	6.9 N	122.1 E
050	Palmer Station, Antarctica, USA	64.7 S	64.4 W
051	Mawson Station, Antarctica, Australia	67.6 S	63.0 E
052	Wilkes Station, Antarctica, Australia	66.2 S	110.6 E
053	McMurdo Station, Antarctica, USA	77.8 S	166.7 E
055	Ascension Island, UK	8.0 S	14.3 W
059	Christmas Island, USA	2.0 N	157.4 W
060	Culgoora, Australia	30.3 S	149.6 E
061	South Georgia Island, UK	54.3 S	36.5 W
063	Dakar, Senegal	14.7 N	17.5 W
064	Ft. Lamy, Chad	12.2 N	15.0 E
065	Hohenpeissenberg, Germany	47.8 N	11.0 E
067	Natal, Brazil	5.9 S	35.4 W
068	Johannesburg, South Africa	25.9 S	27.7 E
069	Tristan da Cunha Island, UK	37.0 S	12.3 W
072	Chieng Mai, Thailand	18.8 N	99.0 E
073	Diego Garcia, Chagos, Mauritius	7.3 S	72.5 E
075	Mahé, Seychelles, UK	4.7 S	55.5 E
111	Wrightwood, California, USA	34.4 N	117.7 W

The triangulation method based on photogrammetric principles is described in detail in chapter 2.

1.3 References

(1) Schmid, H., "Reformatory and Revolutionary Changes in Geodesy," *Bulletin Geodesique*, No. 80, June 1966, pp. 141–147.

(2) Kozai, Y., "The Earth Gravitational Potential Derived from Satellite Motion," *Space Science Reviews*, D. Reidel Publishing Co., Dordrecht-Holland, Vol. 5, 1966, pp. 818–879.

(3) Kaula, W. M., "Evaluation of Results Relative to Those Obtained by Other Means," United States National Report, 1963–1967, Fourteenth General Assembly, IUGG, *Transactions*, American Geophysical Union, Vol. 48, No. 2, June 1967, pp. 343–345.

(4) Schmid, H., "Satellitengeodäsie—das Mittel zur Erstellung eines globalen geodätischen Bezugssystems," Wild-Heerbrugg, 50-Jahr-Festschrift (Satellite Geodesy—a method for the establishment of a worldwide geodetic reference system. Wild-Heerbrugg publication honoring the 50th anniversary of the Wild-Heerbrugg, Ltd.) 1971, pp. 104–113.

Figure 2.—Portion of the world net showing ties between four continents bordering the Atlantic Ocean.

2. GEOMETRIC SOLUTION OF SATELLITE GEODESY

2.1 Introductory Considerations

In the classical treatment of geometric geodesy, i.e., that part of geodesy that deals with the derivation of rigorous geometric results, difficulties arise from the fact that the measured quantities cannot be rigorously related to the geometric model to be established. Physical influences are responsible for this dilemma. The so-called measurements of horizontal and vertical angles are vitiated to an unknown extent by systematic influences such as anomalies in the gravity field and refraction. The reduction of base line measurements is, in principle, similarly affected.

In addition, the classical method of triangulation is forced to adopt a number of complex postulates whose geometric content is based on certain hypotheses. A typical example is the present day correction methods generally known as "isostatic reduction procedures." The physical principles underlying these procedures are the assumption of homogeneity and hydrostatic equilibrium of the masses within the Earth's crust. The resulting corrections to all geodetic observations will prejudice the end result in favor of Clairaut's theory. Aside from the physical assumptions, an unavoidable characteristic of classical geodetic triangulation is the practical limitation of sight length between points on or near the surface of the Earth. Not only are such geodetic triangulations incapable of making intercontinental connections but the first order nets must be pieced together with an excessive number of individual arcs. The disadvantage of this method arises not so much from the large number of stations involved as from the fact that accuracy is impaired by error propagation, especially in extensive nets.

As a consequence geodetic theory has developed complex methods of adjustment designed to eliminate the contradictions in the data by iteration, permitting the results of partly geometric and partly geophysical adjustment operations to interact until all results become internally consistent.

Although attractive from a theoretical standpoint, such methods have practical limitations. For this reason a purely geometrically defined, three-dimensional, worldwide, geodetic reference system is desired in order to transcend the shortcomings of the classical geodetic triangulation method. Moreover such a worldwide geometric solution is superior to a mere connection of the various geodetic datums which has at times been called the purpose of satellite geodesy. The geometrically defined reference system will make possible a more significant dynamic-physical analysis of measured satellite orbital perturbations and thus contribute to the solution of those problems which have to do with the location of the Earth's mass center and the description of gravity anomalies on or near the surface of the Earth as needed for the study of the physical structure of the crust as well as for the computations of the orbit of ballistic missiles flying in the immediate vicinity of the Earth.

The significance of a three-dimensional triangulation method, emphasized repeatedly in the recent history of geodesy, becomes especially apparent in connection with the field of satellite geodesy, which, because of its geometric and geophysical aspects, demands a three-dimensional solution.

Perhaps the greatest significance of geometric satellite triangulation, however, lies in the fact that, for the first time in the history of geodesy, with this method there exists the possibility for the creation of a world-wide three-dimensional reference system supported by a minimum of a priori hypotheses, in particular without reference to either the magnitude or direction of the force of gravity.

Establishing geometric correspondence among a number of selected, nonintervisible points of the physical surface of the Earth can be accomplished with spatial triangulation by means of auxiliary targets elevated sufficiently above the Earth's surface.

The generation of light signals visible over great distances is possible by means of artificial satellites. Because of the high velocity of such targets,

observation of directions to them can, at present, be made only with precision photogrammetric cameras. Because of the physical and chemical properties of the photogrammetric measurement components, the absolute accuracy as well as the reproducibility of the observation conditions in this method are limited. To get observational results with maximum absolute accuracy, the adjustment of the photogrammetric measurements must be based on a method of interpolation.

A suitable reference system into which an elevated target can be intercalated is obviously the right ascension-declination system of metric astronomy. This system is all the more attractive from the geodetic point of view because one of its axes is parallel to the Earth's axis of rotation. A large number of fixed stars whose coordinates are tabulated in catalogues are available as reference points. These control points being practically at infinite distance, it follows that their direction coordinates are insensitive to a parallel displacement of the observer and hence can not be used for scale determination. It is therefore necessary to determine the scale of the satellite triangulation independently, e.g., by measuring the distance between two adjacent stations. As will be shown in section 3.3, it is necessary to carry out such scale determinations in several portions of the worldwide triangulation net.

2.2 Geometric Foundations

We turn our attention now to a three-dimensional method of triangulation that is based on direction measurements and is designed to determine the coordinates of nonintervisible triangulation stations.

The relevant geometric solution is not new. In fact there is little room for originality in applying photogrammetry to ballistic and related problems. The use of star photography for the calibration of photogrammetric cameras is a proven method, especially with astronomers. The use of star images to orient photogrammetric cameras and the corresponding triangulation of additionally photographed target points was used successfully in the 1930's by Hopmann and Lohmann [1] for tracking missiles before this method was applied in the development of the V–2 rocket at Peenemünde, Germany, and, subsequently, in various other countries.

Väisälä proposed the same principle in the reports on the meetings of the Finnish Academy of Sciences, 1946, under the title "An Astronomical Method of Triangulation" [2].

There are several ways to present the geometric principles of this triangulation method. Väisälä's

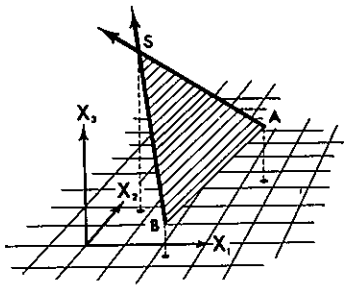

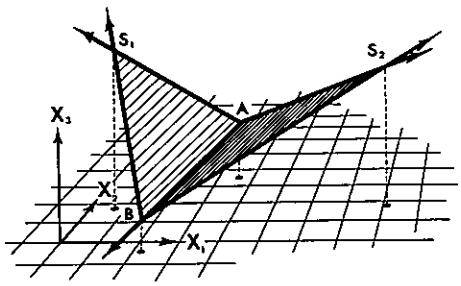

Figure 3.—Geometry of satellite triangulation.

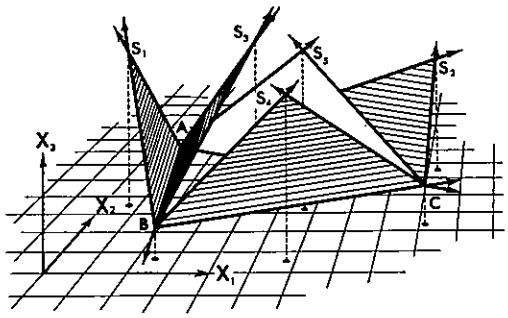

Figure 4.—Geometry of satellite triangulation.

proposal contains a lucid, geometric explanation. Two rays issuing from the end points of a given base line and directed at a common point define a plane in space whose orientation can be determined from the direction cosines of the rays. When two such planes have been fixed, the direction in space of the base line can be computed as the intersection of the two planes. The principle involved is shown in figure 3.

After two directions *AB* and *AC* (fig. 4) issuing from station *A* have been determined in this fashion, the shape and spatial orientation of the station triangle *ABC* is fixed by intersecting *AB* and *AC* with a plane whose orientation is known from observing the satellite position S_5 from *B* and *C*. Thus 5 planes are necessary and sufficient to fix the shape and orientation of a station triangle. Each of these planes contains two stations and one point of the satellite orbit. Therefore, there are 5

positions of the orbit together with the positions of the three stations A, B, and C, or $(5 + 3) \times 3 = 24$ unknowns to be determined.

Since each pair of simultaneous observations of a satellite position or, in other words, the determination in space of two intersecting lines, gives rise to 4 equations, there are in all 5×4, or 20 equations of condition available. Hence $24 - 20$, or 4 additional, independently determined geometric quantities are required for a complete solution of the triangle. The most obvious of the many theoretically available choices are the 3 coordinates of one of the stations which, in principle, can be assumed arbitrarily, for example, as the origin of the coordinate system. It is equally logical to choose as the fourth assumption the length of one of the sides of the triangle, which fixes the scale for the whole triangulation. For purposes of explaining the principle of satellite triangulation, it is sufficient to introduce this side length as the unit of length.

It is interesting to note that three of the five necessary planes can be determined with a single pass of the satellite if the subpoint of the observed satellite lies near the middle of the station triangle (see fig. 5). For this case a unique solution can be obtained with the determination of $(3 + 3) \times 3$, or 18 unknowns from 7×2, or 14 available condition equations. Again, it is necessary to introduce four additional, independently determined geometric parameters.

From the viewpoint of analytical photogrammetry the geometric principle of satellite triangulation can be explained by identifying the unknown positions of the triangulation stations and the unknown orientations of the observing cameras with the corresponding conditions in classical aerial photogrammetry. The unknown orbital positions of the satellite correspond to the relative control points of the stereo model, and the stars play the role of absolute control points, with the restriction that they cannot furnish scale since they lie at an infinite distance.

The geometric concept of photogrammetric satellite triangulation must, however, be interpreted in the light of the fact that, at each station, the stars (absolute control points) are used for the determination of the elements of the interior orientation needed for the reconstruction of the photogrammetric bundle, *together with* the determination of the three rotation elements of the exterior orientation. The condition of intersection of the rays resulting for each satellite image observed from more than one station is used exclusively to determine the three elements of translation of the exterior orientation. This circumvents the unfavorable correlation between the elements of rotation and translation that is typical in aerial triangulation, an advantage that is reflected in the favorable error propagation characteristics of satellite triangulation (cf. sec. 3.3).

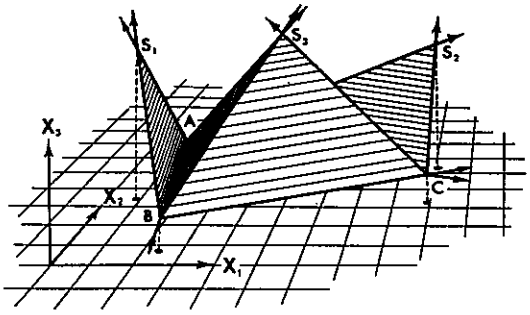

Figure 5.—Simultaneous observation of satellite from three stations.

The geometric content of satellite triangulation, in complete agreement with the corresponding concepts in the general field of analytical photogrammetry, is thus based on a multitude of individual rays whose directions must be determined from the relevant photograms. Hence the idealized conditions must be satisfied; these are that the three points—objective (satellite), center of projection (triangulation station), and image (photographed satellite image)—lie on one straight line. This condition is the geometric basis for satellite triangulation, just as it is the necessary and sufficient criterion for any photogrammetric triangulation [50].

It is obvious that, after fixing the first station triangle in space, nothing prevents the addition of further stations as vertices of triangles adjacent to the first. Postulating the possibility of scale determination, either by direct measurement of a side of one of the space triangles or by simultaneous distance measurement from at least 4 stations to a satellite position, the positions of a number of points on the physical surface of the Earth can be determined in a homogeneous three-dimensional reference system. In practice the arrangement of the stations and, hence, the shape of the configuration is to a great extent dictated by the geographical distribution of islands over the oceans.

Aside from using the method to determine a worldwide geodetic reference system, the same technique can be used to establish the frames for continental triangulations which, on the basis of accuracies in the determination of directions attained even today and of the basically favorable error propagation characteristic of satellite triangulation, are equivalent or superior to classical first-order nets, particularly where such nets cover extensive areas (cf. fig. 6).

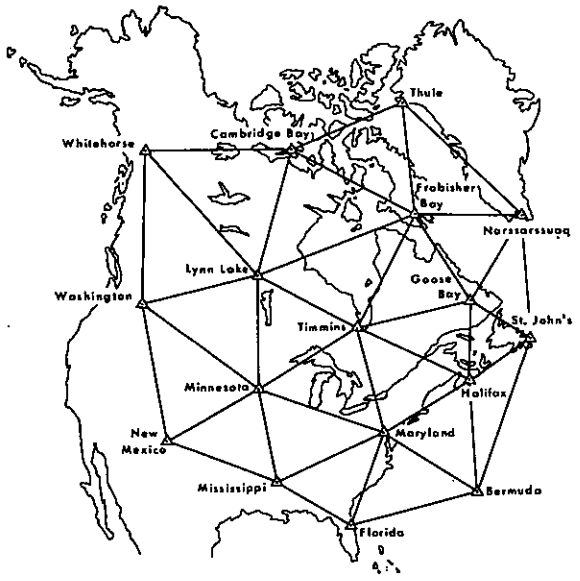

Figure 6.—Densification network in North America.

Judging by present technical standards, satellites orbiting at altitudes below 1,000 km will probably not be used because of their limited life span. Thus, in consequence of the nearly linear decrease in triangulation accuracy with increased height (cf. 3.3), the practically acceptable shortest average distance between points of a continental satellite triangulation net should be 500 to 1,000 km. Without changing the geometric principle, the described method of satellite triangulation becomes a type of three-dimensional triangulation with elevated targets—although the influence of the physical parameters is different and not necessarily more favorable from the standpoint of measuring technique. The method uses present day capabilities to generate a large number of light flashes or future capabilities to burn pyrotechnic signals on airplanes that may soon be expected to fly at heights of 20 to 25 km. In addition to the theoretically desirable, three-dimensional character of the triangulation method, it will be a question of economic feasibility whether such a technique will, in part, replace classical first order triangulation in certain areas of the Earth.

Quite independently of the measurements of the individual spatial triangulation figures, the basic geometrical concept underlying the method of satellite triangulation requires, at least in principle, the simultaneously executed observations of directions to the target—in our case the satellite—from at least two stations. Clearly, the requirement to measure directions, rather than merely angles, implies the necessity of orienting the observed bundle in each case relative to a uniquely defined system of reference. This is otherwise self evident in that our objective is to represent a consistent spatial reference system.

A spatial coordinate system to which a direction to a target sufficiently elevated above the horizon can be referred is the right ascension-declination system.

This reference system surrounding the whole Earth is qualitatively as well as quantitatively suitable, and a great number of precisely measured reference points are readily available. Of especial significance to the photogrammetric mensuration principle is the abundance of such absolute control points. Because of the physical and chemical nature of its numerous components and procedures, the photogrammetric method can satisfy the requirements for highest accuracy only if the corresponding observation and adjustment procedures are executed in a close-interval interpolation process.

We emphasize here, therefore, that the claim of satellite triangulation to produce results without the aid of physical hypotheses and practically free of systematic errors derives chiefly from the fact that photogrammetric direction determination in satellite triangulation operates not only with the aid of geometric interpolation within the reconstructed photogrammetric bundle but represents equally an interpolation into the physical process of astronomic refraction (cf. 2.5). This also means that the absolute accuracy of photogrammetric satellite triangulation depends primarily on the quality of the right ascension-declination system, particularly on its freedom from systematic errors. Because of the importance of the astronomic reference system to satellite triangulation, some relevant remarks on data processing in satellite triangulation will be made in the next section.

2.3 Astronomical Reference System[2]

In satellite triangulation, photographing the fixed stars serves a) to reconstruct and b) to uniquely orient the photogrammetric bundle in space. The problem of reconstructing the bundle is fundamentally identical with the problem of calibrating a photogrammetric camera. The geometric interpretation of the relevant parameters is independent of camera orientation. It would therefore suffice to have the relative geometric arrangement of the images of the stars on a particular plate given in an arbitrary coordinate system. However, the determination of an unambiguous orientation for all the bundles of rays serving the triangulation

[2] For the proper interpretation of the computations in the following, it is necessary that the reader first study sec. 2.7.1 and 2.7.2.

is predicated on the fact that all given control points (the totality of fixed stars used) are given in a uniquely defined reference system that can be uniquely transformed to an Earth-fixed coordinate frame. The right ascension-declination system of metric astronomy furnishes the metric basis for geometric satellite triangulation. The point of departure is the apparent position coordinates of stars tabulated for a given epoch in star catalogues such as: "Apparent Places of (1535) Fundamental Stars" published by the Astronomisches Rechen-Institut, Heidelberg; or the "General Catalogue" with approximately 33,000 apparent star positions; or, probably the most complete catalogue to date, the Smithsonian Astrophysical Observatory Star Catalog [3] in which over 250,000 stars and their apparent places are tabulated.

The choice of stars selected for the purpose of satellite triangulation depends primarily on the accuracy of their coordinates. Stars with large proper motions should be avoided and double stars should not be used. To counteract the influence of spectral differences of the stars, a special lens is used (cf. sec. 2.6). Finally, the selection is limited by the star magnitude registered by the specific optical system and emulsion used. With the BC–4 system and the Eastman Kodak emulsion 103 F in use today, stars of the 7th and 8th magnitude still produce good, measurable images over the entire plate. Using very bright stars at the same time as lower magnitude stars introduces the problem of the influence of relative, systematic errors in locating the centroid of the image. The existence of a magnitude effect, not negligible in astronomical measurements, has, with the focal length currently in use for satellite triangulation, not as yet been demonstrated quantitatively.

In [3] the distribution over the celestial sphere with respect to right ascension and declination of the stars listed in the Smithsonian Catalogue is described from the standpoint used in the selection.

Geometric satellite triangulation can at best, therefore, attain the accuracy of the astronomical reference system (cf. sec. 3.1). Hence, for a critical study of the theoretical accuracy of satellite triangulation, the observation and adjustment procedures used in metric astronomy to establish star catalogues are of fundamental importance. However, within the limits of this presentation, it must suffice to refer to the literature [4,5,6,7,8,9,10] on these highly specialized and complex procedures.

But to understand geometric satellite triangulation it is necessary to interpret correctly the qualitative (geometric) and quantitative (statistical) data listed in the star catalogues. Such interpretations are necessary to understand the reductions needed to transform the time and space dependent geometry of the individual photogrammetric exposures into a homogeneous, geometric system. The problems arising here are basically the same as those faced in the reduction of astronomic-geodetic field observations.

The star catalogues list for apparent places a pair of spherical coordinates for a specified epoch, right ascension α and declination δ. Their meanings are indicated on the unit sphere in figure 7. Right ascension α has its origin at the intersection of the celestial Equator and the ecliptic (the equinox) and is measured toward the east along the Equator; the declination δ is measured from the Equator along the (spherical) meridian, positive toward the North Pole. The specification that the catalogued values refer to a given epoch (generally the beginning of the tropical year 1950.0 in the newer catalogues) means that time dependent corrections must be added to the star coordinates before they represent the actual position at the instant of observation (in our case, the time of exposure).

The reason for these corrections is found primarily in the dynamics of the universe, although purely physical corrections must also be taken into consideration. Theoretical explanations are described in detail in standard works on geodetic astronomy, e.g., references 11 through 18. Nevertheless it seems useful to outline here, in terms of formulas, the sequence of corrections used. For one thing, this outline presents a computerized method designed to reduce the large number of star places, including circumpolars, needed in geometric satellite triangulation. For another, such a presentation helps to clarify the contribution of the individual corrections to the overall adjustment procedure of satellite triangulation and helps the reader to judge the technical and economical aspects involved.

The following computations are for deriving, from the star catalogue data for a specific epoch, the unit vector (see fig. 7) that designates the apparent geocentric direction of a star with reference to the true equinox and at the instant T of observation. The solution shown here is based on the method currently in use at the U.S. Naval Observatory. The pair of lower indices to the right of the matrices designate respectively the equinox and the epoch to which the coordinates are referred. To begin with, the heliocentric unit vector $\mathbf{x}_{00}$, referred to the epoch and equinox of the catalog used, is computed with the catalog entries α and δ.

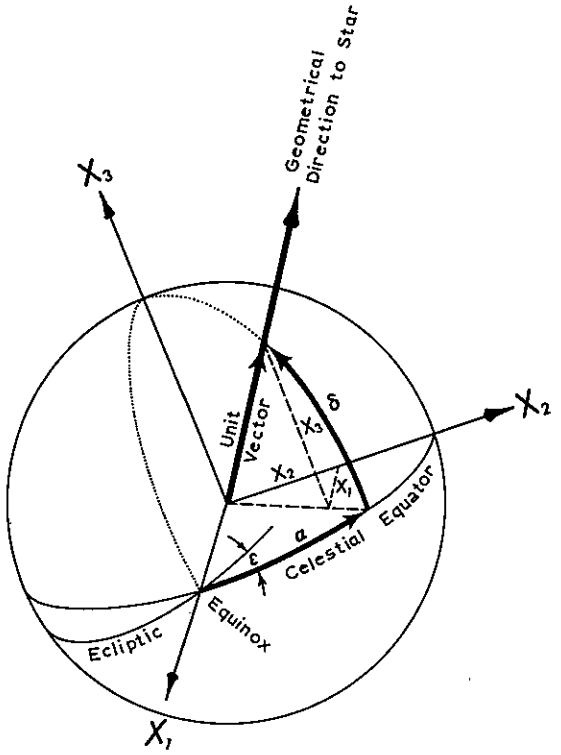

Figure 7.—Astronomic reference systems.

$$\mathbf{x}_{00} = \begin{bmatrix} x_1 \\ x_2 \\ x_3 \end{bmatrix}_{00} = \begin{bmatrix} \cos\delta\cos\alpha \\ \cos\delta\sin\alpha \\ \sin\delta \end{bmatrix}_{00} \tag{1}$$

Then the star coordinates are corrected for the star's proper motion. The corresponding μ_x correction vector is computed, using the proper motion components in right ascension μ_α and in declination μ_δ listed in the catalog, and by differentiating the vector (1), since $\mu_x = \frac{dx}{dt}$ by definition,

$$\mu_x = \begin{bmatrix} -\cos\delta\sin\alpha & -\sin\delta\cos\alpha \\ \cos\delta\cos\alpha & -\sin\delta\sin\alpha \\ 0 & \cos\delta \end{bmatrix}_{00} \begin{bmatrix} \mu_\alpha \\ \mu_\delta \end{bmatrix}_{00} \tag{2}$$

$$= \begin{bmatrix} -x_2 & -x_3x_1(1-x_3^2)^{-\frac{1}{2}} \\ x_1 & -x_3x_2(1-x_3^2)^{-\frac{1}{2}} \\ 0 & (1-x_3^2)^{\frac{1}{2}} \end{bmatrix}_{00} \begin{bmatrix} \mu_x \\ \mu_r \end{bmatrix}_{00}$$

with μ_α and μ_δ in radians.

A second differentiation yields the components of the secular variations. The corresponding vector $\dot{\mu}_x$ is then

$$\dot{\mu}_x = -\mu^2\mathbf{x}_{00}, \text{ where } \mu^2 = \mu^2_{x_1} + \mu^2_{x_2} + \mu^2_{x_3}. \tag{3}$$

In case the radial velocity of the stars is to be applied, (3) is augmented to

$$\dot{\mu}_x = -\mu^2\mathbf{x}_{00} - 0.000205\pi V\mu_x \tag{4}$$

in which π is the star's parallax in seconds of arc and V the radial velocity of the star in km/s. The second term in (4) is quite small and needs to be considered for only a few stars.

With (1), (2), and (3) or (4), the unit vector $\mathbf{x}_{0T}$ referred to epoch T and the catalog equinox is

$$\mathbf{x}_{0T} = \mathbf{x}_{00} + \begin{bmatrix} \mu_{x_1}\dot{\mu}_{x_1} \\ \mu_{x_2}\dot{\mu}_{x_2} \\ \mu_{x_3}\dot{\mu}_{x_3} \end{bmatrix} \begin{bmatrix} T \\ \frac{1}{2}T^2 \end{bmatrix} \tag{5}$$

Expression (5) is the Taylor-Maclaurin expression of vector $\mathbf{x}$ in time to a second order. The time interval T is in tropical years or centuries, depending on the interval for which μ_α and μ_δ are listed in the particular catalog used. T includes the fraction τ of the year in which the observation is made. Values for τ are taken from the volume of [20] in question. The result (5) can be transformed for convenience in programming to

$$\mathbf{x}_{0T} = \left(1 - \frac{\mu^2T^2}{2}\right)\mathbf{x}_{00} + (T - 0.0001025\pi VT)\mu_x \tag{6}$$

The next step rotates the vector $\mathbf{x}_{0T}$ from (5) or (6) in accordance with precession, so that the transformed rectangular coordinates are referred to the mean equinox for the beginning of the Besselian year T' nearest the date of observation. The transformation is

$$\mathbf{x}_{T'T} = \mathbf{R}(-\underset{3}{\zeta}, \underset{2}{\theta}, -\underset{3}{z})\mathbf{x}_{0T} \tag{7}$$

in which the rotation matrix has the following meaning:

$$\mathbf{R}(-\underset{3}{\zeta}, \underset{2}{\theta}, -\underset{3}{z}) = \mathbf{R}(-\underset{3}{z})\mathbf{R}(\underset{2}{\theta})\mathbf{R}(-\underset{3}{\zeta}) =$$

$$\begin{bmatrix} \cos z & -\sin z & 0 \\ \sin z & \cos z & 0 \\ 0 & 0 & 1 \end{bmatrix} \begin{bmatrix} \cos\theta & 0 & -\sin\theta \\ 0 & 1 & 0 \\ \sin\theta & 0 & \cos\theta \end{bmatrix} \tag{8}$$

$$\begin{bmatrix} \cos\zeta & -\sin\zeta & 0 \\ \sin\zeta & \cos\zeta & 0 \\ 0 & 0 & 1 \end{bmatrix}$$

The indices under the angles in the rotation matrices designate the axis around which the rotation takes place (for direction of rotation cf. 2.7.2.2). Using Newcomb's constants the rotation angles are

$$\begin{aligned} \zeta &= (2304''.250 + 1.396\,T_0)T + 0''.302\,T^2 + 0''.018\,T^3 \\ z &= \zeta + 0''.791\,T^2 \\ \theta &= (2004''.682 - 0''.853\,T_0)T - 0''.426\,T^2 - 0''.042\,T^3 \end{aligned} \tag{9}$$

The geometric meaning of the angles is given in [21]. T_0 (in tropical centuries) is the interval between 1900.0 and the epoch of the catalog used. T, also in tropical centuries, is the difference between the Besselian year T' nearest date of observation and the epoch of the catalog.

The vector of (7) is next corrected for annual aberration, for which daily values are listed in [20]. Since these tabulated values are computed from the true motion of the Earth with reference to the mean equinox at the beginning of the Besselian year nearest the date for which they are published, they can be applied directly to this vector. The annual aberration corrections must be interpolated with first and second differences to the date of observation. The resulting constants $-D$, C, and $C \tan \epsilon$ in radian measure may be regarded as displacements of the rectangular coordinates. Thus, the position vector of a star for the epoch T, referred to the mean equinox T' and including the aberration is

$$\mathbf{x}_{(T'T)} = \mathbf{x}_{T'T} + \begin{bmatrix} -D \\ +C \\ C \tan \epsilon \end{bmatrix} \tag{10}$$

with the mean inclination of the ecliptic,

$$\epsilon = 23^\circ 26' 44''.840 - 46''.850\, T - 0''.003\, T^2 + 0''.002\, T, \tag{11}$$

with T as above.

The transformation (7) accounts for precession up to the beginning of the Besselian year nearest the date of observation. An additional rotation is necessary to transform the position coordinates from the corresponding mean equinox to the true equinox at the time T of observation.

With allowable neglect of terms of second and higher order which do not contain the factor $\tan \delta$ one obtains

$$\mathbf{x}_{(TT)} = \mathbf{R}(B, A, -f)\,\mathbf{x}_{(T'T)} \tag{12}$$

where A, f and B are in radians and interpolated from [20] to second differences. The rotation matrix in (12) has the meaning

$$\mathbf{R}(B, A, -f) = \mathbf{R}(-f)\mathbf{R}(A)\mathbf{R}(B) =$$

$$\begin{bmatrix} \cos f & -\sin f & 0 \\ \sin f & \cos f & 0 \\ 0 & 0 & 1 \end{bmatrix} \begin{bmatrix} \cos A & 0 & -\sin A \\ 0 & 1 & 0 \\ \sin A & 0 & \cos A \end{bmatrix} \tag{13}$$

$$\begin{bmatrix} 1 & 0 & 0 \\ 0 & \cos B & \sin B \\ 0 & -\sin B & \cos B \end{bmatrix}$$

or with sufficient accuracy:

$$\mathbf{R}(B, A, -f) = \begin{bmatrix} 1 & -f & -(A + Bf) \\ f & 1 & (B - Af) \\ A & -B & 1 \end{bmatrix}. \tag{14}$$

The rectangular coordinates used up to this point are heliocentric and it is necessary to transform them to geocentric coordinates whenever the absolute parallax π appearing in the "General Catalogue of Trigonometric Stellar Parallaxes" [22] exceeds 0".010. This last correction is obtained with

$$\mathbf{x}_{TT} = \mathbf{x}_{(TT)} + \begin{bmatrix} -C \sec \epsilon \\ -D \cos \epsilon \\ -D \sin \epsilon \end{bmatrix} \frac{\pi}{k} \tag{15}$$

with C, D, and ϵ as in (10). The aberration constant $k = 20''.496$. The $\mathbf{x}_{TT}$ vector indicates the apparent geometric direction to a star for the observation epoch and the corresponding true equinox. The corresponding apparent right ascension and declination are obtained with the inversion of (1) from (15) as

$$\begin{aligned} \alpha &= \tan^{-1} x_2/x_1 \\ \delta &= \tan^{-1} x_3/(x_1^2 + x_2^2)^{\frac{1}{2}} \end{aligned} \tag{16}$$

For a computer program a convenient sequence of operations is obtained by combining the individual steps chosen in (6), (7), (10), (12), and (15). In connection with (1), (2), (3), (8), (9), (11), and (13) or (14), auxiliary computations are required using tabulated or, where necessary, interpolated values. The geocentric directions computed with the rectangular coordinates (15) or the orthogonal spherical coordinates (16) can be adopted without change as topocentric directions, since the stars are sufficiently remote, i.e., no additional parallax correction is needed. The situation is shown in figure 8a, where the basically geometric astronomic reference system $x_{1,2,3}$ is shown, in parallel displacement to an arbitrary point of the Earth's surface on a unit sphere surrounding this point.

The orientation of this assumed spatially stationary, astronomic system differs, therefore, from the orientation of a geocentric coordinate system $y_{1,2,3}$ that rotates with the Earth by an angle θ_{Gr} that corresponds to this rotation and is formed by the plane of the Earth-fixed null meridian of longitude ($\lambda' = 0$) and the plane of the astronomic null meridian ($\alpha = 0$). The geometrical meaning of the angle θ_{Gr} is apparent from figure 9. It is the sidereal time of the null meridian and is computed from universal time (mean Greenwich time) by converting mean to sidereal time, i.e., by multiplication with the ratio 366.2427/365.2427, or 1.00273791, and adding to θ_{0Gr}. The angle θ_{0Gr} is listed in [20] for 0^h UT of each day. The introduc-

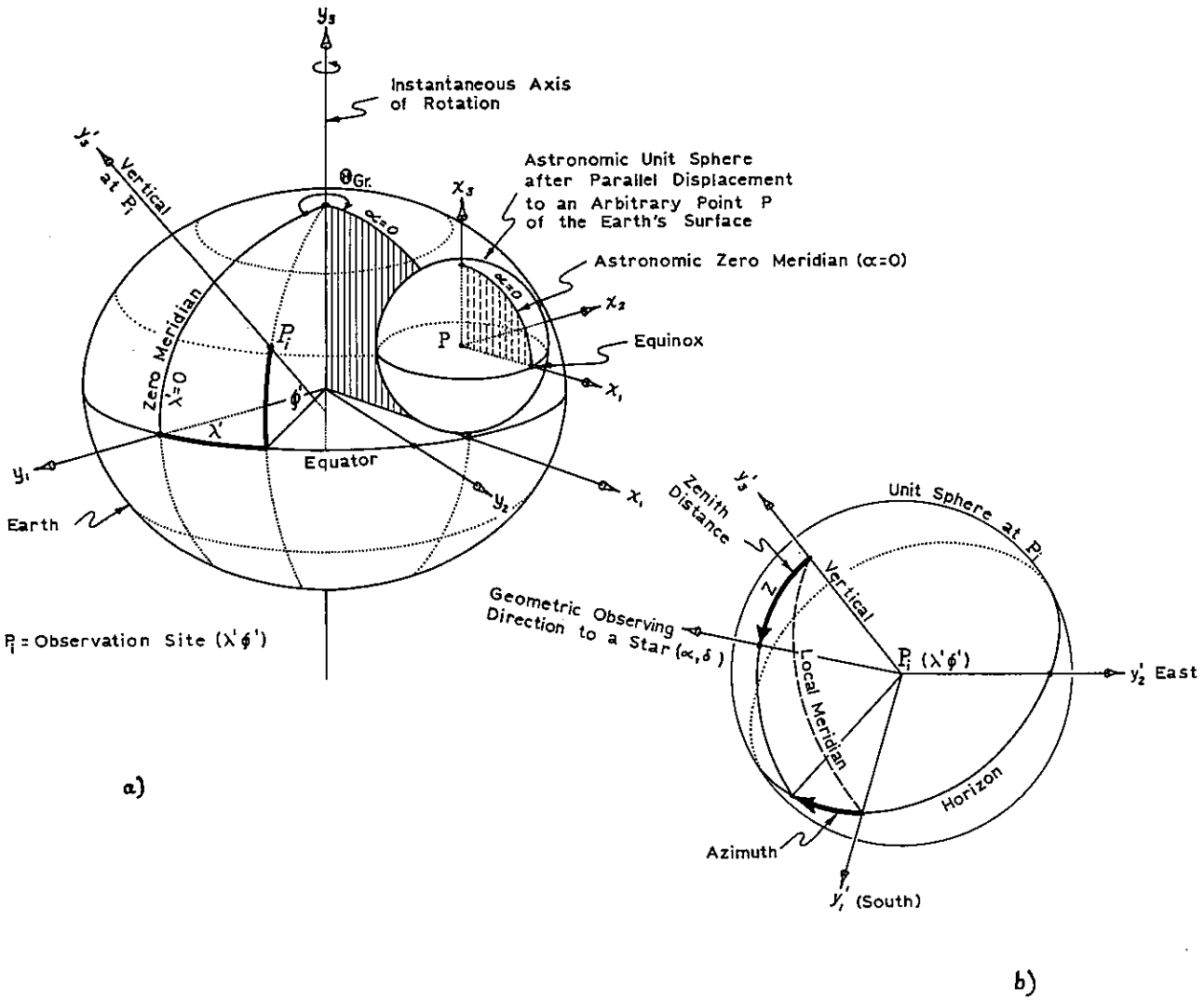

Figure 8.—Geocentric and topocentric coordinate systems.

tion of universal time for the instant of observation makes it necessary to raise certain questions in connection with the measurement of time. This train of thought is presented in sec. 2.4.

By studying the further steps in the reduction, it will become apparent that it is advantageous to change the space orientation of the astronomical reference system $x_{1,2,3}$ in a way to simplify the form of certain corrections.

The first is diurnal aberration. In consequence of the daily rotation of the Earth-fixed observation stations with respect to the right ascension-declination system, assumed stationary, we must, in addition to the annual aberration caused by the Earth's movement around the Sun, consider a so-called diurnal aberration. This is a function of the true position (φ', λ') of the observation site on the Earth and the angle θ_{Gr} (fig. 8a), as well as of the direction of observation, i.e., of the α and δ of the star. After turning the x system of figure 8a through the angle θ about the x_3 axis (cf. fig. 9) the resulting x_1' direction lies in the meridian plane of the observation site and x_2' points to the east, i.e., in the direction of the linear velocity vector $\mathbf{v}_{\varphi'}$ of the Earth's rotation.

Figure 10a shows a unit circle in the plane that contains the unit vector $\mathbf{x}_0'$ (direction to the star) and its x_2 component, and hence also the $\mathbf{v}_{\varphi'}$ vector.

From this the length of the aberration vector Δ is

$$|\Delta| = \frac{v_{\varphi'}}{c} \cos \gamma \qquad (17)$$

in which $v_{\varphi'}$ is the linear velocity of the Earth's rotation in latitude φ', and c is the velocity of light.

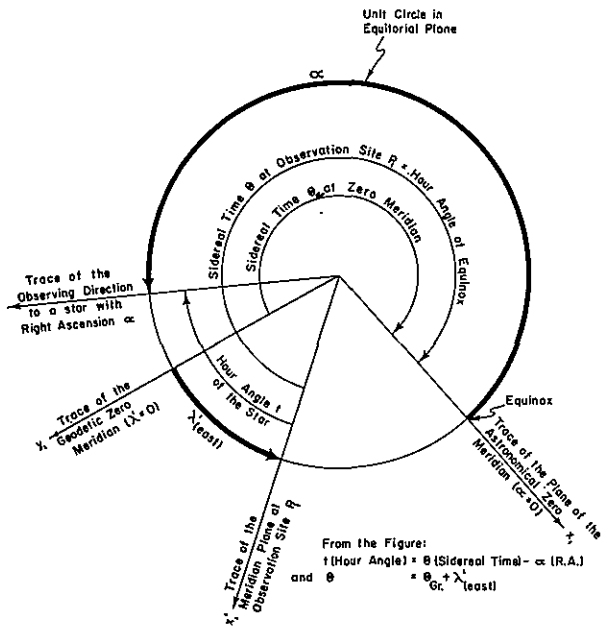

Figure 9.—Orientation of rotating astronomic system relative to assumed fixed system.

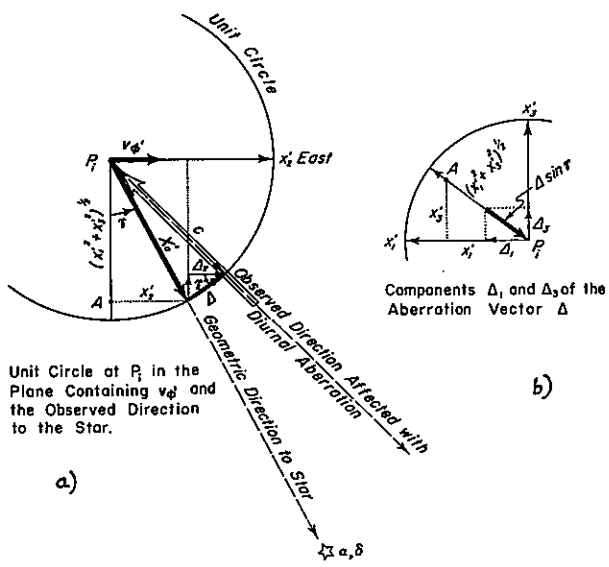

Figure 10.—Components of the aberration vector Δ.

The components of Δ in the $x'_{1,2,3}$ directions (cf. fig. 10a and b and eq. (73)), are

$$\Delta = \begin{bmatrix} -x'_1x'_2 \\ (1-x'^2_2) \\ -x'_3x'_2 \end{bmatrix} \cdot k' \tag{18}$$

with $k' = v_{\varphi'}/c$, or sufficiently close for the purpose

$$k' = 0''.319 \cos \varphi' \tag{19}$$

To compute (18) we must first rotate the x system to which the $\mathbf{x}_{TT}$ vector (15) is referred through the angle θ. This results in

$$\mathbf{x}'_{TT} = \underset{3}{\mathbf{R}}(\theta)\mathbf{x}_{TT} \tag{20}$$

where

$$\underset{3}{\mathbf{R}}(\theta) = \begin{bmatrix} \cos\theta & \sin\theta & 0 \\ -\sin\theta & \cos\theta & 0 \\ 0 & 0 & 1 \end{bmatrix} \tag{21}$$

The unit vector $\mathbf{x}'_{TT}$ corrected for diurnal aberration is, with (18) and (19)

$$\mathbf{x}'_{(TT)} = \mathbf{x}'_{TT} + \begin{bmatrix} -x'_1 \cdot x'_2 \\ (1 - x'^2_2) \\ -x'_3 \cdot x'_2 \end{bmatrix} \cdot k' \tag{22}$$

To account for astronomic refraction a further correction is necessary. Since astronomic refraction is most conveniently computed as a function of the geometric zenith distance z of the observed direction, the x'_{TT} system (20) is rotated through $(90° - \varphi')$ about its x'_2 axis into the local rectangular y' system (see fig. 8b). The resulting unit vector from (22) is

$$\mathbf{y}' = \underset{2}{\mathbf{R}}(90° - \varphi')\mathbf{x}'_{(TT)} \tag{23}$$

where

$$\underset{2}{\mathbf{R}}(90° - \varphi') = \begin{bmatrix} \sin\varphi' & 0 & -\cos\varphi' \\ 0 & 1 & 0 \\ \cos\varphi' & 0 & \sin\varphi' \end{bmatrix} \tag{24}$$

and, correspondingly, with (16) from (23) the azimuth A (positive from south through west) and zenith distance z are

$$\begin{aligned} A &= \tan^{-1}\frac{y'_2}{y'_1} \\ z &= \tan^{-1}\frac{(y'^2_1 + y'^2_2)^{\frac{1}{2}}}{y'_3} \end{aligned} \tag{25}$$

The astronomic refraction r_∞ is next computed on the basis of the mathematical model described in sec. 2.5, as a function of the weather data obtained during the observation (air temperature, pressure, relative humidity, etc.). The vector $\mathbf{y}'$ of (23) is corrected for this refraction, in accordance with (74) of sec. 2.7.2 (cf. also (42)) giving

$$\mathbf{y}_r' = \mathbf{y}' + \begin{bmatrix} -\cos\left(z - \frac{r_\infty}{2}\right)\cos A \\ \cos\left(z - \frac{r_\infty}{2}\right)\sin A \\ \sin\left(z - \frac{r_\infty}{2}\right) \end{bmatrix} 2\sin\frac{r_\infty}{2} \tag{26}$$

When r_∞ is small in a differential sense relative to the expected limit of accuracy, (26) simplifies in accordance with (73) to

$$\mathbf{y}_r' = \mathbf{y}' + \begin{bmatrix} -y_1'y_3' \\ -y_2'y_3' \\ (1 - y_3'^2) \end{bmatrix} r_\infty (1 - y_3'^2)^{-\frac{1}{2}} \qquad (27)$$

where r_∞ is in radians.
Corresponding spherical coordinates can be obtained from (26) or (27) with (25).

More suitable for further development of our problem are the rectangular coordinates ξ and η in the plane tangent at the zenith of the observer to a unit sphere, as shown in figure 24 of sec. 2.7.2. These coordinates are commonly designated standard coordinates in astronomy and are computed with the expressions on the left of (26) or (27) in accordance with (66) and (67) of sec. 2.7.2.1:

$$\begin{aligned} \xi_r &= y_1'/y_3' \\ \eta_r &= y_2'/y_3' \end{aligned} \qquad (28)$$

Hence (cf. (64) and (65) sec. 2.7.2.1)

$$\begin{aligned} A &= -\tan^{-1}\eta_r/\xi_r \\ z_r &= \tan^{-1}(\xi_r^2 + \eta_r^2)^{\frac{1}{2}} \end{aligned} \qquad (29)$$

The correction steps of the preceding paragraphs can again be combined in a sequence of steps convenient for programmed computation. From (20), (22), (23) and (26) or (27), results the direction vector $\mathbf{y}_r'$ in the local coordinate system as derived from the $\mathbf{x}_{TT}$ vector (15) in the astronomic x system. These directions represent a stationary oriented bundle of rays at the point of observation for the instant T (expressed in UT) of the observation. The rays forming this bundle pierce the tangent plane of the unit sphere at the zenith of the observing station in points whose locations are defined by their coordinates ξ_r, η_r. The ξ, η system corresponds in its orientation to the y' system. By obtaining the coordinates ξ_r, η_r, therefore, we have transformed the spherical coordinates, originally tabulated in a star catalogue for a specified epoch, into three-dimensional rectangular coordinates so that all the reference points lie in a plane tangent to the unit sphere. The coordinates assigned to these points with reference to the center of the sphere as origin and axes parallel to the directions $y_{1,2,3}'$ are therefore (ξ_r, η_r, + 1).

The images of the stars corresponding to these control points lie in the plane of the photographic plate on which their position is determined with reference to an arbitrarily oriented, plane, rectangular coordinate system (x, y) introduced into the plate plane (cf. fig. 29 in sec. 2.7.2.5). There remains the problem of establishing the projective correspondence between the two sets of points on the two planes, one set defined by coordinates (ξ_r, η_r), the other by corresponding image coordinates (x, y). This principal problem of the photogrammetric measuring technique is solved by the application of the principles of generalized central perspective. The mathematical model for this solution is described in detail in sec. 2.7.3. For the present, it is only necessary to accept the fact that this step establishes, either directly or indirectly, the orientation of the photogram with respect to the coordinate system in which the control points are given, in our case with reference to the local y' system. Likewise all the derived rays from this oriented bundle, such as the directions to the additionally photographed individual satellite positions (cf. sec. 2.7.5.1), are obtained in this coordinate system. Since in the subsequent triangulation (cf. sec. 2.7.5.2) all directions from the various stations must be referred to a common coordinate system, one can rotate the locally introduced coordinate systems to make their axes parallel to those of the common system chosen for the spatial triangulation *before* the photogrammetric reduction of the individual single cameras. This rotation can also be effected *after* the reduction of the single camera. The rotation matrices that determine the orientation of the photogrammetric exposure and refer to the local y' systems are transformed for this purpose so they refer with their elements of orientation to the common coordinate system chosen for the triangulation. Hence the next step in the computation is the transformation of either the local y' system established at the point of observation $P(\varphi', \lambda')$, or of the local orientation matrix $\mathbf{R}_y'(\alpha, \omega, \kappa)$ obtained in the photogrammetric reduction into a z-system selected for the subsequent triangulation (cf. sec. 2.7.2.6).

First the local y' system is transformed to the corresponding geocentric y system. The necessary rotations are through the angle $(270° + \varphi)$ about the 2 axis and then through the angle $(-\lambda_{east})$ about the turned 3 axis. This gives

$$\mathbf{y} = \mathbf{R}(-\lambda_{east}') \underset{3}{} \mathbf{R}(270° + \varphi') \underset{2}{} \mathbf{y}_r' =$$

$$\begin{bmatrix} \cos\lambda' & -\sin\lambda' & 0 \\ \sin\lambda' & \cos\lambda' & 0 \\ 0 & 0 & 1 \end{bmatrix} \begin{bmatrix} \sin\varphi' & 0 & \cos\varphi' \\ 0 & 1 & 0 \\ -\cos\varphi' & 0 & \sin\varphi' \end{bmatrix} \mathbf{y}_r' \qquad (30)$$

or analogously

$$\mathbf{R}_y(\alpha, \omega, \kappa) = \mathbf{R}(-\lambda_{east}') \underset{3}{} \mathbf{R}(270° + \varphi') \underset{2}{} \mathbf{R}_y'(\alpha, \omega, \kappa) \qquad (31)$$

where $\mathbf{R}_\gamma(\alpha, \omega, \kappa)$ corresponds in the γ system to the photogrammetric orientation matrix.

Basically the aim of the reductions so far discussed is to refer all the photographically registered directions to stars—observed from different stations and, in general, at different times—to a consistent stationary coordinate system. The computations would produce a rigorous geometric solution only if we could assume that the direction of the Earth's axis of rotation, i.e., the γ_3 direction of figure 8a, labeled instantaneous axis of rotation, remains invariant in space. We know, however, that the poles describe more or less irregular loops in a period of approximately 430 days about a mean position which may have a secular displacement. From a geometrical point of view it is immaterial whether this so-called polar motion is treated as an additional motion relative to the astronomic reference system (a sort of additional precession and nutation) or whether one accepts the direction of the rotation axis as invariant and ascribes the phenomenon to a displacement of the crust. However, in addition to this purely geometric and computable effect the influence of polar motion is coupled with the problem of time determination at the observation site. For this reason the discussion of these corrections will be combined with the questions of time determination in the next section.

2.4 Meaning and Measurement of Time

The significance of time determination for the problem of geometric satellite triangulation is twofold. First, because of the dynamic characteristics of the universe, i.e., the Earth's motion in space, we must determine the instant of the photographic exposure of the star image within the time sequence of the astronomic observations. In addition, because of the satellite's own motion, the instants of observation of the satellite at all stations observing the pass must be correlated with respect to an otherwise arbitrary measuring frequency, which amounts to a relative time determination.

With this, one interpolates points along the satellite track whose images, from a geometric standpoint, represent basically arbitrary but uniquely defined points on the orbit. In registering the pass of a satellite whose track is marked by short duration light flashes this requirement is not necessary. Because of the finite speed of light, not all the photons emitted in the flash will arrive at the different observation sites simultaneously, but, for that very reason, they will produce images whose positions on the various photograms correspond to a single point in space—the origin of the flash—and thus fulfill automatically the "geometric condition of simultaneity." In the following we will discuss, first of all and in more detail, those problems concerned with the impact on satellite triangulation of the time of observation needed for star imagery. We emphasize again that the requirement for time correlation in star observations is purely geometric in nature. This conclusion follows from the fact that the spatial position of the Earth and its observation stations changes with time relative to the astronomic reference system. The measurement of time, therefore, serves to refer the space orientation of the Earth at the instant of observation to an orientation assumed as a normal position and corresponding to an orientation at a specified epoch.

For the motion of the Earth around the Sun it is necessary to refer the Julian day and fraction of a day, as represented by UT for the instant of observation, to the beginning of the corresponding tropical year. The latter represents a point of time independent of all calendar reckoning and the same for all meridians (cf. [23]). The interval T so determined is needed for all the reductions described in sec. 2.3. The interval derived from the time of day serves as the basis for determining local sidereal time in accordance with the steps given in the previous section. There now arises in satellite triangulation the problem of the geometrical meaning of universal time.

The time of day is transmitted by radio signals from numerous stations distributed all over the world. Aside from the delays due to physical causes in the transmitters, receivers, and antennas, and variations in the propagation velocity of light caused by atmospheric influences, these time signals represent a sequence of precisely regular intervals. They are monitored by atomic clocks of great stability ($\pm 10^{-10}$ sec. over a period of months with daily variations $< 10^{-11}$ sec.).

In principle these transmitted signals do not represent a time referenced to Earth rotation but to a definite signal sequence. For most daily and public purposes, however, it can be considered directly as the "time of day." By means of star observations at a group of observatories linked in an international service, the relation between these time signals and time referenced to Earth rotation is established. In addition, this international working group is concerned with the determination of the instantaneous pole position. These figures are published in the form of preliminary and, later, definitive values. One set lists the position of the instantaneous pole with respect to a selected null position, while other tables give time corrections to

convert the transmitted signals to universal time 1 (UT-1) and universal time 2 (UT-2). The results from the various observatories—approximately 60 are participating at this time—are combined at the Bureau International de l'Heure (B.I.H.) into a "mean observatory" value. To some extent this eliminates statistically neglected influences such as refraction anomalies, secular pole motions, irregular changes in the Earth's rotation, and other factors. Likewise it smooths out the errors in the determination of time due to the systematic biases caused by the assumed nominal longitudes of the various observations and long term refraction influences. UT-2 in this system is with reference to a fictitious Earth that is practically independent of periodic, chiefly seasonal changes in the rate of the Earth's rotation.

UT-1 is characterized by the fact that it, like the original observation, contains the periodic, seasonal variations of the Earth's rotation and therefore represents a measure of the instantaneous amount of rotation. Hence it is a more suitable time for the present purpose, and a time interval so determined can be converted to the corresponding sidereal interval by multiplication with 1.00273791. Since 24 hours of sidereal time represents exactly 1 revolution of the Earth relative to the right ascension-declination system, the computed sidereal time is proportional to an angle of rotation (the geometric equivalent of the time coordinate) and represented in fig. 9 as sidereal time of the null meridian (cf. fig. 8a). By introducing two great circles to include this angle, one obtains a definition valid for all instantaneous positions of the pole. One great circle is the meridional trace of the plane containing the instantaneous axis and pole of the Earth's rotation, and the point of the celestial equator that represents the equinox of the observation period. The other great circle is the null meridian, which is the trace of a plane again containing the instantaneous axis of rotation, and an arbitrary, but uniquely defined point of the Earth's surface. This point, by international convention, has the coordinates longitude $\lambda_0 = 0$ and latitude $\varphi_0 = 0$ in the universally recognized geodetic system of latitudes and longitudes referenced to the mean position of the pole for the period 1900–05. Unfortunately this point lies in the Atlantic Ocean, so no direct observations are possible from it.

The ultimate refinements in time determination are not of decisive importance in the method of geometric satellite triangulation treated here since the accuracy required in timing the instant of star exposures is at most ±3 msec. UT-1 consequently furnishes geometric satellite triangulation with a time coordinate whose geometric equivalent, when transformed into a sidereal interval, is compatible with the coordinate transformation (20).

In the past, the above situation was complicated by the fact that universal times UT-1 and UT-2 were not referred to the C.I.O. (Conventional International Origin) pole of 1900–05 but, until 1958, were referred to the Cecchini pole and thereafter had as a reference a periodically displaced pole with a "secular" motion. Since for all these various positions of the pole the corresponding null meridian passed through Greenwich, its intersection with the conventional Equator was correspondingly displaced. As a consequence, for the period 1958 to Dec. 31, 1967, UT-1 can not be used as a rigorous measure for rotation.

After Jan. 1, 1968, the time pole is stationary and identical with the C.I.O. in accordance with a resolution of the International Astronomical Union (Lucerne 1967). It should be noted, however, that the classical null meridian of Greenwich must be replaced by either a correspondingly rotated geodetic meridian or by an equivalent discontinuity introduced into universal time on Jan. 1, 1968. After that date the situation is clarified; our basic considerations have validity and UT-1 can be accepted as a measure of Earth rotation. Under these assumptions, the y system obtained with (30) represents a reference system corresponding to an instantaneous position of the Earth to which the photogrammetric rotation matrix $\mathbf{R}_y(\alpha\omega\kappa)$ (computed with (31)) is referenced as well. From the above geometric considerations, it follows readily that for the eventual geometric normalization of the observation results, i.e., for the transformation of these data into the system chosen for the triangulation of the station coordinates, it is necessary to rotate the y system referenced to the observation period into the z system of the epoch selected for the spatial triangulation.

From figure 11 it is apparent that only two rotational components are needed. The y system must first be turned about its 2 axis through the angle $-a$ and then about its 1 axis through the angle $-b$. The obtained 3 axis will then define the direction of the rotation axis for the epoch chosen, while the intersection of the 1 axis with the sphere represents the origin of the system of time measurement adopted by international agreement, its meridian corresponding to the classical Greenwich meridian. From fig. 11 this transformation is

$$\mathbf{z} = \mathbf{R}(\underset{2}{-a}, \underset{1}{-b})\mathbf{y} \qquad (32)$$

with

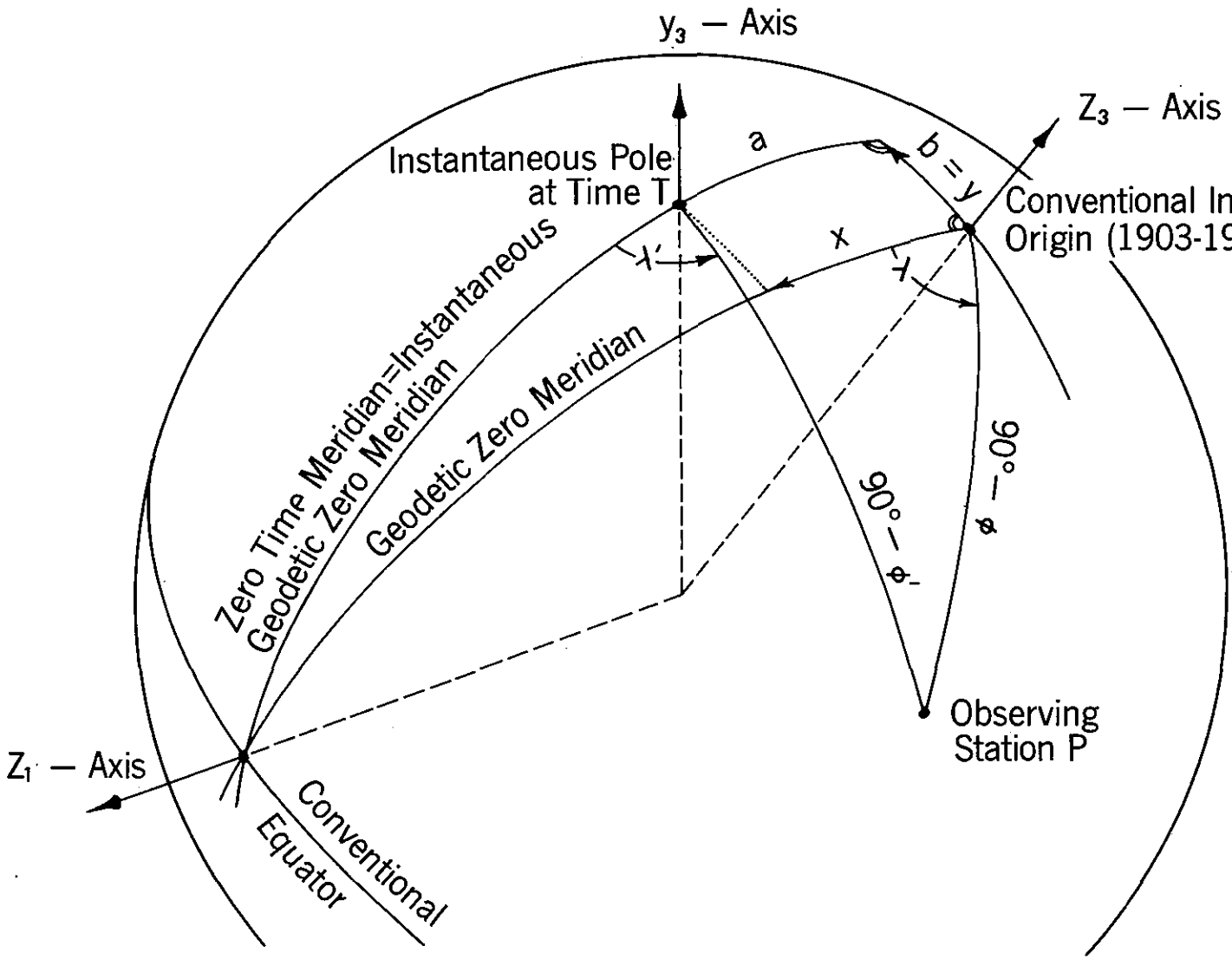

Figure 11.—Relations between the instantaneous pole and the Conventional International Origin.

$$\mathbf{R}(-a, -b) = \mathbf{R}(-b)\mathbf{R}(-a)$$

$$= \begin{bmatrix} 1 & 0 & 0 \\ 0 & \cos b & -\sin b \\ 0 & \sin b & \cos b \end{bmatrix} \begin{bmatrix} \cos a & 0 & \sin a \\ 0 & 1 & 0 \\ -\sin a & 0 & \cos a \end{bmatrix} \quad (33)$$

The rotation angles a and b are small and equal to the differential displacements x and y published by the B.I.H. to define the instantaneous pole with respect to the conventional origin. The rotation (33) becomes, therefore,

$$\mathbf{R}(-x, -y) = \begin{bmatrix} 1 & 0 & x \\ 0 & 1 & -y \\ -x & y & 1 \end{bmatrix} \quad (34)$$

The $\mathbf{R}_y$ matrix of (31) transforms into the corresponding photogrammetric rotation matrix

$$\mathbf{R}_z(\alpha, \omega, \kappa) = \mathbf{R}(-x, -y)\mathbf{R}_y(\alpha, \omega, \kappa). \quad (35)$$

When the satellite triangulation is adjusted within a local, rectangular coordinate system, which could be entirely practical within a given geodetic datum, the expression (35) must be further rotated. If, for example, the rectangular Cartesian coordinate system to be used in the final triangulation is to be erected at the point $P(\varphi, \lambda_{east}, h = 0)$ we will have, analogous to the preceding transformations,

$$\mathbf{z}' = \mathbf{R}(\lambda_{east}(90^\circ - \varphi))\mathbf{z} \quad (36)$$

with

$$\mathbf{R}(\lambda_{east}, (90^\circ - \varphi)) = \mathbf{R}(90^\circ - \varphi)\mathbf{R}(\lambda_{east}) =$$

$$\begin{bmatrix} \sin\varphi & 0 & -\cos\varphi \\ 0 & 1 & 0 \\ \cos\varphi & 0 & \sin\varphi \end{bmatrix} \begin{bmatrix} \cos\lambda & \sin\lambda & 0 \\ -\sin\lambda & \cos\lambda & 0 \\ 0 & 0 & 1 \end{bmatrix} \quad (37)$$

and similarly for the transformation of the photogrammetric orientation matrix

$$\mathbf{R}_z'(\alpha, \omega, \kappa) = \mathbf{R}(_{east}, (90^\circ - \varphi))\mathbf{R}_z(\alpha, \omega, \kappa). \quad (38)$$

2.5 Additional Geometric and Physical Influences

In sec. 2.4 all the coordinate transformations (based on the given star catalogue data) have been treated that are needed to reconstruct analytically the photogrammetric bundle of rays and to orient it in space. The analytical reconstruction is by means of those parameters that simulate interior orientation and distortion, while the exterior elements express the orientation in space of the bundle with respect to a uniquely defined, Earth-fixed coordinate system. To reproduce the oriented bundle, a mathematical model described in detail in sec. 2.7.3 and 2.7.4 is used. For the present, assume that this problem is solved and we pass on to an explanation of the corrections needed to derive, from the image coordinates of the satellite points and the parameters from bundle reconstruction, those directions needed later in the triangulation of the station coordinates. It is assumed further that the measured images of the satellite trail have been made to conform to the mapping principle of a rigorous central perspective by means of the parameters obtained in the bundle reconstruction. Then the direction in space corresponding to any point image computed with the corresponding elements of interior and exterior orientation will be tangent at the center of projection to the ray of light representing the physical light bundle. The center of projection here is the center of the unit sphere. The unit vector $\mathbf{y}'_{0r}$ in this direction is derived from the photogrammetric bundle vector $\mathbf{p}$ by use of (81), sec. 2.7.2. In sec. 2.3 it was explained that this direction refers to the same coordinate system as the photogrammetric rotation matrix in use. Hence by use of the $\mathbf{R}'_y(\alpha\omega\kappa)$ matrix mentioned there, one obtains the unit vector $\mathbf{y}'_{0r}$, corresponding to an arbitrary image where in accordance with (61)

$$\mathbf{y}'_{0r} = \begin{bmatrix} y'_1 \\ y'_2 \\ y'_3 \end{bmatrix}_r \equiv \mathbf{y}_r'. \quad (39)^3$$

This observed direction must first be corrected for refraction. The problem of refraction is shown schematically in figure 12 for both star and satellite images. Astronomical refraction r_∞ for zenith distances up to 85° can be computed to sufficient accuracy with, for example, Garfinkel's [24] formula:

$$r_\infty = \mathbf{T}^{\frac{1}{2}}W\left(\tau_1 \tan\frac{\beta}{2} + \tau_2 \tan^3\frac{\beta}{2} + \tau_3 \tan^5\frac{\beta}{2} + \tau_4 \tan^7\frac{\beta}{2}\right) \quad (40)$$

in which

$\mathbf{T} = T/T_0$, where $T_0 = 273.16\ K^0$
$W = P/T_0$, where $P = p/p_0$, and $p_0 = 760$ mm Hg.
$\tan\beta = (\mathbf{T}^{\frac{1}{2}}/\gamma)\tan z_r$, where $\gamma = 8.7137$ and
z_r = observed zenith distance.

If the coefficients τ_1 to τ_4 are with reference to geometric zenith distances, then an iteration loop

[3] The subscript "0" used to designate a unit vector, will be omitted in the following unless needed for better understanding.

must be provided for the computation of refraction from observed zenith distances.

Refraction for a satellite observation r_s is, according to [25],

$$r_s'' = r_\infty''\left(1 - \frac{a \cdot s}{d \cos z_r}\right) \tag{41}$$

where: $a = r + H$ = Earth radius + height above sea level of observing site,

$s = RT_0/r$, where $R = 29.2745$, the gas constant, hence

$s = 0.001255$, and

d = distance from satellite to station in meters.

The unit vector corrected for refraction is obtained from (39) using (25), (26) or (27), as

$$\mathbf{y}' = \mathbf{y}_r' - \begin{bmatrix} -\cos\left(z_r + \frac{r_s}{2}\right)\cos A \\ \cos\left(z_r + \frac{r_s}{2}\right)\sin A \\ \sin\left(z_r + \frac{r_s}{2}\right) \end{bmatrix} 2 \sin\frac{r_s}{2}, \tag{42}$$

or with (73) in sec 2.7, by

$$\mathbf{y}' = \mathbf{y}_r' + \begin{bmatrix} y_1'y_3' \\ y_2'y_3' \\ -(1-y_3'^2) \end{bmatrix} r_s (1 - y_3'^2)^{-\frac{1}{2}} \tag{43}$$

where r_s is in radians.

To compute the refraction r_s for the direction to the satellite in (41) the distance d between the station and satellite is needed. This quantity is also necessary for the computation of subsequent corrections. However, only a good approximation for the distance is needed and it will also be sufficient in computing $\mathbf{y}'$ from (42) or (43) to replace r_s with r_∞. With (79), (85) and (86) from sec. 2.7.2, the relevant coordinates of the images can be computed. In conjunction with the $\mathbf{R}(\alpha\omega\kappa)$ matrix from (35) or (38) and the approximated station coordinates, these coordinates can be used to make a preliminary triangulation of the satellite positions and to compute the distance d needed. For the adjustment procedure in practice see sec. 2.7.5.1.

A further correction is necessary to account for the fact that the satellite images are not, rigorously, common target points. The flashes emitted by the "active" satellites (e.g., ANNA, GEOS A, GEOS B) can be treated as uniquely defined target points in space. The present day "passive" geodetic satellites (ECHO I and II,[4] PAGEOS) are

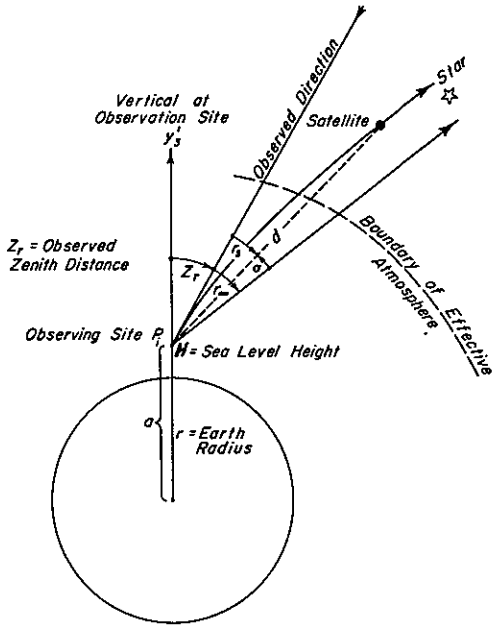

Figure 12.—Schematic of star and satellite refraction.

balloons that merely reflect sunlight, and must be sufficiently large to reflect an adequate amount of light. Those in use to date have a diameter of 30 m. The surface of the balloon reflects the image of the sun; the position of this image on the balloon sphere is a function of the geometric arrangement of the sun, the satellite, and the observing site at the instant of exposure. The necessary correction is analogous to an eccentric reduction in surveying. The correction varies not only for every station observing the target but also for each direction at a given station. The correction is to reduce each observed direction to the center of the balloon; this is called a phase correction because the position of the Sun's image depends on the illumination phase of the satellite. It is assumed that the satellite has the spherical shape it had when launched into orbit. Figure 13 shows schematically the geometry involved.

It can be assumed that the Sun is at a great enough distance so that the direction to the Sun, indicated by the unit vector **l** at the satellite, is the same at the point of observation. In accordance with Snell's reflection law, the points B (balloon center), center of the Sun, the image S of the Sun on the balloon, and the point of observation P_i all lie in one plane. so that the unit vectors **l, m, m***, **n** and the vector $B'B$ are coplanar.

From figure 13, it follows directly that

$$\mathbf{n} = \overline{BB}_l + BB_m \tag{44}$$

[4] Echo I terminated its orbit on May 23, 1968 and Echo II on June 7, 1969.

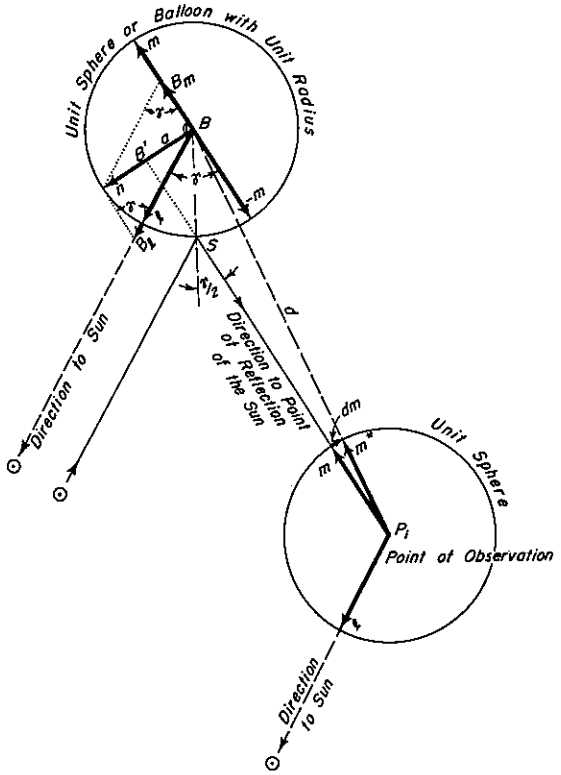

Figure 13.—The satellite phase correction.

or

$$\mathbf{n} = \frac{1}{\sin\gamma}(\mathbf{l} + \cos\gamma\,\mathbf{m}). \tag{45}$$

The scalar product of the unit vectors $\mathbf{l}$ and $-\mathbf{m}$ is

$$\cos\gamma = \mathbf{l} \cdot (-\mathbf{m}). \tag{46}$$

Again, from figure 13,

$$\overrightarrow{B'B} = -a\mathbf{n}. \tag{47}$$

The distance d between the observer and the satellite is large relative to the balloon radius, hence to a, so that to a sufficient degree of approximation

$$d\mathbf{m} = -\frac{a}{d}\,\mathbf{n}, \tag{48}$$

or with (45)

$$d\mathbf{m} = -\frac{a}{d\sin\gamma}(\mathbf{l} + \cos\gamma\mathbf{m}). \tag{49}$$

The displacement a from the center for a reflecting satellite with radius ζ is, from figure 13,

$$a = \zeta\sin\frac{\gamma}{2}. \tag{50}$$

For a balloon with a diffusively reflecting surface it can be argued that the centroid of the satellite image corresponds to the centroid of the illuminated portion of the balloon surface as seen from the observation site. In this case we have

$$a = \frac{\zeta}{2}(1 - \cos\gamma). \tag{51}$$

Finally, with (50) or (51),

$$\mathbf{m}^* = \mathbf{m} + d\mathbf{m}. \tag{52}$$

To compute (49) the unit vectors $\mathbf{l}$ and $\mathbf{m}$ are needed. Up to this point we have assumed only that they are referenced to an arbitrary but consistent coordinate system. Therefore, by (43) we set

$$\mathbf{m} = \mathbf{y}' \tag{53}$$

With the right ascension $\alpha_\odot$ and declination $\delta_\odot$ values of the Sun interpolated for the time of observations, the $\mathbf{x}_\odot$ vector is computed with (1), neglecting refraction and other corrections, and then the $\mathbf{x}'_\odot$ vector, using local sidereal time $\theta = 1.00273991\ (\text{UT-1}) + \lambda'_{\text{east}}$ and (20) and (21). Finally the $\mathbf{y}'_{\text{east}}$ vector is derived with (23) and (24). Then

$$\mathbf{y}'_\odot = \mathbf{l}. \tag{54}$$

Likewise, with (52), the unit vector $\mathbf{y}'$ in the direction of the balloon's center is

$$\mathbf{y}' = \mathbf{m}^*. \tag{55}$$

A detailed explanation of the phase correction is given in [26].

To interpret the direction of (55) correctly in a geometric sense, it is necessary to bear in mind that the satellite, serving as a target, as well as the station site, are subject to independent motions. The satellite in orbiting the Earth shares the motion of the Earth around the Sun, so that the annual aberration effect is canceled.

However, due to the Earth's rotation the linear velocity component of the observation stations creates a displacement of the observed directions corresponding to diurnal aberration. In addition the relative spatial relation between the satellite and observing station changes in the time required for the light to travel from satellite to station. This situation is shown schematically in figure 14 for the case of a flash emitted from the satellite.

The position of the observing station (φ', λ') and its Earth-fixed y' reference system (symbolized by the y_3 direction) is shown at the instant t of the

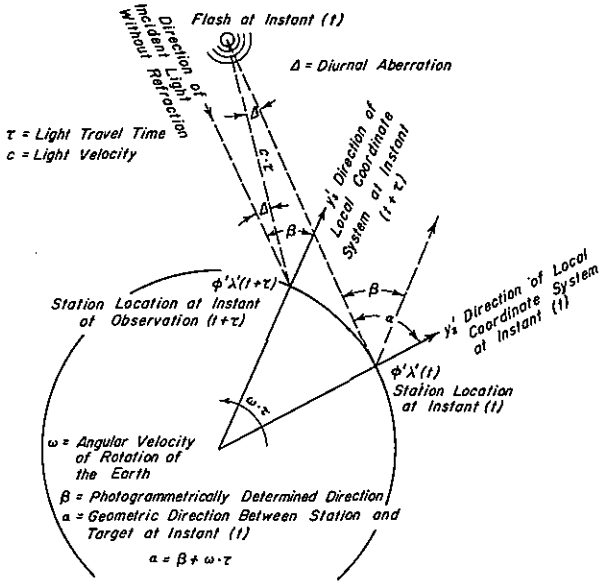

Figure 14.—Influence of diurnal aberration and Earth rotation when recording light flashes from satellite.

emission. Let the geometric direction at time t from the station to the flash be indicated by the direction angle α. Due to its finite propagation velocity c, the light requires an interval τ to reach the station by traversing the distance d

$$\tau = \frac{d}{c} \tag{56}$$

During the interval τ, however, the station has reached a position differing from the initial by the angle $\omega\tau$, where $\omega = 15''/s$ is the Earth's angular velocity. From the aberration theory (cf. [27]) it follows that the apparent direction of observation differs from the corresponding geometrical direction by the aberration angle Δ. This latter direction is parallel to the geometrical direction existing between station and satellite at the instant t. This statement is rigorous to the order to which the Earth's rotational velocity may be considered linear and constant. It follows that the flash is observed at the directional angle β relative to the local coordinate frame. The angle α needed in the subsequent treatment of the problem is therefore obtained from

$$\alpha = \beta + \omega\cdot\tau \tag{57}$$

The situation is complicated somewhat for the case in which satellite triangulation is carried out not with flashes but by means of a continuously illuminated satellite. The shutter mechanism of the observing camera permits the chopping of the satellite trail into a series of separate images. Thus the individual images are formed at times t_1, t_2, . . . t_n, to which appertain corresponding light travel durations τ_1, τ_2, . . . τ_n. The images corresponding to instants $t_1 + \tau_1$, $t_2 + \tau_2$, . . . $t_n + \tau_n$ must now be interpolated into the image sequence. Strictly speaking, according to figure 15 the interpolation should be for the instants $t_1 + \tau_1^*$, $t_2 + \tau_2^*$, . . . $t_n + \tau_n^*$, where

$$\tau_1^* = \tau_1 + \frac{\tau_2 - \tau_1}{t_2 - t_1}\tau_1, \text{ etc.}$$

The difference $\tau_i^* - \tau_i$ is, however, negligible. To effect the interpolation a time-related function of position is set up, expressing the photographic image sequence.

Figure 15 shows the relations existing between the recorded time, satellite position, and the observation station, the symbols used having the same meaning as in figure 14. The principle of interpolation is shown, in considerably simplified form, for only two observations occurring at instants t and $(t + \Delta t)$. As before, the needed direction angle α is obtained from the interpolated observed direction β by means of (57).

The direction α thus obtained reproduces the geometry between station and satellite existing at the instant t. From a similar treatment of the observations at other stations observing the same pass, directions to the satellite's position at the instant t can be computed. These, then, are geometrically coherent directions with which the eventual space triangulation of the observing stations will be carried out. The interpolation of fictitious satellite images referred to above also serves the purpose of taking into account the time differences between the station clocks at the various sites (cf. sec. 2.6). The time differences can be considered as shifts in the origins of the time bases at the several observation stations at the same time.

In order to execute the various reductions just described, it is necessary to derive the corresponding image coordinates $\bar{x}$, $\bar{y}$ with (85) and (86), referenced to the vector $\mathbf{y}'$ of (55). On the assumption that the exposure sequence has been carefully monitored (the practice with the BC–4 system is to within 50 μs.), the following polynomials can be set up as interpolation functions:

$$\begin{aligned}\bar{x} &= a_0 + a_1 t + a_2 t^2 + a_3 t^3 + a_4 t^4 + a_5 t^5 + \ldots \\ \bar{y} &= b_0 + b_1 t + b_2 t^2 + b_3 t^3 + b_4 t^4 + b_5 t^5 + \ldots\end{aligned} \tag{58}$$

The coefficients a_0, a_1, . . . a_n and b_0, b_1, . . . b_n are obtained from an adjustment (cf. 2.7.5.1). The degree assumed for the polynomial depends chiefly on the length of the recorded satellite trail,

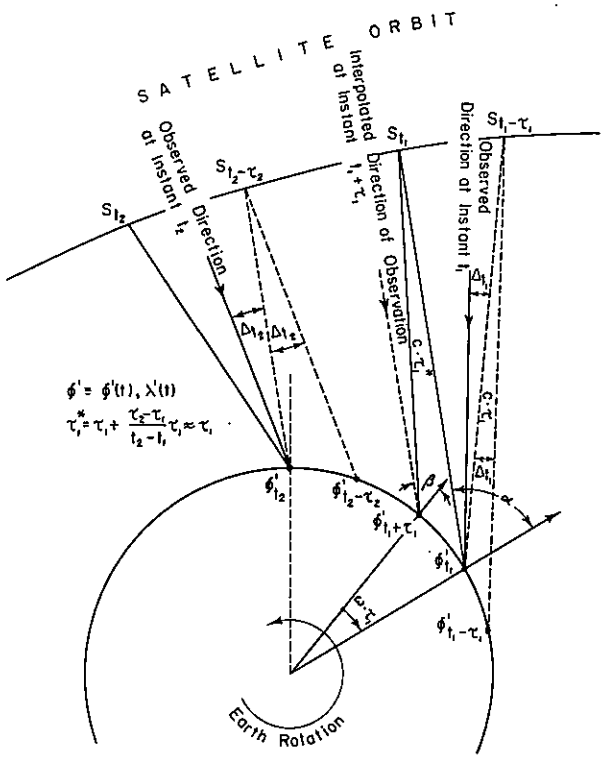

Figure 15.—Influence of diurnal aberration and Earth rotation on light reflected from continuously illuminated satellite.

i.e., more or less on the aperture of the camera used. With the BC–4 system a polynomial of the 5th degree, at least for the component in the direction of the trail, is necessary (cf. sec. 2.1). Several hundred satellite images are used to compute the polynomial. The adjustment effects a smoothing which is of decisive importance for the accuracy of satellite triangulation, since it eliminates the influence of scintillation. Regardless of its amplitude which, depending on local meteorological conditions, can attain several seconds of arc, scintillation is always characterized by a nearly ideal normal distribution and hence can be eliminated almost completely with a Gaussian adjustment, provided a sufficiently large number of satellite images are available. This condition is not met with the use of present-day light flashes.

The polynomials (58) are now used to interpolate fictitious satellite images. Image coordinates $\bar{x}$, $\bar{y}$ are computed for the instant (in station time) that corresponds to the satellite position at time T. Since, as indicated above, the times assigned to the various observing stations are not necessarily referenced to the same null point, the local $t_i + \tau_i$ values must be reduced to a consistent clock time by the addition of ΔT_i (represented schematically in figure 16).

To repeat, the station times $t_i + \tau_i$, $t_j + \tau_j$, $t_k + \tau_k$, etc., used for interpolation at station i, j, k, . . . do not represent the same instant T at the clock, but fix image coordinates which are geometrically consistent, i.e., they satisfy the "geometric condition of simultaneity" mentioned in sec. 2.4.

With the image coordinates $\bar{x}$, $\bar{y}$ thus obtained, the corresponding $\mathbf{y}'$ vector is recomputed from the corresponding bundle vector $\mathbf{p}$ of (81). The last correction modifies the orientation of this vector to account for the Earth's rotation during the light travel time τ. Theoretically, this is accomplished by rotating the local y' system about its 2 axis through an angle $-(90° - \varphi')$, which brings the 3 axis into coincidence with the Earth's rotation axis. Next, the system is rotated about this latter axis through the angle $-\omega\tau$. This cancels the effect of the Earth's rotation. Finally, the twice rotated 2 axis is turned through the angle $(90 - \varphi)$, resulting in a system with the unit vector $\mathbf{y}_s$. The necessary computations are therefore:

$$\mathbf{y}'_s = \mathbf{R}(90° - \varphi')\mathbf{R}(-\omega\tau)\mathbf{R}(90° - \varphi')\mathbf{y}' =$$

$$\begin{bmatrix} \sin\varphi' & 0 & -\cos\varphi' \\ 0 & 1 & 0 \\ \cos\varphi' & 0 & \sin\varphi' \end{bmatrix} \begin{bmatrix} \cos\omega\tau & -\sin\omega\tau & 0 \\ \sin\omega\tau & \cos\omega\tau & 0 \\ 0 & 0 & 1 \end{bmatrix}$$

$$\begin{bmatrix} \sin\varphi' & 0 & \cos\varphi' \\ 0 & 1 & 0 \\ -\cos\varphi' & 0 & \sin\varphi' \end{bmatrix} \mathbf{y}'. \qquad (59)$$

Since $\omega\tau$ is small, (59) simplifies to

$$\mathbf{y}'_s = \mathbf{y}' + \begin{bmatrix} -y'_2 \sin\varphi' \\ y'_1 \sin\varphi' + y'_3 \cos\varphi' \\ -y'_2 \cos\varphi' \end{bmatrix} \cdot \omega\tau. \qquad (60)$$

The transformation of the direction of the unit vector $\mathbf{y}'_s$ into the chosen z or z' system can now be effected in accordance with (30) and (32) or (36), as the case may be. This completes the discussion of all the steps needed in preparation for the satellite triangulation proper. The next section describes the observation technique, since familiarity with the field operations contributes to an understanding of the geometry of satellite triangulation. Then, in sec 2.7, the mathematical formulation of geometric satellite triangulation is presented as a whole, with back references to the results derived in 2.3, 4, and 5.

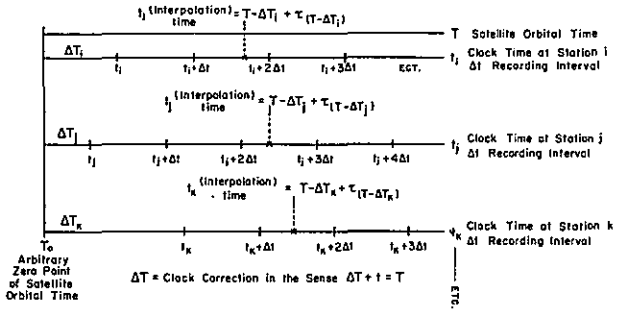

Figure 16.—Principle of time interpolation for the "geometric condition of simultaneity."

2.6 Measuring Procedures of the Geometric Method

2.6.1 Photogrammetric Camera

The techniques used in the measurement of rocket trajectories, particularly because of their high accuracy requirements, had an early influence on the development of photogrammetric data acquisition and evaluation instrumentation. Characteristic in this field of application is the necessity to combine a great number of observations in a single photogram in which, in turn, each individual observation is generally registered very accurately against a time or frequency standard. Consequently there is a requirement on the photogrammetric instrumentation for great stability over extended periods of observation. This requirement led to the development of the so-called ballistic camera which, on the whole, is based on the phototheodolite of terrestrial photogrammetry. In order to adapt the instruments to the unorthodox requirements of the geometry encountered in tracking rocket trajectories and at the same time increase the accuracy of the direction determination, cameras were developed that could be oriented arbitrarily and whose objectives had long focal lengths. A corresponding decrease in viewing angle is inevitable because of practical limitations on the size of the plate. Exact elements of exterior orientation are obtained with the use of elements from the classical, geodetic angle measuring instruments such as precision spindles, circles, and hyper-sensitive levels.

The development of instrumentation reflecting these concepts reached a high point in the 1940s with the Askania phototheodolite [28]. This camera had a 370-mm focal length, f/5.5, 13 × 18-cm plate format and a synchronous drive for the rotary shutters, producing 1.5, 3, 6, and 12 exposures per second with a synchronization accuracy of 10^{-3} s. In addition, a louvered shutter was available to block out certain exposures in the sequence or to generate time-related star trails. The horizontal and vertical circles could be set to within 3^{cc}.

These instruments were used in Peenemünde for measuring the V–2 trajectory up to the point of engine cutoff. On the resumption of similar projects in the USA after 1945, interest in photogrammetric precision metrology faded because of, as it turned out, too optimistic expectations from electronic approaches to the problem of trajectory measurements. When it became apparent that neither these electronic approaches nor the capability of the cinetheodolite could do justice to the developing rocket technique, the author had the opportunity, in connection with his duties at the Ballistic Research Laboratories of the Aberdeen Proving Ground, Md., to initiate plans for improved precision theodolites. With the active and sympathetic cooperation of the Swiss firm Wild-Heerbrugg, this resulted in today's well-known BC–4 phototheodolite system. At the time, the experience gained in the various fields of experimentation created a demand for the development of a series of cameras with different angles of view, to be used interchangeably on the same mount. In addition to the necessary variation in picture sequence over a wide range, the requirement for maximum accuracy in exposure synchronization was considered of utmost importance. The development of the complete system covered a period of 10 years. The general concept is described in [29] and technical details of the BC–4 phototheodolite are explained in [30].

In the early sixties the idea of applying the photogrammetric technique for geometric satellite triangulation to the establishment of a continental net began to be seriously considered [31]. The technical requirements for such a project differ from those of conventional trajectory mensuration, first, in that the exterior orientation of the camera is not determined with graduated circles, but from the photogram itself on the basis of the photographed control points (star images). Secondly, the requirement for unusually high accuracy demands that the parameters needed for the reconstruction of the photogrammetric bundle (the generalized model of interior orientation) be recomputed for each individual plate. This makes it necessary to effect a compromise between focal length (increase of intrinsic accuracy) and a field of view sufficiently large to enable the observer to record a sufficient number of available catalogued stars in any portion of the sky. Absolute synchronization between the widely separated stations is complicated, actually impossible in theory, in view of the unknown light travel time at the instant of observation. Hence, in satellite triangulation it is merely

necessary to record the instants of satellite observation very accurately (to at least 10^{-4} sec) against the frequency standard at each station. However, the station clocks (frequency standards) must be calibrated with respect to a basically arbitrary, but uniquely defined time sequence. Synchronization of the clocks to within about 10^{-5} sec is attained by periodic comparison at all stations with a traveling calibration clock, which in turn is compared at regular intervals with an atomic standard (e.g., the U.S. Naval Observatory). Stations with limited accessibility are additionally equipped with a cesium standard. The transmission, via satellites, of time signals for clock comparisons has proved quite satisfactory, with accuracies of from ± 2 to ± 10 μsec, depending on the electronic equipment available at the receiving station. These procedures ensure the elimination of the error source due to uncertainties in the propagation of light, and reduce all other timing errors below the overall error level of the system. All other residual errors can therefore be neglected in the adjustment.

Reference [32] contains a description of the BC–4 installation as modified to the specifications of the U.S. Coast and Geodetic Survey from the original missile trajectory instrumentation. The present BC–4 phototheodolite differs from the installation described there mainly in the optic now in use, a special objective designed by Dr. Bertele and constructed by the Wild-Heerbrugg Co. which, taking all theoretical and practical considerations into account, represents an optimal solution for satellite triangulation. The Cosmotar objective lens has a focal length of 450 mm with a relative opening of 1:3.4, its chief advantage lying in the fact that it has minimal change of radial distortion within the visible spectrum. This practically eliminates differences in radial distortion for the centroids of images of stars of various colors and of the Sun's image reflected from the satellite. Figure 17 shows a camera with the Cosmotar objective and the Henson capping shutter mentioned in the next section. Figure 18 is a picture of a typical BC–4 installation. A satellite observing instrument with tracking capability, developed in recent years by the firm of Carl Zeiss-Oberkochen, is illustrated in figure 19.

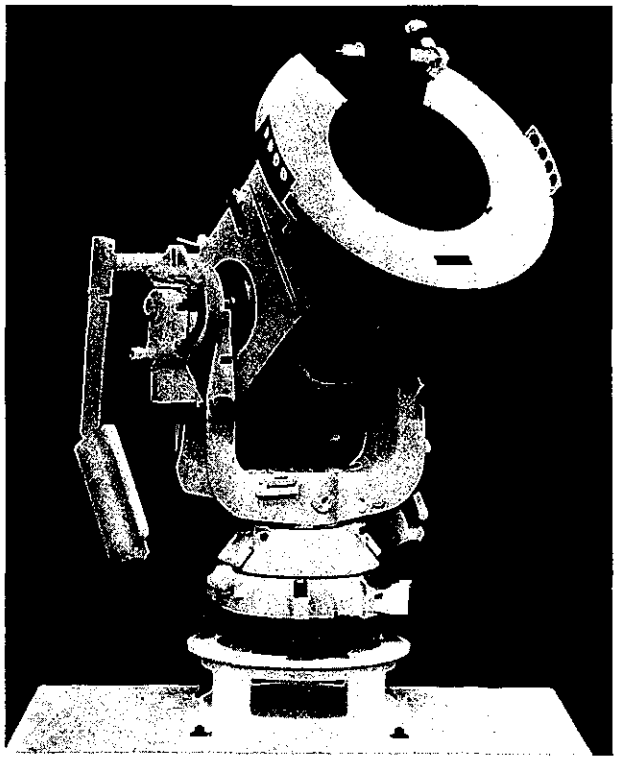

Figure 17.—Wild BC–4 camera with external Henson shutter assembly.

2.6.2 Camera Shutters and Their Mechanical Drives

When continuously illuminated satellites are used for triangulation, the tracks of the stars and of the satellites on the photogram must be chopped into a sequence of individual time-related images. The star trails are the result of the Earth's rotation, shared by the Earth-fixed camera, while the track of the satellite is largely due to its own motion although the Earth rotation during the satellite pass contributes a component to the track. The track interruptions on the plate are effected in the BC–4 camera by three rotating disk shutters inserted between the lens elements, approximately in the principal plane of the lens system. Two of the disks rotate at equal rates in opposite directions to achieve maximum symmetry in the exposure and a high degree of efficiency (about 70%) of the shutter. The third disk subdivides the primary image sequence generated by the rotation velocity of the first two disks which, in addition, fixes the exposure interval of the individual images. The most useful combinations of primary image sequence or exposure interval and actual exposure sequence in satellite triangulation, within the technical limitations of the BC–4, are shown in table 2.

This shutter is activated by a synchronous motor specially developed for a frequency of 500 Hz. Registration of the image centroid is initiated by an adjustable, magnetic pick-up. Further technical details of the shutter drive developed and manu-

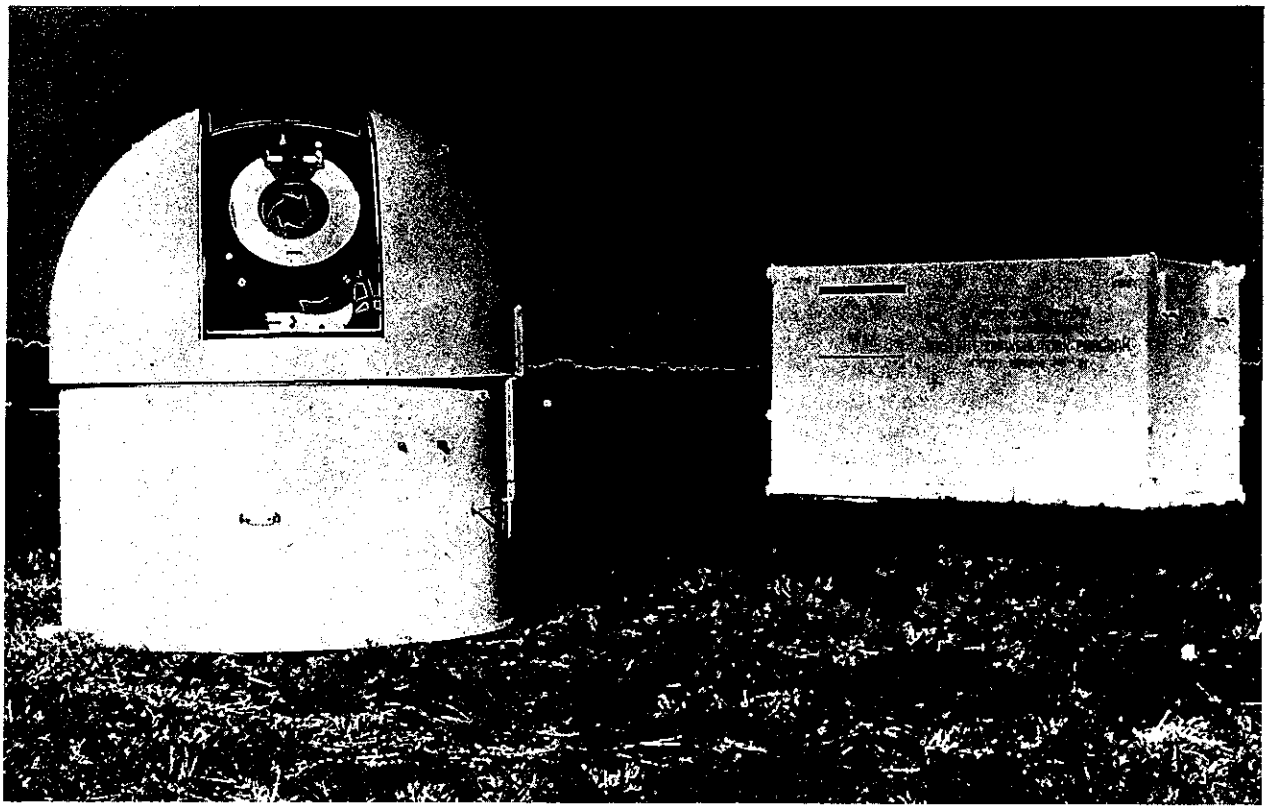

Figure 18.—Typical setup on observation site with camera shelter and recording equipment shelter.

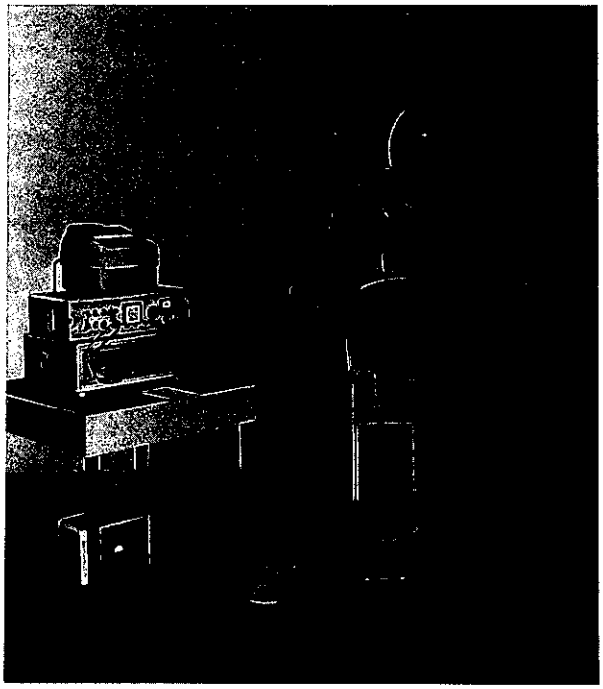

Figure 19.—Zeiss satellite tracking camera with recording unit.

factured by Fred C. Henson Co., Pasadena, Calif., are published in [33]; the shutter mechanism itself is pictured in figure 20.

Corresponding to the combination selected from table 2, the rotating disk shutter generates a chronologically regular sequence of images. In order to create arbitrary groupings in this sequence for the purpose of identification, or to further subdivide this primary image sequence, an additional iris type shutter is installed in front of the exchangeable filter element of the BC–4, also

TABLE 2.—*Most useful combinations of primary image sequence, exposure interval, and actual exposure sequence*

Images per sec	Exposure interval (100% efficiency) (sec)	Optimal subdivision with third shutter	Accuracy of timing (10^{-6} sec)
20	1/20	:2, :3, :4, :5	±20
10	1/60		±40
5	1/30		±60
2.5	1/15		±70

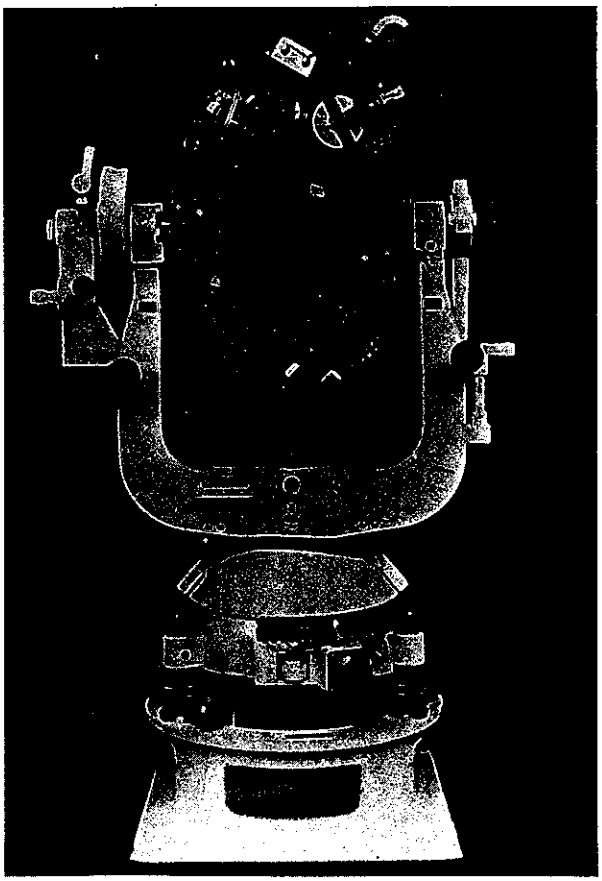

Figure 20.—Henson capping shutter assembly (cover removed).

made by the Henson Co. and known in the trade as a capping shutter. This is activated through solenoids and makes it possible to open or close the shutter in between two successive exposures generated by the rotating shutters. Technical details of the shutter operation are given in [33].

Although it would be desirable from the photogrammetric standpoint to register the stars, as well as the satellite, by means of a shutter located in the principal plane of the lens system, i.e., by means of, say, the rotating disks, a compromise is imposed by the limitations of the f-stop. While it is possible, even necessary, (cf. sec. 2.7.4) to record stars during the period of the satellite's passage, only low magnitude stars will register adequately, and their number is insufficient for the adjustment. It is necessary, therefore, to expose stars with the aid of the capping shutter before and after the activation of the disk shutters, that is, before and after the satellite exposure proper. In order to obtain the correct time correlation for these images, signals for the opening and closing of this shutter are generated with the aid of adjustable contacts, so that the mean of the corresponding two instants of time is associated with the midpoint of the segment of the so created star trail, which is of finite length even for relatively short intervals of exposure.

2.6.3 Electronic Control Instrumentation

The electronic console controls the following principal functions:

a. Drives the 500-Hz synchronous motor of the rotary disk shutter from the built-in station frequency standard,

b. controls the station clock with the same frequency standard,

c. synchronizes the signal from the magnetic pickup of the rotating disk shutter with the station clock,

d. programs remote control of both shutter systems,

e. illuminates the fiducial marks and the auxiliary data for later identification and evaluation,

f. drives the nine-channel registration equipment which records the course of the observation program and

g. compares the station clock with an external time standard or signal and monitors the accuracy of the rate of the station's frequency standard by means of a received calibration frequency (VLF).

In order to synchronize the rotating disk shutter with the station clock the exposure sequence for a satellite pass is set mechanically by a suitable selection of gear ratio in the camera control (see table 2), with a similar electronic program in the synchronization system. This results in a display on the oscilloscope of a pulse sequence for the time code generator corresponding to the selected program (for example two exposures per second). Simultaneously, the pulses from the magnetic pickup, indicating the mid-open position of the shutters, are fed to the oscillograph. By a phase comparison the two signals, which are initially different in time, are brought into coincidence, effecting synchronization between station clock and exposure. Due to practical limitations in the mechanical precision of the drive there are slight irregularities in the shutter rates, causing the signal returning from the cameras to vary irregularly in time with the comparison signal originating in the station clock. These deviations vary from about ± 20 to ± 40 μs. The actual synchronization process is therefore to give the signal from the station clock an adjustable bandwidth to each side of, for example, 100 μs. If the signal from the BC–4 falls within this gate it is registered as synchronous on the Brush tape, otherwise not (cf. 2.6.3f). The rate of the frequency standard is

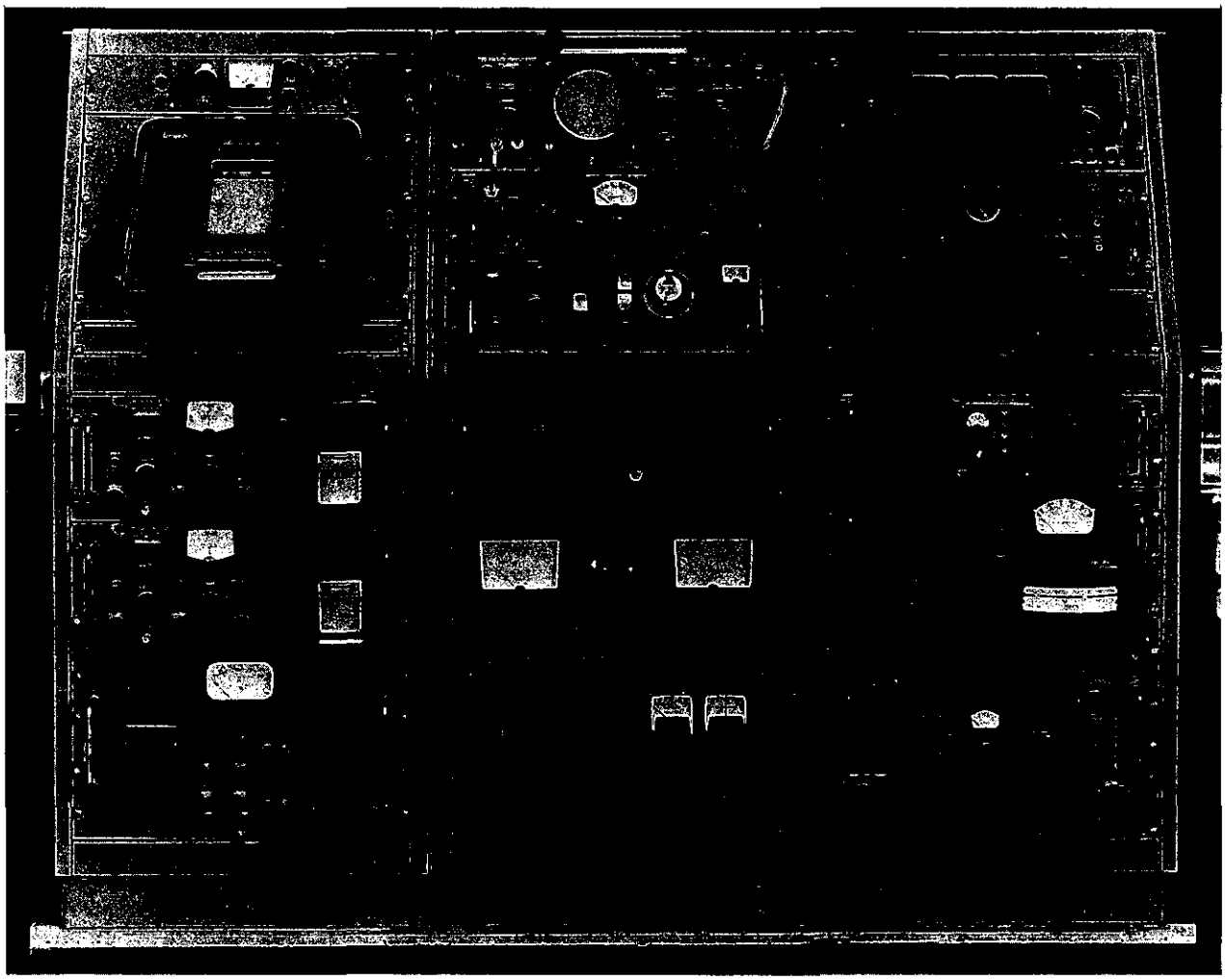

Figure 21.—(a) BC–4 electronics control console, and (b) schematic.

WWV LORAN C RECEIVER	OSCILLOSCOPE	TIME CODE GENERATOR
CHART RECORDER	CAMERA SYNCHRONIZER	PROGRAMMER
	CAMERA CONTROL	(BLANK)
VLF RECEIVER	PAPER TAPE READER	OSCILLATOR
VLF RECEIVER	24 VOLT POWER SUPPLY	500 HERTZ AMPLIFIER
VOLTAGE REGULATOR	BATTERY BACK-UP	POWER CONTROL
	(BLANK)	AUXILIARY PANEL

Figure 21.—(b) BC–4 electronics console schematic.

monitored with a received frequency (VLF), and absolute time is assigned as described at the end of par. 2.6.1.

When the auxiliary capping shutter is in operation for star exposure, with the rotating disk shutters at rest, its opening and closing is recorded on the Brush tape together with the station clock signals. This determines time for the star exposures. A control console built by the Electronics Engineering Co. of California, which at this time is part of all the BC–4 systems, is shown in figures 21a and b.

2.6.4 Photogrammetric Registration

The format of the BC–4 plates is 18 × 18 cm. They are either 6 or 10 mm thick and those of best quality have a flatness of 3 μm. A good compro-

mise between sensitivity and grain size is found in the Eastman-Kodak emulsion 103-F. After accurately controlled developing of the plate particular care must be exercised in the drying process, turning the plate continuously. The essential information content of an individual photogram consists of the point-shaped star images and the satellite trail. For star registration a sequence of five successive individual images is necessary, for statistical reasons. To obtain uniform star images independent of star magnitude, it is necessary to expose several such sequences with various shutter speeds. In addition, the selection of optimal exposure time is dependent on the range in declination of the stars. Star photography, using the capping shutter, is executed before and after the satellite's pass. During the satellite pass additional images of the brighter stars in the field of view are generated by programming the rotating disk shutters. These star images are of particular importance for the exterior orientation since they are recorded simultaneously with the satellite trail. With suitable choice of exposure interval it is possible to obtain a presentation of both stars and the satellite in a series of similar, point-shaped images.

In measuring the negative itself one is presented with the problem of centering a black measuring mark within a dark, point-shaped image.[5] A series of experiments has shown that the plate measurement process is faster and more reliable if a diapositive is first produced, so that the black measuring mark can be set within a white, round image.

The negatives are copied in almost monochromatic blue light under vacuum onto a 6-mm thick glass plate covered with an exceedingly fine-grained emulsion. Statistical tests have shown that the copying process introduces no marked deterioration in accuracy. Figure 22 shows the star and satellite images schematically. The sequences A, B, C, and D, E, F, represent 5 star images, each taken with the capping shutter and various shutter speeds, before and after the satellite pass, the upper star trails representing a brighter star. The sequences a, b, c symbolize images of the satellite and of stars recorded simultaneously by means of the rotating disk shutter. Because of the limited resolution of the objective and emulsion, the three satellite images designated b correspond to only a single, approximately point-shaped star image b, whereas the star imagery corresponding to the satellite exposure intervals a and c appear as star trails, unresolved into individual images. Stars that

[5] To date, ring-shaped measuring marks with a diameter of 20 to 30 μm are not available.

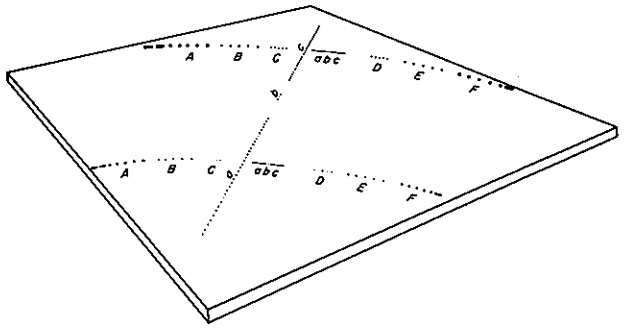

Figure 22.—Schematic of the star and satellite images.

are insufficiently bright produce no measureable image b and those of higher magnitude are not recorded at all through the rotating disk shutter. Figure 23 is a magnified portion of a plate showing trails of the balloon satellites Echo I and II generated by the rotating disk shutter.

2.6.5 Coordinate Measurements on the Comparator and Their Reduction

Measurement of the photograms, either of the original negative or of a diapositive copy, produces rectangular coordinates with an arbitrary origin in the plane of the plate. The comparator used does not necessarily have to operate on this principle but can, for example, measure polar coordinates instead [34]. These must, however, be transformed to the x, y coordinates needed later in the adjustment and the corresponding weight matrix, correlated in this case, must be computed.

The measurement of photograms is one of the most essential phases of analytical photogrammetry and has been discussed in detail in the literature. Furthermore, the specific measuring method used depends not only on the type of comparator used by also on the organizational and environmental conditions. Accordingly, only those phases will be discussed that are typical for the problem in question.

If a high degree of accuracy in the end results of geometric satellite triangulation is to be achieved it is necessary to bear in mind from the outset the fact that a large number of points (600 to 750 star and up to 600 satellite images) must be measured on each photogram, requiring 5 to 8 hours for the measurement. Special care must therefore be exercised in the selection of the type of comparator, the environmental conditions, and the arrangement of working procedures, so that systematic error influences can be held to a minimum or can be corrected computationally. A description of the current procedures at the National Ocean Survey follows.

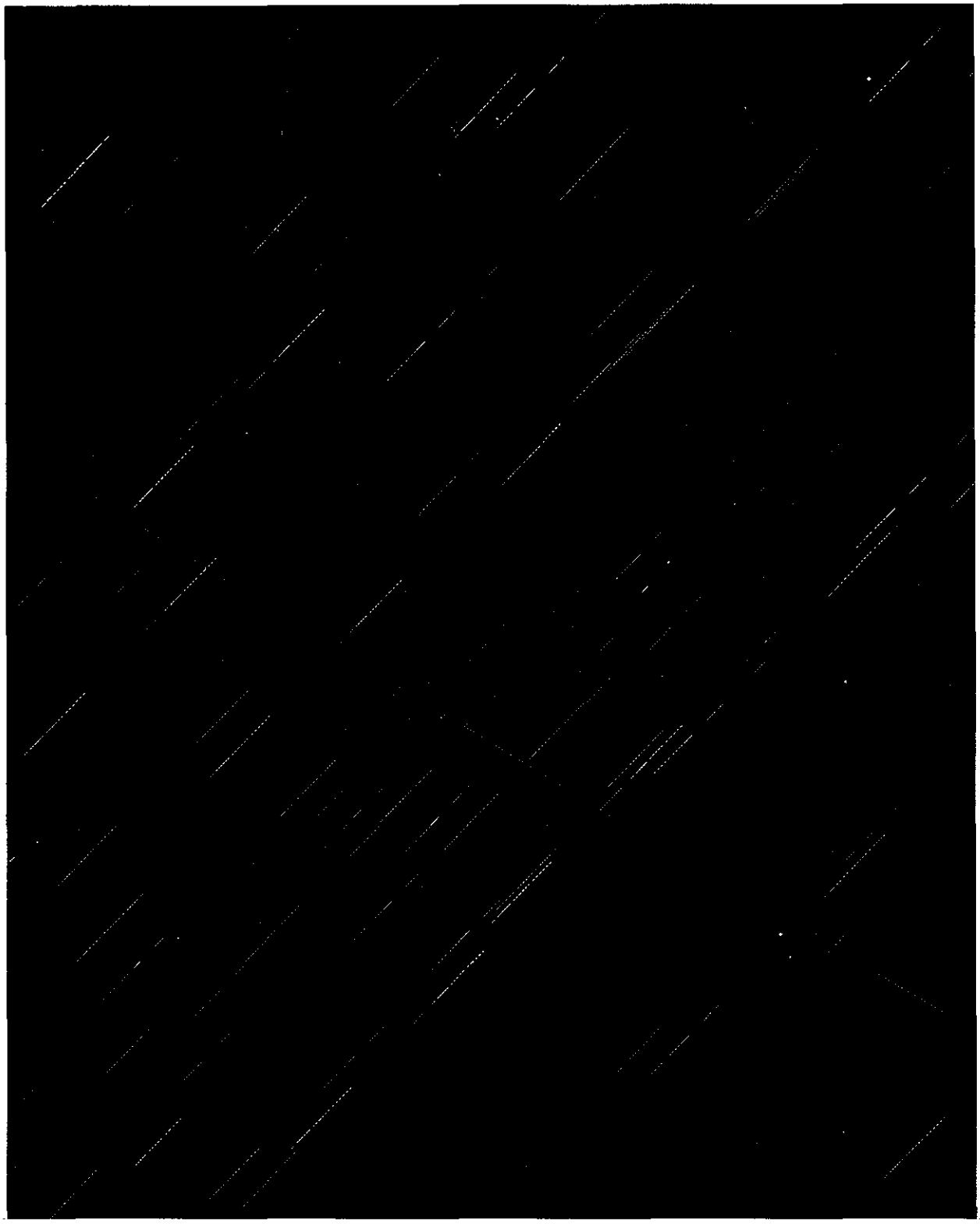

Figure 23.—Star plate with trails of two satellites.

The measurements are made on comparators equipped with independent x and y spindles with a working length of about 225 mm each. The instruments, manufactured by the firm of David Mann, Lincoln, Mass., are equipped with a direct, binocular observing optic with magnification adjustable in steps up to 40× and a circular measuring mark with a diameter of about 30 μm. The comparators are operated in a controlled environment (temperature 22° C ±0.5 C, humidity 50% ±5%) and tested about every 2 months for linear and periodic scale errors in the x and y spindles as well as for orthogonality of the motions. Calibrated grid plates in each of four positions are measured for this purpose by each of three observers. The coordinates measured to the nearest micron are registered electronically on a typewriter, punch tape, or card. The initial operations revealed the fact that the operator's body heat generated an unacceptably large systematic error in the measurements because the optic of the comparator was not constructed in accordance with the Abbe principle. It was necessary therefore to modify the construction so as to project the measuring mark into the plane of measurement. Extensive tests have shown that the comparators now are stable for operating periods of from 2 to 3 hours. However, it is still necessary to subdivide the measurement of a plate into several such periods.

The first step is to drill 8 circular holes into the emulsion, approximately 40 to 50 μm in diameter. These are located at the four corners, at the extremities of the legs of the conventional fiducial marks pointing toward the center, and four additional at the approximate center of each edge. These drill holes are measured at the beginning and end of each measuring session, and the differences are used to check the stability of the instrument during that period. Before continuing with the description of the measuring procedure, some essentials in the preparation for plate measurement must be mentioned.

The readings on the circles in the field give an orientation of the camera in azimuth and elevation to within 10 to 20 seconds. With the time of observation and approximate station coordinates, a range in right ascension and declination on the celestial sphere can be computed. The computer searches the star catalogue tape for all stars in this portion of the sky and their coordinates together with the nominal camera constants and the approximated orientation data are used to compute plate coordinates for these stars. These points are projected on a cathode ray tube associated with the electronic computer and photographed to the scale of the photogram to produce a star chart. The stars are subdivided into three groups of magnitudes and labeled accordingly. Another symbol designates a group of at least eight stars, as bright as possible and located in a circular ring 3 cm wide near the edges of the plate. Since the registration on the original photogram or diapositive varies according to magnitude, it is easy to bring the photogram and the "computed star chart" into coincidence on a light table. At the same time a grid template is superimposed, dividing the plate format into 100 equal squares. The photogram is now examined under the binocular magnification of the comparator. In each of the squares a star of the series, before and after the satellite pass, that coincides with an image on the star chart is selected and marked. In addition all stars recorded during the satellite pass (cf. fig. 20) and the specially selected bright stars near the edge of the plate are marked with an identification symbol.

After this preparation the plate is placed in the comparator. In order to eliminate as far as possible the influence of unknown systematic errors, a subgroup of stars and satellite images covering the whole extent of the plate is measured at each of the two or three sessions required. After completion of the measurements all premarked stars and satellite images will have been measured. The satellite trail crosses the plate within at most a few mm from the center, and its images are measured to a maximum distance of 6 cm from the center in order to avoid edge effects in the emulsion. In order to combine the readings obtained from the two or three necessary comparator sittings in a consistent system, the individual sets are translated, rotated, and stretched with two scale corrections in an adjustment to best fit the configuration of the relevant drill holes. The residuals of the reference points after these transformations are typically ±0.3 μm. The entire measuring process is then repeated with the plate turned through approximately 180°. Both results are then meaned by fitting this latter result to the first, again by means of an adjustment (determination of two components of translation, a rotation, and two scale factors). From the residual differences between corresponding double measurements in this adjustment a characteristic mean error of ±1.6 μm results, as a measure of precision of the measured coordinates (cf. sec. 3.2).

In addition, the plate coordinates of all premarked star and satellite images are referenced to the plate center as determined by the fiducial marks. The coordinates of the above-mentioned bright stars near the edges of the plate that are easily identifiable in the catalogue are now used to

compute an approximate orientation. With this result right ascensions and declinations are computed from the image coordinates of all measured stars (cf. sec. 2.7.5.1). The same program compares these values with the tape containing the star catalog, identifies the stars, and updates them to the observation epoch and true equinox (cf. sec. 2.3, eqs. (1) to (15)).

The step in the overall adjustment procedure of satellite triangulation here under discussion represents a mutually interacting combination of human effort and electronic computing. The contributions from the human element are the critical operations, such as the execution of the measurements and evaluation of the statistical intermediate results, while the computing system prepares star charts, presents catalogued data, and makes the necessary computations.

After completion of this operation, measured coordinates for all selected stars and satellite images are available, as well as the star coordinates reduced to a certain point. These data are now further reduced in a numerical adjustment to be discussed in the next section.

2.7 Numerical Adjustment

2.7.1 Introductory Remarks

In this section the attempt will be made to present the mathematical concept of the method of geometric satellite triangulation, considering the problem from the standpoint of analytical photogrammetry. The *principle of the photogrammetric measuring method* is most conveniently identified with the concept of a direction fixed within a certain coordinate system. It is therefore reasonable to expect a clear and computationally economical solution with a vectorial presentation. It should be borne in mind that the mathematical expression for a direction in space can be changed either by rotating the coordinate system to which the direction is referred, or by a change in direction within the fixed reference frame. The latter can be accomplished either by rotating the given vector or by the addition of a correction vector. From a mathematical standpoint, rotating the coordinate system and changing the direction are equivalent. However, this interpretation helps to explain the measuring process geometrically. One difference between the two cited operations becomes apparent when one considers that a rotation of the coordinate system does not affect the geometry existing between the object points. The concept of a linear coordinate transformation, including translations if necessary, therefore seems meaningful. A change in direction within a given coordinate system on the other hand effects a change of the spatial position of this direction in object space. The designation "change in direction" will therefore be reserved for this operation.

Finally, as simple a representation as possible shall be given of the photogrammetric measuring method, whose concept rests on the principles of a central perspective. For this purpose it is merely necessary to get a mental picture of a unit vector $\mathbf{x}_0$ assigned to a specified direction in object space, with reference to an arbitrary but uniquely defined coordinate system. With the assumption that the starting point of this vector coincides with the center of projection of the central perspective (e.g., at the center of the unit sphere), the photogrammetric bundle vector $\mathbf{p}$ in object space, reduced to unit length, is, geometrically speaking, identical with the above-mentioned vector $\mathbf{x}_0$. Since the photogrammetric bundle vector $\mathbf{p}$ is referred to the coordinate system $\bar{x}$, $\bar{y}$, c of the camera, a rotation of the coordinate system transforms the vector $\mathbf{x}_0$ into vector $\mathbf{p}$ or vice versa. This step, described above as a coordinate transformation, represents the fundamental analytical operation of the photogrammetric measuring method (cf. sec. 2.7.2.1). It now remains only to consider those displacements of the image from the central perspective concept that are the result of the physical photographic process. Before an adjustment algorithm is developed from this line of thought, the more important mathematical aids needed in this discussion will be listed in logical order.

2.7.2 Mathematical Aids

2.7.2.1 Various mathematical expressions for the unit vector

From figure 24 directly:

$$\mathbf{x}_0 = \begin{bmatrix} x_1 \\ x_2 \\ x_3 \end{bmatrix} = \frac{\mathbf{x}}{\mathbf{x}}$$

$$= \begin{bmatrix} X - X_0 \\ Y - Y_0 \\ Z - Z_0 \end{bmatrix} [(X - X_0)^2 + (Y - Y_0)^2 + (Z - Z_0)^2]^{-\frac{1}{2}}$$

$$= \begin{bmatrix} \xi \\ \eta \\ 1 \end{bmatrix} (\xi^2 + \eta^2 + 1^2)^{-\frac{1}{2}} \tag{61}$$

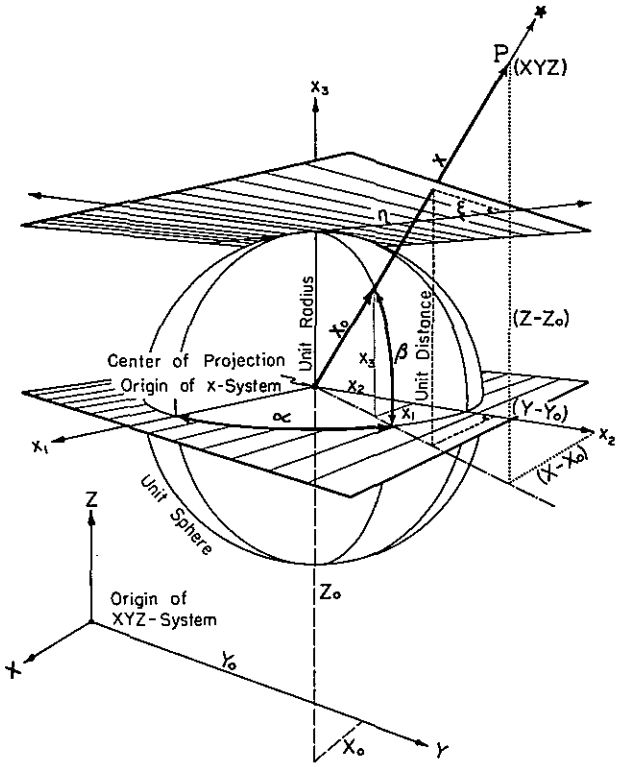

Figure 24.—Basic coordinate systems used in the numerical evaluation.

where either

$$\mathbf{x} = \begin{bmatrix} (X - X_0) \\ (Y - Y_0) \\ (Z - Z_0) \end{bmatrix} \text{ or } \mathbf{x} = \begin{bmatrix} \xi \\ \eta \\ 1 \end{bmatrix}. \tag{62}$$

Furthermore:

$$\mathbf{x}_0 = \begin{bmatrix} \cos\beta \cos\alpha \\ \cos\beta \sin\alpha \\ \sin\beta \end{bmatrix}, \tag{63}$$

where from figure 22

$$\tan\alpha = \frac{x_2}{x_1} = \frac{\eta}{\xi}. \tag{64}$$

$$\tan\beta = \frac{x_3}{(x_1 + x_2)^{\frac{1}{2}}} = (\xi^2 + \eta^2)^{-\frac{1}{2}} \tag{65}$$

and

$$\xi = \frac{(X - X_0)}{(Z - Z_0)} = \frac{x_1}{x_3} \tag{66}$$

$$\eta = \frac{(Y - Y_0)}{(Z - Z_0)} = \frac{x_2}{x_3} \tag{67}$$

2.7.2.2 Coordinate transformation

$$\mathbf{x}' = \mathbf{R}(\gamma_1\gamma_2\gamma_3)\,(\mathbf{x} + \Delta\mathbf{x}) \tag{68}$$

where the rotation matrix has the following meaning

$$\mathbf{R}(\gamma_1\gamma_2\gamma_3) = \mathbf{R}(\gamma_3)\,\mathbf{R}(\gamma_2)\,\mathbf{R}(\gamma_1). \tag{69}$$

The γ's designate the angles through which rotation takes place in the indicated order, the indices under the angle showing the axis around which rotation takes place. Counter-clockwise rotation (as seen from above) is positive.

2.7.2.3 Change of direction

From figure 25

$$\mathbf{x}_0' = \mathbf{x}_0 + \Delta\mathbf{x} \tag{70}$$

The differential $d\mathbf{x}_0$ of a unit vector $\mathbf{x}_0$ is a vector of infinitesimal length with a direction perpendicular to $\mathbf{x}_0$, since the length of $\mathbf{x}_0$ is constant by definition. The vector $\mathbf{x}_0$ can therefore turn through only an infinitesimal angle ϵ whose measure in radians is equal to the length of the linear displacement $d\mathbf{x}_0$. Therefore, for small displacements the following equalities follow from figure 25:

$$|\Delta\mathbf{x}| = |d\mathbf{x}_0| = \epsilon = \sin\epsilon = \tan\epsilon \tag{71}$$

and hence

$$\mathbf{x}_0' = \mathbf{x}_0 + d\mathbf{x}_0. \tag{72}$$

For the special case where $d\mathbf{x}_0$ is coplanar with one of the coordinate axes, e.g., with x_3, it follows from figure 26:

$$d\mathbf{x}_0 = \begin{bmatrix} -x_1 \cdot x_3 \\ -x_2 \cdot x_3 \\ +(1 - x_3^2) \end{bmatrix} \epsilon\,(1 - x_3^2)^{-\frac{1}{2}} \tag{73}$$

ϵ in radians. $\mathbf{x}_0'$ then follows from (72).

Similar expressions for the other axes are obtained by cyclic permutation of the subscripts and the vector components in (73) in the order (1)→(2)→(3)→(1).

For larger values of ϵ one obtains from (63)

$$\mathbf{x}_0' = \begin{bmatrix} \cos(\beta + \epsilon)\cos\alpha \\ \cos(\beta + \epsilon)\sin\alpha \\ \sin(\beta + \epsilon) \end{bmatrix}$$

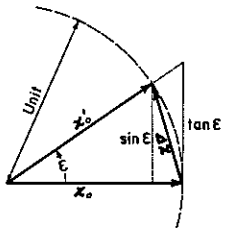

Figure 25.—Increment of a unit vector.

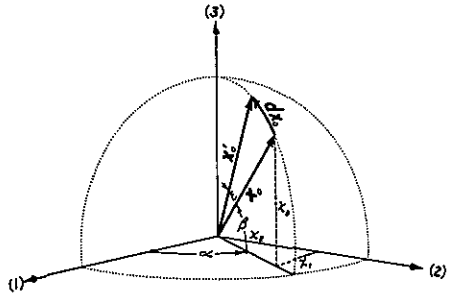

Figure 26.—Increment coplanar with a coordinate axis.

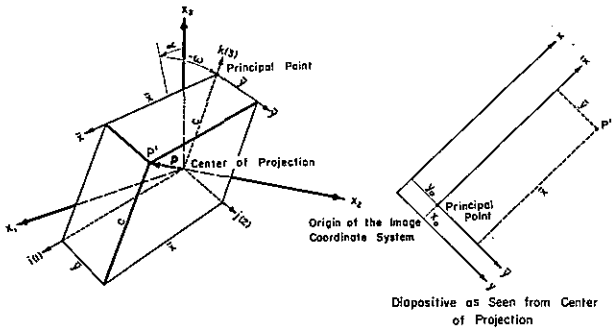

Figure 27.—The photogrammetric bundle vector **p**.

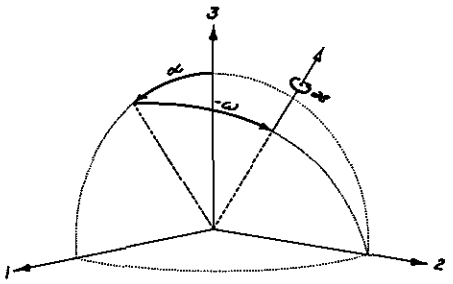

Figure 28.—Sense of direction of exterior elements of orientation.

2.7.2.4 Central perspective

From figure 27 the photogrammetric bundle vector **p** is

$$\mathbf{p} = \bar{x}\ \mathbf{i} + \bar{y}\ \mathbf{j} + c\ \mathbf{k} = \begin{bmatrix} x \\ y \\ c \end{bmatrix} \tag{75}$$

and, with (61)

$$\mathbf{p}_0 = \frac{\mathbf{p}}{|\mathbf{p}|}, \text{ where } |\mathbf{p}| = (\bar{x}^2 + \bar{y}^2 + c^2)^{-\frac{1}{2}}. \tag{76}$$

From (68), with $\Delta\mathbf{x} = 0$, follows the fundamental equation of analytical photogrammetry

$$\mathbf{p}_0 = \mathbf{R}(\alpha, \omega, \kappa)\ \mathbf{x}_0 \tag{77}$$

where

$$\mathbf{R}(\alpha, \omega, \kappa) = \mathbf{R}(\kappa)\ \mathbf{R}(\omega)\ \mathbf{R}(\alpha) = \begin{bmatrix} r_{11} & r_{12} & r_{13} \\ r_{21} & r_{22} & r_{23} \\ r_{31} & r_{32} & r_{33} \end{bmatrix} \tag{78}$$

The r_{ij} in the orthogonal matrix (78) are actually the direction cosines, i.e., the components of the corresponding unit vectors, in the x coordinate system of the corresponding axes after the indicated rotations through angles α, ω and κ shown in figure 28. They are found to be:

$$\begin{aligned} r_{11} &= \cos\alpha\cos\kappa + \sin\alpha\sin\omega\sin\kappa \\ r_{12} &= \cos\omega\sin\kappa \\ r_{13} &= -\sin\alpha\cos\kappa + \cos\alpha\sin\omega\sin\kappa \\ r_{21} &= -\cos\alpha\sin\kappa + \sin\alpha\sin\omega\cos\kappa \\ r_{22} &= \cos\omega\cos\kappa \\ r_{23} &= \sin\alpha\sin\kappa + \cos\alpha\sin\omega\cos\kappa \\ r_{31} &= \sin\alpha\cos\omega \\ r_{32} &= -\sin\omega \\ r_{33} &= \cos\alpha\cos\omega \end{aligned} \tag{79}$$

For the orthogonal matrix $\mathbf{R}(\alpha, \omega, \kappa)$

$$\mathbf{R}^{-1}(\alpha, \omega, \kappa) = \mathbf{R}^*(\alpha, \omega, \kappa) \tag{80}$$

so that with (77), (78) and (79)

$$\mathbf{x}_0 = \frac{\mathbf{x}}{|\mathbf{x}|} = \mathbf{R}^*(\alpha, \omega, \kappa)\ \frac{\mathbf{p}}{|\mathbf{p}|}. \tag{81}$$

Furthermore, from (77) with (78), (61) and 75)

$$\begin{bmatrix} \bar{x} \\ \bar{y} \\ c \end{bmatrix} = \begin{bmatrix} r_{11} & r_{12} & r_{13} \\ r_{21} & r_{22} & r_{23} \\ r_{31} & r_{32} & r_{33} \end{bmatrix} \begin{bmatrix} (X - X_0) \\ (Y - Y_0) \\ (Z - Z_0) \end{bmatrix} \frac{|\mathbf{p}|}{|\mathbf{x}|} \tag{82}$$

so that

$$\frac{\bar{x}}{c} = \frac{r_{11}(X - X_0) + r_{12}(Y - Y_0) + r_{13}(Z - Z_0)}{r_{31}(X - X_0) + r_{32}(Y - Y_0) + r_{33}(Z - Z_0)} = \frac{m}{q} \tag{83}$$

and

$$\frac{\bar{y}}{c} = \frac{r_{21}(X - X_0) + r_{22}(Y - Y_0) + r_{23}(Z - Z_0)}{r_{31}(X - X_0) + r_{32}(Y - Y_0) + r_{33}(Z - Z_0)} = \frac{n}{q}. \tag{84}$$

Finally, for (83 and (84)

$$\bar{x} = \frac{cm}{q} \tag{85}$$

$$\bar{y} = \frac{cn}{q}. \tag{86}$$

2.7.2.5 Deviations from the central perspective bundle

Refraction effects a displacement in direction which, with (73) [cf. also (26) and (27)], can be applied to the unit vector in the direction in question or which, with (74), leads directly to the unit vector corrected for refraction.

We consider next those influences that displace the image from its central perspective position that are due to the constructive properties of the camera. It is known from experience that the image of the object point P is formed not at P' but at P^*, which is displaced relative to P' by a vector $\boldsymbol{\Delta}$ lying in the plane of the photograph.
From figure 29 we have

$$\bar{x} = x - x_0 - \Delta x \tag{87}$$

$$\bar{y} = y - y_0 - \Delta y \tag{88}$$

in which Δx and Δy are the components of $\boldsymbol{\Delta}$.

The coordinates x and y are obtained from the corresponding comparator coordinates, corrected for the nonorthogonality ϵ of the comparator spindles as shown in figure 29, from

$$x = x_{meas} + y \cdot \epsilon \tag{89}$$

$$y = y_{meas} \tag{90}$$

Since the vector $\boldsymbol{\Delta}$ is always small, a sufficiently accurate linear scale correction results from replacing the scale factor c in (85) and (86) by c_x and c_y. Thus

$$\bar{x} = \frac{c_x m}{q} \tag{91}$$

$$\bar{y} = \frac{c_y n}{q} \tag{92}$$

The required expressions for Δx and Δy are, from figure 29,

$$\Delta x = \Delta R_x + \Delta T_x \tag{93}$$

$$\Delta y = \Delta R_y + \Delta T_y \tag{94}$$

The symmetric radial distortion ΔR is, as usual, expressed as a polynomial in odd powers of the distance d. Omitting the first power, which is equivalent to a scale correction, one obtains

$$\Delta R = K_1 d^3 + K_2 d^5 + K_3 d^7 \tag{95}$$

where

$$d = [(\bar{x} - x_s)^2 + (\bar{y} - y_s)^2]^{\frac{1}{2}} \tag{96}$$

and

$$\Delta R_x = \frac{\Delta R(\bar{x} - x_s)}{d} = (\bar{x} - x_s)(K_1 d^2 + K_2 d^4 + K_3 d^6) \tag{97}$$

$$\Delta R_y = \frac{\Delta R(\bar{y} - y_s)}{d} = (\bar{y} - y_s)(K_1 d^2 + K_2 d^4 + K_3 d^6) \tag{98}$$

A model for the distortion due to the unavoidable residual errors in centering the individual elements of the lens system was given by Conrady in [35] (cf. also [36]). In figure 29 the minimal component of this distortion is purely tangential and designated ΔT_0. For high grade objectives ΔT_0 can be expressed sufficiently accurately with two terms of an even polynomial in d:

$$\Delta T_0 = K_4 d^2 + K_5 d^4. \tag{99}$$

According to Conrady the components of this nonsymmetric distortion are—using the designations in figure 29—in the tangential direction

$$\Delta T_t = \Delta T_0 \cos(\varphi_T + \beta) \tag{100}$$

and in radial direction

$$\Delta T_r = 3\Delta T_0 \sin(\varphi_T + \beta). \tag{101}$$

Hence

$$\Delta \mathbf{T} = \begin{bmatrix} \Delta T_x \\ \Delta T_y \end{bmatrix} = \begin{bmatrix} \cos\beta & \sin\beta \\ -\sin\beta & \cos\beta \end{bmatrix} \begin{bmatrix} \Delta T_t \\ \Delta T_r \end{bmatrix}. \tag{102}$$

Finally with (99), (100) and (101) one obtains from (102)

$$\Delta \mathbf{T} = \begin{bmatrix} \Delta T_x \\ \Delta T_y \end{bmatrix} = (K_4 + K_5 d^2) \times$$

$$\begin{bmatrix} 2(\bar{x} - x_s)(\bar{y} - y_s) & 3(\bar{x} - x_s)^2 + (\bar{y} - y_s)^2 \\ 3(\bar{y} - y_s)^2 + (\bar{x} - x_s)^2 & 2(\bar{x} - x_s)(\bar{y} - y_s) \end{bmatrix} \begin{bmatrix} \sin\varphi_T \\ \cos\varphi_T \end{bmatrix}. \tag{103}$$

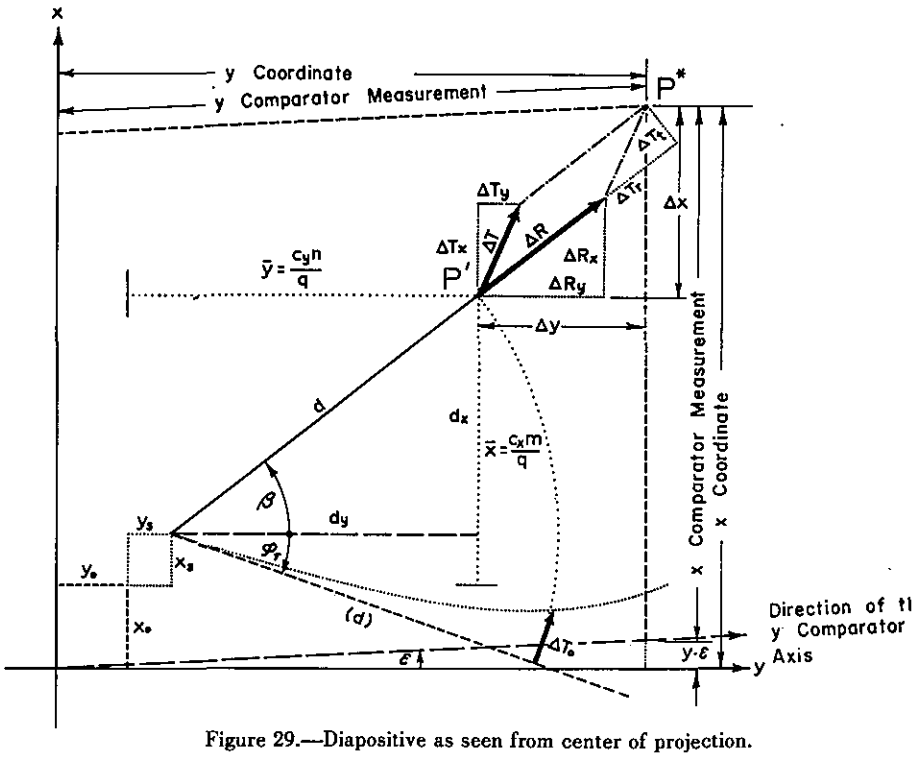

Figure 29.—Diapositive as seen from center of projection.

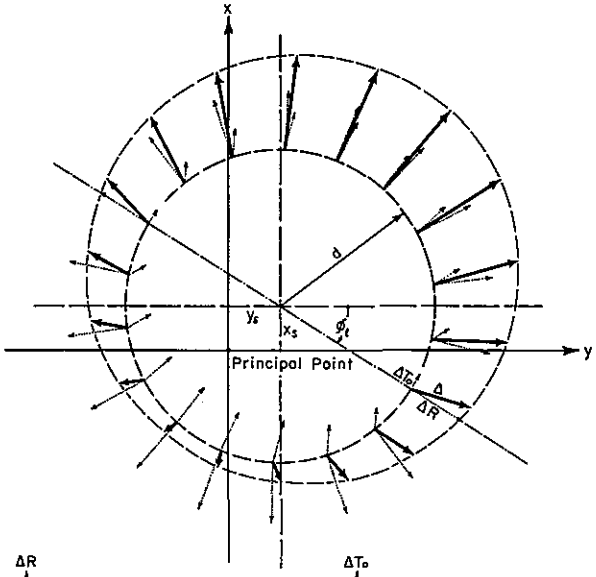

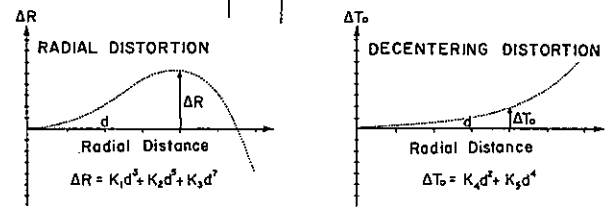

Figure 30.—Components of distortion.

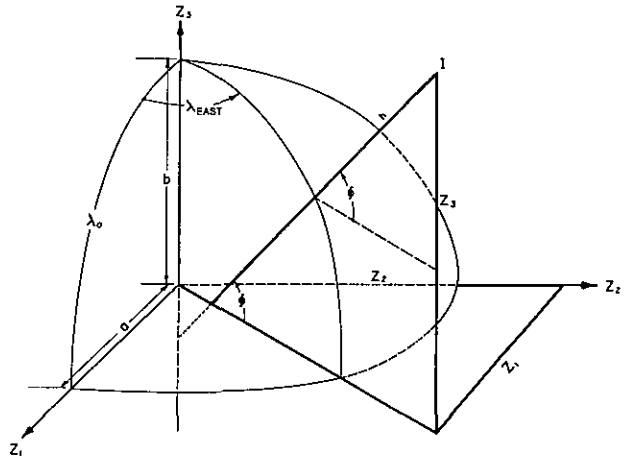

Figure 31.—Earth ellipsoid parameters and coordinates.

Figure 30 shows schematically the components for radial and decentering distortion for a certain distance d.

Finally one obtains with (89), (90), (97), (98) and (103) in accordance with (87), (88) and (93), (94) and figure 29:

$$\bar{x} = x + y'\cdot\epsilon - (\bar{x} - x_s)(K_1d^2 + K_2d^4 + K_3d^6) - (K_4 + K_5d^2)\{2(\bar{x} - x_s)(\bar{y} - y_s)\sin\varphi_T + [3(\bar{x} - x_s)^2 + (\bar{y} - y_s)^2]\cos\varphi_T\} - x_0 \tag{104}$$

$$\bar{y} = y - (\bar{y} - y_s)(K_1d^2 + K_2d^4 + K_3d^6) - (K_4 + K_5d^2)\{[3(\bar{y} - y_s)^2 + (\bar{x} - x_s)^2]\sin\varphi_T + 2(\bar{x} - x_s)(\bar{y} - y_s)\cos\varphi_T\} - y_0 \tag{105}$$

where the meaning of d is defined by (96), and x and y are the comparator coordinates measured on the photogram.

2.7.2.6 Description of the rectangular coordinate systems

In order to make the computations for the adjustment of geometric satellite triangulation as clear and synoptic as possible, three rectangular coordinate systems are used. Each of the three systems has a subgroup. The three principal systems are designated x, y, and z systems, and the corresponding subsystems are x', y', and z'. The x system corresponds to the astronomic reference system in that the x_3 axis points to the celestial North Pole and the x_1 axis intersects the Equator at the vernal equinox (cf. fig. 7). The origin of this system is the center of the unit sphere that circumscribes the Earth's center (origin of the rectangular geometric coordinates) or any arbitrary point of observation.

Turning the x system about its x_3 axis through the hour angle θ of the equinox (local sidereal time at observation site P) results in the x' system

$$\mathbf{x}' = \underset{3}{\mathbf{R}}(\theta)\mathbf{x} \tag{106}$$

The y system (cf. fig. 8a) designates the rectangular geocentric coordinate system that corresponds to the orientation of the Earth for a specific epoch and in which the y_3 axis points to the instantaneous North Pole. The intersection of the instantaneous null meridian with the instantaneous Equator determines the direction of the y_1 axis. The instantaneous null meridian is defined on the reference ellipsoid as the trace of the plane containing the instantaneous axis of rotation of the Earth and that point whose ellipsoidal coordinates in the conventional geodetic reference system (1900–05 Pole) are $\varphi = 0, \lambda = 0$.[6]

At an arbitrary point of observation in the y system the corresponding instantaneous ellipsoidal coordinates are φ' and λ'_{east}. If the y system is rotated first through the angle λ'_{east} about its y_3 axis the local y' system is obtained. In this system the y'_3 axis points to the station zenith while the y'_1 axis lies in the plane of the meridian as well as of the horizon, and hence points south. Therefore

$$\mathbf{y}' = \underset{2}{\mathbf{R}}(90^\circ - \varphi')\,\underset{3}{\mathbf{R}}(\lambda'_{east})\,\mathbf{y} = \underset{2}{\mathbf{R}}(90^\circ - \varphi')\,\mathbf{x}'. \tag{107}$$

Cf. also (23) and (30), the latter being the inverse transformation.

Finally we have the z and z' systems that coincide essentially with the y and y' systems except that the z systems are referenced to the conventional (1900–05) pole. If the displacement of the instantaneous pole relative to the conventional pole is given, as is the practice, by the components x and y (cf. sec. 2.4 and fig. 11) the transformation is effected by

$$\mathbf{z} = \underset{1}{\mathbf{R}}(-y)\,\underset{2}{\mathbf{R}}(-x)\,\mathbf{y} \tag{108}$$

and

$$\mathbf{z}' = \underset{2}{\mathbf{R}}(90^\circ - \varphi)\,\underset{3}{\mathbf{R}}(\lambda_{east})\,\mathbf{z} \tag{109}$$

(cf. also (32), (34), (36) and (37)).

Ellipsoidal coordinates corresponding to the z system are designated φ and λ.

2.7.2.7 Transformation of ellipsoidal coordinates φ, λ, h into rectangular coordinates and inversely.

The astronomical systems x and x' introduced in the previous section are, with respect to their information content, essentially two-dimensional, defining merely directions in three space (cf., e.g., fig. 7). On the other hand, the y, y', z, z' systems are used in the three-dimensional positioning of points on the Earth's surface (station coordinates) (cf., e.g., figs. 8a and 8b). In the course of reduction of the satellite triangulation it is therefore necessary to transform geodetic ellipsoidal coordinates into three-dimensional rectangular coordinates and vice versa. It is also necessary to make provisions for the introduction of given ellipsoidal coordinates with their weights into the adjustment of the spatial triangulation. This brings up the problem of a purely geometric solution for

[6] cf. remark in sec. 2.4.

ellipsoid transformations. Finally the problem of determining ellipsoid constants arises when one desires to reference the rectangular station coordinates resulting from an extended satellite triangulation to a best-fitting ellipsoid for this area. In consequence of our assumption that electronic computers are being used, such computations are rigorously performed with closed formulas rather than the differential transformations of classical geodesy.

Such a solution, in programmed form, can be found in [37] from which the necessary formulas are excerpted.

The designations for the constants of the reference ellipsoid are taken from figure 31:

a = semimajor axis

b = semiminor axis

$$e = \text{eccentricity} = \left(\frac{a^2 - b^2}{a^2}\right)^{\frac{1}{2}} \tag{110}$$

Figure 32 represents the plane of the meridian λ.

To transform the φ, λ, h into geocentric rectangular coordinates z_1, z_2, z_3 (cf. sec. 2.7.2.6 and fig. 31) the following formulas are used

$$z_1 = [a^2(a^2 + b^2 \tan^2\varphi)^{-\frac{1}{2}} + h \cos\varphi] \cos\lambda \tag{111}$$

$$z_2 = [a^2(a^2 + b^2 \tan^2\varphi)^{-\frac{1}{2}} + h \cos\varphi] \sin\lambda \tag{112}$$

$$z_3 = (a^2 + b^2 \tan^2\varphi)^{-\frac{1}{2}} b^2 \tan^2\varphi + h \sin\varphi \tag{113}$$

For the inverse transformation

$$\tan\lambda = \frac{z_2}{z_1} \tag{114}$$

$$\tan\psi^0 = z_3 (z_1^2 + z_2^2)^{-\frac{1}{2}} a \cdot b^{-1} \tag{115}$$

$$\Delta\psi = -\frac{\tan\psi^0 - ae^2(z_1^2 + z_2^2)^{-\frac{1}{2}} \sin\psi^0 - a^{-1}bz_3(z_1^2 + z_2^2)^{-\frac{1}{2}}}{1 + \tan^2\psi^0 - ae^2(z_1^2 + z_2^2)^{-\frac{1}{2}} \cos\psi^0} \tag{116}$$

[7]

$$\psi = \psi^0 + \Delta\psi \tag{117}$$

$$\tan\varphi = ab^{-1} \tan\psi \tag{118}$$

$$h = [(z_1^2 + z_2^2)^{\frac{1}{2}} - a \cos\psi] \sec\varphi \tag{119}$$

If necessary the geocentric rectangular coordinates may be transformed into local rectangular or vice versa by using (68) with (30) or (36). Such a transformation represents the link between the y and y' or z and z' systems of sec. 2.7.2.6. For example with the z systems:

$$\mathbf{z}' = \mathbf{R}(\lambda_0, (90° - \varphi_0))\,(\mathbf{z} - \mathbf{z}_0) \tag{120}$$

[7] Use of (116) requires an iteration loop to avoid the alternative of solving a 4th-degree equation. Transforming φ to reduced latitude ψ accelerates the convergence of (116). See ref. [37], also A. R. Wooten, BRL Memo Rep. No. 1322, Ballistic Res. Lab., Aberdeen Proving Ground, Md., 1961.

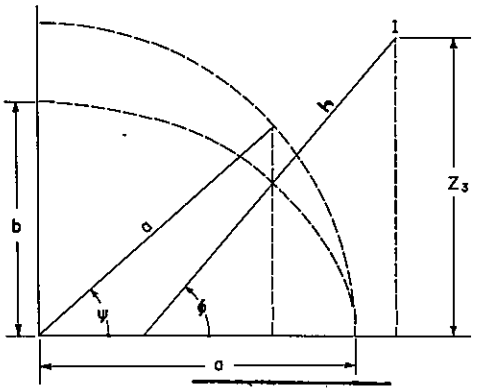

Figure 32.—Parameters for the transformation of ellipsoidal to Cartesian coordinates.

where the $\mathbf{z}_0$ vector is computed from (111), (112), (113) with φ_0, λ_0, h_0, the ellipsoidal coordinates of the selected origin of the z' system.

In introducing certain ellipsoidal coordinates

$$\varphi = \begin{bmatrix} \varphi \\ \lambda \\ h \end{bmatrix} \tag{121}$$

with their given weights

$$\mathbf{P}_\varphi = \begin{bmatrix} P_\varphi & P_{\varphi,\lambda} & P_{\varphi,h} \\ P_{\varphi,\lambda} & P_\lambda & P_{\lambda,h} \\ P_{\varphi,h} & P_{\lambda,h} & P_h \end{bmatrix} \tag{122}$$

into the adjustment of the spatial satellite triangulation as additional conditions it should be noted that

$$\mathbf{z}' = \begin{bmatrix} z_1' \\ z_2' \\ z_3' \end{bmatrix} \tag{123}$$

can be represented as a vector function of $\boldsymbol{\varphi}$.

Hence we can compute

$$\frac{d\mathbf{z}'}{d\varphi} = \mathbf{T}_\varphi = \begin{bmatrix} \frac{\partial z_1'}{\partial\varphi} & \frac{\partial z_1'}{\partial\lambda} & \frac{\partial z_1'}{\partial h} \\ \frac{\partial z_2'}{\partial\varphi} & \frac{\partial z_2'}{\partial\lambda} & \frac{\partial z_2'}{\partial h} \\ \frac{\partial z_3'}{\partial\varphi} & \frac{\partial z_3'}{\partial\lambda} & \frac{\partial z_3'}{\partial h} \end{bmatrix} \tag{124}$$

and

$$\Delta\mathbf{z}' = \mathbf{T}_\varphi \Delta\varphi \tag{125}$$

Since furthermore

$$\frac{d\varphi}{d\mathbf{z}'} = \mathbf{T}_\varphi^{-1} \tag{126}$$

we have

$$\Delta\varphi = \mathbf{T}_\varphi^{-1}\Delta\mathbf{z}' \tag{127}$$

From similar considerations we have, in addition:

$$\mathbf{P}_z' = (\mathbf{T}_\varphi^{-1})^*\mathbf{P}_\varphi\mathbf{T}_\varphi^{-1}. \tag{128}$$

The partial derivatives in the $\mathbf{T}_\varphi$ matrix (124) are computed with the coordinates φ_0, λ_0, of the origin of the local system:

$$\mathbf{T}_\varphi = \mathbf{R}(\lambda_0, (90^\circ - \varphi_0))\frac{d\mathbf{z}}{d\varphi}, \tag{129}$$

where $\frac{d\mathbf{z}}{d\varphi}$ is computed by differentiation of the expressions (111), (112) and (113) as follows:

$$\frac{d\mathbf{z}}{d\varphi} = \begin{bmatrix} -I\cos\lambda & -II\sin\lambda & \cos\varphi\cos\lambda \\ -I\sin\lambda & II\cos\lambda & \cos\varphi\sin\lambda \\ I\cot\varphi & 0 & \sin\varphi \end{bmatrix} \tag{130}$$

c. Transforming these rectangular coordinates into ellipsoidal coordinates, using (114) to (119), taking into account the parameters of the new reference ellipsoid.

This type of transformation is common, especially in connection with comparison of the final results of satellite triangulation with classical geodetic surveys.

The determination of the constants of a reference ellipsoid that best fits the results of an extended satellite triangulation is treated in [38]. Such solutions must include the results of dynamic satellite geodesy, and the formulas so far developed serve as the basis for sueh a solution, since with (110) and (119) the geoid undulation N can be written, after suitable transformation, as

$$N = h - H = (z_1^2 + z_2^2)^{\frac{1}{2}}\sec\varphi - a(1 - e^2\sin^2\varphi)^{\frac{1}{2}} - H \tag{133}$$

If the leveling height H be assumed free of error the other partial derivatives are

$\frac{\partial N}{\partial z_1}$	$\frac{\partial N}{\partial z_2}$	$\frac{\partial N}{\partial z_3}$	$\frac{\partial N}{\partial a}$	$\frac{\partial N}{\partial f}$
$\cos\varphi\cos\lambda$	$\cos\varphi\sin\lambda$	$\sin\varphi$	$-W$	$b\sin^2\varphi\,W^{-1}$

(134)

where

$$I = \{a^2b^2\tan\varphi\,[\cos^2\varphi\,(a^2 + b^2\tan^2\varphi)^{3/2}]^{-1} + h\sin\varphi\}\rho^{-1} \tag{131}$$

$$II = [a^2(a^2 + b^2\tan^2\varphi)^{-\frac{1}{2}} + h\cos\varphi]\,\rho^{-1} \tag{132}$$

with $\rho = 206\,264''.8$

The $\Delta\boldsymbol{\varphi}$ ($\Delta\varphi$, $\Delta\lambda$, Δh) vector computed with (127) is in seconds of arc for $\Delta\varphi$ and $\Delta\lambda$ and in meters for Δh; corresponding values are substituted in (125).

The classical ellipsoidal coordinates of the triangulation stations, referenced at times—especially in the world net—to different datums, are most conveniently recomputed on a common reference ellipsoid before they are introduced into the spatial triangulation as initial approximations, as described later on. These purely geometric ellipsoid transformations can be accomplished with the formulas above by

a. Computing from the given coordinates φ, λ, h with (111), (112), (113), geocentric coordinates pertaining to a specific ellipsoid,

b. If necessary, translating the origin—the ellipsoid center—of these rectangular coordinates and

with

$$W^2 = (1 - e^2\sin^2\varphi) \tag{135}$$

By means of an adjustment three translation components Δz_1, Δz_2, Δz_3 and new ellipsoid parameters a and $f = 1 - \frac{b}{a}$ can be computed, subject to the condition $\Sigma v_N^2 = \min$.

2.7.3 Setting up the General Photogrammetric Observation Equations

The general photogrammetric observation equations are obtained through combination of the expressions given in (91), (92), (104) and (105), with reference to the relations (79), (83), (84), and (96).

The mathematical model is

$$F = \bar{x} - y\epsilon + (\bar{x} - x_s)(K_1d^2 + K_2d^4 + K_3d^6) + \{2(\bar{x} - x_s)(\bar{y} - y_s)\sin\varphi_T + [3(\bar{x} - x_s)^2 + (\bar{y} - y_s)^2]\cos\varphi_T\}(K_4 + K_5d^2) + x_0 - x_{\text{meas}} = 0 \tag{136}$$

$$G = \bar{y} + (\bar{y} - y_s)(K_1 d^2 + K_2 d^4 + K_3 d^6) + \{[3(\bar{y} - y_s)^2 + (\bar{x} - x_s)^2] \sin \varphi_T + 2(\bar{x} - x_s)(\bar{y} - y_s) \cos \varphi_T\}(K_4 + K_5 d^2) + y_0 - y_{meas} = 0 \quad (137)$$

where, according to figure 29 and (91), (92) and (96):

$$\bar{x} = \frac{c_x m}{q} \quad (138)$$

$$\bar{y} = \frac{c_y n}{q} \quad (139)$$

and

$$d^2 = \left(\frac{c_x m}{q} - x_s\right)^2 + \left(\frac{c_y n}{q} - y_s\right)^2. \quad (140)$$

The meaning of m, n, and q is apparent from (83), (84), the direction cosines r_{ij} being obtained from (79).

Substituting (138), (139), and (140) in (136) and (137), taking into account (83), (84), and (79), results in expressions for the equations F and G which represent the mathematical model for the generalized central perspective.

Since, especially at the beginning of the adjustment, the approximation values for the exterior orientation parameters are not necessarily good ones, it is better to adopt the following computation procedure which converges more rapidly and leads to a simpler solution with sufficiently close approximation. It should be noted that the radial distortion (95) and particularly the decentering distortion ΔT_0 (99), as functions of d, are small and vary little with a change in d.

At the beginning of each iteration step of the adjustment, $\bar{x}$ and $\bar{y}$ are computed using the comparator coordinates x and y, neglecting the influence of their measuring error, in accordance with figure 29 and (87), (88), (89), (90), (93), and (94). Since the coordinates x and y are replaced by the actual measurements l_x and l_y, the designations $l_{\bar{x}}$ and $l_{\bar{y}}$ will now be introduced for $\bar{x}$ and $\bar{y}$.

$$l_{\bar{x}} = l_x + l_y \cdot \epsilon - x_0 - \Delta R_x - \Delta T_x \quad (141)$$

$$l_{\bar{y}} = l_y - y_0 - \Delta R_y - \Delta T_y \quad (142)$$

With this,

$$(\bar{x} - x_s) - (l_{\bar{x}} - x_s) = d_x \quad (143)$$

$$(\bar{y} - y_s) = (l_{\bar{y}} - y_s) = d_y, \quad (144)$$

and

$$d^2 = d_x^2 + d_y^2. \quad (145)$$

The radial and Conrady components of distortion ΔR_x, ΔR_y, ΔT_x, and ΔT_y in (141) and (142) are computed with (97), (98), and (103). Since the mathematical models of the distortion and hence also the distance d with its components d_x and d_y refer to the geometry of the central perspective (cf. fig. 29), an iteration loop must be designed for computing all the distortion components used in (141) and (142). In (97), (98) and (103), $\bar{x}$ and $\bar{y}$ are first replaced by

$$\bar{x} = l_{\bar{x}} \approx l_x + l_y \cdot \epsilon - x_0 \quad (146)$$

and

$$\bar{y} = l_{\bar{y}} \approx l_y - y_0 \quad (147)$$

The ΔR_x, ΔR_y, ΔT_x and ΔT_y so computed are substituted in (141) and (142) to give new $l_{\bar{x}}$, $l_{\bar{y}}$ values, with which distortion components are again computed, followed by new $l_{\bar{x}}$ and $l_{\bar{y}}$ values. This iteration is continued until the difference between successive $l_{\bar{x}}$ and $l_{\bar{y}}$ becomes less than a prescribed tolerance.

Introduction of l_x and l_y and substitution for m, n, and q in accordance with (83) and (84) changes (136) and (137) to

$$F = -l_y \cdot \epsilon + \frac{c_x[r_{11}(X - X_0) + r_{12}(Y - Y_0) + r_{13}(Z - Z_0)]}{r_{31}(X - X_0) + r_{32}(Y - Y_0) + r_{33}(Z - Z_0)} + x_0 + (l_{\bar{x}} - x_s)(K_1 d^2 + K_2 d^4 + K_3 d^6) + \{2(l_{\bar{x}} - x_s)(l_{\bar{y}} - y_s) \sin \varphi_T + [3(l_{\bar{x}} - x_s)^2 + (l_{\bar{y}} - y_s)^2] \cos \varphi_T\}(K_4 + K_5 d^2) - l_x = 0 \quad (148)$$

$$G = \frac{c_y[r_{21}(X - X_0) + r_{22}(Y - Y_0) + r_{23}(Z - Z_0)]}{r_{31}(X - X_0) + r_{32}(Y - Y_0) + r_{33}(Z - Z_0)} + y_0 + (l_{\bar{y}} - y_s)(K_1 d^2 + K_2 d^4 + K_3 d^6) + \{[3(l_{\bar{y}} - y_s)^2 + (l_{\bar{x}} - x_s)^2] \sin \varphi_T + 2(l_{\bar{x}} - x_s)(l_{\bar{y}} - y_s) \cos \varphi_T\}(K_4 + K_5 d^2) - l_y = 0 \quad (149)$$

in which d^2 from (145) is

$$d^2 = (l_{\bar{x}} - x_s)^2 + (l_{\bar{y}} - y_s)^2 \qquad (150)$$

The meaning of the r_{ij} is apparent from (78) and (79), and the $l_{\bar{x}}$, $l_{\bar{y}}$ are computed iteratively with (141) and (142).

Equations (148) and (149) are analytical expressions for the generalized central perspective principle. The influences requiring generalization are:

a. Skew ϵ of the comparator carriage; its effect is simulated by the term ϵl_y in (148).

b. Linear scale error in the measuring spindles of the comparator; their influence is adequately accounted for with the scale factors c_x and c_y in (148) and (149), respectively.

c. Distortion; the two last terms in each of (148) and (149) simulate the components of the distortion vector Δ as the sum of radial and decentering distortion. In addition, the actual conditions are more closely approximated by displacing the origin (x_s, y_s) of the distortion from the principal point (x_0, y_0). These relations are shown schematically in figures 29 and 30.

For the further treatment of the expressions (148) and (149) it is only necessary to note that the direction cosines (cf. (62), (83) and (84)) in the third term of (148) and in the second term of (149) refer to refracted corrections.

The next step is to set up the observation equations. In the adjustment a generalized adjustment algorithm, described in [39] and [40], is used. The mathematical model is given with the two functions F and G of (148) and (149), and the general observation equations are obtained by expanding these functions in Taylor series and neglecting terms of the second and higher order as

$$\frac{\partial \mathbf{F}}{\partial \mathbf{u}} \Delta\mathbf{u} + F_0 = 0 \qquad (151)$$

$$\frac{\partial \mathbf{G}}{\partial \mathbf{u}} \Delta\mathbf{u} + G_0 = 0 \qquad (152)$$

in which $\mathbf{u}$ is the vector of all parameters in the mathematical model, including the measured quantities. The symbols designating the various partial derivatives of F and G are listed in (153).

$\mathbf{u}$	$\alpha\ \omega\ \kappa\ X_0\ Y_0\ Z_0\ c_x\ c_y\ x_0\ y_0\ X\ Y\ Z\ K_1\ K_2\ K_3\ x_s y_x\ K_4\ K_5\ \varphi_T\ \epsilon\ l_x\ l_y$
$\frac{\partial F}{\partial \mathbf{u}}$	$A_x\ B_x\ C_x\ D_x\ E_x\ F_x\ G_x\ -\ H_x I_x\ J_x\ K_x\ L_x\ M_x N_x\ O_x\ P_x\ Q_x\ R_x\ S_x\ T_x\ U_x\ Z_x\ -$
$\frac{\partial G}{\partial \mathbf{u}}$	$A_y\ B_y\ C_y\ D_y\ E_y\ F_y\ -\ G_y\ H_y I_y\ J_y\ K_y\ L_y\ M_y N_y\ O_y\ P_y\ Q_y\ R_y\ S_y\ T_y\ U_y\ -\ Z_y$

(153)

where

$$J_x = -D_x \quad K_x = -E_x \quad L_x = -F_x$$
$$J_y = -D_y \quad K_y = -E_y \quad L_y = -F_y.$$

The corresponding analytical expressions including the necessary auxiliary quantities are:

$$\begin{aligned}
① &= (\bar{x} - x_0)/c_x & ⑤ &= ①F - r_{13} \\
② &= (\bar{y} - y_0)/c_y & ⑥ &= ②D - r_{21} \\
③ &= ①D - r_{11} & ⑦ &= ②E - r_{22} \\
④ &= ①E - r_{12} & ⑧ &= ②F - r_{23} \\
& & ⑨ &= ②r_{12} - ①r_{22}
\end{aligned} \qquad (154)$$

$$\begin{aligned}
A_x &= +c_x(① \cdot ⑨ + ⑦) \\
B_x &= +c_x[(1 + ①^2) \sin\kappa + ① \cdot ② \cos\kappa] \\
C_x &= +c_x② \\
D_x &= \frac{c_x}{q} ③ \\
E_x &= \frac{c_x}{q} ④ \\
F_x &= \frac{c_x}{q} ⑤ \\
G_x &= ① \\
H_x &= 1 + P_x \\
I_x &= Q_x \\
M_x &= d_x d^2 \\
N_x &= d_x d^4 \\
O_x &= d_x d^6 \\
A_y &= +c_y② \cdot ⑨ \\
B_y &= +c_y[(1 + ②^2) \cos\kappa + ① \cdot ② \sin\kappa] \\
C_y &= -c_y① \\
D_y &= \frac{c_y}{q} ⑥ \\
E_y &= \frac{c_y}{q} ⑦ \\
F_y &= \frac{c_y}{q} ⑧ \\
G_y &= ② \\
H_y &= P_y \\
I_y &= 1 + Q_y \\
M_y &= d_y d^2 \\
N_y &= d_y d^4 \\
O_y &= d_y d^6
\end{aligned} \qquad (155)$$

$$
\begin{aligned}
P_x &= -\frac{\Delta R}{d} - d_x^2 D_r - d_x D_w \cos\varphi_T \\
&\quad - 4d_x[K_x + (2d_x^2 + d_y^2)K_5]\cos\varphi_T \\
&\quad - 2d_y[K_4 + (d_x^2 + 3d_y^2)K_5]\sin\varphi_T \\
P_y &= -d_x d_y D_r - d_x D_w \sin\varphi_T \\
&\quad - 2d_y\{[K_4 + (3d_x^2 + d_y^2)K_5]\cos\varphi_T \\
&\quad + 2d_y K_5 \sin\varphi_T\} \\
Q_x &= -d_x d_y D_r - d_y D_w \cos\varphi_T \\
&\quad - 2d_x\{[K_4 + (d_x^2 + 3d_y^2)K_5]\sin\varphi_T \\
&\quad + 2d_x d_y K_5 \cos\varphi_T\} \\
Q_y &= -\frac{\Delta R}{d} - d_y D_r - d_y D_w \sin\varphi_T \\
&\quad - 2d_x[K_4 + (d_x^2 + 2d_y^2)K_5]\cos\varphi_T \\
&\quad - 4d_y[K_4 + (d_x^2 + 2d_y^2)K_5]\sin\varphi_T
\end{aligned}
$$

where

$$
\begin{aligned}
d_x &= (l_{\bar{x}} - x_s) \qquad d_y = (l_{\bar{y}} - y_s) \\
D_r &= [2K_1 + 4K_2 d^2 + 6K_3 d^4] \\
D_w &= [2K_4 + 4K_5 d^2] \\
d^2 &= d_x^2 + d_y^2 \\
R_x &= d^2\cos\varphi_T + 2(d_x^2\cos\varphi_T + d_x d_y \sin\varphi_T) \\
R_y &= d^2\sin\varphi_T + 2(d_y^2\sin\varphi_T + d_x d_y \cos\varphi_T) \\
S_x &= d^4\cos\varphi_T + 2d^2(d_x^2\cos\varphi_T + d_x d_y \sin\varphi_T) \\
S_y &= d^4\sin\varphi_T + 2d^2(d_y^2\sin\varphi_T + d_x d_y \cos\varphi_T) \\
T_x &= -\sin\varphi_T(K_4 d^2 + K_5 d^4) \\
&\quad + 2(K_4 + K_5 d^2)(d_x d_y \cos\varphi_T - d_x^2 \sin\varphi_T) \\
T_y &= \cos\varphi_T(K_4 d^2 + K_5 d^4) \\
&\quad + 2(K_4 + K_5 d^2)(d_y^2\cos\varphi_T - d_x d_y \sin\varphi_T)
\end{aligned}
$$

$$
\begin{aligned}
U_x &= l_y \qquad U_y = 0 \\
Z_x &= -1 \qquad Z_y = -1
\end{aligned}
\tag{155a}
$$

With an arbitrarily selected mean error of unit weight m_0 before adjustment, the weight matrix [cf. (196)] assigned to the observation equations (151) and (152) is computed. The adjustment then determines the $\Delta\mathbf{u}$ vector subject to the condition

$$\Delta\mathbf{u}^*\mathbf{P}\Delta\mathbf{u} = \text{Min} \tag{156}$$

The required parameters are then

$$\mathbf{u} = \mathbf{u}_0 + \Delta\mathbf{u} \tag{157}$$

where $\mathbf{u}_0$ are the approximations for the parameters [cf. (208) to (210)].

2.7.4 Mathematical Model for the Photogrammetric Camera

The various applications of the photogrammetric measurements method each require the development of an analytical expression from the general formulation. A special application will now be shown as the first step in satellite triangulation. As outlined initially in sec. 2.3 the parameters needed for the reconstruction of the bundle from the star images (in this case: ϵ, c_x, c_y, x_0, y_0, x_s, y_s, K_1, K_2, K_3, K_4, K_5, φ_T) and of the exterior orientation (α, φ, κ) are to be computed.

Since the directions to the fixed stars refer to the center of the unit sphere at the center of projection, the coordinates X_0, Y_0, Z_0 of (148) and (149) are set to zero. Furthermore it was shown toward the end of sec. 2.3 that the coordinates expressing the direction to a star can be transformed to standard coordinates ξ_r, η_r, 1 (cf. fig. 24 and (66), (67) with (61)). This changes (148) and (149) into

$$
\begin{aligned}
F &= -l_x - l_y \cdot \epsilon + \frac{c_x[r_{11}\xi_r + r_{12}\eta_r + r_{13}]}{r_{31}\xi_r + r_{32}\eta_r + r_{33}} + x_0 \\
&\quad + (l_{\bar{x}} - x_s)(K_1 d^2 + K_2 d^4 + K_3 d^6) \\
&\quad + \{2(l_{\bar{x}} - x_s)(l_{\bar{y}} - y_s)\sin\varphi_T + [3(l_{\bar{x}} - x_s)^2 \\
&\quad + (l_{\bar{y}} - y_s)^2]\cos\varphi_T\}(K_4 + K_5 d^2) = 0
\end{aligned}
\tag{158}
$$

$$
\begin{aligned}
G &= -l_y + \frac{c_y[r_{21}\xi_r + r_{22}\eta_r + r_{23}]}{r_{31}\xi_r + r_{32}\eta_r + r_{33}} + y_0 \\
&\quad + (l_{\bar{y}} - y_s)(K_1 d^2 + K_2 d^4 + K_3 d^6) \\
&\quad + \{[3(l_{\bar{y}} - y_s)^2 + (l_{\bar{x}} - x_s)^2]\sin\varphi_T \\
&\quad + 2(l_{\bar{x}} - x_s)(l_{\bar{y}} - y_s)\cos\varphi_T\}(K_4 + K_5 d^2) = 0.
\end{aligned}
\tag{159}
$$

We note, first of all, that right ascension α and declination δ, together with their mean errors, are given quantities. Consequently it is necessary to minimize the sum of the $v_\alpha v_\alpha + v_\delta v_\delta$), weighted in accordance with the weight matrix $\mathbf{P}_{\alpha,\delta}$ given for the stars, not the sum of squares of the v_ξ and v_η residuals. To accomplish this the ξ_r and η_r are differentiated with respect to α and δ, and the coefficients in the observation equations used to compute the $\Delta\xi$ and $\Delta\eta$ are multiplied accordingly. After appropriate arrangement coefficients are obtained in the observation equations which do not refer to the corrections $\Delta\xi$ and $\Delta\eta$, but to v_α and v_δ. Using (66) and (67) one obtains in the y' system

$$\xi_r = \frac{y_1'}{y_3'} \tag{160}$$

$$\eta_r = \frac{y_2'}{y_3'} \tag{161}$$

from which, omitting the index r

$$d\xi = \frac{y_3' dy_1' - y_1' dy_3'}{y_3'^2} \tag{162}$$

$$d\eta = \frac{y_3' dy_2' - y_2' dy_3'}{y_3'^2} \tag{163}$$

From (1) with (20), (23) and figure 9 follows:

$$\mathbf{x}' = \begin{bmatrix} x_1' \\ x_2' \\ x_3' \end{bmatrix} = \begin{bmatrix} \cos\delta\cos t \\ -\cos\delta\sin t \\ \sin\delta \end{bmatrix} = \begin{bmatrix} \sin\varphi' & 0 & \cos\varphi' \\ 0 & 1 & 0 \\ -\cos\varphi' & 0 & \sin\varphi' \end{bmatrix} \begin{bmatrix} y_1' \\ y_2' \\ y_3' \end{bmatrix}. \tag{164}$$

Differentiating (164), noting that $dt = -d\alpha$, gives

$$d\mathbf{x}' = \begin{bmatrix} -x_2' & -\sin\delta\cos t \\ x_1' & \sin\delta\sin t \\ 0 & \cos\delta \end{bmatrix} \begin{bmatrix} d\alpha \\ d\delta \end{bmatrix} \tag{165}$$

From (23)

$$d\mathbf{y}' = \mathbf{R}(90° - \varphi')d\mathbf{x}' \tag{166}$$

which with (165) gives

$$d\mathbf{y}' = \begin{bmatrix} -x_2'\sin\varphi' & -(x_3'\cos t\sin\varphi' + \cos\delta\cos\varphi') \\ x_1' & x_3'\sin t \\ -x_2'\cos\varphi' & (-x_3'\cos t\cos\varphi' + \cos\delta\sin\varphi') \end{bmatrix} \times \begin{bmatrix} d\alpha \\ d\delta \end{bmatrix}. \tag{167}$$

With the relations found in (160), (161) and (164), the application of (167) with (162) and (163) yields

$$\frac{d\eta}{d\alpha} = \frac{-y_2'\sin\varphi'}{y_3'} + \xi_r\frac{y_2'\cos\varphi'}{y_3'} = \eta_r(\xi_r\cos\varphi' - \sin\varphi') \tag{168}$$

$$\frac{d\eta}{d\alpha} = \frac{y_1'}{y_3'} + \eta_r{}^2\cos\varphi' = \xi_r\sin\varphi' + (1 + \eta_r{}^2)\cos\varphi' \tag{169}$$

and similarly, omitting the intermediate steps:

$$\frac{d\xi}{d\delta} = -\cos t\,(1 + \xi_r{}^2 + \eta_r{}^2) \tag{170}$$

$$\frac{d\eta}{d\delta} = \sin t\,\sin\varphi'\,(1 + \xi_r{}^2 + \eta_r{}^2) \tag{171}$$

Other quantities needed are

$$\frac{\partial F}{\partial\alpha} = J_x{}^* = J_x\cdot\frac{d\xi}{d\alpha} + K_x\cdot\frac{d\eta}{d\alpha} \tag{172}$$

$$\frac{\partial F}{\partial\delta} = K_x{}^* = J_x\cdot\frac{d\xi}{d\delta} + K_x\cdot\frac{d\eta}{d\delta} \tag{173}$$

$$\frac{\partial G}{\partial\alpha} = J_y{}^* = J_y\cdot\frac{d\xi}{d\alpha} + K_y\cdot\frac{d\eta}{d\alpha} \tag{174}$$

$$\frac{\partial G}{\partial\delta} = K_y{}^* = J_y\cdot\frac{d\xi}{d\delta} + K_y\cdot\frac{d\eta}{d\delta} \tag{175}$$

in which $\frac{d\xi}{d\alpha}, \frac{d\xi}{d\delta}, \frac{d\eta}{d\alpha}, \frac{d\eta}{d\delta}$ are given with (168) to (171) and J_x, J_y, K_x, and K_y are computed from (153) to (155).

If one accepts the coordinates corrected for refraction ξ_r and η_r, the corresponding linearized observation equations can be set up directly with (158), (159), and the introduction of (172) to (175). Just as the central perspective bundle was altered by additional physical influences, the direction given with the coordinates ξ_r, η_r can be subjected to a further refraction correction by further improving the τ constants used for the original refraction correction.

In consonance with (40) one can therefore write

$$\Delta r_\infty = \mathbf{T}^{\frac{1}{2}}\mathbf{W}\left(\tan\frac{\beta}{2}\Delta\tau_1 + \tan^3\frac{\beta}{2}\Delta\tau_2 + \tan^5\frac{\beta}{2}\Delta\tau_3 + \tan^7\frac{\beta}{2}\Delta\tau_4\right) \tag{176}$$

Assuming further that refraction does not affect azimuth, we have ξ_r/η_r = constant and therefore

$$\frac{\Delta\xi}{\Delta\eta} = \frac{\xi_r}{\eta_r} \tag{177}$$

and, in analogy with (66) and (67)

$$\xi_r{}^2 + \eta_r{}^2 = \tan^2 z_r = \frac{y_1'^2 + y_2'^2}{y_3'^2}. \tag{178}$$

Differentiating (178) gives

$$\xi_r\Delta\xi + \eta_r\Delta\eta = \tan z_r(1 + \tan^2 z_r)\Delta z. \tag{179}$$

Substituting (171) in (179) gives

$$\Delta z = \Delta r_\infty \tag{180}$$

$$\Delta\xi = \xi_r \frac{(1+\tan^2 z_r)}{\tan z_r}\Delta r_\infty = \frac{2\xi_r}{\sin 2z_r}\Delta r_\infty \tag{181}$$

$$= \frac{y_1'}{y_3'^2}(y_1'^2 + y_2'^2)^{-\frac{1}{2}}\Delta r_\infty$$

$$\Delta\eta = \eta_r \frac{(1+\tan^2 z_r)}{\tan z_r}\Delta r_\infty = \frac{2\eta_r}{\sin 2z_r}\Delta r_\infty \tag{182}$$

$$= \frac{y_2'}{y_3'^2}(y_1'^2 + y_2'^2)^{-\frac{1}{2}}\Delta r_\infty,$$

in which Δr_∞ is given with (176).

Taking into consideration (176), (181), and (182), and using the designations of (153), the partial derivatives of the functions F and G needed in the refraction correction are now introduced, giving

$$\frac{\partial F}{\partial \tau} = \begin{bmatrix} V_x \\ W_x \\ X_x \\ Y_x \end{bmatrix} = \begin{bmatrix} \tan\frac{\beta}{2} \\ \tan^3\frac{\beta}{2} \\ \tan^5\frac{\beta}{2} \\ \tan^7\frac{\beta}{2} \end{bmatrix} \cdot \tau_x \tag{183}$$

$$\frac{\partial G}{\partial \tau} = \begin{bmatrix} V_y \\ W_y \\ X_y \\ Y_y \end{bmatrix} = \begin{bmatrix} \tan\frac{\beta}{2} \\ \tan^3\frac{\beta}{2} \\ \tan^5\frac{\beta}{2} \\ \tan^7\frac{\beta}{2} \end{bmatrix} \cdot \tau_y \tag{184}$$

where

$$\tau_x = \mathbf{T}^{\frac{1}{2}} W \frac{J_x y_1' + K_x y_2'}{y_3'^2(y_1'^2 + y_2'^2)^{\frac{1}{2}}} = \mathbf{T}^{\frac{1}{2}} W \frac{2(J_x\xi_r + K_x\eta_r)}{\sin 2z_r} \tag{185}$$

and

$$\tau_y = \mathbf{T}^{\frac{1}{2}} W \frac{J_y y_1' + K_y y_2'}{y_3'^2(y_1'^2 + y_2'^2)^{\frac{1}{2}}} = \mathbf{T}^{\frac{1}{2}} W \frac{2(J_y\xi_r + K_y\eta_r)}{\sin 2z_r} \tag{186}$$

with $\mathbf{T}$ and W as in (40).

The observation equations (151), (152) for the single camera are therefore set up in accordance with (158), (159), (153) to (155) and with (172) to (175), (183), and (184). Since the skew of the comparator axes ϵ is always small the term $v_{l_y}\epsilon$ is negligible. We thus have the system of observation equations

$$\mathbf{A}\mathbf{v}_u + \mathbf{l} = 0 \tag{187}$$

with the weight matrix $\mathbf{P}_u = m_0^2\boldsymbol{\sigma}_u^{-1}$, where, in general, we have for each pair of observation equations

$\mathbf{v}_u^*$ $\quad$ $\boldsymbol{\Delta}^*$ $\quad$ $\mathbf{v}_{l_{x,y}}^*$ $\quad$ $\mathbf{v}_{\alpha,\delta}^*$ $\quad$ $\boldsymbol{\Delta}_0^*$

$$\mathbf{A} = \begin{array}{c|cc|ccccccccccccccccccccc} & l_x & l_y & \alpha^1 & \delta & \alpha & \omega & \kappa & c_x & c_y & x_0 & y_0 & K_1 & K_2 & K_3 & x_s & y_s & K_4 & K_5 & \varphi_T & \epsilon & \tau_1 & \tau_2 & \tau_3 & \tau_4 \\ \hline & -1 & - & J_x^* & K_x^* & A_x & B_x & C_x & G_x & - & H_x & I_x & M_x & N_x & O_x & P_x & Q_x & R_x & S_x & T_x & U_x & V_x & W_x & X_x & Y_x \\ & - & -1 & J_y^* & K_y^* & A_y & B_y & C_y & - & G_y & H_y & I_y & M_y & N_y & O_y & P_y & Q_y & R_y & S_y & T_y & - & V_y & W_y & X_y & Y_y \end{array}$$

$-\mathbf{A}_l$ $\quad$ $\mathbf{B}_{\alpha,\delta}$ $\quad$ $\mathbf{B}_0$ $\quad$ $\mathbf{B}$

α^1 = right ascension

(188)

$\mathbf{l}$ is computed [cf. (151), (152)] from the approximation and measured values as

$$\mathbf{l}_i = \begin{bmatrix} F_0 \\ G_0 \end{bmatrix}_i \tag{189}$$

$$\mathbf{P}_u = \begin{bmatrix} \mathbf{P}_{l_x, l_y} & 0 & 0 & 0 \\ 0 & \mathbf{P}_{\alpha,\delta} & 0 & 0 \\ 0 & 0 & \mathbf{P}_0 & 0 \\ 0 & 0 & 0 & \mathbf{P}_\tau \end{bmatrix} \tag{190}$$

Theoretically, the $\mathbf{P}_u$ matrix (190) could be completely filled but it is necessary to normalize all weights with respect to a selected value for m_0 and, in addition, the mean errors of the rotation parameters must be in radians. This makes it possible to account for all existing correlations. In practice however, as indicated in (190), there are uncorrelated groups since no correlation exists between the $\boldsymbol{\sigma}_l$ matrix specifying the accuracy of comparator measurements, the $\boldsymbol{\sigma}_{\alpha,\delta}$ matrix specifying the accuracy of the star coordinates, the $\boldsymbol{\sigma}_0$ matrix specifying the accuracy of the other, chiefly photogrammetric, parameters and the $\boldsymbol{\sigma}_\tau$ matrix that specifies the accuracy of the refraction determination.

Since in what follows it will be repeatedly necessary to compute accuracy criteria, the meaning of the various designations used will now be explained.

2.7.4.1 Measures of accuracy before adjustment

The mean error of unit weight arbitrarily fixed before the adjustment is m_0. The mean error of a measurement i is designated m_i. Hence

$$p_i = \frac{m_0^2}{m_i^2} \tag{191}$$

The corresponding weight matrix, e.g., for the comparator measurements l_x, l_y is

$$\mathbf{P}_{l_i} = \begin{bmatrix} p_{l_x} & p_{l_{x,y}} \\ p_{l_{x,y}} & p_{l_y} \end{bmatrix} = m_0^2 \begin{bmatrix} \sigma_{l_x}^2 & \sigma_{l_{x,y}} \\ \sigma_{l_{x,y}} & \sigma_{l_y}^2 \end{bmatrix}^{-1} = m_0^2 \boldsymbol{\sigma}_{li}^{-1} \tag{192}$$

with $\sigma_{l_{x,y}} = (\rho_{x,y}\, \sigma_{l_x}\, \sigma_{l_y})$; $\rho_{x,y}$ denotes the correlation coefficient which = 0 for comparator measurements when the comparator has independent mechanisms for measuring x and y.

2.7.4.2 Measures of accuracy after adjustment

The mean error of unit weight after the adjustment is

$$s_0 = \left(\frac{\mathbf{v}^* \mathbf{P} \mathbf{v}}{n - u} \right)^{\frac{1}{2}} \tag{193}$$

and the mean error of an observation after the adjustment is

$$s_i = \frac{s_0}{m_0} m_i \tag{194}$$

With respect to the unknowns u computed in the adjustment there exists the relation

$$s_0^2 \mathbf{N}_u^{-1} = \mathbf{s}_u^2 = \boldsymbol{\sigma}_u = \underbrace{\begin{bmatrix} \underline{s_{u_1 u_1}} & s_{u_1 u_2} & \cdots & s_{u_1 u_n} \\ & \underline{s_{u_2 u_2}} & \cdots & s_{u_2 u_n} \\ & & \ddots & \vdots \\ & & & \underline{s_{u_n u_n}} \end{bmatrix}}_{\text{Covariance matrix}} \tag{195}$$

in which $s_{u_i u_j} = \rho_{ij} s_{u_i} s_{u_j}$. With (193) and (195) we obtain

$$\mathbf{P}_u = m_0^2 \boldsymbol{\sigma}_u^{-1} = \frac{m_0^2}{s_0^2} \mathbf{N}_u. \tag{196}$$

Omitting the index u in order to simplify the notation we have $s_{ij} = \rho_{ij} s_i s_j$ and the dimensionless correlation matrix that corresponds to (195) is then

$$\boldsymbol{\rho} = \begin{bmatrix} s_1^{-1} & & & \\ & s_2^{-1} & & \\ & & \ddots & \\ & & & s_n^{-1} \end{bmatrix} \mathbf{s}^2 \begin{bmatrix} s_1^{-1} & & & \\ & s_2^{-1} & & \\ & & \ddots & \\ & & & s_n^{-1} \end{bmatrix} = \begin{bmatrix} 1 & \rho_{12} & \cdots & \rho_{1n} \\ \rho_{12} & 1 & & \vdots \\ \vdots & & \ddots & \vdots \\ \rho_{1n} & \cdots & & 1 \end{bmatrix} \tag{197}$$

in which all $\rho_{ii} = 1$ and the numerical values of the correlation coefficients ρ_{ij} as well as that of the determinant $|\rho|$ lie between 0 and 1.

Finally it is desirable to compute the axes and orientation of error ellipses and of the error ellipsoids arising in connection with the spatial triangulation to be discussed later. In a solution designed for electronic computation it is convenient to treat the relatively simple two-dimensional case as a special case of the three-dimensional solution here given.

On development of the determinant, the characteristic equation

$$\begin{bmatrix} s_x^2-\lambda & s_{x,y} & s_{x,z} \\ s_{x,y} & s_y^2-\lambda & s_{y,z} \\ s_{x,z} & s_{y,z} & s_z^2-\lambda \end{bmatrix} = 0 \qquad (198)$$

becomes a polynomial equation in λ, the eigenvalues of the covariance matrix.

$$\lambda^3 - r\lambda^2 + s\lambda - t = 0 \qquad (199)$$

The lengths of the semiaxes of the error ellipsoid are square roots of the roots, λ_1, λ_2, λ_3 of this equation. To obtain the direction cosines of the axes the eigenvectors $\mathbf{x}_1$, $\mathbf{x}_2$, and $\mathbf{x}_3$ are computed in 3 separate steps by substituting in turn each of the $\lambda_{1,2,3}$ values in (198) and solving the 3 sets of simultaneous, linear, homogeneous equations:

$$\begin{bmatrix} s_x^2-\lambda & s_{x,y} & s_{x,z} \\ s_{x,y} & s_y^2-\lambda & s_{y,z} \\ s_{x,z} & s_{y,z} & s_z^2-\lambda \end{bmatrix} \begin{bmatrix} x_{i1} \\ x_{i2} \\ x_{i3} \end{bmatrix} = 0 \qquad (200)$$

Each of the three solutions $(x_{i_1}, x_{i_2}, x_{i_3})$ contains a free variable with which the vector $\mathbf{x}_i$ can be expressed in length λ_i or as a unit vector, thus defining the direction of the axis. The procedure is described in [40].

For the two-dimensional case the 2×2 covariance matrix is extended to a 3×3 matrix by introducing the number 1, or any other number, as the third diagonal term and zeros for the other additional entries to account for the fictitious third dimension. The capacity of the larger electronic computers makes it attractive to design a program which can compute eigenvalues and vectors for the n-dimensional case. However the computational effort increases with the third power of n.

If maximum accuracy is desired in satellite triangulation it is necessary to recalibrate the camera for each event. Hence $\mathbf{P}_0$ is a null matrix. The need for an additional refraction correction is questionable because of the existing correlation between the τ values and the elements of exterior orientation, especially when the cameras are equipped with objectives requiring small viewing angles. When the $\Delta\tau_i$ corrections are not computed the $\mathbf{P}_u$ matrix consists of only the $\mathbf{P}_l$ and $\mathbf{P}_{\alpha,\delta}$ portions. As shown in (188) $\mathbf{A}_l$ is always a unit matrix. Introducing, for the moment, $\mathbf{P}_{\alpha,\delta}$ as a null matrix and with $\mathbf{P}_l$ from (192), the normal equations system corresponding to the observation equations (187) is

$$\sum_{i=1}^{m} [\mathbf{B}^*\mathbf{P}_l\mathbf{B}]_i\Delta + \sum_{i=1}^{m} [\mathbf{B}^*\mathbf{P}_l\mathbf{l}]_i = 0 \qquad (201)$$

m = number of star images.

Each pair of observation equations for an individual star image i contributes to the normal equations system (201) in the following manner:

$$\mathbf{B}_i^*\mathbf{P}_{l_i}\mathbf{B}_i\Delta + \mathbf{B}^*\mathbf{P}_{l_i}\mathbf{l}_i = 0. \qquad (202)$$

Subdividing the $\mathbf{B}$ matrix further by using the notations introduced in (188) results in the following scheme for (202)

$$\begin{matrix} \mathbf{v}_{\alpha,\delta} & \Delta_0 \end{matrix}$$
$$\begin{bmatrix} (\mathbf{B}^*_{\alpha,\delta}\mathbf{P}_l\mathbf{B}_{\alpha,\delta})_i & (\mathbf{B}^*_{\alpha,\delta}\mathbf{P}_l\mathbf{B}_0)_i \\ (\mathbf{B}^*_0\mathbf{P}_l\mathbf{B}_{\alpha,\delta})_i & (\mathbf{B}^*_0\mathbf{P}_l\mathbf{B}_0)_i \end{bmatrix} + \begin{bmatrix} (\mathbf{B}^*_{\alpha,\delta}\mathbf{P}_l\mathbf{l})_i \\ (\mathbf{B}^*_0\mathbf{P}_l\mathbf{l})_i \end{bmatrix} = 0. \qquad (203)$$

The accuracy of the given α, δ values expressed with the $\mathbf{P}_{\alpha,\delta}$ matrix is, in accordance with the concepts developed in [39], taken into consideration by replacing the term $(\mathbf{B}_{\alpha,\delta}\mathbf{P}_l\mathbf{B}_{\alpha,\delta})_i$ in (203) with

$$(\mathbf{B}^*_{\alpha,\delta}\mathbf{P}_l\mathbf{B}_{\alpha,\delta} + \mathbf{P}_{\alpha,\delta})_i. \qquad (204)$$

Elimination of the $\mathbf{v}_{\alpha,\delta}$ vector reduces the normal equations system to

$$\overbrace{\sum^{i} [\mathbf{B}_0^*\mathbf{P}_l\mathbf{B}_0 - \mathbf{B}_0^*\mathbf{P}_l\mathbf{B}_{\alpha,\delta}(\mathbf{B}^*_{\alpha,\delta}\mathbf{P}_l\mathbf{B}_{\alpha,\delta} + \mathbf{P}_{\alpha,\delta})^{-1}\mathbf{B}^*_{\alpha,\delta}\mathbf{P}_l\mathbf{B}_0]_i}^{\mathbf{N}}\Delta_0 +$$
$$\underbrace{\sum^{i} [\mathbf{B}_0^*\mathbf{P}_l\mathbf{l} - \mathbf{B}_0^*\mathbf{P}_l\mathbf{B}_{\alpha,\delta}(\mathbf{B}^*_{\alpha,\delta}\mathbf{P}_l\mathbf{B}_{\alpha,\delta} + \mathbf{P}_{\alpha,\delta})^{-1}\mathbf{B}^*_{\alpha,\delta}\mathbf{P}_l\mathbf{l}]_i}_{-\Delta\mathbf{l}} = 0. \qquad (205)$$

From (205), finally, the vector Δ_0 of parameter corrections is obtained as

$$\Delta_0 = \mathbf{N}^{-1}\Delta\mathbf{l} \tag{206}$$

and

$$\mathbf{O} = \mathbf{O}_0 + \Delta_0 \tag{207}$$

as well as the mean error of unit weight after adjustment from (193).

In consequence of the fact that in linearizing the original functions F and G, terms of the second and higher order were neglected, the result of an adjustment must be iterated until the change in $\mathbf{v}^*\mathbf{P}\mathbf{v}$ in successive iterations becomes equal to, or less than, a prescribed tolerance.

The treatment of given right ascension and declination values in the above manner allows the determination of unknown star coordinates by simply introducing the $\mathbf{P}_{\alpha,\delta}$ matrix as a null matrix. It is, of course, necessary in this case to find adequate approximation values (α_0, δ_0) to replace the normally given α, δ's.

Although the determination of the coordinates of unknown stars is merely incidental to the problem at hand, the use of uncatalogued stars contributes to the calibration of the camera whenever such a star is photographed at sufficiently large intervals of time and at least twice. The corresponding angle of the Earth's rotation can be introduced into the adjustment by means of the associated instants of time to help fix the geometry. Thus the images of such stars furnish additional data and contribute in a small way to the determination of the parameters of interior orientation. In satellite triangulation it is scarcely possible to gain any advantage from this, because the total period of observation of an event, i.e., the interval elapsing between the pre- and postsatellite pass star recordings is deliberately held to a minimum in order to reduce the probability of changes in environmental conditions. Experience has shown that elimination of these changes is not always possible, especially when the requirements for accuracy are high.

For that reason an observation technique was developed to detect small variations in camera orientation occurring during the normal 20- to 30-minute period of observation. The method provides for star observations during the actual period of transit of the satellite, as well as before and after. Since there is no choice but to assume that the elements of interior orientation do not vary significantly within the period of observation, a mathematically closer simulation of the actual situation is obtained by computing three separate and independent exterior orientations, one for each of the three periods—before, after, and during the transit of the satellite across the camera's field of view. The single camera observation equations (187) are therefore augmented to include three sets of corrections to the exterior orientation $\Delta\alpha$, $\Delta\omega$, $\Delta\kappa$ instead of just one subset. The first term in (205), schematically represented, will then have the form shown in figure 33.

In order to increase the internal accuracy of the photogrammetric measuring process, particularly to minimize the influence of the emulsion and scintillation effects, a sequence of (usually) five consecutive single images is measured for each star. This means that each of these l_x, l_y coordinate measurements has its individual residuals, but only one pair of corrections to the star's right ascension and declination values may be postulated. Hence, for a star recorded n times it is necessary first to construct the partial normal equations system (203) as the sum of the corresponding n subsystems, followed by the addition of $\mathbf{P}_{\alpha,\delta}$ just once in accordance with (204) before continuing the computations with the elimination of the v_α and v_δ to set up the final normal equations (205). If $\Delta\tau$ corrections are to be computed it is advisable to first carry out a solution without the $\Delta\tau$, to avoid the unfavorable influence of existing correlations on the numerical adjustment. In a final iteration the $\Delta\tau$ will then be included as additional unknowns to produce the result. If measurements of unknown stars are included in the system, it is best not to set up coefficients for refraction corrections in the relevant observation equations, because of the limited geometrical content of such equations.

Whenever, for example, values for certain photogrammetric parameters, as determined from an independently executed camera calibration e, are to be introduced together with their measures of accuracy into the adjustment, the corresponding weight matrix $\mathbf{P}_{0_e}$ (cf. (196))

$$\mathbf{P}_{0_e} = \frac{m_0^2}{s_{0_e}^2}\mathbf{N}_{0_e} \tag{208}$$

must be added to normal equations system (205). It must be borne in mind that this $\mathbf{P}_{0_e}$ matrix has reference to the given values which are appropriately used as approximation values in the first iteration. Since in the course of the iteration, however, the approximations for the $\mathbf{O}_0$ vector undergo changes, a modification of the vector of absolute terms in the normal equations system is necessary at each iteration step in that a vector

$$\mathbf{P}_{0_e}\Delta\mathbf{l}_{0_e} \tag{209}$$

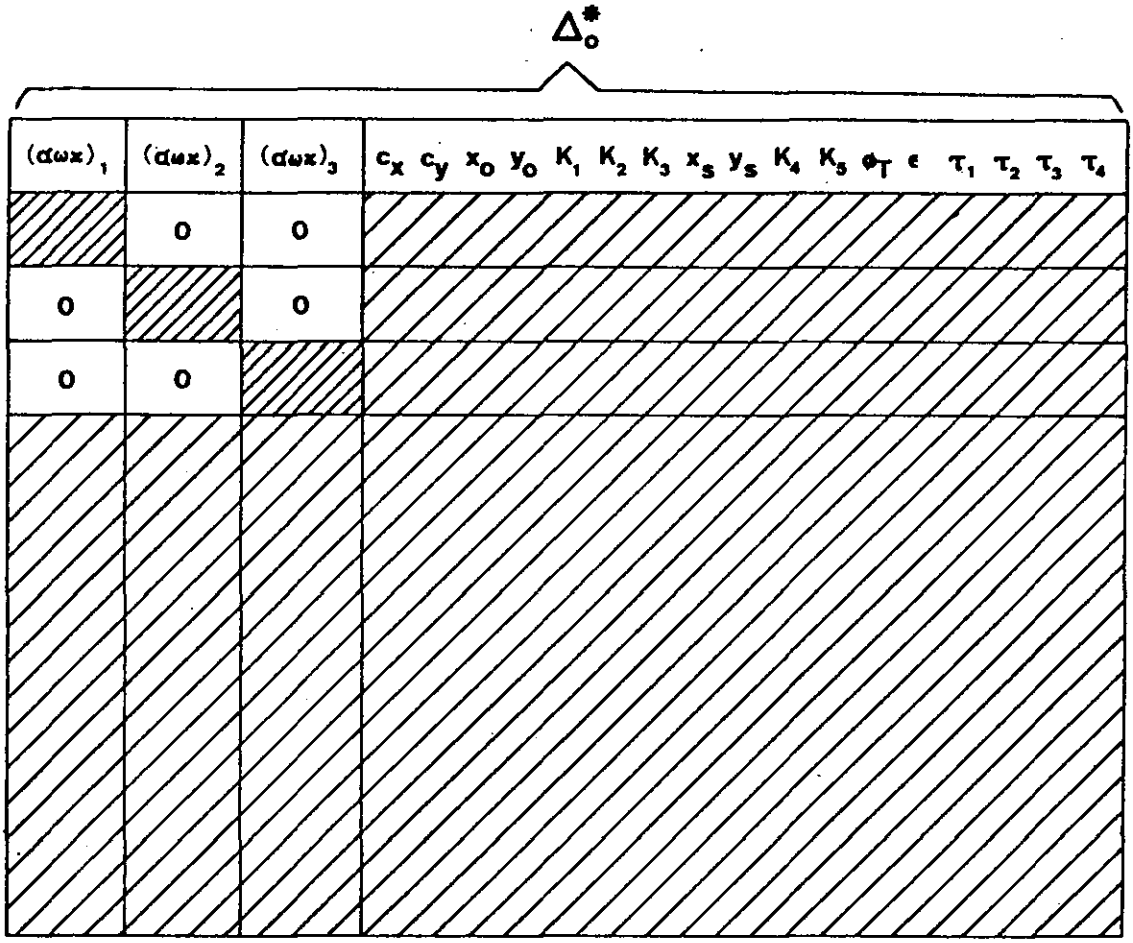

Figure 33.—Schematic of the reduced normal equations system.

is added to the $\Delta\mathbf{l}$ vector for that iteration, where

$$\Delta\mathbf{l}_{0_e} = \mathbf{O}_{0_e} - \mathbf{O}_e. \tag{210}$$

The purpose and effect of this operation is to initialize the $\mathbf{O}_e$ components of the $\mathbf{O}_0$ vector to their given values before proceeding with the next iteration. For parameters that are not given the $\Delta\mathbf{l}_{0_e}$ vector has zero components.

It can be argued that the determination of three different sets of orientation parameters does not lead to an optimum solution in cases where the exterior orientation of the camera does not change at all during the entire observation, so that only one or two sets of α, ω, κ are justified. For this reason we first compute directions in space for a number of fictitious images along the plate diagonal, using the results of the present solution. For each of the fictitious point images whose coordinates x, y are assumed free of error, three unit vectors corresponding to the three orientations are computed by use of (81) in the y' system:

$$\mathbf{y}'_{j=1,2,3} = \mathbf{R}'_{\nu_{j=1,2,3}}(\alpha,\omega,\kappa)\frac{\mathbf{p}}{|\mathbf{p}|} \tag{211}$$

where

$$\mathbf{p} = \begin{bmatrix} \bar{x} \\ \bar{y}\dfrac{c_x}{c_y} \\ c \end{bmatrix} \tag{212}$$

and

$$|\mathbf{p}| = \left[\bar{x}^2 + \left(\bar{y}\frac{c_x}{c_y}\right)^2 + c_x^2\right]^{\frac{1}{2}}. \tag{213}$$

In accordance with (107), premultiplication of the $\mathbf{y}'_{j=1,2,3}$ vectors with $R(270^0 + \phi')$ yields the corresponding $\mathbf{x}'_{j=1,2,3}$ vectors. With the $\mathbf{y}'$ or $\mathbf{x}'$ vectors, as the case may be, compute the corresponding

ξ and η values with (28) and the azimuths and zenith distances or hour angles and declinations with (29).

Next, compute the small angle ϵ_{jk} between the computed directions for each pair from the $\mathbf{y}'_{j=1,2,3}$ or $\mathbf{x}'_{j=1,2,3}$. For the combination 1,2 in an x' system one obtains, for example

$$\epsilon_{1,2} = |\mathbf{x}'_2 - \mathbf{x}'_1| \tag{214}$$

or, in radians,

$$\epsilon_{1,2} = [(x'_{2_1} - x'_{1_1})^2 + (x'_{2_2} - x'_{1_2})^2 + (x'_{2_3} - x'_{1_3})^2]^{\frac{1}{2}}. \tag{215}$$

If the differences between corresponding right ascensions and declinations or azimuths and zenith distances, so computed from the three orientations, exceed their confidence limits, a timing error or camera motion may be the cause. Before one can decide whether these computed differences in direction are significant, one must find the mean errors of either the direction components (α, δ) and (A, z) or at least of the angles ϵ_{jk}, which can be looked upon as combinations in pairs of the computed (α, δ) or (A, z).

Since α and δ are parameters of the mathematical model on which the adjustment is based, the following solution is offered. Using (204) and taking into account the considerations leading to (202) and (203), the first term of the normal equations system (201) can be represented schematically as

$$\begin{bmatrix} (\mathbf{B}^*_{\alpha,\delta}\mathbf{P}_l\mathbf{B}_{\alpha,\delta} + \mathbf{P}_{\alpha,\delta})_1 & \mathbf{O} & \mathbf{O} & (\mathbf{B}^*_{\alpha,\delta}\mathbf{P}_l\mathbf{B}_0)_1 \\ \mathbf{O} & \ddots & \mathbf{O} & \vdots \\ \mathbf{O} & \mathbf{O} & (\mathbf{B}^*_{\alpha,\delta}\mathbf{P}_l\mathbf{B}_{\alpha,\delta} + \mathbf{P}_{\alpha,\delta})_m & (\mathbf{B}^*_{\alpha,\delta}\mathbf{P}_l\mathbf{B}_0)_m \\ (\mathbf{B}^*_0\mathbf{P}_l\mathbf{B}_{\alpha,\delta})_1 & \cdots & (\mathbf{B}^*_0\mathbf{P}_l\mathbf{B}_{\alpha,\delta})_m & \sum_{i=1}^{i=m} (\mathbf{B}^*_0\mathbf{P}_l\mathbf{B}_0)_i \end{bmatrix} = \begin{bmatrix} \mathbf{A}_{11} & \mathbf{A}_{12} \\ \mathbf{A}^*_{12} & \mathbf{A}_{22} \end{bmatrix}. \tag{216}$$

Designate the inverse of the matrix (216) as

$$\begin{bmatrix} \mathbf{A}_{11} & \mathbf{A}_{12} \\ \mathbf{A}_{12} & \mathbf{A}_{22} \end{bmatrix}^{-1} = \begin{bmatrix} \mathbf{Q}_{11} & \mathbf{Q}_{12} \\ \mathbf{Q}_{12} & \mathbf{Q}_{22} \end{bmatrix}. \tag{217}$$

From (216) and (217) it is apparent that for the inverted normal equations system of (206)

$$[\mathbf{A}_{22} - \mathbf{A}^*_{12}\mathbf{A}_{11}{}^{-1}\mathbf{A}_{12}]^{-1} = \mathbf{N}^{-1} = \mathbf{Q}_{22}\,. \tag{218}$$

Furthermore, since

$$\begin{bmatrix} \mathbf{A}_{11} & \mathbf{A}_{12} \\ \mathbf{A}^*_{12} & \mathbf{A}_{22} \end{bmatrix} \begin{bmatrix} \mathbf{Q}_{11} & \mathbf{Q}_{12} \\ \mathbf{Q}^*_{12} & \mathbf{Q}_{22} \end{bmatrix} = \mathbf{I} \tag{219}$$

it follows from (217) that

$$\mathbf{Q}_{11} = \mathbf{A}_{11}{}^{-1} + \mathbf{A}_{11}{}^{-1}\mathbf{A}_{12}\mathbf{N}^{-1}\mathbf{A}^*_{12}\mathbf{A}_{11}{}^{-1}. \tag{220}$$

From the schematic shown in (216) it follows that the computation indicated with (220) can be performed in independent steps for each individual pair i of values α, δ. Hence we can write

$$\begin{aligned} s^2_{(\alpha,\delta)i} = s^2_0[&(\mathbf{B}^*_{\alpha,\delta}\mathbf{P}_l\mathbf{B}_{\alpha,\delta} + \mathbf{P}_{\alpha,\delta})_i^{-1} \\ &+ (\mathbf{B}^*_{\alpha,\delta}\mathbf{P}_l\mathbf{B}_{\alpha,\delta} + \mathbf{P}_{\alpha,\delta})_i^{-1}\,(\mathbf{B}^*_{\alpha,\delta}\mathbf{P}_l\mathbf{B}_0)_i\mathbf{N}^{-1} \\ &\times (\mathbf{B}^*_0\mathbf{P}_l\mathbf{B}_{\alpha,\delta})_i\,(\mathbf{B}^*_{\alpha,\delta}\mathbf{P}_l\mathbf{B}_{\alpha,\delta} + \mathbf{P}_{\alpha,\delta})_i^{-1}]. \end{aligned} \tag{221}$$

With (221) we obtain the covariance matrix for the corrected values of α, δ for the stars originally selected for the adjustment. If the star in question was originally unknown it is merely necessary to set the relevant $\mathbf{P}_{\alpha,\delta}$ equal to a null matrix and to introduce the corresponding $\mathbf{P}_l$ matrix which must, of course, relate to the initially chosen m_0 value. In the present case a further simplification is present since the $\mathbf{B}_{\alpha,\delta}$ matrix is quadratic and nonsingular, hence invertible. The covariance matrix for an originally unknown star is therefore from (221)

$$\mathbf{s}_{\alpha,\delta} = s^2_0(\mathbf{B}^{-1}_{\alpha,\delta}\mathbf{P}_l{}^{-1}\mathbf{B}^{-1*}_{\alpha,\delta} + \mathbf{B}^{-1}_{\alpha,\delta}\mathbf{B}_0\mathbf{N}^{-1}\mathbf{B}^*_0\mathbf{B}^{-1*}_{\alpha,\delta}). \tag{222}$$

Finally, to compute the accuracy of a direction defined by a fictitious, errorless point the $\mathbf{P}^{-1}$ matrix in (222) becomes a null matrix resulting in

$$\mathbf{s}^2_{\alpha,\delta} = s^2_0(\mathbf{B}^{-1}_{\alpha,\delta}\mathbf{B}_0\mathbf{N}^{-1}\mathbf{B}^*_0\mathbf{B}^{-1*}_{\alpha,\delta}). \tag{223}$$

The formula (223) is now applied for a selected fictitious point to the three orientations obtained from the solution of the system (205). The resulting covariance matrix $\mathbf{s}^2_{\alpha,\delta}$ is of dimension 6 × 6. The three 2 × 2 submatrices along the diagonal are the three covariances $\mathbf{s}^2_{(\alpha,\delta)j=1,2,3}$ associated with the three sets of α, δ. The analogous covariance matrices of the azimuth and elevation components are obtained with (107) as

$$\mathbf{s}^2\,(A, z)_{j=1,2,3} = \mathbf{R}(90°_2 - \varphi)\,\mathbf{s}^2_{(\alpha,\delta)j=1,2,3}\,\mathbf{R}^*(90°_2 - \varphi). \tag{224}$$

Finally the variances s_{21}^2, s_{32}^2, s_{31}^2 of the three ϵ angles of (215) are the diagonal terms of the covariance matrix

$$\mathbf{s}_\epsilon^2 = \mathbf{F}^* \mathbf{s}_{\alpha,\delta}^2 \mathbf{F} \tag{225}$$

where

$$\mathbf{F} = \begin{bmatrix} \frac{\partial\epsilon}{\partial\alpha_1} & 0 & \frac{\partial\epsilon}{\partial\delta_1} \\ \frac{\partial\epsilon}{\partial\delta_1} & 0 & \frac{\partial\epsilon}{\partial\delta_1} \\ \frac{\partial\epsilon}{\partial\alpha_2} & \frac{\partial\epsilon}{\partial\alpha_2} & 0 \\ \frac{\partial\epsilon}{\partial\delta_2} & \frac{\partial\epsilon}{\partial\delta_2} & 0 \\ 0 & \frac{\partial\epsilon}{\partial\alpha_3} & \frac{\partial\epsilon}{\partial\alpha_3} \\ 0 & \frac{\partial\epsilon}{\partial\delta_3} & \frac{\partial\epsilon}{\partial\delta_3} \end{bmatrix}. \tag{226}$$

In (226) for each combination j, k:

$$\begin{bmatrix} \frac{\partial\epsilon}{\partial\alpha_j} \\ \frac{\partial\epsilon}{\partial\delta_j} \\ \frac{\partial\epsilon}{\partial\alpha_k} \\ \frac{\partial\epsilon}{\partial\delta_k} \end{bmatrix} = \frac{1}{\epsilon_{jk}} \begin{bmatrix} x'_{j_1}x'_{k_2} - x'_{j_2}x'_{k_1} \\ x'_{j_1}x'_{k_1}x'_{k_3}(1-x'^2_{k_3})^{-\frac{1}{2}} + x'_{j_2}x'_{k_2}x'_{k_3}(1-x'^2_{k_3})^{-\frac{1}{2}} - x'_{j_3}(1-x'^2_{k_3})^{\frac{1}{2}} \\ x'_{j_2}x'_{k_1} - x'_{j_1}x'_{k_2} \\ x'_{k_1}x'_{j_1}x'_{j_3}(1-x'^2_{j_3})^{-\frac{1}{2}} + x'_{k_2}x'_{j_2}x'_{j_3}(1-x'^2_{j_3})^{-\frac{1}{2}} - x'_{k_3}(1-x'^2_{j_3})^{\frac{1}{2}} \end{bmatrix} \tag{227}$$

If all $|\epsilon_{1,2,3}|$ exceed the corresponding quantity $Ks_{\epsilon_{1,2,3}}$ (where K is a constant selected on the basis of personal experience) then it must be assumed that the camera orientation has changed during the three observation periods. In this case the second solution indicated in the schematic of figure 33 will be accepted as definitive, this being the orientation corresponding to the stars recorded during the satellite transit.

On the other hand, if certain values of ϵ are less than the corresponding $K \cdot s_\epsilon$ then these orientations can be combined. Thus

If: $\epsilon_{12} < Ks_{\epsilon_{1,2}}$, combine orientations 1 and 2
$\epsilon_{23} < Ks_{\epsilon_{23}}$, combine orientations 2 and 3
$\epsilon_{13} < Ks_{\epsilon_{1,3}}$, combine orientations 1 and 3 (228)

The result is obtained as shown in [40] in the form

$$\boldsymbol{\Delta}_0 = [\mathbf{N}^{-1} - \mathbf{N}^{-1}\mathbf{C}^*(\mathbf{C}\mathbf{N}^{-1}\mathbf{C}^*)^{-1}\mathbf{C}\mathbf{N}^{-1}] \quad [\boldsymbol{\Delta}\mathbf{l} + \mathbf{N}^{-1}\mathbf{C}^*(\mathbf{C}\mathbf{N}^{-1}\mathbf{C}^*)^{-1}\mathbf{l}] \tag{229}$$

where $\mathbf{N}^{-1}$ and $\boldsymbol{\Delta}\mathbf{l}$ are from the last iteration in the solution of the original system (205) and

$$\mathbf{C} = \begin{bmatrix} 1 & 0 & 0 & -1 & 0 & 0 & 0 & 0 & 0 \\ 0 & 1 & 0 & 0 & -1 & 0 & 0 & 0 & 0 \\ 0 & 0 & 1 & 0 & 0 & -1 & 0 & 0 & 0 \\ 0 & 0 & 0 & 1 & 0 & 0 & -1 & 0 & 0 \\ 0 & 0 & 0 & 0 & 1 & 0 & 0 & -1 & 0 \\ 0 & 0 & 0 & 0 & 0 & 1 & 0 & 0 & -1 \end{bmatrix} \bigcirc \tag{230}$$

$\mathbf{C}$ is a 6×0 matrix (0 = no. of components of the $\boldsymbol{\Delta}_0$ vector), the first nine columns being as indicated and the balance of the matrix consisting of zero entries. The form of the 6×9 portion will vary according to the results of the criteria (228). The form in (230) corresponds to the case of combining all 3 orientations. For such a case, furthermore,

$$\mathbf{l} = \begin{bmatrix} \alpha_2^o - \alpha_1^o \\ \omega_2^o - \omega_1^o \\ \kappa_2^o - \kappa_1^o \\ \alpha_3^o - \alpha_2^o \\ \omega_3^o - \omega_2^o \\ \kappa_3^o - \kappa_2^o \end{bmatrix} \tag{231}$$

The values with the superscript "o" are the approximation values used in the final iteration in the solution of the system shown in figure 33. The correction vector computed with (229) pertains to these approximations. The final result is then

computed with (229) and (207).

The last phase of the computations covers the partial results, and a summary of these results now follows. Values for distortion at a prescribed interval, e.g., in 3-mm steps, are computed to a maximal radial distance d_{max} dictated by the plate format. If the radial distortion for a prescribed distance d_0 is to be made equal 0 the corresponding camera constant c^* is computed with

$$c^* = \frac{c_x + c_y}{2}(1 - K_0) \tag{232}$$

in which

$$K_0 = -(K_1 d_0^2 + K_2 d_0^4 + K_3 d_0^6) \tag{233}$$

The radial distortion is then computed successively for the required distances d with (95). The transformed radial distortion corresponding to c^* is

$$(\Delta R) = d \cdot K_0 + \Delta R \tag{234}$$

Values for the decentering distortion are computed similarly with (99).

If it is desired to study the values of astronomic refraction within the range of the photogrammetric exposure, they can be computed from (40) as a function of z in suitable intervals, either with the given or the newly computed τ values.

Computing distortion and refraction values is of particular significance when star observations are evaluated for the calibration of photogrammetric cameras or used in error studies of individual photographs. In satellite triangulation the computation of such data is highly advantageous for the purpose of gaining insight into the behavior of all cameras in use, in view of the fact that the photogrammetric registration in a continental, and especially in a worldwide net, is exposed to extreme ranges of local and seasonal environmental conditions. It is therefore required to be informed as to the reliability and metric quality of the instrumentation used and it is also expected that a systematic study of these results will allow the drawing of conclusions with respect to the individual photograms.

Finally we must compute the corrections to the given values resulting from the adjustment, the statistical measures of accuracy, such as the mean error of unit weight, the mean errors of the computed quantities as well as mean errors of values, computed as functions of those quantities.

Corrections to the measured images are computed with (189). With the parameters obtained in the adjustment one has

$$\begin{aligned} v_{l_{xi}} &= F_i \\ v_{l_{yi}} &= G_i \,. \end{aligned} \tag{235}$$

To get a better picture of the distribution of these residuals it is useful to compute the radial and tangential components of these corrections. Computation of the corrections v_α and v_δ for each given star is carried out with (203), (204) where, now, $\mathbf{\Delta}_0$ is a zero vector:

$$\mathbf{v}_{(\alpha,\delta)i} = -(\mathbf{B}^*_{\alpha,\delta}\mathbf{P}_l\mathbf{B}_{\alpha,\delta} + \mathbf{P}_{\alpha,\delta})_i^{-1}(\mathbf{B}^*_{\alpha,\delta}\mathbf{P}_l\mathbf{l})_i. \tag{236}$$

Wherever quantities, introduced by means of approximations into the adjustment, differ from free variables, in that corresponding entries in the $\mathbf{P}_u$ matrix (190) (cf. also (208)) represent *a priori* given weights, relevant corrections are computed, using the results from the adjustment, from

$$\boldsymbol{v}_u = u - u_0 \tag{237}$$

where u stands for the adjusted, and u^0 for the initial value of the parameter. Next one computes

$$\sum \mathbf{v}_l^* \mathbf{P}_l \mathbf{v}_l + \sum \mathbf{v}^*_{\alpha,\delta}\mathbf{P}_{\alpha,\delta}\mathbf{v}_{\alpha,\delta} + \sum \mathbf{v}_u^* \mathbf{P}_u \mathbf{v}_u = \sum \mathbf{v}^* \mathbf{P} \mathbf{v} \tag{238}$$

and in accordance with (193) the mean error of unit weight after adjustment s_0 with

$$s_0 = \left[\frac{\sum \mathbf{v}^* \mathbf{P} \mathbf{v}}{n - u}\right]^{\frac{1}{2}}. \tag{239}$$

The mean errors of the computed parameters are obtained by multiplying s_0 with the square root of the corresponding diagonal term in $\mathbf{N}^{-1}$ of (206). The mean errors of the given quantities result from dividing s_0 by the square root of the weight assigned to the quantities.

The mean error of the camera constant (232), as well as the mean error of radial and decentering distortion are computed as mean errors of functions of quantities determined in the adjustment. In general the mean error s_a of a quantity a

$$a = F(u) \tag{240}$$

is

$$s_a = s_0 [\mathbf{f}_a^* \mathbf{N}^{-1} \mathbf{f}_a]^{\frac{1}{2}} \tag{241}$$

in which $\mathbf{f}_a$ is the vector whose components are the partial derivatives $\frac{\partial \mathbf{F}(\mathbf{u})}{\partial \mathbf{u}}$, the components corresponding to parameters not present in (240) being zero. For the cases in question here,

$$\mathbf{f}_c^* = \begin{array}{|c|c|c|c|c|}\hline \multicolumn{5}{|c|}{\partial /} \\ \hline \partial c_x & \partial c_y & \partial K_1 & \partial K_2 & \partial K_3 \\ \hline \dfrac{1-K_0}{2} & \dfrac{1-K_0}{2} & -\dfrac{c_x+c_y}{2}\cdot d_0^2 & -\dfrac{c_x+c_y}{2}\cdot d_0^4 & -\dfrac{c_x+c_y}{2}\cdot d_0^6 \\ \hline \end{array} \tag{242}$$

$$\mathbf{f}_{\Delta R}^* = \begin{array}{|c|c|c|}\hline \multicolumn{3}{|c|}{\partial /} \\ \hline \partial K_1 & \partial K_2 & \partial K_3 \\ \hline d^3 & d^5 & d^7 \\ \hline \end{array} \tag{243}$$

$$\mathbf{f}_{(\Delta R)}^* = \begin{array}{|c|c|c|}\hline \multicolumn{3}{|c|}{\partial /} \\ \hline \partial K_1 & \partial K_2 & \partial K_3 \\ \hline d(d^2-d_0^2) & d(d^4-d_0^4) & d(d^6-d_0^6) \\ \hline \end{array} \tag{244}$$

$$\mathbf{f}_{\Delta T}^* = \begin{array}{|c|c|}\hline \multicolumn{2}{|c|}{\partial /} \\ \hline \partial K_4 & \partial K_5 \\ \hline d^2 & d^4 \\ \hline \end{array} \tag{245}$$

$$\mathbf{f}_\tau^* = \begin{array}{|c|c|c|c|}\hline \multicolumn{4}{|c|}{\partial /} \\ \hline \partial\tau_1 & \partial\tau_2 & \partial\tau_3 & \partial\tau_4 \\ \hline \mathbf{T}^{\frac{1}{2}}W\tan\dfrac{\beta}{2} & \mathbf{T}^{\frac{1}{2}}W\tan^3\dfrac{\beta}{2} & \mathbf{T}^{\frac{1}{2}}W\tan^5\dfrac{\beta}{2} & \mathbf{T}^{\frac{1}{2}}W\tan^7\dfrac{\beta}{2} \\ \hline \end{array} \tag{246}$$

Substituted in (241) the components computed with (242) now give the mean error of the camera constant c^*, with (243), of the radial distortion at the selected distances d, with (244), of the radial distortions corresponding to camera constant c^*, with (245), of the decentering distortion, and with (246), of astronomic refraction as function of selected zenith distances. This concludes the computations in connection with the reduction of the single camera.

In preparation for the next series of computations the orientation matrix $\mathbf{R}'_y(\alpha,\omega,\kappa)$ during the satellite pass must first be transformed from the local y' system into the final z or z' system that has been selected for the eventual spatial triangulation. $\mathbf{R}'_y(\alpha,\omega,\kappa)$ results from (79), either with the second group of elements of orientation in the schematic of figure 33 or, in accordance with the principle of combination of (228), from a group of orientation elements that also includes star recordings simultaneous with the satellite transit.

The necessary transformation is accomplished with (30) and (108) or (109), so that we have

$$\mathbf{R}'_z(\alpha,\omega,\kappa) = \mathbf{R}_3(\lambda_{east}),\ \mathbf{R}_2(90^\circ-\varphi)\ \mathbf{R}_1(-x,-y)\cdot \mathbf{R}_2(270^\circ+\varphi'),\ \mathbf{R}_3(-\lambda_{east})\ \mathbf{R}'_y(\alpha,\omega,\kappa) \tag{247}$$

and with (79) for example,

$$\begin{aligned} \cos\alpha_{z'} &= r_{33}/\cos\omega_{z'} \\ \sin\omega_{z'} &= -r_{23} \\ \cos\kappa_{z'} &= r_{22}/\cos\omega_{z'} \end{aligned} \tag{248}$$

The reduction, just described, of a single observation of stars is suitable, on the one hand, for a camera calibration and, on the other, it represents one of the intermediate steps in the process of photogrammetric satellite triangulation. A description in detail, with flow charts of these programs, is given in [42]. The arrangement of the latter is in accordance with the present practice of the National Geodetic Survey for the adjustment of the single camera in connection with satellite triangulation, as well as for the calibration of aerial cameras. It was unavoidable to keep this program from being influenced by the development of the method. It does not therefore follow in all respects the presentation given here. However, all the operations so far described, as well as some additional, somewhat less essential computations are included, based in part on formulations of spherical trigonometry. The orientations of coordinate axes and definitions of the sense of rotation differ in some cases from the descriptions above.

We now list the intermediate results from the

single camera program that will be needed in the next reduction step.

a. The parameters set up to reconstruct the photogrammetric bundle and computed in the adjustment, namely

(1) the elements of exterior orientation $(\alpha\omega\kappa)_{y'}$ referring to the local y' system, and

(2) in the general case, the parameters: ϵ, c_x, c_y, x_0, y_0, x_s, y_s, K_1, K_2, K_3, K_4, K_5, φ_T, τ_1, τ_2, τ_3, τ_4.

b. The elements of exterior orientation referred to the ultimate triangulation coordinate system, i.e., either $(\alpha\omega\kappa)_z$ or $(\alpha\omega\kappa)_{z'}$.

c. The mean error of unit weight s_0.

d. The inverted normal equations system N^{-1}.

e. Meteorological data at the observation site during the satellite observations.

f. All data necessary for the identification of observation sites and instrumentation.

g. All supplementary information needed for time determination of the satellite images.

2.7.5 Spatial Triangulation

2.7.5.1 Preliminary computations

The principal problem of geometric satellite triangulation is the determination of three-dimensional, rectangular coordinates for the observation sites, the triangulation being executed in either the z or z' coordinate systems introduced in sec. 2.7.2.6. In preparation for these computations the treatment of the single camera (as described at the end of sec. 2.7.4 includes, among other things, the transformation of the elements of exterior orientation to $(\alpha\omega\kappa)_z$ or $(\alpha\omega\kappa)_{z'}$. Now, in order to triangulate, it is necessary to determine, at each of the stations which have recorded simultaneously a specific satellite pass, at least one direction associated with a specific satellite location in space. Just as the elements of exterior orientation of all photograms must refer to a consistent coordinate system, all the directions obtained with such an orientation must be with respect to unambiguously defined target points in space.

This requirement is filled by reducing all measured image coordinates to a rigorous central perspective and then applying all the corrections explained in sec. 2.5.

Reduction of the plate coordinates l_x, l_y to a central perspective is accomplished with (141) and (142). The expressions for ΔR_x, ΔR_y, ΔT_x, ΔT_y are computed from (97), (98) and (103) using (143) to (147) and, as indicated on page 41, with an iteration loop. The coordinates $l_{\bar{x}}$ and $l_{\bar{y}}$ so obtained correspond in measuring to (138) and (139), and must still be reduced to a common scale factor. If in (138) we set $c_x = c$ we obtain, in agreement with (212)

$$l_{\bar{x}_c} = l_{\bar{x}} \tag{249}$$

and

$$l_{\bar{y}_c} = l_{\bar{y}} \cdot \frac{c_x}{c_y} \tag{250}$$

The image coordinates $l_{\bar{x}_c}$, $l_{\bar{y}_c}$ refer to the principal point and the scale factor c, i.e., to the idealized central perspective. Before these fictitious point images can be used in a spatial triangulation they must be corrected for the influences cited in sec. 2.5. These corrections can be classified under the groupings:

a. *Refraction*, subdivided into astronomic and parallactic refraction

b. *Eccentricity of the target* and

c. *Time corrections*, subdivided into clock corrections and light propagation effects.

In the course of the reduction the influence of scintillation is largely eliminated, at the appropriate place, by smoothing the sequence of individual images of the satellite trail with the aid of polynomials.

The computation of some of these corrections requires an approximation to the distance between the camera site and the satellite. To effect these corrections the coordinates $l_{\bar{x}_c}$, $l_{\bar{y}_c}$ ((249) and (250)) and the $\mathbf{R}_{y'}(\alpha,\omega,\kappa)$ matrix from the single camera are used to produce the unit vector $\mathbf{y}'_r$ from (81) and the corresponding standard coordinates ξ_r, η_r with (28), and then, with (29), the observed zenith distance z_r. The astronomic refraction r_∞ follows from (40) by iteration. The unit vector $\mathbf{y}'$ corrected for astronomic refraction is computed with (42) where, as explained on page 20, r_s is replaced with r_∞, or, alternatively, directly with

$$z = z_r + r_\infty \tag{251}$$

and (74), in the form

$$(\mathbf{y}') = \begin{bmatrix} \cos z \cos A \\ \cos z \sin A \\ \sin z \end{bmatrix} \tag{252}$$

In this the azimuth A is derived from (29). With $(\mathbf{y}')$ new values for ξ and η are derived from (28). With these and using $c = c_x$, image coordinates are computed from (85) and (86), taking the direction cosines r_{ij} from $\mathbf{R}'_y(\alpha,\omega,\kappa)$ and substituting ξ, η, 1 for $X - X_0$, $Y - Y_0$ and $Z - Z_0$ respectively. After all satellite images of a given

photogram have been so reduced, the coefficients for polynomials (58) are determined from an adjustment in accordance with (266) to (270). With these polynomials the $l_{\bar{x}_c}$ and $l_{\bar{y}_c}$ are expressed as functions of station-clock time t. Omitting the subscript c we have then, quite generally

$$l_{\bar{x}} = f(t) \tag{253}$$

$$l_{\bar{y}} = g(t) \tag{254}$$

With the notation of figure 16 we obtain observation times referenced to an unambiguous time designation by adding to each locally recorded time t the corresponding clock correction ΔT, which rarely exceeds 10 ms. The normalized instants of time $T_{j_{1,2,\ldots,m}}$ recorded at stations $j_{1,2,\ldots,m}$ will then be

$$T_{j_{1,2,\ldots,m}} = t_{j_{1,2,\ldots,m}} + \Delta T_{j_{1,2,\ldots,m}} \tag{255}$$

In order to obtain an instant of time that is as close as possible to the range of times recorded at each station, we form the arithmetic mean of the T's and convert this mean to corresponding interpolation times referred to the individual station clocks. Thus

$$t_{j_{1,2,\ldots,m}} = \frac{\sum T_{j_{1,2,\ldots,m}}}{m} - \Delta T_{j_{1,2,\ldots,m}} . \tag{256}$$

Based on the relevant t value at each station, $l_{\bar{x}}$, $l_{\bar{y}}$ values are computed with (253), (254) for points along the satellite trail which, since light propagation time has as yet been neglected, refer to simultaneous instants of exposure.

Next, approximate satellite positions are computed with these data. The camera site coordinate approximations (φ^0, λ^0, h^0) are, with (111), (112), (113), transformed to rectangular coordinates in the z system or, if necessary, by the additional transformation (36) into the z' system. With the $\mathbf{R}_z(\alpha,\omega,\kappa)$ or $\mathbf{R}_{z'}(\alpha,\omega,\kappa)$ orientation matrices mentioned previously and the interpolated $l_{\bar{x}}$, $l_{\bar{y}}$ coordinates, once these values are available for all stations, approximate satellite positions can be computed, using for an intersection with m rays (cf. e.g., [43]):

$$\begin{bmatrix} m & 0 & [a_x] \\ 0 & m & [a_y] \\ [a_x] & [a_y] & [a_x a_x + a_y a_y] \end{bmatrix} \begin{bmatrix} z_{s_1} \\ z_{s_2} \\ z_{s_3} \end{bmatrix} + \begin{bmatrix} [b_x] \\ [b_y] \\ [a_x b_x + a_y b_y] \end{bmatrix} = 0 . \tag{257}$$

The $z_{s_{1,2,\ldots,m}}$ are the approximated coordinates of a point on the satellite's orbit. As an auxiliary computation, one forms with (79)

$$a_x = -\frac{r_{11} l_{\bar{x}} + r_{21} l_{\bar{y}} + r_{31} c}{r_{13} l_{\bar{x}} + r_{23} l_{\bar{y}} + r_{33} c} \tag{258}$$

$$a_y = -\frac{r_{12} l_{\bar{x}} + r_{22} l_{\bar{y}} + r_{32} c}{r_{13} l_{\bar{x}} + r_{23} l_{\bar{y}} + r_{33} c} \tag{259}$$

$$b_x = -(a_x z_3^0 + z_1^0) \tag{260}$$

$$b_y = -(a_y z_3^0 + z_2^0) \tag{261}$$

where $z^0_{1,2,3}$ are approximated rectangular station coordinates. The distances between an observation station and the satellite positions are

$$d = [(z_{s_1}^0 - z_1^0)^2 + (z_{s_2}^0 - z_2^0)^2 + (z_{s_3}^0 - z_3^0)^2]^{\frac{1}{2}} \tag{262}$$

Instead of storing the large number of distances corresponding to the 500 to 600 satellite positions, it is preferable to express d as a function of t. As with the functions (253), (254), we again use (58) with one expansion for the d. This results in one polynomial for each station or, in general,

$$d = h(t). \tag{263}$$

We now resume the reduction of the results obtained with (249) and (250), computing first the satellite refraction r_s with (41) and using (263) along with the previously computed astronomic refraction r_∞. Then follows the unit vector $\mathbf{y}'$ corrected for refraction, from the refracted vector $\mathbf{y}'_r$ by use of (42) or (252), where now

$$z = z_r + r_s. \tag{264}$$

Reduction of the $\mathbf{y}'$ vector is continued with the elimination of the influence of eccentricity of the target point.

After the unit vector $\mathbf{y}'_\odot$ in the direction to the Sun has been computed, in accordance with (54) and the Sun's right ascension and declination at the instant of observation and the use of (20), (21), (23) and (24), one obtains the unit vector $\mathbf{y}'_{BM}$ to the center of the balloon with (52) and (49) in the form

$$\mathbf{y}'_{BM} = \mathbf{y}' - \frac{a}{d \sin \gamma} (\mathbf{y}'_\odot + \cos \gamma \mathbf{y}') \tag{265}$$

in which the needed quantities are derived from (263), (50) or (51) and (46).

With the vector (265) corresponding ξ, η values are again computed with (28), as are $l_{\bar{x}}$, $l_{\bar{y}}$ coordinates of the corresponding fictitious satellite images using the $\mathbf{R}_{y'}(\alpha,\omega,\kappa)$ matrix in the manner

described on p. 53. With these values in (58) the final interpolation polynomials are set up which, in complete analogy with the expressions (253) and (254), represent $l_{\bar{x}}$ and $l_{\bar{y}}$ as functions of t (cf. also sec. 2.7). In reference to the degree of the polynomials note the remarks following (58) (cf. also sec. 3.1). Normal equations corresponding to the equations (58) are set up in order to determine the polynomial coefficients where, to simplify the numerical calculations, the t values, assumed free of error, are replaced with a sequence of integers whose increment corresponds to the greatest common divisor of the interval recorded at the various stations involved. The normal equations system for n images has the form

$$\overbrace{\sum_{i=1}^{n} [\mathbf{B}_{\bar{l}}^{*}\mathbf{P}_i\mathbf{B}_{\bar{l}}]_i}^{\mathbf{N}_c}\ \mathbf{c} = \overbrace{\sum_{i=1}^{n} [\mathbf{B}_{\bar{l}}^{*}\mathbf{P}_i\bar{\mathbf{l}}]_i}^{\mathbf{l}_c} \tag{266}$$

in which $\mathbf{P}_i$ is expressed with sufficient accuracy in terms of the weight matrix assigned to the original coordinate measurements [cf. (192)]. For an m^{th} degree polynomial $\mathbf{B}_{\bar{l}}$ is, from (58), for each of the **n** points

$$\mathbf{B}_{l_i} = \left[\begin{array}{cccccc|ccccccc} \cdot & \cdot & \cdot & \cdot & \cdot & \cdot & \cdot & \cdot & \cdot & \cdot & \cdot & \cdot & \cdot \\ 1 & t_i & t_i^2 & t_i^3 & \cdot & t_i^m & & & 0 & & & & \\ \cdot & \cdot & \cdot & \cdot & \cdot & \cdot & \cdot & \cdot & \cdot & \cdot & \cdot & \cdot & \cdot \\ \hline \cdot & \cdot & \cdot & \cdot & \cdot & \cdot & \cdot & \cdot & \cdot & \cdot & \cdot & \cdot & \cdot \\ & & & 0 & & & 1 & t_i & t_i^2 & t_i^3 & \cdot & \cdot & t_i^m \\ \cdot & \cdot & \cdot & \cdot & \cdot & \cdot & \cdot & \cdot & \cdot & \cdot & \cdot & \cdot & \cdot \end{array}\right] \tag{267}$$

c is the vector of coefficients to be determined

$$\mathbf{c}^{*} = [a_0 a_1 a_2 a_3 \ldots a_m\, b_0 b_1 b_2 b_3 \ldots b_m] \tag{268}$$

and $\bar{\mathbf{l}}_i$ is the vector with components $(l_{\bar{x}}, l_{\bar{y}})$ obtained with the $\mathbf{y}'_{BM}$ vector of (265),

$$\bar{\mathbf{l}}_i = \begin{bmatrix} l_{\bar{x}} \\ l_{\bar{y}} \end{bmatrix}_i . \tag{269}$$

The solution for the vector of coefficients **c** follows from (266)

$$\mathbf{c} = \mathbf{N}_c^{-1}\mathbf{l}_c \tag{270}$$

and the covariance matrix associated with the coefficients **c** is, from (195),

$$\mathbf{s}_c^2 = s_{0_c}^2\,\mathbf{N}^{-1}. \tag{271}$$

The mean error s_{0_c} for the satellite trail fit is, from (193)

$$s_{0_c} = \left[\frac{\sum_{i=1}^{n} (\mathbf{v}^{*}\mathbf{P}_i\mathbf{v})_i}{2n - (2m+2)}\right]^{\frac{1}{2}} . \tag{272}$$

The individual v values are computed with (58) and, with the designations used in (253) and (254), are

$$\mathbf{v}_i = \begin{bmatrix} v_{l_{\bar{x}}} \\ v_{l_{\bar{y}}} \end{bmatrix}_i = \begin{bmatrix} f(t) - l_{\bar{x}} \\ g(t) - l_{\bar{y}} \end{bmatrix}_i . \tag{273}$$

If pairs of coordinates $l_{\bar{x}}$ and $l_{\bar{y}}$ for n points are determined by interpolation in (58), the corresponding covariance matrix is, in accordance with (240), (241), (272) and using the designations introduced with (267),

$$(\mathbf{s}_{\bar{l}})^2 = s_{0_c}^2\,[\mathbf{B}_{\bar{l}}\mathbf{N}_c^{-1}\mathbf{B}_{\bar{l}}{}^{*}] . \tag{274}$$

In order to account for all existing correlations the $\mathbf{B}_{\bar{l}}$ matrix must be set up for all n points and is therefore of dimension $2n \times (2m + 2)$.

Interpolation for coordinates of fictitious satellite images by means of the computed polynomials is executed, in agreement with figure 16, by forming interpolation times t corresponding to a selected sequence of orbital times T with

$$t = T - \Delta T + \tau_{(T-\Delta T)}. \tag{275}$$

The $\tau_{T-\Delta T}$ are computed with (56). The necessary distances d are computed with sufficient accuracy for the times $T-\Delta T$ from the polynomial (263). Finally the fictitious image coordinates are computed by substituting the interpolated instants t in (58), whose coefficients have been determined from the solution of (270). After the pairs of coordinates for the selected orbital times T have been computed, the last reduction is made to remove the effect of Earth rotation that took place during the light travel time. As before, a new unit vector $\mathbf{y}'$ must be computed from the coordinate pairs $l_{\bar{x}}$, $l_{\bar{y}}$ just obtained, using (81) and $\mathbf{R}_{y'}(\alpha,\omega,\kappa)$. Then, with (60) and the $\tau_{T-\Delta T}$ values from (56), every $\mathbf{y}'$ vector is transformed into its corresponding $\mathbf{y}'_s$ vector. The final image coordinates $l_{\bar{x}}$, $l_{\bar{y}}$ result from (60) and the use of (85) and (86) where, as before, the direction cosines r_{ij} are taken from $\mathbf{R}_{y'}(\alpha,\omega,\kappa)$, and ξ replaces $X - X_0$, η replaces $Y - Y_0$ and the number 1 replaces $Z - Z_0$. The quantities ξ and η are again derived from $\mathbf{y}'_s$ by the application of (28).

Concerning the needed number of directions so introduced see sec. 3.1. In any case the selection of orbital times T should be such that one of these instants corresponds to a point of the orbit whose image on the several photograms is as close as possible to the principal point.

Having completed these preliminary computations, a pair of image coordinates will be available

for each selected point of the orbit and representing fictitious observations. These image coordinates simulate images that would have been obtained had the following conditions been met:

a. The photogrammetric camera reproduces a rigorous central perspective.

b. The comparator has no linear scale errors and measures in two perpendicular directions.

c. The origin of the image coordinate system coincides with the principal point.

d. The observation was executed in vacuo, i.e., refraction and scintillation do not exist.

e. The images correspond to the center of the balloon.

f. Neither Earth nor satellite have a proper motion, i.e., there is no influence from aberration or time of light propagation.

g. All station clocks run without error with respect to a reference time and the recording times of the stars are rigorously UT-1, and

h. The images at all stations observing a specific satellite pass correspond to uniquely defined positions on the satellite orbital curve.

After processing of all observed data in the manner described, we have at our disposal for the execution of the spatial triangulation: for each of the observing stations and for all satellite passes observed at such stations a photogram, each with a number of fictitious image point coordinates $l_{\bar{x}}$, $l_{\bar{y}}$, the relevant scale factor c, and either the $\mathbf{R}_z(\alpha,\omega,\kappa)$ or $\mathbf{R}_{z'}(\alpha,\omega,\kappa)$ orientation matrix. Since orientation matrices are referred to the same coordinate system—either the z or z' system—the spatial triangulation can now, with the idealized image coordinates $l_{\bar{x}}$, $l_{\bar{y}}$ mentioned above, be carried out in accordance with the geometrical principles of a rigorous central perspective. For this last adjustment step the covariance matrix associated with the computed image coordinates will also be needed.

With (274) a covariance matrix was obtained relating to the smoothing process of the orbital curve. The covariance matrix relating to the single camera reduction is computed, with the designation introduced in (188), from (195) and the results obtained with (206) and (239) of the single camera solution in the form

$$(\mathrm{s}_{l0})^2 = s_0^2\,[\mathbf{B}_0\mathbf{N}^{-1}\mathbf{B}_0^*] \tag{276}$$

Since the two error contributions are independent of each other, the total covariance matrix for the values $l_{\bar{x}}$, $l_{\bar{y}}$ of a specific photogram is, with (274) and (276),

$$(\mathrm{s}_{\bar{l}})^2 = (\mathrm{s}_{\bar{l}_c})^2 + (\mathrm{s}_{\bar{l}_0})^2 \tag{277}$$

with the proviso that all computations are with reference to a common mean error of unit weight (cf. sec. 3.1).

For each station to be triangulated and for all satellite passes observed at the station, the following information is now available:

a. Approximate station coordinates

$$\varphi^0,\ \lambda^0 \text{ and } h^0 \tag{278}$$

b. If given, the weight matrix of these coordinates

$$\mathbf{P}_\varphi = \begin{bmatrix} p_\varphi & p_{\varphi,\lambda} & p_{\varphi,h} \\ p_{\varphi,\lambda} & p_\lambda & p_{\lambda,h} \\ p_{\varphi,h} & p_{\lambda,h} & p_h \end{bmatrix}. \tag{279}$$

c. Corresponding rectangular coordinates $z_{1,2,3}$ or $z'_{1,2,3}$, derived from (111), (112), (113) and, if necessary, transformed with (36).

d. The relevant weight matrices $\mathbf{P}_z$ or $\mathbf{P}_{z'}$ from (128).

e. The elements of orientation $(\alpha\omega\kappa)_z$ or $(\alpha\omega\kappa)_{z'}$ from the single camera program (cf. (248)).

f. The scale factor c (cf. p. 53).

g. The fictitious image point coordinates $l_{\bar{x}}$, $l_{\bar{y}}$ corresponding to the selected satellite positions and associated satellite orbit times. (cf. p. 55), and

h. The covariance matrix (277) of these coordinates.

The information contained in points a. to h. represents the input data for the spatial triangulation proper, the solution and adjustment of which is treated in the next section as the final step in the evaluation.

The evaluation procedures of this section and, in addition, computations relating to alternative approaches to these problems, are described in all details and with pertinent flow charts in [44]. The treatment of the subject to this point has demonstrated the fact that certain computer operations must be repeated frequently. For this reason the computer programs have been designed from the standpoint of optimal economic operation and the flow charts in [44] reflect a corresponding organization of the computations.

2.7.5.2 The adjustment

As stated above, the spatial triangulation of the station coordinates can now proceed in accordance with the law of central perspective. The mathematical model on which the adjustment is based is given with formulas (85), (86) which, with the present nomenclature and in accordance with (148) and (149), are

$$F = \frac{c[(z_{s_1} - z_1)\, r_{11} + (z_{s_2} - z_2)\, r_{12} + (z_{s_3} - z_3)\, r_{13}]}{(z_{s_1} - z_1)\, r_{31} + (z_{s_2} - z_2)\, r_{32} + (z_{s_3} - z_3)\, r_{33}} - l_{\bar{x}} = 0 \tag{280}$$

$$G = \frac{c[(z_{s_1} - z_1)\, r_{21} + (z_{s_2} - z_2)\, r_{22} + (z_{s_3} - z_3)\, r_{23}]}{(z_{s_1} - z_1)\, r_{31} + (z_{s_2} - z_2)\, r_{32} + (z_{s_3} - z_3)\, r_{33}} - l_{\bar{y}} = 0. \tag{281}$$

The $z_{s_{1,2,3}}$ denote the coordinates of a satellite position, and $z_{1,2,3}$ station coordinates. In case the exterior elements of orientation ($\alpha\omega\kappa$) are referred to the z' system the station coordinates are designated as z' without making any other changes in the algorithm.

With the nomenclature of (153) in sec. 2.7.3, the observation equations corresponding to expressions (280) and (281) are, according to (151) and (152)

$$\underbrace{[\Delta z_{s_1} \quad \Delta z_{s_2} \quad \Delta z_{s_3}]}_{\Delta \mathbf{z}_s^*} \underbrace{\begin{bmatrix} -D_x & -E_x & -F_x \\ -D_y & -E_y & -F_y \end{bmatrix}}_{\mathbf{B}_{z_s}} + \underbrace{[\Delta z_1 \quad \Delta z_2 \quad \Delta z_3]}_{\Delta \mathbf{z}^*} \underbrace{\begin{bmatrix} +D_x & +E_x & +F_x \\ +D_y & +E_y & +F_y \end{bmatrix}}_{\mathbf{B}_z} - \underbrace{[v_x \quad v_y]}_{\mathbf{v}_l^*} \underbrace{\begin{bmatrix} 1 & 0 \\ 0 & 1 \end{bmatrix}}_{\mathbf{A}_l} + \begin{bmatrix} F^0 \\ G^0 \end{bmatrix} = \begin{bmatrix} 0 \\ 0 \end{bmatrix} \tag{282}$$

$$-\mathbf{l} \tag{283}$$

in which F^0 and G^0 are computed with approximations for the station coordinates $z_{1,2,3}$ (cf. page 56 under c) and for the satellite position coordinates $z_{s_{1,2,3}}$ (cf. (257)). The definition of the coefficients in (282), (283) is given in (153) to (155). All pairs of coordinates $l_{\bar{x}}$, $l_{\bar{y}}$ computed for a given photogram are correlated, since all directions to the satellite depend on the orientation matrix derived from the single camera solution. Furthermore, for a passive satellite all the coordinate pairs $l_{\bar{x}}$, $l_{\bar{y}}$ of fictitious satellite images are correlated, since they are derived from the smoothing polynomials that are based on an adjustment involving all coordinate measurements of the original satellite images.

According to (277) $(s_{\bar{l}_{i,j}})^2$ is the covariance matrix associated with the n sets of $l_{\bar{x}}$, $l_{\bar{y}}$ derived from the photogram taken at station i, observing the event j. The corresponding weight matrix is, from (196),

$$\mathbf{P}_{\bar{l}_{i,j}} = m_0^2\, ((s_{l_{i,j}})^2)^{-1} \tag{284}$$

If we now set up observation equations (282) and (283) for all the directions introduced into the satellite triangulation net, i.e., for all the coordinate pairs $l_{\bar{x}}$, $l_{\bar{y}}$ derived from measurements of the photograms, taking into account all existing correlations as expressed in the $\mathbf{P}_{\bar{l}}$ matrices, it would be possible to form directly the corresponding normal equations system. The unknowns of such a system would be the coordinates of the observing stations as well as of the orbital points. To make the solution economically more feasible, therefore, the corrections to coordinates of the orbital points are eliminated in the formation of the normal equations, thus producing a final normal equations system that contains only corrections to the camera station coordinates. The procedure, which is analogous to the elimination of relative pass points in numerical aerial photo triangulation (cf. [43]), requires a formation of partial normal equations systems in the following manner.

As stated above, the n pairs of coordinates $l_{\bar{x}}$, $l_{\bar{y}}$ for a particular photogram are correlated by way of the associated $\mathbf{P}_{\bar{l}}$ matrix. With (282), (283) the 2n observation equations pertaining to station i and event j are formed first of all. The normal equations system is then formed which is, with appropriate use of the designations introduced in (282), (283),

$$\begin{array}{cc} \Delta \mathbf{z}_{s_{j_{1,2,3,\ldots,n}}} & \Delta \mathbf{z}_i \\ \left[\begin{array}{c|c} \mathbf{B}^*_{z_{s_j}} \mathbf{P}_{\bar{l}_{i,j}} \mathbf{B}_{z_{s_j}} & \mathbf{B}^*_{z_{s_j}} \mathbf{P}_{\bar{l}_{i,j}} \mathbf{B}_{z_i} \\ \hline \mathbf{B}^*_{z_i} \mathbf{P}_{\bar{l}_{i,j}} \mathbf{B}_{z_{s_j}} & \mathbf{B}^*_{z_i} \mathbf{P}_{\bar{l}_{i,j}} \mathbf{B}_{z_i} \end{array}\right] & = \left[\begin{array}{c} \mathbf{B}^*_{z_{s_j}} \mathbf{P}_{\bar{l}_{i,j}} \mathbf{l}_{\bar{l}_{i,j}} \\ \hline \mathbf{B}^*_{z_i} \mathbf{P}_{\bar{l}_{i,j}} \mathbf{l}_{\bar{l}_{i,j}} \end{array}\right] \end{array} \tag{285}$$

where

$$\Delta \mathbf{z}_{s_{j_{1,2,\ldots,n}}} = \begin{bmatrix} \Delta z_{s_1} \\ \Delta z_{s_2} \\ \cdot \\ \Delta z_{s_n} \end{bmatrix} \tag{286}$$

Each of the partial vectors $\Delta \mathbf{z}_{s_{1,2,\ldots,n}}$ is the vector

of corrections for a specific satellite position. $\Delta \mathbf{z}_i$ is the correction vector for the coordinates of observation station i. The normal equations system shown schematically in (285) must be set up as a unit for all the fictitious points computed for the photogram in question, since the associated $\mathbf{P}_{\bar{l}_{i,j}}$ of dimension $2n \times 2n$ is an indivisible unit.

If a specific satellite event j has been observed from m stations, the partial systems (285) are set up individually for each of the m photograms and combined into the normal equations partial system representing the event j, as shown in the schematic arrangement

$$\begin{array}{c|c|c|c|c|c}
 & \multicolumn{4}{c|}{\overbrace{\qquad\qquad\qquad\qquad\qquad\qquad\qquad}^{\Delta \mathbf{z}_{i_{1,2,\ldots,m}}}} & \\
\Delta \mathbf{z}_{s_{j_{1,2,3,\ldots,n}}} & \Delta \mathbf{z}_{i=1} & \Delta \mathbf{z}_{i=2} & \cdots & \Delta \mathbf{z}_{i=m} & \\
\hline
\sum_{i=1}^{m} (\mathbf{B}^*_{z_{s_j}} \mathbf{P}_{\bar{l}_{i,j}} \mathbf{B}_{z_{s_j}})_i & (\mathbf{B}^*_{z_{s_j}} \mathbf{P}_{\bar{l}_{i,j}} \mathbf{B}_{z_i})_{i=1} & (\mathbf{B}^*_{z_{s_j}} \mathbf{P}_{\bar{l}_{i,j}} \mathbf{B}_{z_i})_{i=2} & \cdots & (\mathbf{B}^*_{z_{s_j}} \mathbf{P}_{\bar{l}_{i,j}} \mathbf{B}_{z_i})_{i=m} & \sum_{i=1}^{m} (\mathbf{B}^*_{z_s} \mathbf{P}_{\bar{l}_{i,j}} \mathbf{l}_{i,j})_i \\
\hline
(\mathbf{B}^*_{z_i} \mathbf{P}_{\bar{l}_{i,j}} \mathbf{B}_{z_{s_j}})_{i=1} & (\mathbf{B}^*_{z_i} \mathbf{P}_{\bar{l}_{i,j}} \mathbf{B}_{z_i})_{i=1} & \mathbf{0} & \mathbf{0} & \mathbf{0} & (\mathbf{B}^*_{z_i} \mathbf{P}_{\bar{l}_{i,j}} \mathbf{l}_{i,j})_{i=1} \\
\hline
(\mathbf{B}^*_{z_i} \mathbf{P}_{\bar{l}_{i,j}} \mathbf{B}_{z_{s_j}})_{i=2} & \mathbf{0} & (\mathbf{B}^*_{z_i} \mathbf{P}_{\bar{l}_{i,j}} \mathbf{B}_{z_i})_{i=2} & \mathbf{0} & \mathbf{0} & (\mathbf{B}^*_{z_i} \mathbf{P}_{\bar{l}_{i,j}} \mathbf{l}_{i,j})_{i=2} \\
\hline
\vdots & \mathbf{0} & \mathbf{0} & \ddots & \mathbf{0} & \vdots \\
\hline
(\mathbf{B}^*_{z_j} \mathbf{P}_{\bar{l}_{i,j}} \mathbf{B}_{z_{s_j}})_{i=m} & \mathbf{0} & \mathbf{0} & \mathbf{0} & (\mathbf{B}^*_{z_i} \mathbf{P}_{\bar{l}_{i,j}} \mathbf{B}_{z_i})_{i=m} & (\mathbf{B}^*_{z_i} \mathbf{P}_{\bar{l}_{i,j}} \mathbf{l}_{i,j})_{i=m}
\end{array} \tag{287}$$

With evident simplification (287) can also be written in the form

$$\begin{bmatrix} \mathbf{A} & \mathbf{C} \\ \mathbf{C}^* & \mathbf{B} \end{bmatrix} \begin{bmatrix} \Delta \mathbf{z}_{s_{j_{1,2,\ldots,n}}} \\ \Delta \mathbf{z}_{i_{1,2,\ldots,n}} \end{bmatrix} = \begin{bmatrix} \Delta \mathbf{l}_{s_j} \\ \Delta \mathbf{l}_{z_{i_{1,2,\ldots,n}}} \end{bmatrix} \tag{288}$$

Now the correction vector $\Delta \mathbf{z}_{s_{j\,1,2,\ldots}}$ for the satellite positions is eliminated, leaving a normal equations partial system for corrections to coordinates of those stations that observed the satellite event j. This system is

$$\begin{aligned} &[\mathbf{B} - \mathbf{C}^*\mathbf{A}^{-1}\mathbf{C}]\, \Delta \mathbf{z}_{i_{1,2,\ldots,m}} \\ &= [\Delta \mathbf{l}_{z_{i_{1,2,\ldots,m}}} - \mathbf{C}^*\mathbf{A}^{-1}\Delta \mathbf{l}_{s_j}] \end{aligned} \tag{289}$$

or simply

$$\mathbf{N}_{z_{i_{1,2,\ldots,m}}} \Delta \mathbf{z}_{i_{1,2,\ldots,m}} = \mathbf{l}_{z_{i_{1,2,\ldots,m}}}. \tag{290}$$

When the partial systems (290) have been formed for all events, the final, complete normal equations system for the corrections to coordinates of all stations involved in the satellite triangulation is formed by adding the individual systems (290) according to station index. The resulting system is

$$\mathbf{N}_z \Delta \mathbf{z} = \mathbf{l}_z \tag{291}$$

In the present form $\mathbf{N}_z$ of (291) is singular and not invertible, since no origin of coordinates or a scale have as yet been introduced (cf. sec. 2.2). To satisfy the first requirement, the introduction of an origin or the equivalent, at least three possibilities are worthy of consideration.

The simplest is to assume one of the stations of the net to be given with its initial coordinates $\mathbf{z}^0_{(1,2,3)i}$ free of error. This imposes on the system (291) the condition that the corresponding $\Delta \mathbf{z}_i$ vector be a zero vector in the solution of the system. This is accomplished by assigning the approximation coordinates an infinite weight, i.e., the quantity 10^n is introduced as weight in the relevant diagonal terms of (291), n being as large as the capacity of the computer allows. This causes the $\Delta \mathbf{z}_i$ vector to vanish for all practical purposes, since the corresponding entries in the $\mathbf{N}^{-1}$ matrix will be multiplied by 10^{-n}.

A second possibility exists, especially in connection with triangulation of a continental satellite net in which the observation stations are part of an established geodetic reference system. For such a case, weight matrices (279) and, after appropriate transformation, corresponding $\mathbf{P}_z$ or $\mathbf{P}_{z'}$ matrices (128) are available as input data. It is then only necessary to add these weight matrices to the system (291) where called for.

A third possibility, which is especially attractive for error studies, is to introduce as origin of coordinates the centroid of all adjusted coordinates. This means adding to the system the supplementary condition

$$\sum (\mathbf{z}^0 + \Delta \mathbf{z}) = \sum \mathbf{z} = 0 \tag{292}$$

This will result in a symmetrical distribution of mean errors for the net, with modifications depending on the shape of the net. For a further

discussion of the problem see [46] and additional contributions in [47].

In order not to endanger the accuracy of the $\mathbf{N}_z$ matrix inversion, it has been found advisable in practice to combine these various possibilities. Initially, one of the stations is held fixed at the origin. After the $\mathbf{N}_z$ matrix inversion the coordinate system is translated. The three condition equations (292) are replaced by the condition valid for each station

$$\hat{\mathbf{z}}_i = \mathbf{z}_i - \frac{\sum^{i-s} \mathbf{z}_i}{s} \tag{293}$$

where s is the number of stations involved in the triangulation. The matrix of weight coefficients for the $\hat{\mathbf{z}}$ values is obtained, since in this case $\mathbf{F}^* = \mathbf{F}$, from

$$\hat{\mathbf{N}}_z^{-1} = \mathbf{F}\mathbf{N}_z^{-1}\mathbf{F} \tag{294}$$

where the $\mathbf{F}$ matrix is obtained as a symmetric quadratic matrix by differentiating the right side of (293). The coefficients of $\mathbf{F}$ are $\frac{s-1}{s}$ along the diagonal and $-\frac{1}{s}$ in the spaces where the correlation between the individual components of the station coordinates should appear. A sequence of operations utilizing the symmetry of the $\mathbf{F}$ matrix is described in detail in [45].

The introduction of scale into the triangulation by means of measured distance between two or more stations of the net is of prime importance in satellite triangulation. Such distances can be derived, for example, from long-line traverses measured with, for instance, a geodimeter (cf. [48] and [49]). Designating the two stations i and j, and the distance between them d, then

$$d_{ij} = [(z_{i1} - z_{j1})^2 + (z_{i2} - z_{j2})^2 + (z_{i3} - z_{j3})^2]^{\frac{1}{2}}, \tag{295}$$

the weight of the distance d_{ij} being expressed as

$$P_{d_{ij}} = \frac{m_0^2}{m_{d_{ij}}} \tag{296}$$

where $m_{d_{ij}}$ is the mean error of the distance d_{ij} in meters. With the designation

$$\mathbf{f}^* d_{ij} = \frac{\partial d_{ij}}{\partial z_{ij}} =$$

∂z_{i_1}	∂z_{i_2}	∂z_{i_3}	∂z_{j_1}	∂z_{j_2}	∂z_{j_3}
$\frac{z_{i_1} - z_{j_1}}{d^0}$	$\frac{z_{i_2} - z_{j_2}}{d^0}$	$\frac{z_{i_3} - z_{j_3}}{d^0}$	$\frac{z_{j_1} - z_{i_1}}{d^0}$	$\frac{z_{j_2} - z_{i_2}}{d^0}$	$\frac{z_{j_3} - z_{i_3}}{d^0}$

(297)

it is merely necessary in the system (291) to add, at the locations corresponding to stations i and j, including location ij on the left side, the appropriate portion of the matrix

$$(\mathbf{f}_d P_d \mathbf{f}_d^*)_{ij} \tag{298}$$

and on the right side

$$(\mathbf{f}_d P_d \Delta \mathbf{l}_d)_{ij} \tag{299}$$

where

$$\Delta l_{d_{ij}} = d_{ij} - d_{ij}^0 \tag{300}$$

and d_{ij}^0 is computed with the approximations for $\mathbf{z}_{ij}^0$ from (295). Any number of scalars can thus be introduced into the adjustment. With the expected development in measuring distances with lasers it should be possible, in the future, to measure distances between the observing stations and the satellite which can then be similarly introduced into the normal equation system (288) before the satellite positions are eliminated using (289).

After the system (291) has been amended with the above described two steps—fixing the origin of coordinates and introducing scale—the vector of coordinate corrections for all the stations in the triangulation can now be computed as

$$\Delta \mathbf{z} = \mathbf{N}_z^{-1}\mathbf{l}_z \tag{301}$$

and the final result of the satellite triangulation is

$$\mathbf{z} = \mathbf{z}^0 + \Delta \mathbf{z} \tag{302}$$

From (235), using the $\mathbf{z}$ vector and expressions (280), (281) the corrections $\mathbf{v}_{\bar{l}}$ are computed, followed by the determination of corrections for all additionally introduced observations. Thus, for example, for *a priori* given station coordinates

$$\mathbf{v}_{z_i} = \Delta \mathbf{z}_i \tag{303}$$

and for distances used as scale control

$$v_{d_{ij}} = \bar{d}_{ij} - d_{ij}, \tag{304}$$

in which $\bar{d}_{ij}$ is computed with the final coordinates out of (295), and d_{ij} is the initially given measurement.

With these v's and their weights, the mean error of unit weight s_0 for the whole triangulation is computed from

$$s_0 = \left[\frac{\mathbf{v}_{\bar{l}}^* \mathbf{P}_{\bar{l}} \mathbf{v}_{\bar{l}} + \mathbf{v}_z^* \mathbf{P}_z \mathbf{v}_z + \sum P_d v_d v_d}{B + Z + D - S}\right]^{\frac{1}{2}}. \tag{305}$$

where B = number of observation equations
Z = number of station coordinates, given *a priori*, with their weights
D = number of distances given, with their weights

S = number of all coordinates, of station locations as well as of satellite points.

If in the course of the observations, e.g., for meteorological or logistic reasons, stations must be moved a short distance, such dual stations must be coupled. Corresponding conditions are introduced and their number is added in the denominator of (305) just as all extraneous metric conditions must be taken into account. With the covariance matrix (195), corresponding to the inverted normal equations system, and the s_0 of (305), the mean error of the individual $z_{1,2,3}$ is obtained with the square roots of the diagonal terms of this covariance matrix and, with (198) to (200), the semiaxes of the error ellipsoid and their direction cosines.

This actually completes the result of the satellite triangulation, at least from the standpoint of photogrammetry. Further processing of the results reverts to a strictly geodetic point of view, such as the conversion of the computed **z** values into an ellipsoidal system, which can be accomplished with (114) to (119).

If the approximations φ^0, λ^0, h^0 were given coordinates a correction vector can be computed with (126)

$$\mathbf{v}_\varphi = \mathbf{T}_\varphi^{-1}\,\mathbf{v}_z$$

and the corresponding station covariance in analogy with (128)

$$\mathbf{s}_\varphi^2 = s_0^2(\mathbf{T}_\varphi^{-1}\,\mathbf{Q}_z\,(\mathbf{T}_\varphi^{-1})^*) = \begin{bmatrix} s_\varphi^2 & s_{\varphi,\lambda} & s_{\varphi,h} \\ s_{\varphi,\lambda} & s_\lambda^2 & s_{\lambda,h} \\ s_{\varphi,h} & s_{\lambda,h} & s_h^2 \end{bmatrix} \tag{306}$$

in which $\mathbf{Q}_z$ is the appropriate 3×3 matrix from $\mathbf{N}^{-1}$. In principle we can say that the measures of accuracy for all quantities derived from the **z** values are to be computed as mean errors of functions of the adjusted **z**'s in conformance with (241). In [45] the structure of a computing program for spatial triangulation is described and the necessary flow charts shown. Likewise, all supplementary computations and statistical controls needed for check and of significance to the computations in an extended triangulation program are explained.

2.8 References

(1) Hopmann und Lohmann, "Ballistische Photogrammetrie (Ballistic Photogrammetry), Hillersleben, 1943.

(2) Väisälä, Y., "An Astronomical Method of Triangulation," *Sitzungsberichte der Finnischen Akademie der Wissenschaften*, (Proceedings of the Finnish Academy of Sciences), 1947, pp. 99–107.

(3) Bossler, John D., "The SAO Star Catalog, Its Qualitative and Quantitative Value to the C&GS Satellite Triangulation Program," U.S. Department of Commerce, Environmental Science Services Administration, Institute for Earth Sciences, Geodetic Research Laboratory, Washington, D.C., Aug. 1966, 52 pp.

(4) Clemence, G. M., "Astronomical Reference Systems," *Basic Astronomical Data*, Vol. III of *Stars and Stellar Systems*, chapter I. Edited by K. Aa. Strand. University of Chicago Press, Chicago and London, 1963, pp. 1–10.

(5) Scott, F. P., "The System of Fundamental Proper Motions," Ib., chapter II, 1963, pp. 11–29.

(6) Vasilevskis, S. "The Reference System of Bright Stars, Intermediate, and Faint Stars and of Galaxies," Ib., chapter III, 1963, pp. 30–39.

(7) Dieckvoss, W. "Photographic Proper Motions," Ib., chapter IV, 1963, pp. 40–45.

(8) Woolard, E. W. and Clemence, G. M., "Spherical Astronomy," Academic Press, New York and London, 1966, 453 pp.

(9) Scott, F. P., "Fundamental Work at Washington," *Transactions of the International Astronomical Union*, Vol. IX, 1955, Cambridge University Press, 1957, pp. 713–716.

(10) Introductory Remarks in "Publications of U.S. Naval Observatory, Second Series," Washington, D.C., U.S.A. and in Publications of Astronomical Observatory Pulkovo, U.S.S.R. (See also special publications containing star catalogs).

(11) König, A., "Astrometry with Astrographs," *Astronomical Techniques*, Vol. II *Stars and Stellar Systems*, edited by W. A. Hiltner, University of Chicago Press, Chicago and London, 1962, 461 pp.

(12) Introductory Remarks in AGK2, Cape and Yale Photographic Star Catalogs.

(13) Clemence, G. M., "Inertial Frames of Reference," *Quarterly Journal of the Royal Astronomical Society*, Vol. 7, Blackwell Scientific Publications, Oxford and Cambridge, 1966, pp. 10–21.

(14) Wayman, P. A., "Determination of the Inertial Frame of Reference," *Quarterly Journal of the Royal Astronomical Society*, Vol. 7, Blackwell Scientific. Publications, Oxford and Cambridge, 1966, pp. 138–156.

(15) Fricke, W. and Kopff, A., "Introductory Remarks," in Fourth Fundamental Catalog, (FK4). Publications of Astronomisches Rechen-Institut Heidelberg, No. 10, G. Braun, Karlsruhe, 1963.

(16) Morgan, H. R., "Catalog of 5,368 Standard Stars, 1950, Based on the Normal System, N30," *Astronomical Papers of the American Ephemeris and Nautical Almanac*, Vol. XII, Part III, U.S. Government Printing Office, Washington, D.C., 1952.

(17) Gliese, W., "The Right Ascension System of the FK4," Publications of Astronomisches Rechen-Institut Heidelberg, No. 12, G. Braun, Karlsruhe, 1963.

(18) Kopff, A., Nowacki, H., and Strobel, W., "Individual Corrections to the FK3 and the Declination System of the FK4," Publications of Astronomisches Rechen-Institut Heidelberg, No. 14, G. Braun, Karlsruhe, 1964.

(19) Scott, F. R. and Hughes, J. A., "Computations of Apparent Places for the Southern Reference Star Program," *The Astronomical Journal*, Vol. 69, No. 5, pp. 368–370.

(20) "The American Ephemeris and Nautical Almanac," U.S. Government Printing Office, Washington, D.C.

(21) "Explanatory Supplement to The Astronomic Ephemeris and The American Ephemeris and Nautical Almanac," Her Majesty's Stationery Office, London, 1961, pp. 28–35.

(22) Jenkins, L. F., "General Catalogue of Trigonometric Stellar Parallaxes," Yale University Observatory, New Haven, Conn., 1952.

(23) Jordan/Eggert, "Handbuch der Vermessungskunde," (Handbook of Surveying), Vol. 3, part 1, Metzlersche Verlagsbuchhandlung, Stuttgart, 1939, 476 pp.

(24) Garfinkel, Boris, "An Investigation on the Theory of Astronomical Refraction," *Astronomical Journal*, Vol. 50, N.P., Feb. 1944, pp. 169–179.

(25) Schmid, Hellmut H., "The Influence of Atmospheric Refraction on Directions Measured to and from a Satellite," U.S. Army Geodesy, Intelligence and Mapping Research and Development Agency, Corps of Engineers, *U.S. Army Engineer Research Note No. 10*, Fort Belvoir, Va., Feb. 1963.

(26) Schmid, Erwin, "Phase Correction for Sun-Reflecting Spherical Satellites," U.S. Department of Commerce, National Oceanic and Atmospheric Administration, National Ocean Survey, Geodetic Research and Development Laboratory, Washington, D.C., *NOAA Technical Report NOS* 43, Rockville, Md., August 1971.

(27) Schaub, Werner, "Vorlesungen über sphärische Astronomie," (Lectures on Spherical Astronomy), Akademische Verlagsgesellschaft Geest & Portig, AG. Leipzig, 1950.

(28) Lacmann, Otto, "Die Photogrammetrie in ihrer Anwendung auf nicht-topographischen Gebieten," (The Application of Photogrammetric Methods to Non-topographic Problems), S. Hirzel Verlag, Leipzig, 1950, 132 pp.

(29) Schmid, Hellmut H., "An Integrated Ballistic Camera System," Ballistic Research Laboratories, Aberdeen Proving Ground, Md. U.S.A. 1959, 14 pp.

(30) Wild Heerbrugg AG., "Prospekt über BC–4 Ballistische Kammer," Heerbrugg, St. Gallen, Switz. (The BC–4 Ballistic Camera), 1959, 7 pp.

(31) U.S. Department of Commerce, "Satellite Triangulation in the Coast & Geodetic Survey," U.S. Department of Commerce, Environmental Science Services Administration, Coast & Geodetic Survey, *Technical Bulletin* No. 24, Washington, D.C., U.S.A., Feb. 1965, 21 pp.

(32) Taylor, Eugene A., "Optical Tracking for Space Geodesy," in The Use of Artificial Satellites for Geodesy, *Proceedings of the First International Symposium on the Use of Artificial Satellites for Geodesy*, Washington, D.C., April 26–28, 1962. North-Holland Publishing Company, Amsterdam, 1963, pp. 187–192.

(33) Henson, Fred C., Co., "Photo-Optical Instrumentation," 3311 E. Colorado St., Pasadena, Calif., U.S.A., P.O. Box 5265, 1966, 15 pp.

(34) Brown, Duane C., "Computational Tradeoffs in the Design of a One-micron Plate Comparator," D. Brown Associates, Inc., P.O. Drawer 550, Melbourne, Fla., U.S.A., *Photogrammetric Engineering*, 1969, pp. 185–194.

(35) Conrady, A., "Decentered Lens Systems," *Monthly Notices of the Royal Astronomical Society*, Vol. 79, 1919, pp. 384–390.

(36) Brown, Duane C., "Decentering Distortion of Lenses," *Photogrammetric Engineering*, American Society of Photogrammetry, Vol. XXXII, No. 3, May 1966, pp. 444–462.

(37) Schmid, Hellmut H., "Some Remarks on the Problem of Transforming Geodetic Ellipsoidal Coordinates into Cartesian Coordinates with the Help of the Reduced Latitudes," *Ordnance Computer Research Report*. Vol. VI, No. 2, Ballistic Research Laboratories, Aberdeen Proving Ground, Md., U.S.A., April 1959.

(38) Schmid, Erwin and Schmid, Hellmut H., "Curve and Surface Fitting with Potential Functions," *Zeitschrift für Vermessungswesen*, Nr. 11, Verlag Konrad Wittwer, Stuttgart, Germany, 1971, pp. 488–497.

(39) Schmid, Hellmut H., "Ein allgemeiner Ausgleichungs-Algorithmus zur Auswertung von hybriden Messanordnungen," (A Generalized Least Squares Solution for Hybrid Measuring Systems), *Bildmessung und Luftbildwesen*. Deutsche Gesellschaft für Photogrammetrie, Vol. 33, 1965, Fasc. 3, pp. 93–102 and 4, pp. 173–176.

(40) Schmid, Hellmut H. and Schmid, Erwin, "A Generalized Least Squares Solution for Hybrid Measuring Systems," U.S. Department of Commerce, Environmental Science Services Administration, Coast & Geodetic Survey, Washington, D.C., June 1965; also *The Canadian Surveyor*, Vol. IX, No. 1, The Canadian Institute of Surveying, Ottawa, Canada, March 1965, pp. 27–41.

(41) Zurmühl, R., "Matrizen," (Matrices) Springer-Verlag, Berlin-Göttingen-Heidelberg. Fourth edition 1965, 146 pp.

(42) Slama, Chester C, "A Mathematical Model for the Simulation of a Photogrammetric Bundle Using Redundant Stellar Control," U.S. Department of Commerce, National Oceanic and Atmospheric Administration, National Ocean Survey, *NOAA Technical Report NOS* 55, Rockville, Md., Dec. 1972.

(43) Schmid, Hellmut H., "A General Analytical Solution to the Problem of Photogrammetry," *Ballistic Research Laboratories Report* No. 1065, Aberdeen Proving Ground, Md., U.S.A., 1959, 83 pp.

(44) Hanson, Robert H. "Satellite Image Reduction." U.S. Department of Commerce, National Oceanic and Atmospheric Administration, National Ocean Survey, Washington, D.C., in preparation.

(45) Hanson, Robert H., "Photogrammetric Satellite Triangulation Network Adjustment." U.S. Department of Commerce, National Oceanic and Atmospheric Administration, National Ocean Survey, Washington, D.C., in preparation.

(46) Poetzschke, Heinz G. "A Comparator Calibration Method. U.S. Army Material Command. *Ballistic Research Laboratories Report* No. 1353, U.S. Army Ballistic Research Laboratories, Aberdeen Proving Ground, Md., U.S.A., Jan. 1967, 33 pp.

(47) Rinner, Karl, "Systematic Investigations of Geodetic Networks in Space," Annual Technical Report, European Research Office, Contract No. 91–591–EUC 3584, 1966, 186 pp.

(48) Meade, Buford K., "High-Precision Transcontinental Traverse Surveys." *Surveying and Mapping*, American Congress on Surveying and Mapping, Vol. 27, Washington, D.C., 20044, 1967, pp. 41–46.

(49) Wolf, Helmut, "Rigorous Computation of the European Traverse Including the Accompanying Strip of Triangulation." M. Kneissl: Die europäische Basis-Traverse Tromso-Catania für ein geodätisches Satelliten-Weltnetz. (The European Traverse Tromso-Catania in the Geodetic Satellite World Net). DGK. Reihe B. Heft Nr. 143 (German Geodetic Commission. Series B. Fasc. No. 143) Munich, 1967, pp. 129 et seq.

(50) Schmid, Hellmut H., "Eine allgemeine analytische Lösung für die Aufgabe der Photogrammetrie." (General Analytical Solution to the Problem of Photogrammetry). *Bildmessung und Luftbildwesen* 1958, Heft 4, pp. 103–113, und 1959, Heft 1, pp. 1–12.

3. ERROR THEORETICAL CONSIDERATIONS

3.1 Error Budget of Geometric Satellite Triangulation

As shown in chapter 1 the principle of the method of geometric satellite triangulation is based on combining a large number of individual directions to satellites in a three-dimensional triangulation. These satellite directions are obtained by interpolating the individual images of the chopped satellite trail into the framework of the star background present on the photograms.

Directions to the star images are first computed, basically as functions of the observing datum, the time of observation (UT-1), and the instantaneous pole coordinates. These directions are referenced either to the astronomic right ascension-declination system for a specific epoch (x system) or, after appropriate rotation, to an Earth-fixed, three-dimensional reference coordinate system (y or z system) in which the observation station locations are to be triangulated (cf. sec. 2.7.2).

The satellite images are recorded in an arbitrary time sequence which is, however, common for all stations observing an event. The satellite images are then interpolated into the directions to the stars, i.e., into the background of stars, and thus fixed in the same reference system to which the star images have been reduced. The three-dimensional position of the observing stations is found by assigning to them a location such that the satellite directions emanating from the various stations lead to the determination of the three-dimensional geometry of all observed satellite transits.

Aside from the practical requirements of the field observer it is not necessary to know in advance the orbit of the satellite. The points of the orbit serve merely as elevated triangulation targets and only the condition for intersection of corresponding rays is needed to fix the positions of the observation sites (cf. sec. 2.2). As a consequent requirement such rays must satisfy the "geometric condition of simultaneity" explained in sec. 2.4. This condition is automatically met, for example, in case the satellite trail is fixed by the recording of a sequence of flashes emitted by the satellite.

Since a sufficient number of such flashes can not be generated to reduce the influence of scintillation adequately (cf. sec. 2.5) we photograph the satellite in the portion of its orbit illuminated by the sun. In this method the trace of the orbit is chopped by means of a rotating disk shutter in the camera (cf. sec. 2.6, figs. 22 and 23) into a series of time-dependent individual images. However for physical as well as technical reasons it is impossible to generate satellite images at the several observing stations that initially satisfy the "geometric condition of simultaneity." It therefore becomes necessary to fit the bundle of directions to the satellite for a particular event as closely as possible to the satellite orbit which is by its nature continuous. Since only a small portion of the orbit (about 1 or 2%) is involved, the observed curve may be considered as part of an elliptical orbit obeying the Keplerian laws of motion. These laws predicate that the satellite directions are referred to an inertial system as approximated, e.g., by the right ascension-declination system.

On the other hand, because of the Earth's rotation, a solution based on satellite directions referred to an Earth-fixed coordinate system requires the assumption of a twisted space curve as a model for the satellite orbit.

In such a procedure satellite triangulation is subject to five sources of error. First are the uncertainties in the star catalogue data. Second are the accidental errors in time determination for the star and satellite exposures. Third are the accidental errors in coordinate measurement of the star and satellite images, fourth the influence of scintillation acting as an accidental error source and, finally, the irregular distortion of the photographic emulsion. All must be taken into consideration.

Such a presentation of the error budget assumes first that the corresponding systematic errors are sufficiently small and, secondly, that the mathematical model used to reconstruct the photographic process is sufficiently close to reality. Furthermore the assumption must be valid that the photographed sections of the satellite orbit must be usable qualitatively for interpolation. All these assumptions must hold within such accuracy limits that the influence of the remaining imperfections on the triangulation computations remain a magnitude smaller then the propagation of the five cited error sources.

All further secondary corrections such as pole displacement (cf. end sec. 2.4), astronomic and parallactic refraction, satellite phase angle and light travel time (For all these corrections see sec. 2.5.) must correspond to geometric-physical reality with such accuracy that the effect of remaining biases is negligibly small.

Even from this point of view the rigorous error theoretical treatment of the satellite triangulation method leads to a mutually correlated matrix schematic. The individual plates are uncorrelated with respect to the photogrammetric reduction so far as processing the measured star and satellite coordinates is concerned. However, for all plates introduced into a satellite triangulation system only

one set of reference stars is available, and these are limited in number and distribution.

Hence the same group of stars appears repeatedly on the same plate as a result of star registration before, during, and after the event. In addition, such groups are recorded on a number of plates.

In the observations for the world net, stars up to 8th magnitude and with maximum mean position errors of 0".4 were selected from the SAO star catalogue. This gives us about 20,000 stars at our disposal ([3] of sec. 2). With an average frequency of about 100 stars per plate and approximately 3,000 plates in the world net this means that each star appears, on the average, on 15 plates. Since, strictly speaking, there can result only one pair of corrections for each observed star in the adjustment, the mathematical reconstructions of all the photogrammetric bundles and their orientations are correlated to such a degree that they should really be adjusted as a unit even if, for lack of knowledge of existing correlations, one accepts independent weight matrices for the star coordinates.

In the spatial triangulation of the observing stations the satellite directions are now combined to reconstruct the geometry of the recorded satellite orbit curve. The intersection condition for the rays applied in this process—either direct or indirect by way of fitting to a spatial model of the orbit—contains additional orientation information, similar to the relative orientation in the classical photogrammetric restitution process. But since all photogrammetric bundle parameters that determine directions to the satellite and their orientation quantities are correlated, there results a correlation between all recorded satellite events; i.e., observing station positions and all observed satellite orbital curves should be obtained from one common adjustment with the use of the covariance matrix involving all reconstructed photogrammetric bundles and their orientations.

Processing the approximately 2,500 plates available in the world net requires the computation of nearly 50,000 interpolation parameters. For the approximately 1,400 recorded events, close to 7,000 orbital parameters would have to be determined. A simultaneous adjustment of such a large number of correlated unknowns is at present, even with the largest available computer, neither economically feasible nor, because of the required computational accuracy, capable of realization.

One has, therefore, to make concessions. From the error theoretical point of view, probably the most serious compromise is the necessity of separately determining the photogrammetric interpolation parameters for each plate, since these parameters determine absolute directions to the interpolated satellite images and are therefore of decisive significance in fixing the spatial positions of the observation stations. In conformance with the weights given with the star data, a pair of corrections for the star coordinates is obtained in each bundle reconstruction adjustment, independent of the number of images of the particular star. On completion of all the bundle reconstructions under consideration there will therefore be for each star as many corrections available as the number of times such a star was recorded on the various plates. On the basis of the observation data in the world net this averages out to 15 times. Arguing from the concept that every adjustment represents a weighted arithmetic mean, there is a possibility of computing for each star a unique set of corrections in the form of the arithmetic mean of the individual pairs. Care need only be taken to insure, by use of appropriate weights, that the mean error of unit weight after adjustment is the same for all the bundle reconstructions. One could then add this average of the corrections to the original star data and repeat the bundle reconstruction computations. With an appropriate choice of weights for these corrected star data the latter could then be held correspondingly fixed in the repeated bundle reconstruction.

The justification for such an expensive iteration depends on how close the averaged star coordinate corrections come to the solution from a rigorous adjustment. The significance of such a solution hinges, therefore, on the extent to which these "improved star coordinates" represent in their totality a reference system which is superior to the star catalogue available originally. In the processing of the world net the "improved star coordinates" for the 20,000 stars being used are being computed in order to be able to present these amended right ascensions and declinations to the astronomers for critical evaluation. Repetition of the computations for bundle reconstructions is, however, not contemplated for financial reasons.

As mentioned previously the accidental errors of time designations for the star and satellite recordings must be taken into consideration. In the adjustment for the single camera this is taken care of automatically by carrying corrections to the right ascensions. These being geometrically equivalent to UT-1 it is necessary only to compute weights for the introduced right ascension values, taking into account the uncertainties in time associated with the recorded instants of observation. For the instrumentation used in the world net this accidental timing error amounts to less than a

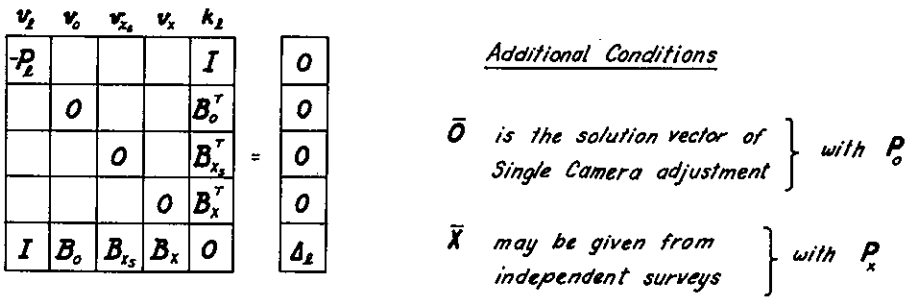

Figure 34.—Basic normal equations system corresponding to observation equations $Bv = \Delta$. The weights P range from 0 to ∞.

millisecond so far as the registration of the shutter action is concerned. Since the available UT-1 is in itself scarcely better than ±2 ms (which acts as a system error in the orientation for the individual plate) the assumption of a ±3 ms overall uncertainty in the determination of time for the star exposures seems reasonable. The inaccuracy of a direction corresponding to this time uncertainty is ±0".045, a magnitude considerably less than the photogrammetric measuring accuracy with the BC–4 system and the 450-mm lens, hence negligible.

A similar conclusion can be drawn with respect to the influence of random errors of the synchronization procedure on the satellite images. By means of periodic control of timing (cf. sec. 2.6.1) the instants of observation at the various stations are fixed relative to each other within at least ±100 μs. The most critical situation would arise for the Echo satellite with a speed of 8 km/s and minimum distance of 1,000 km, where 100 μs corresponds to a change in direction of ±0".16. With the Pageos satellite used in the world net, because of its greater distance and consequent slower speed, a timing error of ±100 μs results in a maximal direction uncertainty of only ±0".04. Although this is negligibly small, a calculation employed in the adjustment discussed later on—which is designed primarily to eliminate scintillation with polynomial curve fitting—serves to adjust as well any existing random timing errors in the synchronization.

Existing correlations between the separately reconstructed bundles of directions to stars are neglected, as detailed above. Thus, for each single camera computation individual parameters are determined for the interpolation model including the covariance matrix associated with these parameters. This is significant for further evaluations.

The locations of the observing stations are computed in the step of the adjustment which now follows. Their position in space is fixed by the condition that the bundles of directions to the satellite issuing from these stations must lead to the geometry of all satellite orbital curves that have been recorded. Since each bundle of directions is obtained by the interpolation of the corresponding satellite images into the relevant interpolation model and, since these models are now no longer correlated, it follows that the individual satellite orbit determinations are likewise uncorrelated. This results in a simplification of the data processing as the orbit determinations can be processed sequentially and care need only be taken that their cumulative effect bears on the station determination.

The condition of intersection on which the determination of the geometry of the observed satellite orbits is based—either directly or indirectly by way of a fit to a spatial orbital model—contains additional information for determining the parameters of the relevant interpolation models. The coordinates of the stations and the parameters specifying the geometry of the satellite orbit, plus all parameters of all interpolation models involved together with their individual variance-covariance matrices referred to above, must appear as unknowns in the adjustment.

The resulting system of normal equations is $\mathbf{Bv} = \mathbf{\Delta}$ with a range in weights $\mathbf{P}$ from zero to infinity. Designating the vector of corrections to the measured satellite image coordinates by $\mathbf{v}_l$, the correction vector for the previously computed bundle interpolation parameters $\mathbf{0}$ by $\mathbf{v}_0$, the correction vector for the approximated satellite orbital positions by $\mathbf{v}_{x_s}$, and finally the correction vector for the approximated station coordinates by $\mathbf{v}_x$, the corresponding normal equations system can be written as indicated in figure 34. The $\mathbf{X}$ are supplementary conditions that may exist between the stations to be triangulated such as, for example, measured distances for scale determination.

Figure 35 shows the normal equations system after these functional relations have been intro-

Introducing $\Delta_0 = \bar{0} - 0^\circ$ *and* $\Delta_x = \bar{x} - x^\circ$

v_l	v_0	v_{x_s}	v_x	k_l	k_0	k_x		
$-P_l$				I				0
	0			B_0^T	I			0
		0		$B_{x_s}^T$				0
			0	B_x^T		I	=	0
I	B_0	B_{x_s}	B_x	0				Δ_l
	I				σ_0			Δ_0
			I			σ_x		Δ_x

$\sigma_0 = P_0^{-1}$

$\sigma_x = P_x^{-1}$

After elimination of v_l v_0 k_l k_0 *and* k_x

v_{x_s}	v_x		
$-B_{x_s}^T(\sigma_l + B_0\sigma_0 B_0^T)^{-1}B_{x_s}$	$-B_{x_s}^T(\sigma_l + B_0\sigma_0 B_0^T)^{-1}B_x$	=	$B_{x_s}^T(\sigma_l + B_0\sigma_0 B_0^T)^{-1}(\Delta_l - B_0\Delta_0)$
$-B_x^T(\sigma_l + B_0\sigma_0 B_0^T)^{-1}B_{x_s}$	$-P_x - B_x^T(\sigma_l + B_0\sigma_0 B_0^T)^{-1}B_x$		$P_x\Delta_x + B_x^T(\sigma_l + B_0\sigma_0 B_0^T)^{-1}(\Delta_l - B_0\Delta_0)$

Figure 35.—The normal equations system augmented with additional constraints. The lower portion shows the reduced matrix after elimination of the auxiliary parameters v_l, v_o, k_l, k_o and k_x.

duced. The corresponding set of correlates are designated by **K**. The system reduced down to satellite orbit and station coordinates is given in the lower portion of figure 35.

The image coordinates can be expressed as functions of the interpolation parameters describing the photogrammetric bundle of the coordinates of the satellite position and of the relevant coordinates of the observing station. Since the individual bundle reconstructions are uncorrelated, it is possible to replace the correction vector to the interpolation parameters by a corresponding correction vector to the image coordinates, thus reducing decisively the number of unknowns to be carried.

As is apparent from the lower portion of figure 35, this computation procedure is completely rigorous only when the expression $\mathbf{\Delta}_0$ is carried along on the right-hand side of the reduced normal equations system, i.e., with the vector of absolute terms; hence, a rigorous elimination of the **0**-parameters is not possible. However, since in the first iteration loop the **0**-values as obtained from the single camera adjustment are introduced into the triangulation adjustment as approximation values, $\mathbf{\Delta}_0$ is initially a zero vector. This means that the elimination of the **0**-parameters is valid to within the first order of $\mathbf{\Delta}_0$ terms. Moreover, due to the large number of absolute control points (in our case about 100 stars per plate), the influence of the orientation contribution resulting from the intersection condition is quite small. Thus the procedure is justified by the considerable gain in simplicity derived by the elimination of these parameters in the triangulation adjustment.

This leaves the unknowns that are to be determined by the condition of intersection of the rays: the coordinates of the observing station and the parameters describing the geometry of the satellite orbital curves. From a conceptual point of view this means that the bundles of directions to a satellite assigned to a particular satellite pass must conform as closely as possible in the sense of an adjustment to the orbital curve. This curve is subject to the geometric consequences of Kepler's first law, according to which the orbit can be expressed, in an inertial system, by the equation of an ellipse.

Furthermore, the fitting process must do justice to the dynamic content of Kepler's second law, according to which the true anomaly is a function of time. It seems convenient in the application to develop the true anomaly as a series in the eccentricity and the mean anomaly. Basically speaking one can say that Kepler's first law accomplishes the fit of the bundle perpendicular to the direction of the orbital curve and the second law along the orbit curve. Kepler's third law can

not be made use of because the orbital period of the observed satellite is not known. Moreover, the balloon satellite with its typically unfavorable mass ratio is exposed to disturbing influences such as residual atmospheric pressure and the Sun's radiation pressure, so that the orbital period could yield only limited information in a geometrical sense. All computation schemes must furthermore take into account the fact that the recorded times for satellite imagery refer to the instants of exposure and these data must therefore be corrected for light travel time and Earth rotation during this light travel time before they can be further processed with the application of the principles of celestial mechanics.

The practical application of orbital determination by means of bundle fitting is faced with two further obstacles. As stated at the end of sec. 2.5, a large number of satellite images is needed in the adjustment to sufficiently reduce the scintillation effect. In the world net the number of images averages 300 per plate. Since the corresponding 300 directions are derived from the same group of interpolation parameters they are correlated, which means that for each of the satellite direction bundles to be introduced into the fit a 600×600 completely filled covariance matrix must be taken into consideration. If the event has been observed by more than two stations this quickly leads to undesirably large demands on the memory of the computer. Even more decisive is the fact that the scintillation effect depends on the meteorological conditions during the event which can be quite different at the contributing stations. To prevent this "noise" from being averaged between the contributing stations to an event in the triangulation adjustment, the appropriate weight matrices for the individual direction bundles must be computed, using the mean scintillation characteristic for each station. This quantity is not yet available.

Alternatively to the bundle fitting concept one could also fix the satellite orbital curve by smoothing the spatial coordinates of the triangulated satellite points with polynomials as functions of time [11]. Such a solution assumes that the orbital curve is designated by a series of short duration flashes emitted from the satellite, the time sequence of the flashes being sufficiently well known. Only then will there be recorded images on the individual plates which lead to the triangulation of the corresponding orbital points. On the other hand if, as is necessary for practical reasons at this time, the satellite images are produced on the various plates by chopping the trail of the continuously illuminated satellite with a rotating disk shutter into separate points, then one would first have to compute the necessary light travel times iteratively with approximated satellite positions. In principle this would give sufficient information to interpolate on each photogram for the event image points satisfying the "geometric condition of simultaneity." From an error theoretical standpoint, however, such interpolation is open to question for the very reason that the position of the individual images is influenced to different and unknown extent by scintillation. From the computational standpoint still another disadvantage accrues to this solution in that all the satellite directions on the selected plates are correlated, leading to variance-covariance matrices whose consideration would require an intolerable amount of memory space.

The theoretical and practical difficulties of the above method of solution are circumvented by modifying the approach and evaluating each plate independently to the greatest extent possible.

This concept is valid also from the standpoint of error theory and is based on the fact that the measurements at a given observing station, i.e., the photogrammetric registration of the star images and satellite orbit together with the relevant recordings of time, are self-sufficient in the sense that the information so obtained is completely independent of similar operations at other stations. Transforming these measuring data into time-correlated satellite directions requires only the additional assumption that the satellite orbital curve is continuous.

Knowing the geometric-dynamic properties of the photographed portion of the satellite orbit as described above, it should be possible to postulate the form of this trail on the photogram, in direction of the trail and at right angles to it, in terms of the central perspective laws, light propagation time, and the aberration due to the Earth's rotation. The formalization would lead to an infinite series expansion in which higher order terms could be neglected. An adjustment to this theoretical model of the orbital projection could then be made by fitting the satellite images to it. Another possibility and the one adopted here is to smooth the satellite images with polynomials. Just as the triangulated spatial coordinates of discrete orbital points can be fitted to polynomial functions of time, the recorded sequence of time-related satellite images can be similarly smoothed, resulting in positions of the satellite on the photogram as a function of time. A curve fit is justifiable all the more from the standpoint of error theory inasmuch as the simplest conceivable projection model exists between the continuous orbit and the corresponding satellite image sequence. The measured satel-

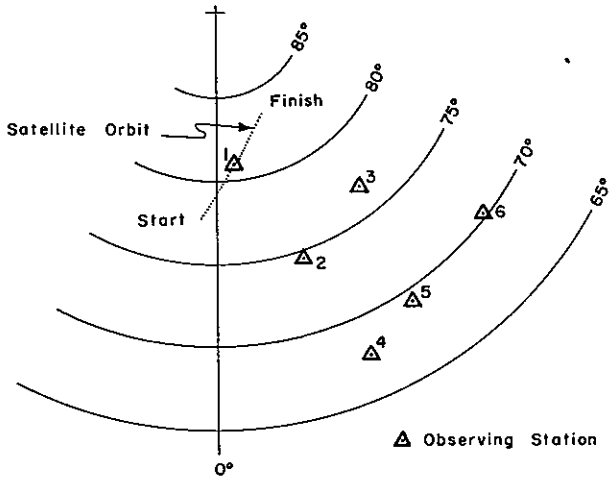

Figure 36.—Schematic of the portion of the satellite orbit observed and the typical location of observing stations.

lite image coordinates are therefore reduced to the concept of a rigorous central perspective (i.e., the concept of an ideal photograph) by means of the bundle reconstruction parameters obtained from an adjustment based on reference stars and their images. Then one applies the principle of an adjustment to compute best-fitting polynomials. To the extent that the central perspective nature of the images of the satellite orbital points has been reproduced, this adjustment has the function of neutralizing the random errors of the comparator measurements, random emulsion shrinkage, and scintillation effects. In addition, it yields an indication of the accuracy of the smoothing polynomials in the form of statistical functions.

In order to verify the required degree for these polynomials, 380 satellite space coordinates were recorded for a simulated Pageos orbit at intervals of 0.8 s, corresponding to the average length of the Pageos arc observed with the BC–4 camera. The satellite orbit was integrated with a 10th-order Cowell-Störmer process. The Earth's gravity field was introduced by means of an expansion in spherical functions to the 4th degree and 4th order using the coefficients of the "1966 Smithsonian Institution Standard Earth." Radiation pressure of the Sun and attraction of the Moon and Sun were also included in the integration computations. The resulting coordinates of satellite positions were then transformed into a geostationary system.

Six fictitious observing stations (see fig. 36) were distributed relative to the computed orbit, to simulate the geometrical distribution of stations. By applying the time of light propagation for each of the 380 fictitious points of the orbit, corresponding plate coordinates were computed at each of the six

TABLE 3.—*Curve fit of 380 fictitious satellite images with polynomials of degree 1 to 11; x in the direction of the trail, y normal to it*

	Degree of polynomial	σ_x [μm]	σ_y [μm]
Obs. sta. 1 ------	1	404.166	215.720
	2	53.445	1.853
	3	1.267	0.289
	4	0.090	0.006
	5	0.003	0.001
	6	0.000	0.000
Obs. sta. 2 ------	1	461.861	133.736
	2	54.919	0.964
	3	1.479	0.166
	4	0.099	0.004
	5	0.004	0.000
	6	0.000	0.000
Obs. sta. 3 ------	1	226.233	169.385
	2	50.510	0.229
	3	0.709	0.204
	4	0.076	0.002
	5	0.002	0.000
	6	0.000	0.000
Obs. sta. 4 ------	1	494.437	57.121
	2	53.362	0.209
	3	1.571	0.039
	4	0.099	0.000
	5	0.004	0.000
	6	0.000	0.000
Obs. sta. 5 ------	1	356.618	82.163
	2	51.751	0.223
	3	1.116	0.077
	4	0.085	0.001
	5	0.003	0.000
	6	0.000	0.000
Obs. sta. 6 ------	1	145.585	157.387
	2	48.951	0.476
	3	0.458	0.184
	4	0.070	0.000
	5	0.001	0.000
	6	0.000	0.000

stations to reproduce an exact central perspective mapping of the orbital geometry. These plate coordinates were then subjected to polynomial curve fits from the first to the eleventh degree in sequence. The resulting mean errors of the computed coordinates after adjustment are listed in table 3 below, σ_x referring to the coordinate component in direction of the trail and σ_y at right angles to the trail.

For polynomials of 7th to 11th degree all entries are the same as they are for the 6th degree.

From table 3 it is seen that the required accuracy can be obtained with a polynomial of the 5th degree along the trail and of the 4th degree across the trail. At the same time no undesirable effect of "oversmoothing" is apparent with polynomials of higher degree, at least up to the eleventh. This degree is of consequence in that from an

adjustment polynomial of the nth degree only $(n+1)$ computed values can be used, otherwise the corresponding covariance matrix becomes singular, while the use of fewer values does not exhaust the available information content completely.

In processing the world net, polynomials of the 6th degree are used in smoothing both x and y, so that seven fictitious directions can be used in the final triangulation, provided that the trace of the portion of the satellite orbit common with other stations extends over the whole plate. Thus the polynomials provide the adjusted location of the satellite trace as a function of the recorded time. This relation simplifies the application of the influence of time corrections such as clock differences and light propagation. After having transformed a selected satellite orbital time to a corresponding time of registration on the plate, it is necessary to compute only x and y coordinates for the corresponding fictitious plate image from the relevant polynomial with this latter time. By using this procedure on all photograms that have observed a common event, a fictitious image is obtained on each photogram satisfying the "geometric condition of simultaneity" (cf. sec. 2.4). An approximate preliminary triangulation of the relevant orbital points will be needed to determine the variable propagation time of light for each registered orbital image. It should be noted in this connection that an error of 3 km in the approximated distance will create an error of only 10 μs in the time. Along with the coefficients of the curve fit polynomials one obtains the mean dispersion of the individual images and hence the variance-covariance of the polynomial parameters. Since the fictitious satellite image positions corresponding to specified times are computed as functions of the polynomial parameters (cf. (58) and (270)), the corresponding error propagation computation will produce their variance-covariance matrix. This matrix rigorously displays the correlations among the individual satellite images resulting from the polynomial smoothing. If 7 such fictitious satellite images are used, as for example in the world net, a 14×14 covariance matrix for these points must also be computed.

At this stage the following evaluation data are available for each satellite orbit observation at a station:

a. The bundle parameters describing the interpolation model, including the exterior elements of orientation, and the associated 20×20 covariance matrix scaled to an *a priori* introduced error of unit weight.

b. The 7 pairs of coordinates for the selected fictitious satellite images together with their 14×14 covariance matrix, also referred to the error of unit weight mentioned in (a).

The last processing step, computing the three-dimensional geometry of the observing stations, amounts to determining the spatial directions corresponding to the fictitious satellite images in order to triangulate the satellite orbit points and all the observation sites by means of an adjustment, subject to the condition that the sum of squares of weighted corrections to the fictitious satellite image coordinates be a minimum. The weight matrices of the satellite direction bundles are compounded at each station by the joint influence of the covariances of the relevant interpolation parameters (cf. (a) above) and the covariances of the plate coordinates of the fictitious satellite images (cf. (b) above).

Whenever additional *a priori* given information relative to the geometry of the observing sites, such as spatial distance between them (as for scale determination), position coupling between adjacent stations (eccentric reductions), or the like is used as input data, such data can be introduced into the adjustment without difficulty after having computed the necessary functional weights, referred to the *a priori* selected error of unit weight. This is true also for the case where additional geometric data will become available through, for example, laser distance measurement between satellite and station.

In the world net such scalars will be introduced in the form of measured distances of edges of the world net polygon primarily in the United States, Europe, Africa, and Australia, as shown in figure 37.

These basic ideas underlying the error budget of geometric satellite triangulation are presented here in explanation of the error theoretical considerations that lead to the adjustment algorithm described in sec. 2.7. Moreover, by pointing out computational possibilities differing from the present solution and leading eventually to completely rigorous adjustment and error propagation, it is hoped that impetus will be given to perfecting the method of geometric satellite triangulation.

The next section reports some results on accuracies in the various evaluation phases obtained in the processing of the observed data for the world net.

3.2 Analysis of the Essential Sources of Error and the Error Propagation into the Spatial Triangulation.

In sec. 3.1 it was shown that the method of geometric satellite triangulation is subject to five

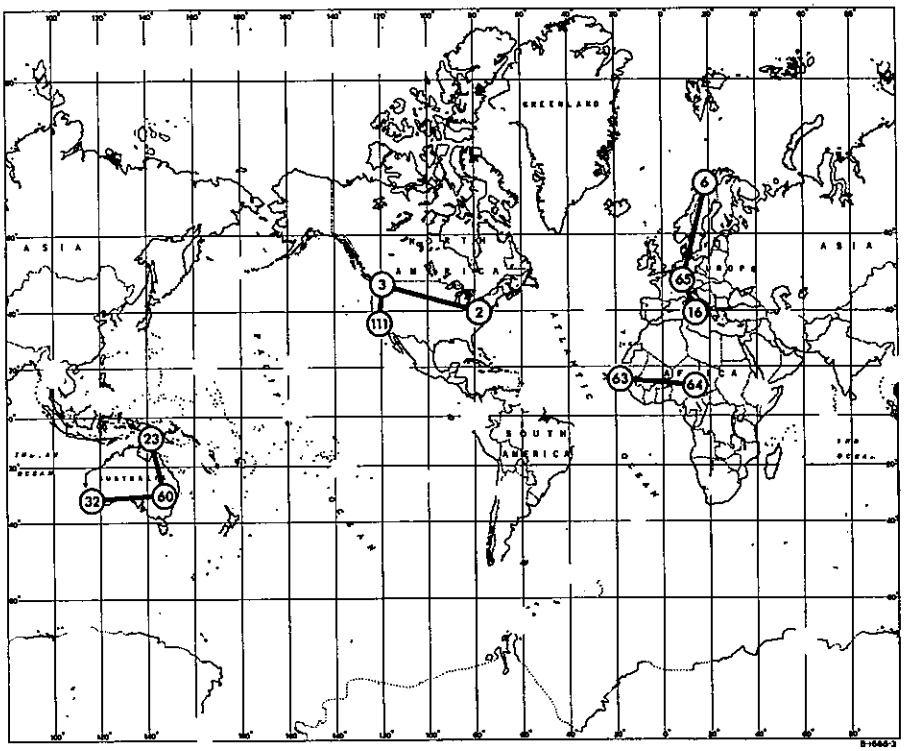

Figure 37.—Scalars connecting observing stations actually measured in the world net program.

random error sources. The accidental errors from these sources arise in connection with:

a. the comparator measurements of star and satellite images.

b. the reference data from the star catalogues.

c. the designated times of the star and satellite recordings.

d. atmospheric scintillation affecting the directions to the recorded star and satellite orbit points, and

e. accidental emulsion shifts generated in the process of developing the plate.

This idealized situation will, however, exist only to the degree to which sufficient precautions are exercised to either model the following systematical error sources or eliminate them by operational procedures during the field observations and in the data processing.

a. Observation Phase

(1) Elimination of possible static instability of the camera during the average half-hour period of observation.

(2) Elimination of systematic errors in recording the instant of shutter operation which is needed to within a few ms of Universal Time and, relative to all involved cameras, to within 1/10 ms.

b. Measurement Phase

(1) Strict adherence to the Abbe comparator principle.

(2) Correction for the lack of perpendicularity of the comparator axes.

(3) Accounting for at least linear differences in the comparator scales.

c. Adjustment phase

(1) Determination of the elements of interior orientation existing in the operational environment.

(2) Determination of the comparator constants outlined in b(2) and (3) above.

(3) Modeling of astronomic and parallactic refraction, the latter because of the finite distance of the satellite.

(4) Modeling the phase angle of the satellite illumination as function of size and shape of the satellite, its reflective property, and the geometric positions of the sun, satellite and observing station during the event.

(5) Considering influence of light travel time on stations synchronization and aberration.

(6) Introducing with sufficient accuracy the spatial orientation of the instantaneous rotation axis of the Earth (pole wandering) with respect to individual camera orientations as

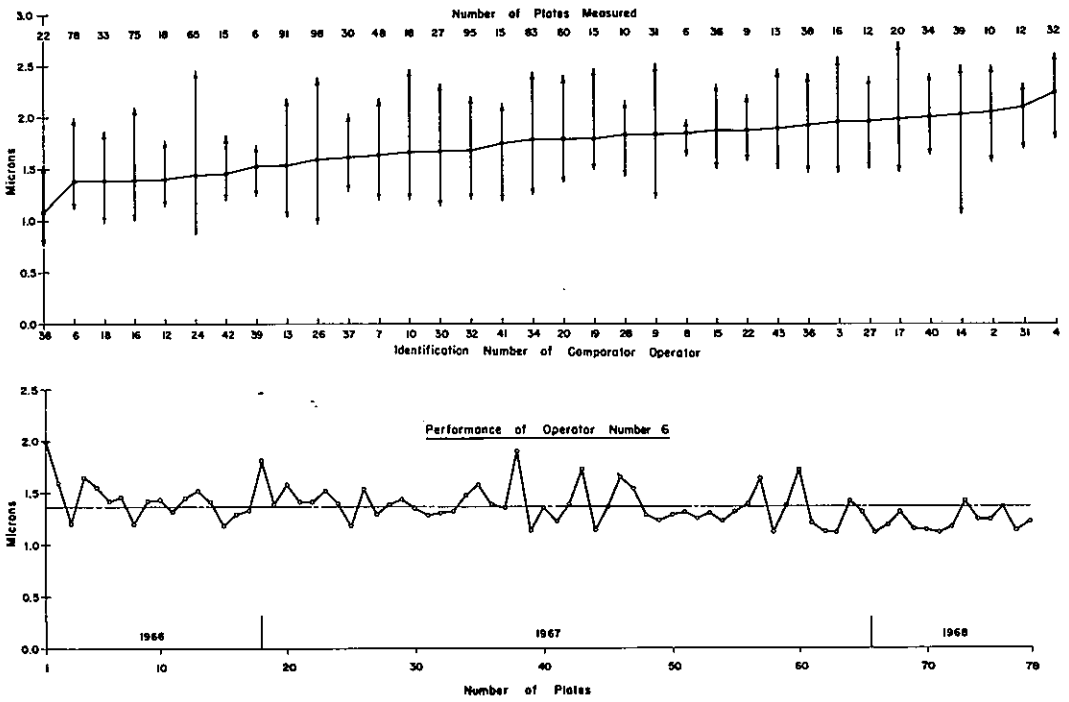

Figure 38.—Comparison of the measuring accuracies attained by a group of comparator operators and the individual performance of one.

well as with respect to the use of UT-1 (true angle of Earth's rotation).

(7) Reduction of star places to time of observation, involving precession, nutation, proper motion, radial velocity, annual and diurnal aberration, as well as the influence of the spectral characteristics and magnitude of the star on the photogrammetric imagery.

Quantitative results will now be given with respect to the above mentioned random errors and their propagation into the end results of the spatial satellite triangulation, errors in time determination, as previously mentioned, being considered negligible [1], [2], [3], [4], [5].

3.2.1 Accuracy of the Comparator Measurements

We discuss first of all the result of measuring 1,210 photograms, representing practically half of the observed data from the world net.

On each photogram, on the average, 100 fixed stars were recorded before and after the satellite transit and also during the event. With repeated exposure 500 to 800 star images are thus registered. In addition there are about 300 satellite images so that on each photogram at least 800 images must be measured. In order to complete these measurements in the time alloted to the world net program, six comparators of similar design were in operation. Of significance also is the fact that a group of operators is involved in the measurements. Each photogram is measured on the comparator in two positions differing by approximately 180° (cf. sec. 2.6.5). By means of a two-component translation, two scale factors and a rotation, the two sets of measurements are brought into coincidence by an adjustment. The internal accuracy of the measuring process (precision of the comparator measurements) can then be judged on the basis of residual differences from double measurements. From the selected photograms with their 1,291,744 double measurements there resulted a mean error for the arithmetic mean of a double measurement of $\pm 1.63\ \mu$m. No significant difference between the precision of the x and y coordinates was detected.

It is of interest to group the measurement of plates by individual operators. The separately computed average measuring accuracy for each of the 34 comparator operators, arranged in sequence of increasing absolute amounts, is shown in figure 38. The number at the top of each arrow represents the number of photograms measured by the operator, and the ordinates of the arrow heads indicate the range over which the mean errors of the individual plate measurements vary for that operator.

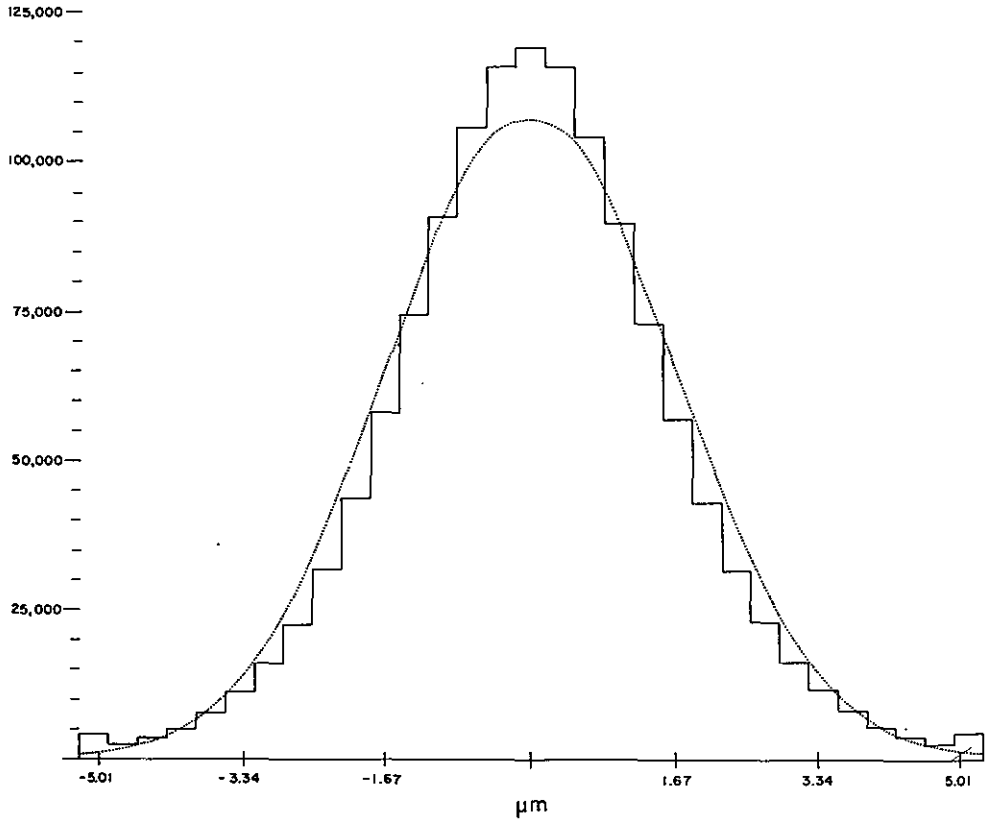

Figure 39.—Histogram of 1,291,744 double measurement differences.

It can be seen that the mean measuring precision attained ranges from ± 1.1 μm (for operator no. 38) to ± 2.2 μm (for operator no. 4). The best single result was ± 0.76 μm by operator no. 38 and the worst was ± 2.66 μm by operator no. 20. As an explanation of these fairly surprising differences one must assume chiefly the varying capabilities of the operators but also the influence of environmental conditions on image quality. The lower diagram in figure 38 shows the mean error of the 78 photograms measured in chronological order by operator no. 6 over a period of 18 months. Although the average mean error of $\pm 1.37$$\mu$m by this operator is relatively low, the dispersion is typical for the behavior of all operators with respect to the quality of their individual measuring results. In addition to displaying the variation in precision from plate to plate the diagram indicates a steady though small improvement in the measuring operation.

Figure 39 shows the histogram of the 1,291,744 double measurements. From the similarity of the histogram with the superimposed theoretical normal distribution one can conclude a sufficiently close absence of bias errors, all the more so taking into consideration the fact that the data for the histogram are composed of samples with differing mean errors. On the basis of these results one can well imagine that these measurements were all made by one fictitious operator on one fictitious comparator instead of by 34 operators on 6 comparators. Hence for the further error theoretical studies we shall assume that the internal accuracy of image coordinates, meaned from double measurement, is sufficiently well expressed in their totality by a mean error of ± 1.63 μm.

The mean errors m_l computed separately for each photogram are plotted in figure 40 for 500 photograms selected for further study. The observed data selected are derived from 35 stations of the world net plotted according to latitude. Table 4 shows the number of plates for each station. The location of the stations is shown in figures 47 to 52. See also table 1 in sec. 1.2.

3.2.2. Accuracy of the Reconstructions of the Photogrammetric Bundles and Their Orientations.

The parameters for reconstructing the bundle and its orientation are obtained by relating the

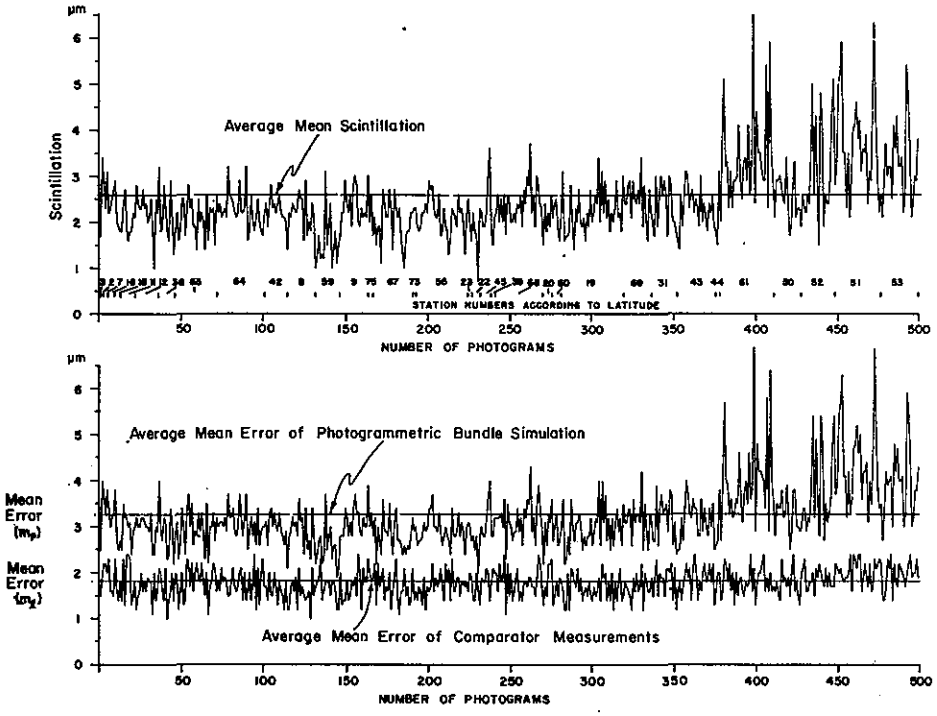

Figure 40.—500 photograms, arranged according to increasing latitude of observing station, showing, in the top diagram, the amount of scintillation for each plate and, below, the mean errors of the bundle simulation and the comparator measurements, respectively.

measured star image coordinates to the corresponding star catalogue data with an adjustment to a mathematical model. The total of these quantities, previously designated as interpolation parameters, includes in addition to the purely photogrammetric parameters a second scale factor and an angle to correct for the *a priori* assumed perpendicularity of the comparator spindles. The introduction of these extra parameters is justified insofar as one may assume that the homogeneity of the scale of the astronomic reference system (unit sphere) and the orthogonality of its coordinates are superior, with respect to systematic errors, to the corresponding mechanical components of the comparators. After the linear scale difference between the x and y spindles[7], and the deviation from perpendicularity has been determined in this manner, the mean error of ± 1.63 μm computed as a measure of precision for the image coordinates can be considered a measure of accuracy for the subsequent treatment. Assuming a mean error of $\pm 0''.3$ for the astronomic coordinates α, δ of FK–4 stars reduced to the observation datum, and $\pm 0''.4$ for all other stars, and that the mathematical model for simulation of the bundle is sufficient, then, since time errors are negligible, the mean error of coordinate corrections resulting from an adjustment executed with appropriate weights will

[7] Periodic screw errors are independently tested for in comparator calibrations.

TABLE 4.—*Identification of the 500-plate sample used in figure 40*

Seq. no.	Obs. sta. no.	No. of processed plates	Seq. no.	Obs. sta. no.	No. of processed plates
1	2	1	19	44	2
2	3	1	20	45	7
3	7	3	21	50	17
4	8	17	22	51	29
5	9	17	23	52	20
6	11	10	24	53	24
7	12	14	25	55	32
8	15	3	26	59	15
9	16	4	27	60	10
10	19	39	28	61	33
11	20	1	29	63	25
12	22	5	30	64	29
13	23	2	31	67	25
14	31	16	32	68	29
15	38	10	33	69	17
16	39	2	34	73	2
17	42	14	35	75	2
18	43	23			
				Sum:	500

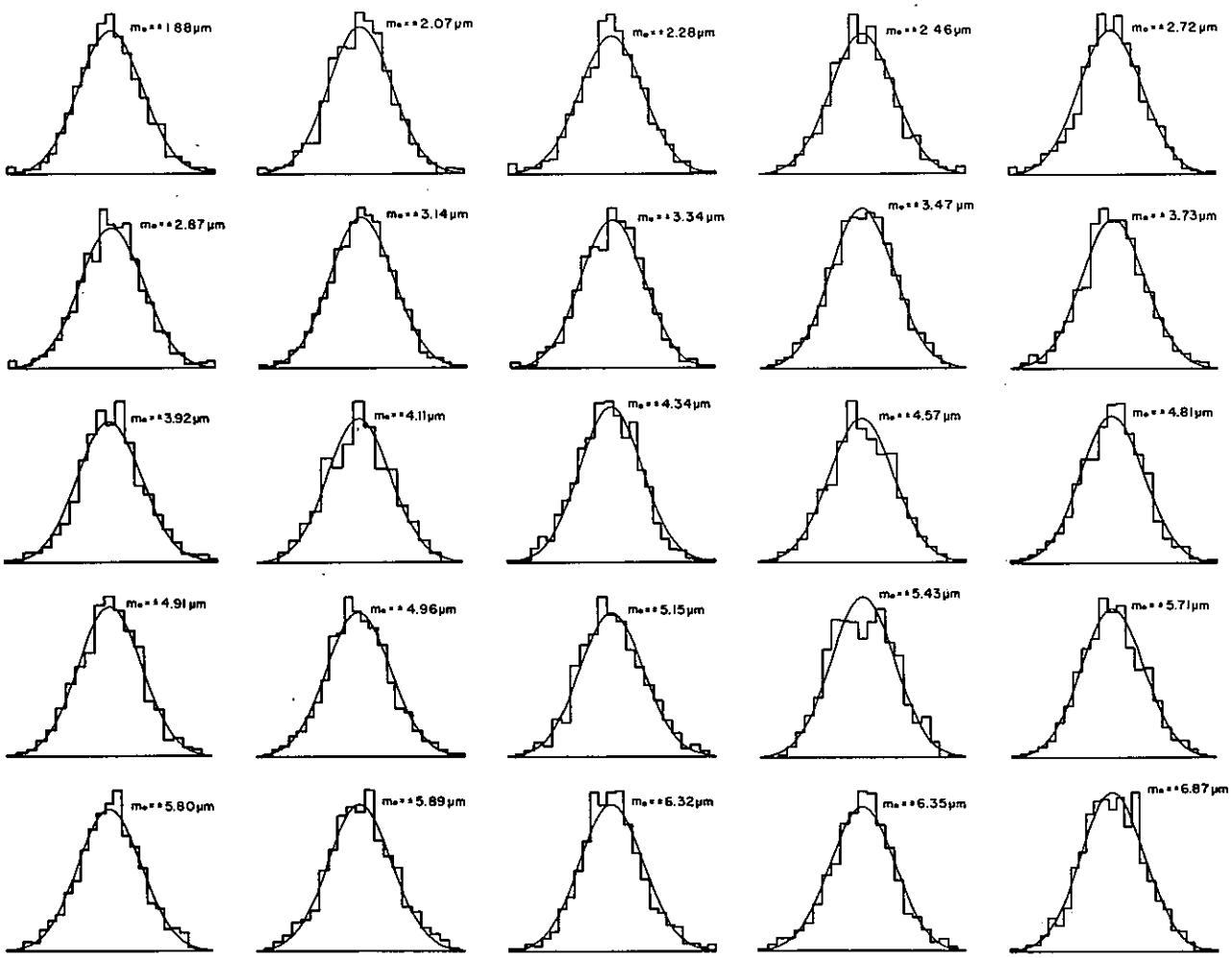

Figure 41.—Histograms of x and y plate residuals for 25 typical single camera adjustments.

express the additive influence of the random errors produced by the comparator measurement, scintillation, and emulsion shift. Figure 40 lists the values for m_p and m_l and the rms for all the data for the 500 selected photograms. The m_p is the mean error of the image coordinates for the photogram as obtained from the adjustment for the photogrammetric bundle reconstruction, and m_l the expression for the accuracy of the corresponding comparator measurements. A mean error of ± 1.0 μm is assumed for the influence of random emulsion shift [7]. Hence the contribution to the total mean error m_p by the scintillation is

$$m_s = \pm (m_p^2 - m_l^2 - 1.0^2)^{\frac{1}{2}}. \qquad (307)$$

This error component is also listed in figure 40. The rms values for the 500 plates are

$m_p = \pm 3.31$ μm, $m_l = \pm 1.81 \mu m$, and $m_s = \pm 2.58$ μm

Figure 41 shows the histogram of combined x and y coordinate corrections with corresponding normal distribution curves for 25 single camera adjustments. These were selected to cover uniformly the range of mean coordinate errors after adjustment actually obtained, i.e., from ± 1.88 μm to ± 6.87 μm. The histograms illustrate the typical behavior of the totality of evaluated observed data.

3.2.3 Accuracy of the Trace of the Satellite Orbit After the Polynomial Fit.

The mean deviation of a measured satellite point from the smoothing polynomial of degree 6 varies between ± 1.6 μm and ± 8.6 μm with rms of ± 3.75 μm for the fit in direction of the satellite trail and between ± 1.3 μm and ± 9.3 μm with rms of ± 3.28

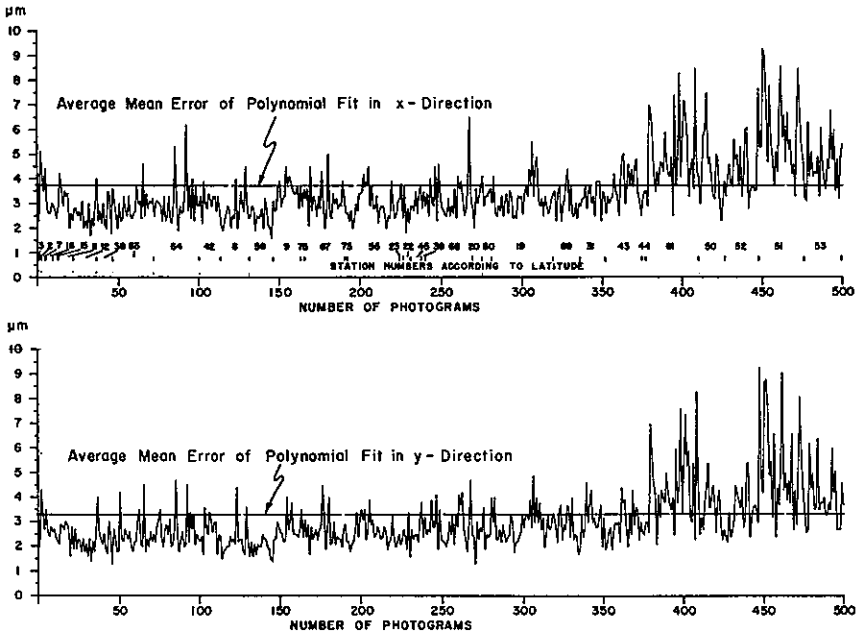

Figure 42.—Plot of the mean errors of the individual polynomial fits to the satellite trail for each of the 500 plates of figure 40. The top diagram refers to the polynomials fitted to displacements in the direction of the trail and the bottom one to the fits perpendicular to the trail.

μm perpendicular to the trail (cf. fig. 42). The corresponding x, y mean value is ± 3.52 μm.

The individual mean displacement is a measure of how well the satellite images on a given photogram fit the polynomial. These quantities are the sums of the superimposed random errors of the comparator measurements, the emulsion shifts, and again the scintillation. The mean deviation in the direction of the satellite trail is, on the average, 0.47 μm larger than at right angles to the trail. This is not so much due to random time errors of the recording sequence that operate in the direction of the trail as it is to the fact that the comparator measurements of the trail images have a larger mean error in this direction than in the direction perpendicular to the trail, because of image blur from the satellite motion.

About 300 satellite image measurements are available per plate. From the double measurements and their differences, the accuracy of the comparator measurements is again determined. This is on the average ± 1.79 μm for the x and y measurements, or practically the same value as for the star image measurements. Again, with the assumption of ± 1.0 μm for the mean random emulsion shift, the opportunity is given to isolate the scintillation effect as

$$m_s = [3.52^2 - 1.79^2 - 1.0^2]^{\frac{1}{2}} = \pm 2.86 \ \mu\text{m} \tag{308}$$

The treatment of the scintillation as a random source of error is based on the fact known from astronomical observations [8], that the mean amplitude of scintillation operates as an irregular error source in all directions. Computing for each plate the scintillation effect on the star images in accordance with (307) and comparing these values with the corresponding similar values obtained from the curve fit with (308), the correlation coefficient $\rho = 0.81 \pm 0.02$ is obtained with the formula

$$\rho = \frac{\sum_{i=1}^{n=500} \Delta s_1 \cdot \Delta s_2}{\left[\sum_{i=1}^{n=500} \Delta s_1^2\right]^{\frac{1}{2}} \left[\sum_{i=1}^{n=500} \Delta s_2^2\right]^{\frac{1}{2}}} \tag{309}$$

where the Δ's represent deviations of the individual amounts of scintillation from their mean value and the indices 1 and 2 refer respectively to the scintillation computed from the bundle reconstructions and from the polynomial fit.

Figure 43 shows the mean scintillation at each observing station with the stations arranged by latitude. From this it is seen that scintillation, with an overall mean for all stations of ± 2.58 μm for the star images and ± 2.86 μm for satellite images, represents a considerable error contribution to the total error budget. Also apparent is the increase in scintillation with increasing latitude which is to be

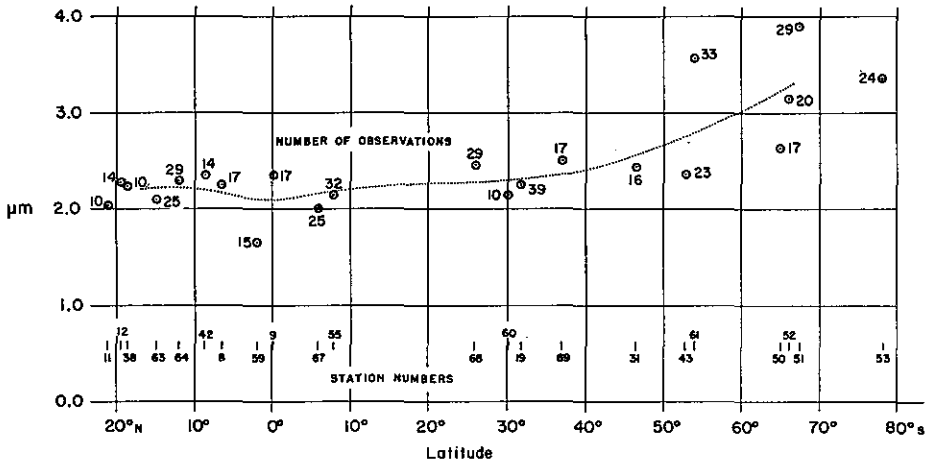

Figure 43.—Average scintillation at a number of observing stations arranged according to latitude, showing a corresponding trend curve.

expected in consequence of the theory presented by Nettelblad [9], according to which scintillation is least in warm, maritime air masses and greatest in cold, continental climates. The amplitude of the scintillation depends, in addition, on the exposure time, which may be the cause for the fact that the mean scintillation for the star exposures of between 0.2 and 3.2 s is ± 2.58 μm and for the satellite images exposed from 1/15 to 1/30 s is ± 2.86 μm.

Obviously the use of short-duration flashes (1/1,000 s) will increase the scintillation effect for the individual flash, thus making it all the more desirable to have a considerable number of such flashes before an accurate triangulation can be performed.

3.2.4 Error Propagation into the Spatial Triangulation

In sec. 3.2.1, 2, 3 quantitative results have been given for the significant random error contributions that must be considered in setting up an error budget for spatial triangulation. Table 5 presents average values from the processing of the selected 500 photograms.

The figure in column 7 of table 5 indicates that an average uncertainty of 1".57 in direction should be associated with a bundle reconstruction that is not overdetermined. Actually this value is a function of the position of a ray within this bundle [3] and to be completely rigorous, in accordance with error theory, should be computed with the covariance matrix obtained from the individual bundle reconstruction adjustment. Since the bundles under consideration here are relatively narrow however (the angle of vision for the BC–4 camera is about 20°) we can, for the present, ignore this fact in a general examination of the error propagation. In order to determine uniquely the 20 required interpolation parameters of an oriented bundle reconstruction, at least 10 reference stars are required, so that the use of an average of 100 stars per plate represents 10 solutions in the adjustment. Each star being measured five times on the average, it can be expected that the direction uncertainty for a central ray after adjustment of the bundle reconstruction will, from a combination of tabulated values in table 5, be as follows:

The error sources affecting the individual image coordinates add quadratically to

$$(m_l) = \pm(1.81^2 + 1.0^2 + 2.58^2)^{\frac{1}{2}} = \pm 3.31 \ \mu\text{m} \tag{310}$$

(cf. table 5, cols. 2, 3, 4, and 5). Assuming the five images for each reference star combined into one fictitious image, then the coordinates will have an accuracy of $3.31/\sqrt{5} = \pm 1.48$ μm. Combined with the mean star catalogue uncertainty of $\pm 0".4 = \pm 0.87$ μm (col. 6) we have a mean uncertainty in direction of ± 1.72 μm $= \pm 0".79$. The combination of 10 independent solutions in one adjustment reduces this error to approximately $0".79/\sqrt{10} = 0".25$.

The figures of table 6 are results from a bundle reconstruction adjustment with a mean error of ± 3.31 μm for the image coordinates after adjustment involving 648 star images of 105 reference stars distributed approximately evenly over the plate. The results shown are mean accuracies of directions corresponding to various image positions on the plate assumed free of error [3].

The mean error $\pm 0".23$ from this table for the

TABLE 5.—*Statistics for the 500-plate sample*

Photogrammetric camera: Wild BC–4, Lens: Cosmotar f = 450 mm, aperture 132 mm
Target: PAGEOS balloon satellite for 496 photograms and ECHO satellite for 4 photograms
Program: World Net
Period of observation: October 1966—September 1969
Observation material: 500 selected photograms with corresponding time recordings from 35 stations in the World Net

		(1) Type of imagery	(2) Mean errors of comparator measurements	(3) Assumed mean of irregular emulsion shift	(4) Average of mean scintillation		(5) Mean coordinate error after adjustment in photogrammetric bundle simulation $[(2)^2 + (3)^2 + (4)^2]^{\frac{1}{2}}$	(6) Introduced mean error of reduced star catalog data		(7) Total noise in photogrammetric bundle simulation adjustment $[(2)^2 + (3)^2 + (4)^2 + (6)^2]^{\frac{1}{2}}$		(8) Mean error of polynomial smoothing $[(2)^2 + (3)^2 + (4)^2]^{\frac{1}{2}}$	
			m_r (μm)	(μm)	(μm)	(")	(m_r)(μm)	(μm)	(")	(μm)	(")	(μm)	(")
Average values	a	Stars	±1.81	±1.00	±2.58	±1.18	±3.31	±0.87	±0.40	±3.42	±1.57	—	—
	b	Satellite	±1.79	±1.00	±2.86	±1.31	—	—	—	—	—	±3.52	±1.61
Minimal values	c	Stars	±0.97	±1.00	±1.01	±0.46	±1.88	±0.87	±0.40	±1.93	±0.88	—	—
	d	Satellite	±0.87	±1.00	±1.07	±0.47	—	—	—	—	—	±1.46	±0.67
Maximal values	e	Stars	±2.45	±1.00	±6.46	±2.96	±6.87	±0.87	±0.40	±7.03	±3.22	—	—
	f	Satellite	±2.68	±1.00	±6.84	±3.14	—	—	—	—	—	±8.96	±4.11

TABLE 6.—*Mean direction accuracies corresponding to image positions on a typical single plate*

Image coordinates (x in mm/y in mm)	0/0	10/10	20/20	30/30	40/40	50/50	60/60	70/70
Mean accuracy of direction	±0".23	±0".25	±0"19	±0"21	±0".21	±0".25	±0".44	±2".77

central ray ($x = y = 0$) is in good agreement with the value 0".25 obtained before from general considerations. Using the mean satellite image error figure of 1".61 from table 5, col. 8, the 6th-degree polynomial fit over 300 satellite points will contribute an uncertainty in direction after adjustment of $\pm 1".61/\sqrt{300/7} = 0".25$. The error sources being uncorrelated the total expected error in direction for the central ray is $(0".25^2 + 0".25^2)^{\frac{1}{2}} = \pm 0".35$.

The use of 6th-degree polynomials makes seven directions available for satellite triangulation in each photographed bundle. However, as we know, these are mutually correlated. One reason is that they are all obtained with a specific group of interpolation parameters from one single camera and, for another, they all derive from a single pair of smoothing polynomials. From a study of the relevant covariance matrices in a rigorous adjustment whose reproduction here would far exceed the available space, it becomes apparent that the use of seven directions distributed evenly over the satellite trail yields a gain of 32% for the geometry of the bundles as against the use of a single central direction. This means that the use of all seven directions has about the same information content that would be obtained from two central rays that are not correlated.

Hence, if we conceive of the total information used in the evaluation of a specific photogram as compressed to determine a central fictitious direction we may expect for such a direction an accuracy of $m_r = \pm 0".35 - 32\%(\pm 0".35) = 0".24$.

According to sec. 3.1 the adjustment algorithm is based on the assumption that the results of bundle reconstructions at the individual stations are uncorrelated. Consequently the directions to the satellite for a given event derived at the individual stations are likewise uncorrelated. To obtain a measure of the mean accuracy to be expected for the spatial triangulation of the observing sites one can therefore assume that the mean accuracy 0".24 of a direction computed above for a fictitious central direction containing all the information content is an uncorrelated function of the station. In the adjustment algorithm this accuracy of triangulation directions associated with a specific evaluation of a photogram is expressed in the form of the weight matrix associated with the coordinates of the seven fictitious satellite images, the weight matrix being computed from the corresponding covariance matrix derived with (277) of sec. 2.7. In sec. 3.1 it was mentioned that in the mathematical formulation to be set up for the final triangulation, only the satellite and station positions were to be determined as unknowns. From the basic triangulation geometry shown in figure 3

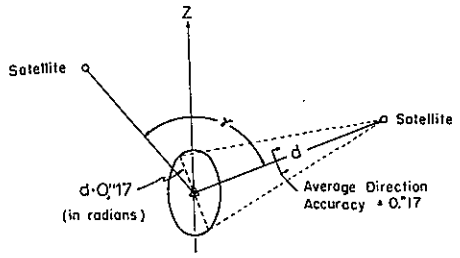

Figure 44.—Section of error ellipsoid at observation station intersected from two satellite positions.

it is then obvious that the accuracy of the triangulation results to be expected in a direction perpendicular to the direction station-satellite is proportional both to the directional accuracy and the station-to-satellite distance. This is indicated schematically and reduced to two dimensions in figure 44.

The accuracy in direction of the z coordinate is a function of the angle γ in which the station-satellite planes intersect. From analysis of the inverted normal equations systems, which contain the geometry of the actual satellite observations it follows, quite generally, that the mean error of the triangulated station in direction of the geodetic latitude and longitude, assuming errorless scale, is proportional to the product $m_R \cdot d$, where m_R is the mean accuracy of direction and d the mean station-to-satellite distance; on the other hand, the average mean error in the direction of height is three times as large [5]. These relations are shown in figure 45, in which $\sqrt{Q}$ is the error propagation factor (sometimes called the weight reciprocal) for the position coordinate.

The same result is shown schematically in another form in figure 46. From this, by comparison of antipodal stations, it is apparent that the uncertainty in height determination within a world triangulation eventually has the effect of an uncertainty in scale. One can expect therefore that additional scale control will have particularly favorable influence on the accuracy of height coordinates but will represent no real gain for the determination of the position coordinates φ, λ. This fact is illustrated in figure 46 showing the effect of from 1 to 4 scale determinations. The lower part of figure 45 shows that even under the assumption of errorless scalars (weight 10^4) only the stations directly involved in the scale determinations show a gain in the determination of their latitude φ and longitude λ. On the other hand, the error propagation coefficient for the height determination reduces from 3 to 1.8 with the use of four scalars, even when a more realistic weight of 1 is used in the scale determination [5], [10].

In the world net the Pageos satellite was observed almost exclusively. Its normal circular orbit elevated about 4,600 km above the surface of the Earth resulted in an average station-to-satellite distance of 6,000 km. With a mean direction accuracy of 0".24 and the propagation factors of figure 45 a triangulation solution based on two

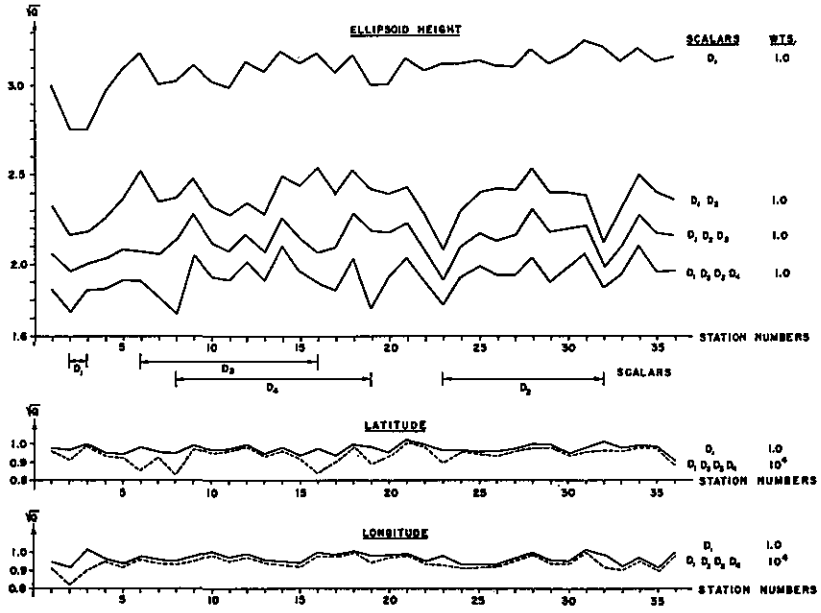

Figure 45.—Error propagation factors for ellipsoid height, latitude, and longitude using from one to four scalars.

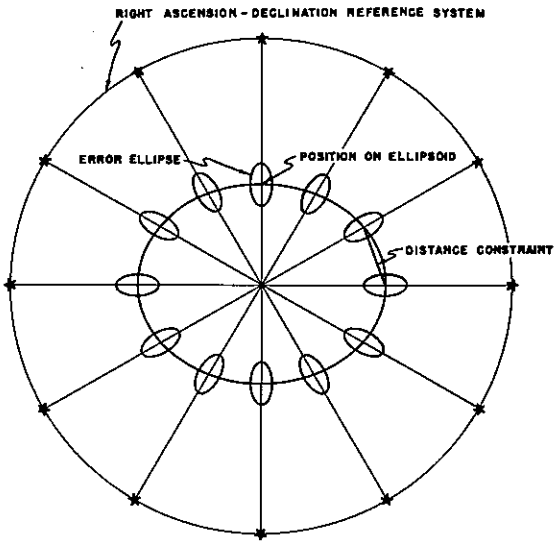

Figure 46.—Error propagation of the method of geometric satellite triangulation.

satellite transits or events per triangle side, assuming an errorless scale, produces position coordinates for the observing stations with mean errors $m_\varphi = m_\lambda = \pm 7.0$ m and $m_H = \pm 21.0$ m. At this time 2,350 plates have been reduced for evaluation in the world net. The distribution of the corresponding events is shown in figures 47 to 52. These observations correspond to about five independent solutions. An adjustment of all these events should therefore yield an accuracy of $m_\varphi = m_\lambda = \pm 7.0/\sqrt{5} = \pm 3.1$ m and $m_H = \pm 21.0/\sqrt{5} = \pm 9.4$ m. Introducing the planned four scalars, measured independently and with an accuracy of at least 1:1,000,000, the expected mean error in height reduces to $m_H = \pm 3.1\text{m} \times 1.8 = \pm 5.6$ m (cf. fig. 45) and the mean position error of a station

$$M = \pm\left(\frac{m_\varphi^2 + m_\lambda^2 + m_H^2}{3}\right)^{\frac{1}{2}} = \pm 4.1 \text{ m} \quad (311)$$

or M is roughly 1:1,500,000 of the mean station-to-satellite distance.

In the next paragraphs the result of the worldwide geometric satellite triangulation program is presented with an associated error analysis based on the statistical information obtained during the final triangulation adjustment.

3.3 Result of the Worldwide Geometric Satellite Triangulation

The quantitative result of the worldwide geometric satellite triangulation program consists of the

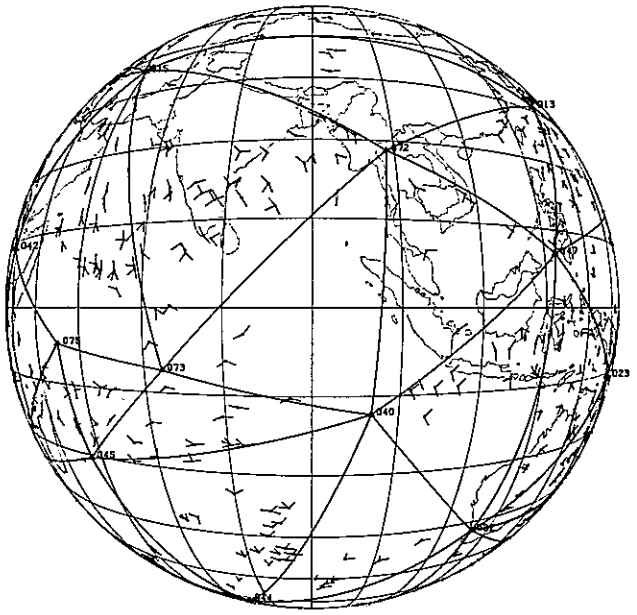

Figure 47.—Geographic distribution of stations and observations. Center of view: latitude 0°, longitude 90°E.

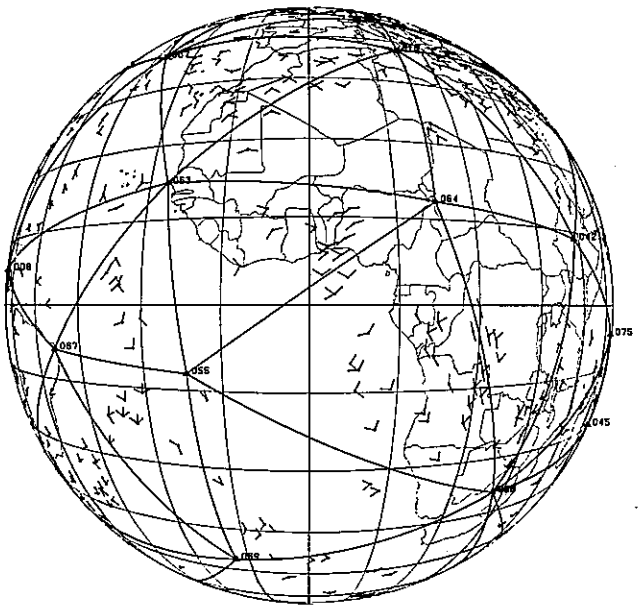

Figure 48.—Geographic distribution of stations and observations. Center of view: latitude 0°, longitude 0°.

three-dimensional positions of 45 stations. Their locations can be seen from figure 53 and table 1.

The corresponding Cartesian reference coordinate system has, as explained before, one of its axes parallel to the rotation axis of the Earth for a certain epoch (CIO). The origin of the system and

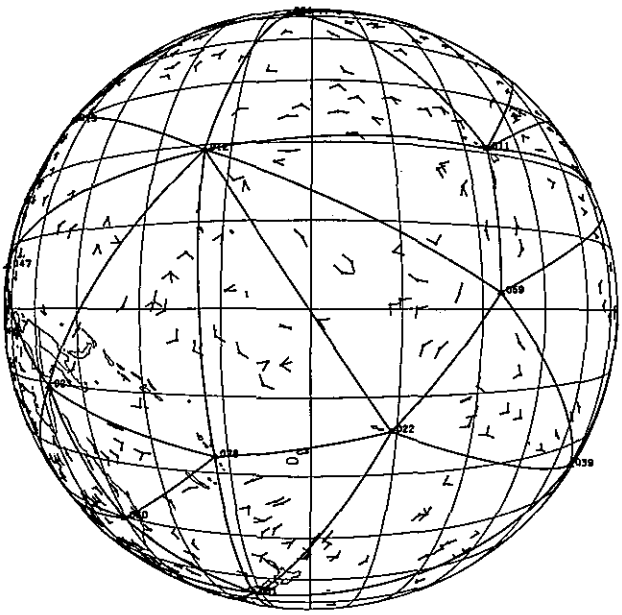

Figure 49.—Geographic distribution of stations and observations. Center of view: latitude 0°, longitude 180°.

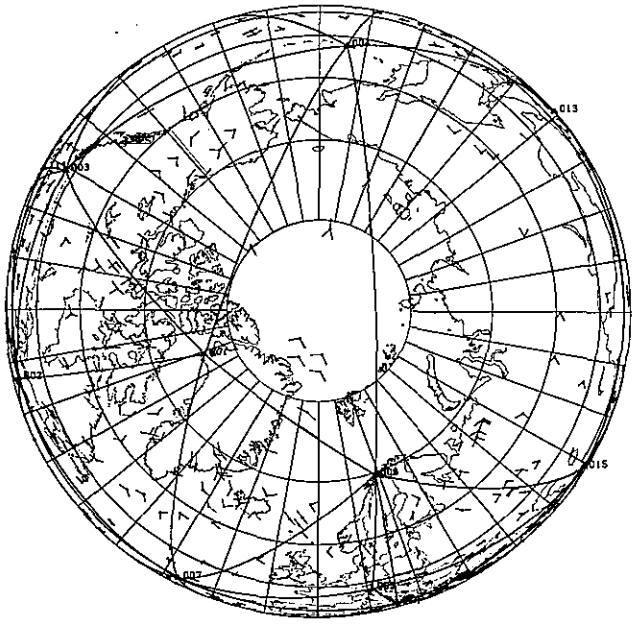

Figure 51.—Geographic distribution of stations and observations. Center of view: North Pole.

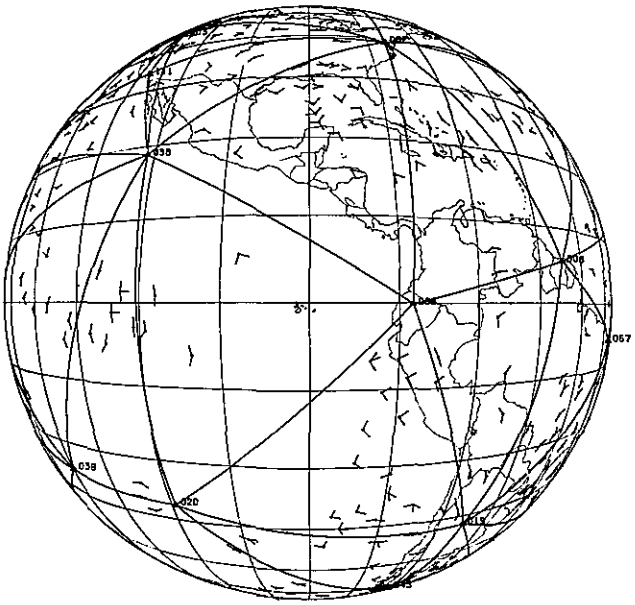

Figure 50.—Geographic distribution of stations and observations. Center of view: latitude 0°, longitude 90°W.

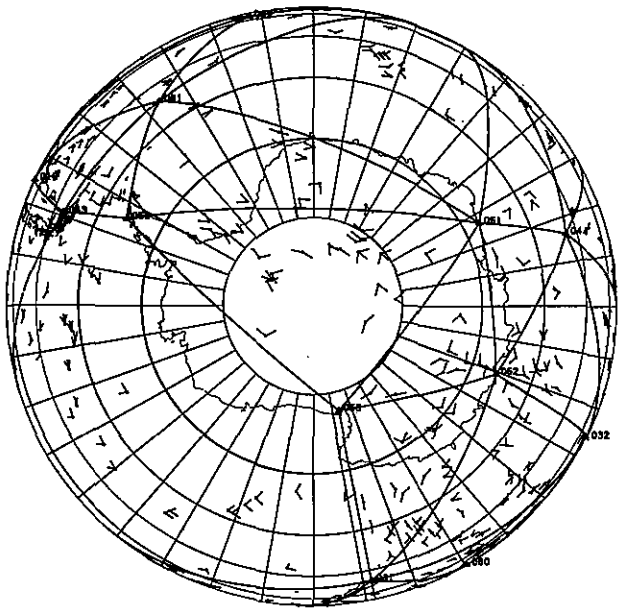

Figure 52.—Geographic distribution of stations and observations. Center of view: South Pole.

the selection of the X direction is arbitrary for reasons inherent to the method of geometric satellite triangulation. It was fixed by enforcing for station No. 2, Beltsville, Md., U.S.A., the following coordinates, which are approximations for a mass-centered position.

Station	Spatial coordinates X (m)	Y (m)	Z (m)
No. 2 (Beltsville)	1130761.500	4830828.597	3994704.584

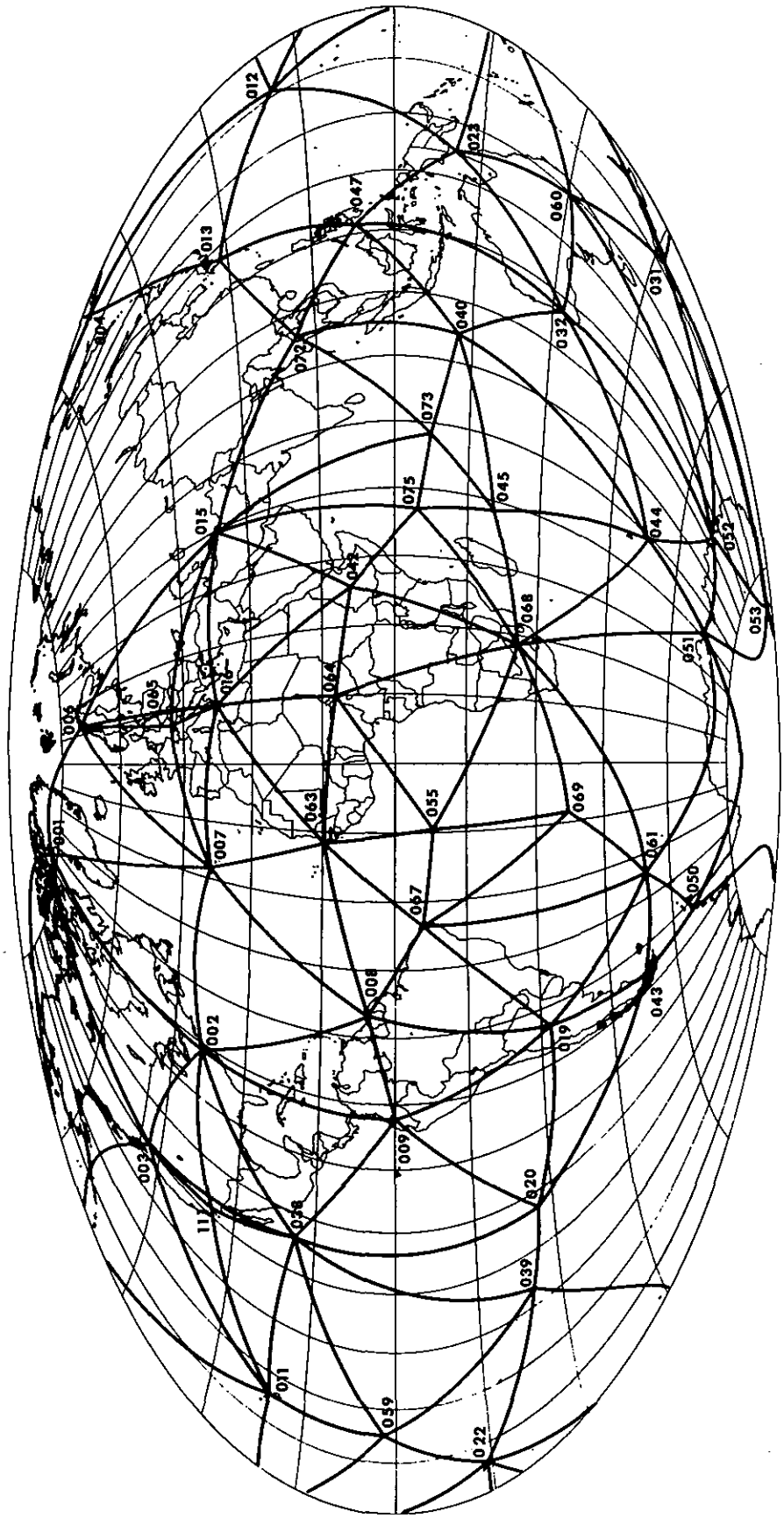

Figure 53.—The 45 stations of the worldwide BC–4 photogrammetric satellite triangulation network with station number designations.

As discussed in the analysis of the results in the next paragraph, it was decided to enforce all eight scalars with their measured values.

Table 7 lists the three-dimensional Cartesian coordinates[8] for the 45 stations and their mean errors (one sigma level) as obtained from the final adjustment. The coordinates refer to the projective center of the BC–4 cameras. The elevation of this point above the permanent station mark is in each case +1.5 m.

3.4 Analysis of the Triangulation Adjustment

The input of the triangulation adjustment refers to the information obtained from the evaluation of 2,350 photographic plates. Specifically, the observation from 856 two-station, 194 three-station, and 14 four-station satellite events were used. The 1,064 satellite events chosen for evaluation required the determination of the spatial positions of the tracking stations and the triangulation of 6,604

TABLE 7.—*Adjusted Cartesian coordinates of world net stations*

No.	Station name	X (m)	σ_x ± (m)	Y (m)	σ_y ± (m)	Z (m)	σ_z ± (m)
1	Thule	546567.862	2.297	1389990.609	3.447	6180239.602	3.960
2	Beltsville	1130761.500	0	4830828.597	0	3994704.584	0
3	Moses Lake	−2127833.613	.790	3785861.054	2.976	4656034.740	2.906
4	Shemya	−3851782.861	4.888	−396404.016	5.654	5051347.586	6.673
6	Tromso	2102925.118	3.663	−721667.562	4.772	5958188.868	4.748
7	Azores	4433636.070	4.737	2268143.467	4.362	3971656.223	4.945
8	Surinam	3623227.823	4.563	5214231.698	4.502	601551.302	5.716
9	Quito	1280815.597	4.338	6250955.436	5.800	−10793.013	5.717
11	Maui	−5466020.732	5.045	2404435.198	4.352	2242229.885	4.703
12	Wake	−5858543.398	5.308	−1394489.166	5.281	2093807.584	5.391
13	Kanoya	−3565865.509	5.200	−4120692.866	6.694	3303428.249	6.131
15	Mashhad	2604346.389	3.988	−4444141.147	5.513	3750323.381	4.974
16	Catania	4896383.234	4.080	−1316167.822	4.463	3856673.791	4.698
19	Dolores	2280603.832	4.190	4914545.588	4.789	−3355412.286	6.839
20	Easter	−1888616.886	4.845	5354892.780	6.246	−2895739.444	7.217
22	Pago Pago	−6099954.446	5.392	997367.321	4.710	−1568567.088	5.883
23	Thursday Is.	−4955371.694	4.671	−3842221.799	5.689	−1163828.451	5.852
31	Invercargill	−4313815.856	4.687	−891322.098	5.238	−4597238.676	6.398
32	Perth	−2375397.874	4.579	−4875524.035	5.746	−3345372.936	6.170
38	Revilla	−2160983.561	2.008	5642711.612	3.653	2035371.417	4.062
39	Pitcairn	−3724766.403	6.502	4421236.249	6.480	−2686072.609	7.288
40	Cocos	−741969.205	4.859	−6190770.789	6.606	−1338530.638	5.843
42	Addis Ababa	4900734.926	4.844	−3968226.427	5.481	966347.675	5.103
43	Sombrero	1371358.188	4.171	3614760.271	4.969	−5055928.396	8.156
44	Heard	1098896.432	6.448	−3684591.597	7.801	−5071838.356	9.919
45	Mauritius	3223422.870	4.472	−5045312.452	6.019	−2191780.736	6.065
47	Zamboanga	−3361946.845	4.909	−5365778.338	6.501	763644.128	6.121
50	Palmer	1192659.730	5.174	2450995.361	7.275	−5747040.896	10.171
51	Mawson	1111335.585	5.189	−2169243.189	5.456	−5874307.692	8.002
52	Wilkes	−902598.435	4.912	−2409507.607	5.700	−5816527.805	7.901
53	McMurdo	−1310841.759	4.993	−311248.105	5.500	−6213251.231	7.886
55	Ascension	6118325.238	5.260	1571746.070	4.816	−878595.457	5.507
59	Christmas	−5885331.078	5.213	2448376.867	4.435	221683.837	5.446
60	Culgoora	−4751637.577	4.552	−2792039.266	5.653	−3200142.319	5.866
61	So. Georgia	2999903.036	4.896	2219368.228	6.055	−5155246.454	8.547
63	Dakar	5884457.561	4.898	1853492.773	4.257	1612863.206	5.072
64	Chad	6023375.533	4.690	−1617924.383	4.242	1331742.422	4.834
65	Hohenpeissenberg	4213552.554	3.730	−820823.968	4.444	4702787.513	4.620
67	Natal	5186398.560	5.260	3653936.203	4.854	−654277.651	5.569
68	Johannesburg	5084812.984	5.229	−2670319.559	5.065	−2768065.639	6.586
69	De Cunha	4978412.958	8.167	1086867.619	6.918	−3823159.761	9.443
72	Thailand	−941692.348	5.593	−5967416.884	6.919	2039317.530	5.461
73	Chagos	1905130.320	4.345	−6032252.624	6.702	−810711.562	5.751
75	Mahe	3602810.169	4.910	−5238217.287	6.393	−515928.653	5.650
111	Wrightwood	−2448854.721	2.088	4667988.213	3.367	3582758.969	3.185

[8] The XYZ system is a left-handed system (west longitude positive). The complete covariance matrix for the triangulated station coordinates, which for space reasons can not be presented here, is available.

satellite positions. The adjustment provided for 9,162 degrees of freedom. Two station-to-station couplings were introduced as additional constraints in order to tie together the stations 111–134 (California) and 012–066 (Wake Island) where, for technical reasons, satellite observations were collected from neighboring observation piers. Eight scalars were rigorously introduced, representing the spatial distances between the following stations:

Stations between which scalars were measured	Spatial distances (m)	σ_d (m)
002–003	3,485,363.232	±3.53
003–111	1,425,876.452	±1.59
006–065	2,457,765.810	±0.80
065–016	1,194,793.601	±1.43
006–016*	3,545,871.454	±1.64
023–060	2,300,209.803	±0.88
032–060	3,163,623.866	±0.98
063–064	3,485,550.755	±2.10

*The scalar 006–016 is not a truly independent scalar.

The measuring and computation of these scalars was executed by various national agencies. For references, the following information is given:

Scalar	Measured by	Computed by	Documentation
002–003 and 003–111	National Geodetic Survey (U.S.A.)	National Geodetic Survey Triangulation Branch (U.S.A.)	Office memos from NGS Triangulation Br. to Geodetic Research & Development Lab. for 002–003—B. K. Meade dated 3/29/71. for 003–111 John G. Gergen dated 8/5/73.
006–065 065–016 006–016	Geodetic Agencies of Norway, Sweden, Denmark, German Federal Republic, Austria, Italy	National Geodetic Survey (U.S.A.) Triangulation Branch	Office memo from NGS Triangulation Br. to GRDL—B. K. Meade dated 4/9/70. Office memo from NGS, New Datum Br. to GRDL—John G. Gergen dated 8/5/73. Further reference literature, the results of which were not used here: Computation of the European Baseline Tromso-Catania by R. Kube and K. Schnädelbach, Deutsches Geodätisches Forschungsinstitut, München (1973).
023–060 032–060	Dept. of National Development, Division of National Mapping, Australia	Division of National Mapping, Australia	Dept. of National Development, Div. of National Mapping, Australia Technical Report No. 11 by K. Leppert, Canberra, Australia, March 1972, entitled "Two Australian Baselines for the Pageos World Triangulation."
063–064	Department of Defense, Defense Mapping Agency and Institute Geographique Nationale (France)	Department of Army, Commanding Officer, US Army Engineer Topographic Production Center (Code 14400), Army Topographic Stations Wash., DC 20315	Transmittal letters to Dr. H. H. Schmid, GRDL, NGS, NOAA, Rockville, Md. 20852 U.S.A. dated June 4, 1971, and July 22, 1971.

To obtain a measure for the precision of the strictly photogrammetric triangulation, a first triangulation adjustment was executed with only the scalar between stations 002–003 enforced. This adjustment produced a sum of the squares of the weighted residuals in terms of plate coordinate corrections $[pvv] = (3.064 \pm 0.045) \times 10^{-8}\,(m^2)$.

A comparison of the measured baselines with the corresponding triangulation results provides a first insight into the internal accuracy of the geometric world net. The differences between the computed and measured distances with a complete constraint on scalar 002–003 are shown in table 8.

TABLE 8.—*Comparison of measured baselines with the geometric triangulation result*

Scalar	Δd = meas. − comp. (m)	σ of scalar as obtained from the triang. adjust. (m)
002–003	0	0 held fixed
003–111	−7.3	±2.8
006–065	−2.0*	±4.9
065–016	+9.3	±5.1
023–060	+5.8	±3.9
032–060	+8.5	±4.6
063–064	−5.1	±5.2
Sum	+9.16	±15.61(σ of $\sum d$)

*The German Geodetic Research Institute gives for the baseline 006–065 a value which is 1.9 *m* larger than the one used here. The corresponding Δ values would then be only 1 decimeter.

The sum Σd of the lengths of the measured scalars is 17,513,184 m, so that

$$\frac{\sum \Delta d}{\sum d} = 1{:}1,\,911,\,920 \qquad (312)$$

As can be seen from table 8 the difference $\Sigma\Delta d$ is only about 0.6 of the standard deviation associated with the sum of the triangulated distances.

It was therefore concluded that the scalars, at least in their totality, are probably of higher accuracy than the geometric satellite triangulation itself. This conclusion is further evidenced when considering the standard errors for these scalars computed by the various computing centers.

An adjustment where all scale lines were enforced with weights corresponding to an accuracy of one part in two million of their respective lengths gave the following result as shown in table 9.

TABLE 9.—*Corrections to baselines weighted 1:2,000,000 in the adjustment*

Scalar	Assumed mean error (m)	Correction from the adjustment (m)
002–003	±1.75	−0.06
003–111	±0.72	+1.50
006–016	±1.78	−0.26
006–065	±1.23	+0.10
016–065	±0.60	+0.42
023–060	±1.15	−0.98
032–060	±1.58	−2.76
063–064	±1.75	+2.60

The [*pvv*] of this adjustment was 3.068×10^{-8}, a value only 0.004×10^{-8} units larger than in the single scalar adjustment mentioned above. This difference is only 1/10 of the associated sigma. It can, therefore, be safely concluded that the scalars do not exercise undue constraint on the triangulation system.

If all 8 scalars are rigorously enforced the [*pvv*] sum increases to 3.071×10^{-8}, a solution which is equally defensible from a statistical standpoint.

The numerical solution is iterated on the CDC 6600 computer (usually three times) until the maximum increment to the triangulated coordinates becomes <1 mm. Multiplying the normal equations matrix pertaining to the final iteration by its corresponding inverse matrix one obtains, as a check, the expected unit matrix to within a unit in the 10th decimal place.

For all these solutions the mean error of unit weight after adjustment is 1.830 ± 0.014 against the expectation of 1.0, indicating the presence of additional unmodeled error sources. If the increase in the overall error budget can be ascribed to additional random error sources then the effect is relatively harmless, resulting only in a corresponding increase in the mean errors of the triangulated station positions. But if the effect of systematic errors (which are distributed in the adjustment in accordance with the least squares principle) is involved, the situation is more serious.

To gain some insight into the stability of the camera during the average half-hour period of operation, star photographs taken immediately before and after the satellite transit were adjusted and sets of camera orientation parameters computed. Thus for each plate the change in azimuth ΔA and in elevation ΔH of the central ray with a corresponding rotation component Δ_X was computed. The Δ_X are random and completely within the range of their mean errors. The $\Delta A \cos H$ and, especially, the ΔH component, however, indicate the influence of a systematic error, as shown in the following diagrams (figs. 54 and 55). For an evaluation of the diagrams it should be added that the individual Δ values shown have an average mean error of $\pm 0''.5$. Since star imagery is also available for the satellite transit period it is possible to study these systematic changes in orientation over the period of observation. A roughly linear trend with time is indicated.

To eliminate this source of error, orientation parameters were used in the final adjustment, wherever possible, that were based solely on star images obtained during the period of actual satellite transit. Still we cannot entirely escape the conclusion that the instability of the camera creates an additional error which, as the diagrams show, has a systematic component and acts as a source of additional accidental errors.

For a further analysis of the results it is important to realize that in consequence of the interpolation of each event into the astronomic system, absolute directions are obtained. This means it is possible to triangulate the direction of the chord joining two adjacent stations in the net independently, i.e., with only the satellite passes observed from these two stations. Such computations were made for all 170 lines of the world net. In these adjustments, as well as in the final solution, all covariance matrices resulting from the individual processing steps were included, so that all results can be considered rigorously derived values. The line triangulations yield an average mean value for the ratio of mean error of unit weight before and after adjustment of 1:1.746, with a range of from 1:0.706 to 1:2.429. The theoretical expected average value is of course 1:1. This means that the observed data do not completely fill the accuracy expectations computed in the above cited partial analyses, a fact that was already mentioned in connection with the obtained mean error of unit weight after adjustment in the final triangulation. However, it is gratifying to note

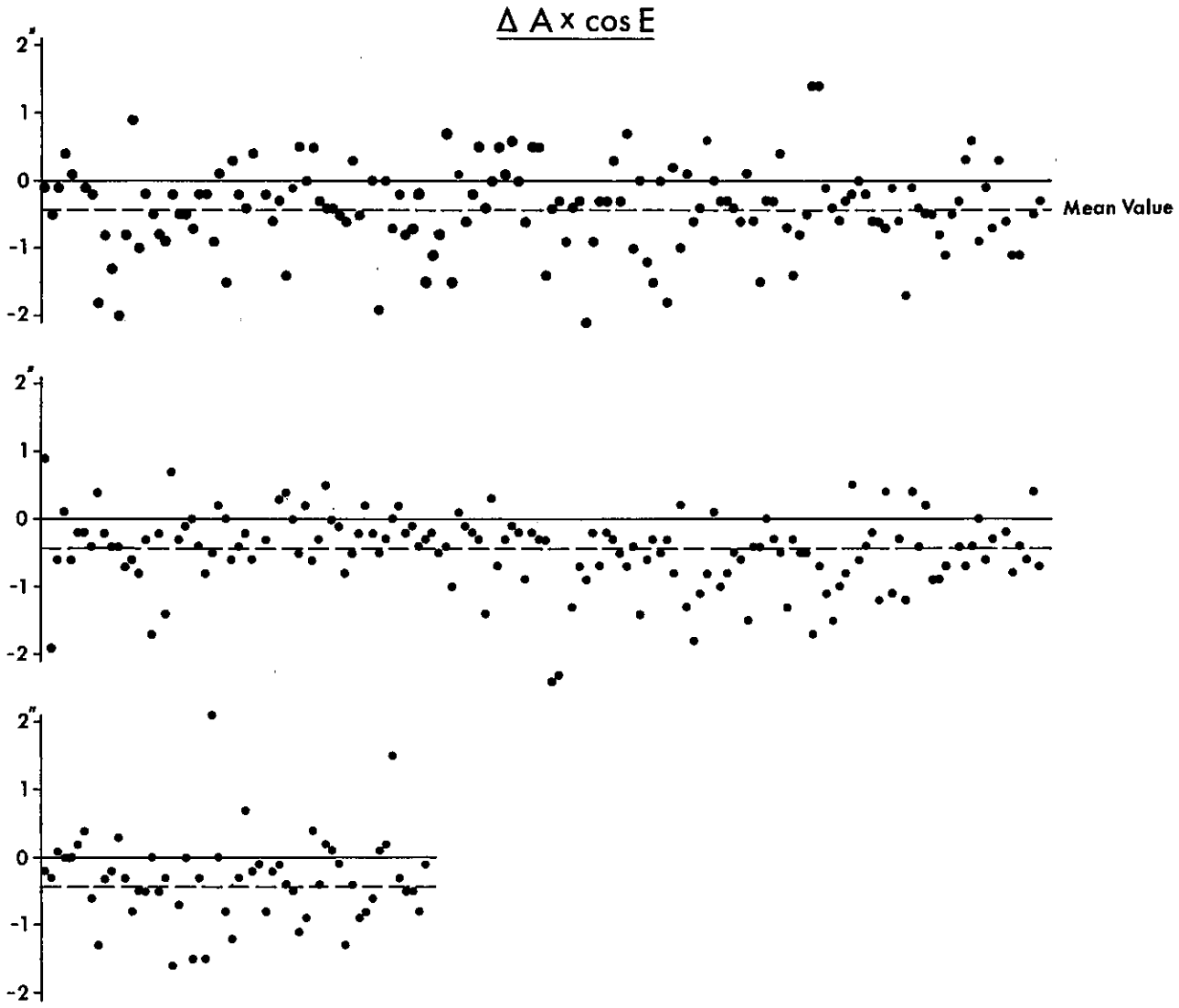

Figure 54.—Plot of the increments in $A \cos E$ from pre- to post-calibration for a number of randomly selected events, in seconds of arc. The three segments are portions of a single graph.

that this value increases only slightly from 1.746 for the average of all individual line adjustments to 1.830 for an adjustment based on the combination of all observations. These figures indicate that the entire body of data is apparently free of perturbing systematic errors and satisfies with practically no constraint the three-dimensional geometrical closure condition of the world net.

In order to strengthen this conclusion a comparison was made between the directions derived from the individual line adjustments and those of the combined solution. The individual resulting azimuth and elevation angle differences are shown in the two following diagrams (figs. 56 and 57) with their 3σ errors and combined in histograms. Although these results do not fully meet ideal, statistical expectations it is not really possible to draw conclusions in any other way regarding the presence of possible systematic error influences in the triangulations of the individual lines.

In order to analyze the accuracy of the shutter synchronization the following argument can be applied to the results of the individual line adjustments. Simple geometric considerations suggest that synchronization discrepancies will lead to larger residual errors in the spatial triangulation the larger the angle is between the orbital plane of the satellite and the line to be triangulated. Because the Pageos satellite has an approximately polar orbit it is sufficient to plot the mean error of

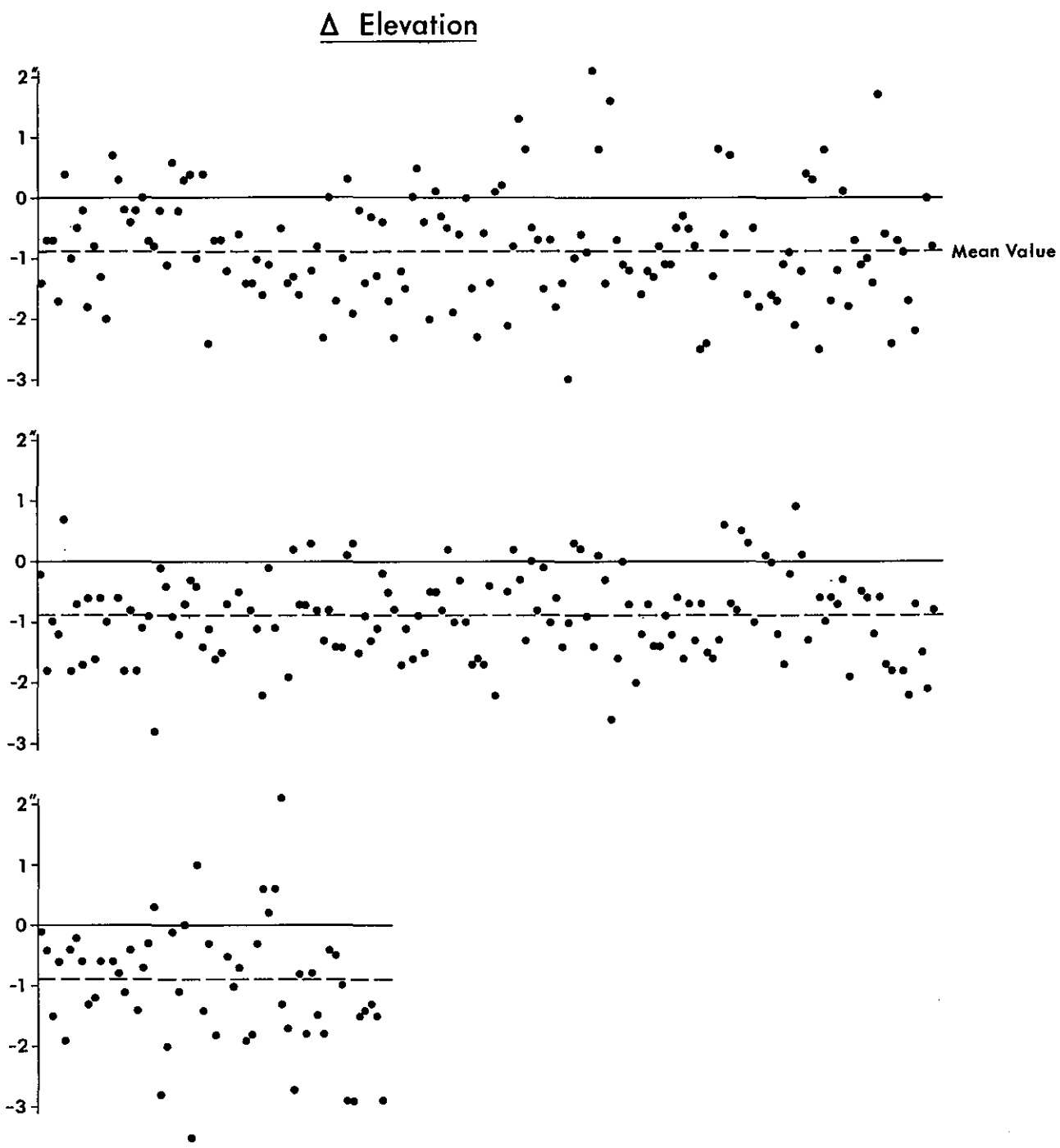

Figure 55.—Plot of the increments in elevation from pre- to post-calibration for a number of randomly selected events, in seconds of arc. The three segments are portions of a single graph.

unit weight after adjustment for the individual line adjustments versus the azimuth, respectively azimuth − 180°, of the triangulated line. As figure 58 shows, the distribution of these values is circular and no dependence on azimuth can be detected. This test at least does not indicate the influence of any synchronization errors.

An examination of the statistical distribution of the 29,104 residuals in the overall adjustment presents a further and obviously necessary oppor-

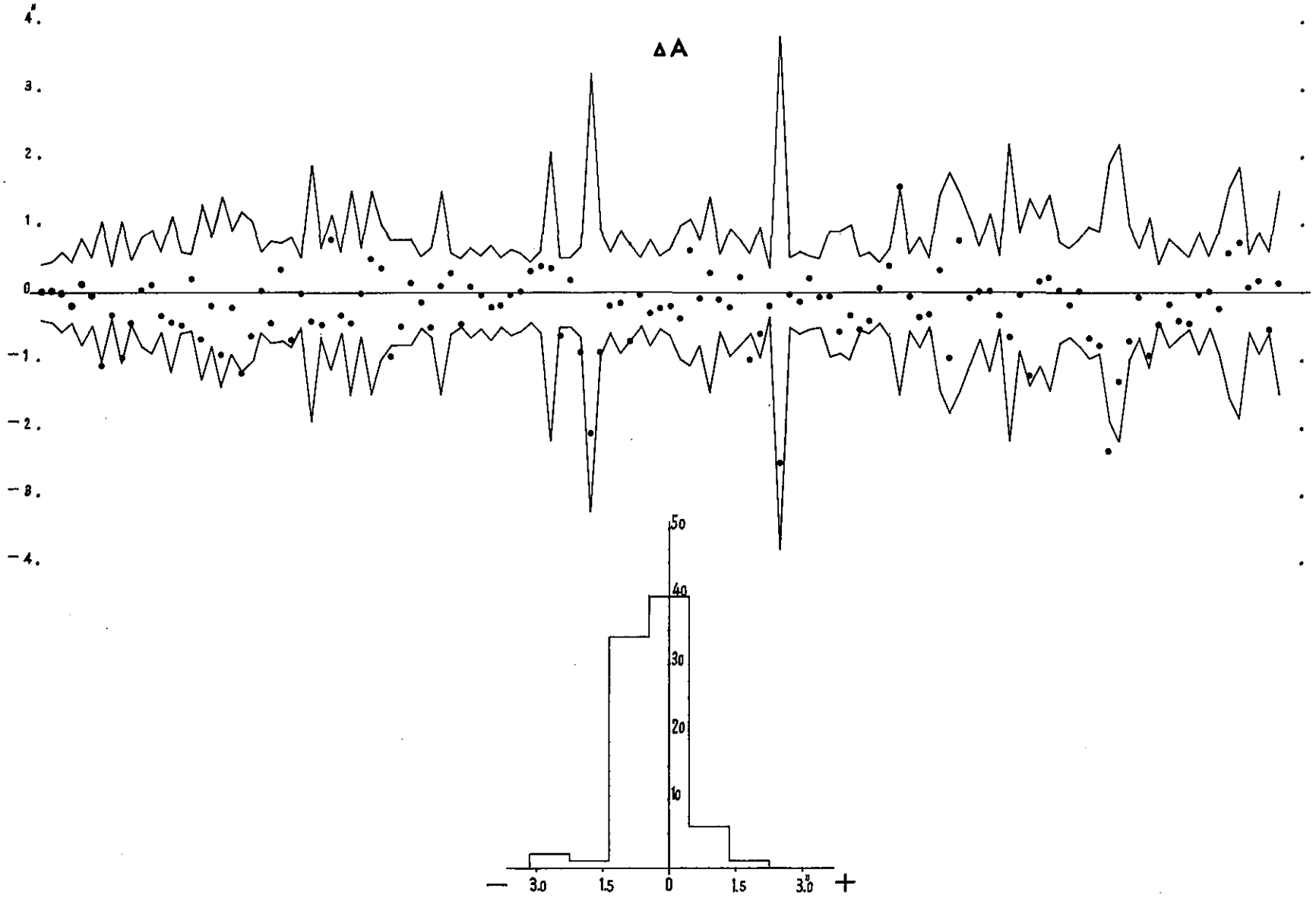

Figure 56.—Differences in azimuth, in seconds of arc, between directions computed as single line adjustments and the corresponding figure from the final adjustment together with the 3σ value of the combined solution. The bottom figure is a histogram of these plotted values.

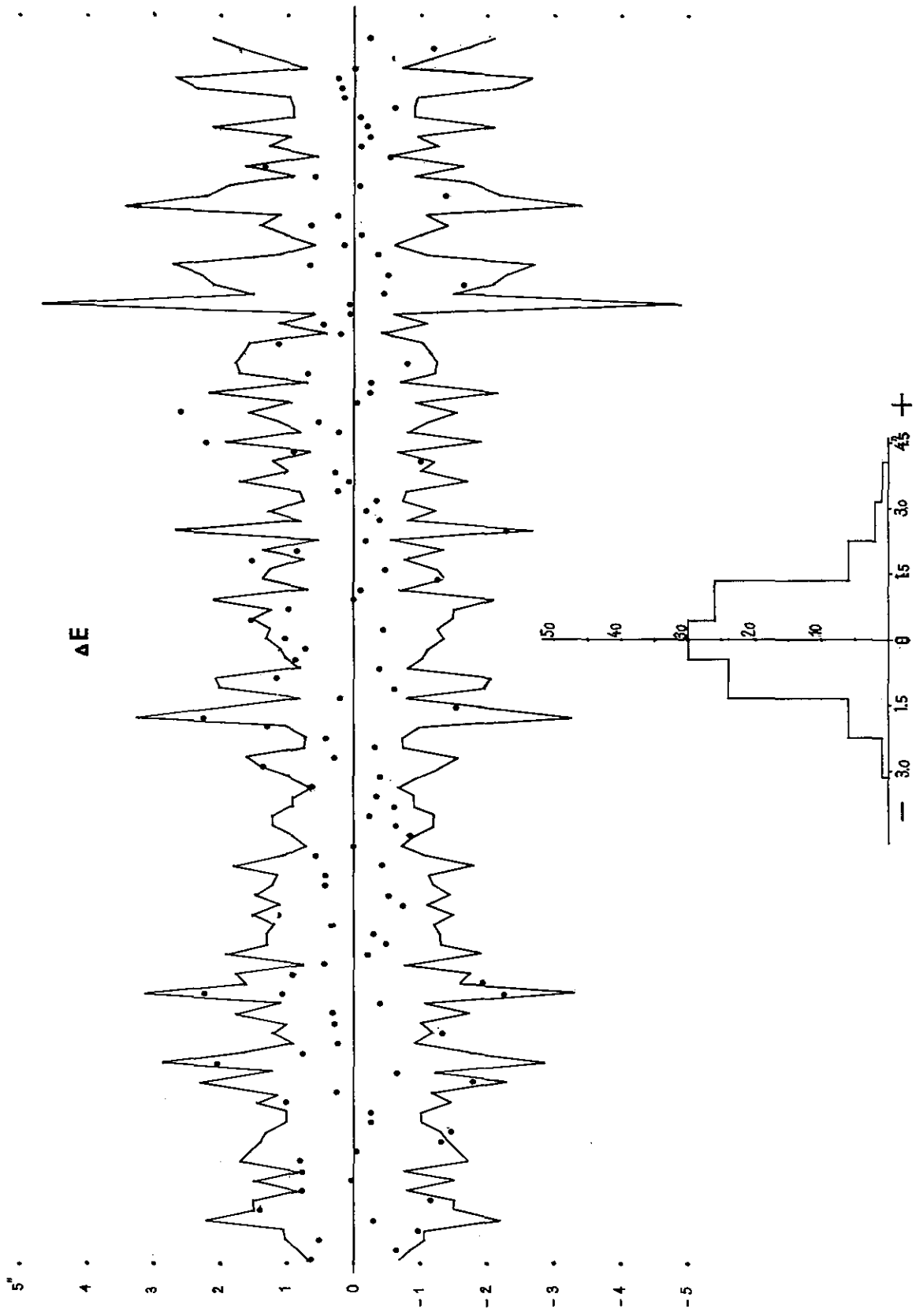

Figure 57.—The elevation differences of the data in figure 56.

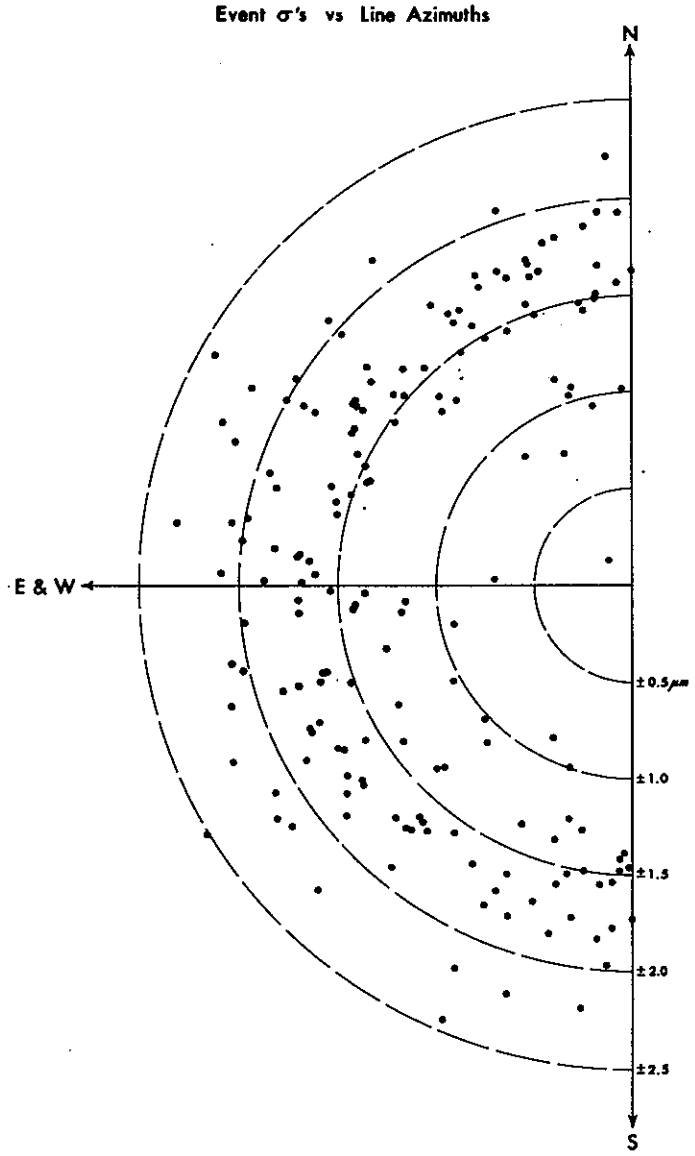

Figure 58.—Mean errors of unit weight σ after single line adjustments plotted in azimuth of the line.

tunity to analyze the data. Figures 59 and 60 are histograms of the residuals in events that were observed from two and three stations respectively. In order to compare these distributions with their theoretical normal distribution curves the residuals would have to be normalized, requiring the computation of the covariance matrix.

$$\sum_{v} = \sum \epsilon - AN^{-1}A^{*}\sigma_0^2. \qquad (313)$$

This is, in the present case, a 29,104 × 29,104 completely filled square matrix, an obvious impossibility. As a result we are forced to neglect the geometric content of the second term of the expression (313) and to normalize the residuals v approximately by dividing each with the mean error of the corresponding observation before adjustment. The greater the number of observations available for the determination of the position of the satellites or, in other words, the greater the

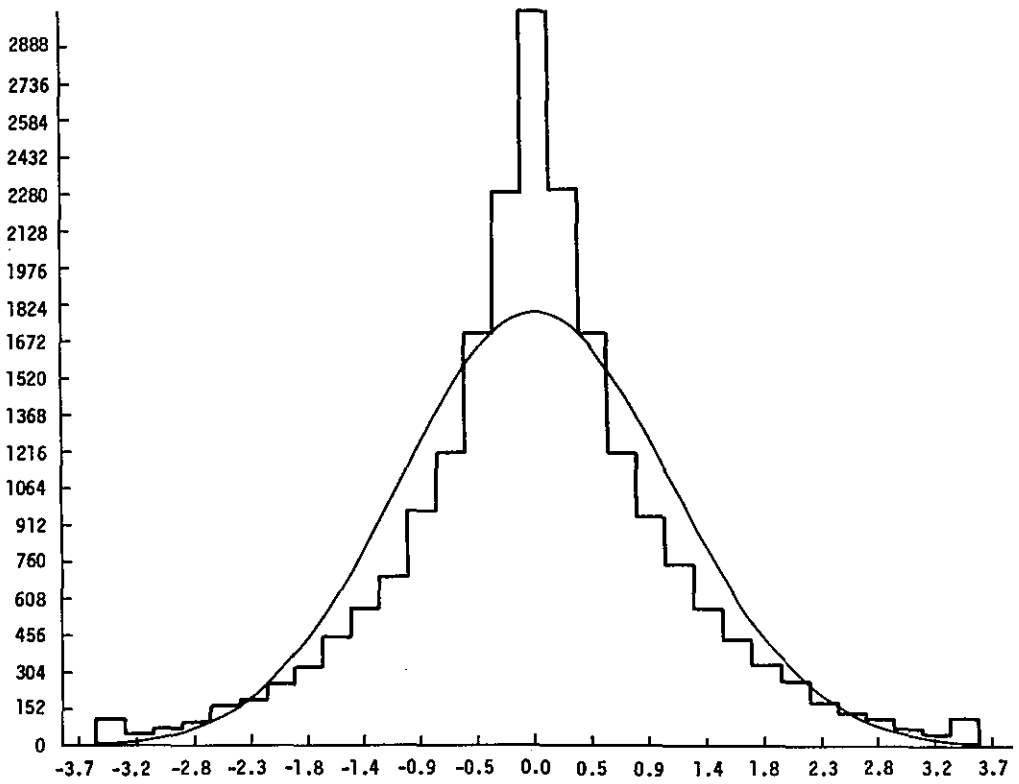

Figure 59.—Plate coordinate residuals for two-plate events (combined x and y values).

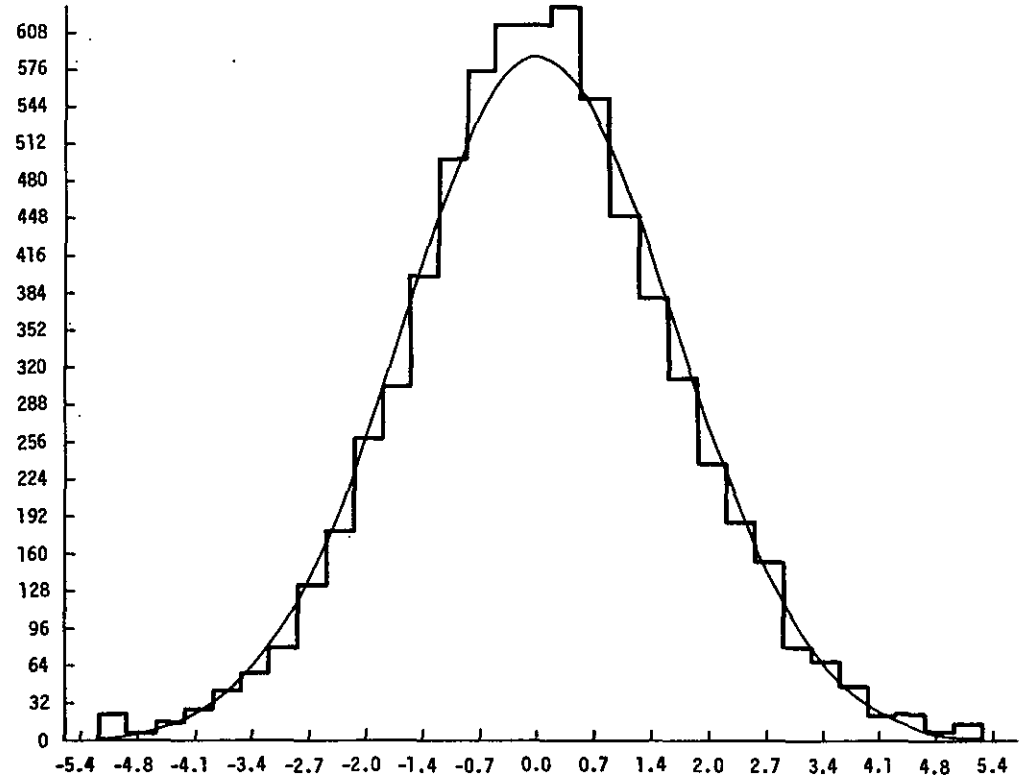

Figure 60.—Plate coordinate residuals for three-plate events (combined x and y values).

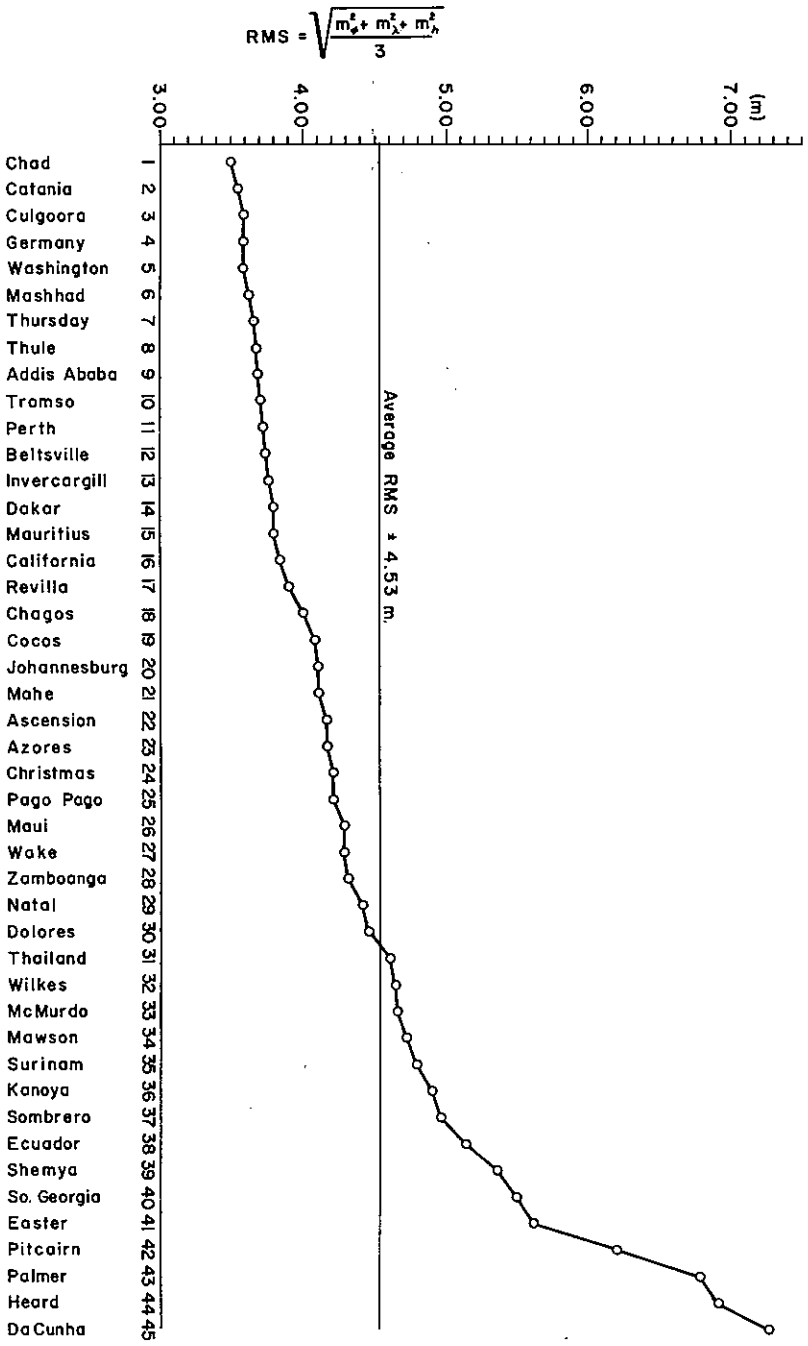

Figure 61.—R.M.S. of mean coordinate errors of adjusted station positions.

number of stations observing the satellite, the more acceptable is the proposed approximation for the normalization of the residuals. This may explain, at least in part, the fact that the fit of the normal curve to the histogram is better for the three station events.

If one accepts the mean error of unit weight after adjustment as a significant measure for the inherent observational accuracy, we have mean coordinate errors for the triangulated stations as shown in figure 61.

It should be noted that although, qualitatively, the material at all stations is uniform, the quantity varies somewhat, resulting in the variations of the coordinate errors.

3.5 References

(1) Schmid, Hellmut H., "Accuracy Aspects of a Worldwide Passive Satellite Triangulation System," *Photogrammetric Engineering*, Vol. XXI, No. 1, Jan. 1965, pp. 104–117.

(2) Schmid, Hellmut H., "The Status of Geometric Satellite Triangulation at the Coast & Geodetic Survey," U.S. Department of Commerce, Environmental Science Services Administration, Coast & Geodetic Survey, 1966, 7 pp.

(3) Schmid, Hellmut H., "Satellite Triangulation," *The Proceedings of the Second International Symposium on the Use of Artificial Satellites for Geodesy*, Athens, Greece, 1967, edited by G. Veis, pp. 245–276.

(4) Schmid, Hellmut H., "Geodetic Satellites: Reduction of Geometric Data," *U.S. National Report (1963–1967), 14th General Assembly Transactions*, American Geophysical Union, Vol. 48, No. 2, June 1967, pp. 333–337.

(5) Schmid, Hellmut H., "Application of Photogrammetry to Three-Dimensional Geodesy, *EOS Transactions*, American Geophysical Union, Vol. 50, No. 1, Jan. 1969, pp. 4–12.

(6) Scott, F. P. and Smith, Jr., C. A., "Comparisons of the SAO and AGK3R Star Catalogs," Conference on Photographic-Astrometric Technique, U.S. Naval Observatory, 1968, pp. 181–190.

(7) Altman, J. H. and Ball, R. C., "On the Spatial Stability of Photographic Plates," *Photographic Science and Engineering*, Vol. 5, No. 5, Sept.–Oct. 1961, pp. 278–282.

(8) Hynek, J. A., "On the Effects of Image Motion on the Accuracy of Measurement of a Flashing Satellite," Cambridge, Mass., Smithsonian Institution Astrophysical Observatory. *Research in Space Science Special Report* No. 33, Feb. 1960, 3 pp.

(9) Nettelblad, F., "Studies of Astronomical Scintillation," *Lund Observatory Publication*, Series II, No. 130, Sweden, 1953, 98 pp.

(10) Rinner, K., "Systematic Investigations of Geodetic Networks in Space," Contract No. 91–591–EUC 3584, Annual Technical Report, European Research Office, Graz, Austria, 1966, 186 pp.

(11) Wolf, H., "Computation of Satellite Triangulation by Spatial Fitting of the Orbit," *German Geodetic Commission*, Series B. No. 153, Munich 1967, pp. 75 et seq.

Acknowledgments

The worldwide geometric satellite triangulation program conducted from mid-1966 to the latter part of 1973 was a cooperative undertaking between the National Aeronautics and Space Administration, which designed and launched the target balloon, and the Defense Department, Defense Mapping Agency (DMA), which contributed the major part in the funding for the observation and data reduction effort and assisted significantly in the field observation phase. The technical supervision of the program was with the National Geodetic Survey (NGS), National Ocean Survey, NOAA. NGS provided the major contribution in the data acquisition and was solely responsible for the data reduction and analysis. The Geodetic Research and Development Laboratory (GRDL, NGS) was responsible for the technical and scientific aspects of the program. The management of the program was in the hands of Capt. L. W. Swanson (NGS). His outstanding and unwavering support to the solution of an endless number of practical problems in conducting this worldwide precision measuring program is thankfully acknowledged. Mr. R. Puhl, Chief of the Data Reduction Branch of NGS, is singled out to convey GRDL's appreciation for responding to often very demanding requests for timely computer results.

Without the splendid cooperation of the international community this program could not have been conducted successfully. The cooperation of the nations who were asked and provided station sites is hereby acknowledged. The participation in the field observation program by teams of the United Kingdom and the German Federal Republic contributed decisively to the required data bank.

The measuring of the necessary scale lines by the geodetic agencies of Australia, Norway, Sweden, Denmark, German Federal Republic, Austria, Italy, and the contribution by France to the African scalar are thankfully mentioned, in recognition of the fact that these results are essential for scaling the worldwide geometric triangulation.

Last, but certainly not least, the dedication and contributions of the members of the Geodetic Research and Development Laboratory are mentioned, which for a decade made their outstanding capabilities available for the solution of many theoretical and computer-oriented problems.

Altogether, nearly 200 employees of the aforementioned U.S. agencies have made their contribution to the program. All of them deserve thanks and recognition for their contributions.

☆ U. S. GOVERNMENT PRINTING OFFICE : 1975 O - 551-598